An Adverse Outcome Pathway Model Approach for Understanding the Effects of Ingested Nanoparticles on the Gastrointestinal Tract

Ke Xu

Department of Food Science and Agricultural Chemistry

McGill University, Montreal

April 2022

A thesis submitted to McGill University in partial fulfillment of the requirements of the degree of Doctor of Philosophy

Table of Contents

Abstract

The past few decades have witnessed an ever-increasing application of nanoparticles (NPs) in the food industry as additives, preservatives, and packaging materials. However, the potential adverse effects of these NPs on the human gastrointestinal (GI) system are not fully understood despite their distinct properties from their bulk counterparts (microparticles, MPs). Traditional *in vivo* toxicity testing using whole animals is resource-intensive and controversial in ethical concerns. As a result, regulatory agencies are calling for a paradigm shift in toxicity assessment from *in vivo* apical tests to alternative, mechanism-based methods using *in vitro* (cell line) models. Adverse Outcome Pathway (AOP) is a framework that organizes key perturbations at different biological levels in a causal manner to support risk assessment, and thus can be used to design integrated toxicity screening platforms. This thesis research addressed (1) the development of a hazard profiling platform based on an AOP model of the human GI tract and (2) the application of the developed platform for hazard identification of ingested NPs.

In this thesis, *in vitro* models of the intestinal epithelium (Caco-2 and HIEC-6) were exposed to a reference library of particles. This reference library consisted of the top three most popular particles in the food sector, including different forms of SiO_2, TiO_2 (food-grade (FG) NPs and MPs, and non-food-grade (NFG) NPs), and AgNPs (citrate-coated AgNP (Citrate-AgNP), and polyethyleneimine-coated AgNP (PEI-AgNP)). Chapter 3 investigated transcriptome-wide changes in 2 cell lines following exposure to the reference library. Comparisons between the 2 cell lines and 8 particles identified chemical-specific and size-dependent responses, allowing the toxicity ranking of the tested particles based on the transcriptomic point of departure (tPOD) values. Functional analysis of the transcriptomic data identified key affected pathways in oxidative stress,

inflammation, and immune responses. Chapter 4 then used bioassays to characterize cellular responses in pathways identified in the previous chapter, as well as intercellular responses at the cellular junction complex and intestinal barrier. This study demonstrated the role of PEI-AgNP in the oxidative stress-dependent disruption of junction complexes and other tested particles in partial disruption of junction complexes without affecting barrier function. More importantly, compromised functional integrity enhanced the transport of food allergen (milk proteins) across the epithelial layer. Based on the outcomes from studies presented in Chapters 3 and 4, the potential role of NPs in disease progression associated with cow milk allergy was examined in Chapter 5. Simultaneous exposure of the NPs and milk affected the antigen delivery across the intestinal epithelium and increased the degranulation of sera-primed mast cells (LAD2). The co-exposure also caused a mechanistic shift from IgE-dependent activation into mixed IgE-dependent and independent activation of mast cells. The identified responses from the previous chapters demonstrated the potential adverse effects of NPs in the GI disease progression and suggested the potential use of the hazard profiling platform developed and tested in Chapter 4 for toxicity screening of other NPs. Chapter 6 examined a multi-component NP model (quantum dots, QD) and quantitively determined the synergistic roles of individual components on the overall toxicity of functional QDs. This chapter also confirmed the critical role of biological transformation in the GI tract in changing the toxicity of the QDs. In summary, this thesis advanced our knowledge of the molecular and cellular mechanisms of the toxicity of ingested NPs and established a high-throughput platform for hazard profiling of NPs likely to enter the human body through the oral route.

Résumé

Il y a récemment eu une croissance des nanoparticules (NP) dans l'industrie alimentaire en tant qu'additifs, conservateurs et matériaux d'emballage. Cependant, les effets indésirables des NP dans le système gastro-intestinal (GI) humain ne sont pas entièrement connu, malgré leurs propriétés distinctes de leurs homologues de plus grande échelle (microparticules, MP). Les tests de toxicité *in vivo* traditionnels utilisant des animaux entiers consomme beaucoup de ressources et sont éthiquement controversé. Donc, les agences de réglementation demandent un changement de paradigme dans l'évaluation de la toxicité des tests apicaux *in vivo* à des modèles *in vitro* (lignée cellulaire). Adverse Outcome Pathway (AOP) est un cadre qui organise les perturbations clés à différents niveaux biologiques de manière causale pour l'évaluation des risques. Cela mène à concevoir des plates-formes intégrées de dépistage de la toxicité. Cette thèse se concentre sur (1) le développement d'une plateforme intégrées basée sur un modèle AOP du GI humain et (2) l'application de cette plateforme pour l'identification des dangers des NP ingérées.

Dans cette thèse, des modèles *in vitro* d'épithélium intestinal (Caco-2 et HIEC-6) étaient exposés à une bibliothèque de référence de particules. Cette bibliothèque comprenait des trois particules les plus populaires dans le secteur alimentaire, SiO_2, TiO_2 (NP et MP de qualité alimentaire et NP de qualité non alimentaire) et AgNPs (citrate-AgNP et polyéthylèneimine-AgNP). Le chapitre 3 a étudié l'échelle du transcriptome dans 2 lignées cellulaires après exposition à cette bibliothèque. Les comparaisons entre les 2 lignées cellulaires et 8 particules ont identifié des réponses chimiques spécifiques et dépendantes de la taille, permettant le classement de la toxicité des particules testées en fonction des valeurs transcriptomiques du point de départ (t-POD). L'analyse fonctionnelle de ces données a identifié les voies principales affectées par le stress oxydatif, l'inflammation et les

réponses immunitaires. Le chapitre 4 a ensuite utilisé des essais biologiques pour examiner les réponses cellulaires des voies identifiées dans le chapitre 3, ainsi que les réponses intercellulaires (jonction cellulaire et barrière intestinale). Cette étude a montré le rôle de PEI-AgNP est dépendante du stress oxydatif des complexes de jonction. D'autres particules on eut une perturbation partielle des complexes de jonction sans affecter la fonction de barrière. Plus important, l'intégrité fonctionnelle a améliorée le transport des allergènes alimentaires (protéines du lait) à travers de la couche épithéliale. Sur la base des chapitres 3 et 4, le rôle potentiel des NP dans la progression de la maladie associée à l'allergie au lait de vache a été examiné (chapitre 5). L'exposition simultanée des NP et du lait a affecté la livraison d'antigènes à travers l'épithélium intestinal et a augmenté la dégranulation des mastocytes amorcés par des sérums. La co-exposition a également provoqué un changement mécaniste de l'activation dépendante des IgE et mastocytes vers une activation indépendante des mastocytes. Les chapitres précédents ont démontré les effets indésirables potentiels des NP dans la progression de la maladie gastro-intestinale et ont suggéré l'utilisation de la plateforme de profilage des risques testée au chapitre 4 dans le dépistage de la toxicité d'autres NP. Le chapitre 6 a examiné un NP modèle avec plusieurs composants (points quantiques, PQ) et a déterminé quantitativement les rôles synergiques des composants individuels sur la toxicité globale. Ce chapitre a également confirmé le rôle critique de la transformation dans le GI dans la modification de la toxicité des PQ. En résumé, cette thèse progresse nos connaissances des mécanismes moléculaires et cellulaires de la toxicité des NP ingérées et a établi une plateforme à haut débit pour le profilage des dangers des NP susceptibles de pénétrer dans le corps humain par le GI.

Acknowledgments

The work conducted in this thesis would not have been possible without the considerable collaboration and constant guidance, and support from several researchers and colleagues. First and foremost, I would like to thank and express my immense gratitude to my supervisor, Dr. Saji George and Dr. Niladri Basu, for their endless patience, encouragement, and invaluable wisdom. I would like to thank all past, current, and honorary George Lab and Basu Lab members for their generous support, advice, help and encouragement throughout. Specifically, I would like to thank Jenny Eng for all the lab training and logistical help throughout my study; Dr. Wut Hmone Phue for her tremendous help with the sample preparation, discussions; and a special thanks to Dr. Aude Bechu for providing the French translation of the abstract.

I would like to thank my supervisory committee, Dr. Jennifer Ronholm and Dr. Stephane Bayen for their guidance over the years, which was a great benefit throughout this research.

The quantum dots study was a collaborative effort with Dr. Aude Bechu from the Moores group in the chemistry department. This study would not have been possible without the cooperation and hard work of everyone involved. Specifically, I would like to thank Dr. Audrey Moores and Dr. Subhasis Goshal for invaluable guidance and encouragement, and for sharing their facilities and expertise with me.

I thank all my friends in Ste. Anne and elsewhere in the world encouraged and supported me throughout. A huge thanks to my friends Yifeng Han and Runyu Shang for always being such strong support for me over the past few years. I would also like to thank my current and former roommates for making my life in Canada so much more enjoyable.

Finally, I thank my family for their constant long-distance support back in China. A huge thanks to my parents, Hailan Huang and Bo Xu, for being so kind patient and such a great source of comfort and encouragement.

This work was supported by the Amy Wong fellowship, The McGill Sustainability Systems Initiative (MSSI), and McGill University Graduate Excellence Award (Xu), as well as the Canada Research Chair program, NSERC Discovery Grants Program (George and Basu).

Table of Figures

Table of Tables

Preface and Contribution to the Knowledge

This thesis is written in the manuscript format, according to McGill's "*Guidelines for Thesis Preparation*." Chapter 1 is a general introduction of the thesis that contains the motivation, objectives, and outlines of this thesis. Chapter 2 surveys related literature for each experimental work. Chapters 3-6 present the introductions, methods, results, and discussions for each of the original studies. Chapter 7 summarizes the thesis with a comprehensive discussion and identifies future research needs. The results presented in Chapter 4 have been published in a peer-reviewed journal. The first part of the study in Chapter 6 has been submitted to a peer-reviewed journal. Chapters 3 and 5 have been prepared for submission, with the candidate being the first author. The second part of Chapter 6 covers the candidate's contribution to a collaborated project that will be submitted for publication after combining with the collaborator's results.

This thesis fills important knowledge gaps and contributes to the advancement of knowledge as follows:

1. Chapter 3 investigated transcriptome-wide changes in two intestinal cell lines following exposure to common dietary NPs. This chapter derived t-POD values for exposed particles, which is a relatively new approach to quantitatively rank hazard potentials while also increasing the understanding of a chemical's mechanism of action. Here, tPODs for all nine NPs were ranked, and comparisons were drawn between the two cell lines. Functional analysis of the transcriptomic data identified critical pathways affected as oxidative stress, inflammation, and immune responses. To the best of our knowledge, this is the first study to characterize transcriptome-wide changes in intestinal cells by dietary NPs, especially in a benchmark dose context. The transcriptomic knowledge and approach can help prioritize chemicals for toxicity screening and identify apical outcomes of concern.

2. Chapter 4 studied the phenotypic effects of common dietary NPs on intestinal epithelial cell models by performing various bioassays targeting the markers of the cellular and intercellular responses identified in the previous chapter. The differential effects of the NPs inferred that the mechanism of toxicity for NPs primarily followed the oxidative stress pathway culminating in the disruption of the cellular junction complex. Subsequent responses of inflammation and immune responses on the intestinal epithelium suggested effects entailing gastrointestinal disorders at higher biological levels, such as food allergy.
3. Chapter 5 examined the potential role that dietary NP exposure might play on the disease progression associated with cow milk allergy. The effects of the particles on changing antigen delivery were investigated across *in vitro* epithelial layers, and degranulation level was studied on sera-primed mast cells (LAD2). The results identified that simultaneous exposure of NPs and milk could initiate mechanism changes from IgE-dependent activation to mixed (IgE-dependent and independent) activation of mast cells. To the best of our knowledge, this is the first study to investigate the effects of NPs in a food matrix on the mechanisms of milk allergy. The results were in good agreement with the responses at molecular (Chapter 3), cellular and intercellular levels (Chapter 4), and taken together they suggest the potential role of NPs in the disease progression of milk allergy.
4. Chapter 6 applied a panel of bioassays used in earlier Chapters to examine the toxicity of a more complex NP model - QDs. This chapter quantitively identified the synergistic roles of individual components on the overall toxicity of multilayered QDs. This chapter also confirmed the critical role of biological transformation (three-phase simulated digestion) in the GI tract in changing the toxicity of the QDs. To the best of our knowledge, this is the first study that attempts to use multilayered-NPs for the in-depth analysis of toxicity after simulated GI tract digestion.

Chapter 1

1. Introduction

1.1. Thesis Motivation, Objectives, and Hypothesis

The widespread application of nanotechnology has revolutionized the food industry in the design, production, processing, packing, and storage of food products.[1] There are currently more than 9,000 commercial products containing NPs on the market, including 363 products in the food sector.[2] However, the application of novel materials may lead to unintended health risks arising from the adverse effects of NPs on the human GI system. As an emerging field of application, knowledge about the toxicity of ingested NPs is still advancing, with prominent knowledge gaps on the fundamental biology of nano-bio interactions and data useful for making regulatory decisions.[3] Traditional toxicity testing involves exposing model animals to the target chemicals for measurable apical outcomes, which can be challenging considering the cost, time, and the number of untested and new materials.[4-7] This realization has resulted in a call for a paradigm shift in toxicology, which is to use New Approach Methodologies (NAMs) based on high-throughput *in vitro* assays to screen, prioritize and predict adverse effects of NPs.[4]

The overall objective of this study is to understand the adverse effects of ingested NPs by organizing the responses at different biological levels using an AOP approach. The optimized assays that probe perturbations at the molecular, cellular and higher biological levels embedded in an adverse outcome would then enable hazard profiling of ingested NPs.

1.2. Specific Aims

Aim 1: Identify key perturbations and toxicity pathways at the molecular level.

The objective of Aim #1 is to identify the transcriptomic changes using RNA sequencing in two intestinal cell lines after exposure to a reference library of dietary NPs. Specifically, the transcriptomic changes were analyzed for

- gaining mechanistic insights into how NPs may perturb intestinal cells. This study measures the changes of a targeted transcriptomic panel containing 989 hallmark genes to calculate tPODs values for all tested particles.
- identifying variable-specific responses of NPs exposure. This chapter is a comparative study involving multiple cell lines (n=2), chemicals and forms (n=9), and concentrations (n=11) to examine chemical-specific and concentration-dependent transcriptomic responses.

The specific hypotheses are 1A: that genes and pathways implicated in oxidative stress, inflammation, and immune responses will be differentially affected by different dietary nanoparticles; 1B: that the differentially expressed genes will be affected in a respond to chemical composition and concentration of tested particles; and 1C: the toxicity of the exposed particles will be ranked similarly in both cell lines based on their t-POD values. The rationale for Aim#1 is to identify key perturbations at the molecular level that can entail apical responses at higher biological levels.

Aim 2: Identify key perturbations at the cellular and the inter-cellular level

The overall goal of Aim #2 is to identify and characterize the *in vitro* phenotypic responses in both cell lines after exposure to the reference NP library. Specific goals are to:

- probe the phenotypic responses including oxidative stress, inflammatory cytokine release, epithelial functions, and immune responses with targeted assays.
- compare the different responses between cell types (n=2), chemical types and forms of NPs (n=9), and concentrations (n=8) and rank particles based on their toxicity.
- propose the toxicity mechanism of NPs to intestinal epithelial cells.

The specific hypotheses for this study are 2A: that the cell models will have different exposure-dependent responses; 2B: that the responses are composition-specific and concentration-dependent; 2C: that the primarily affected responses will be mediated by oxidative stress and pro-inflammatory responses. The results from this chapter, along with the knowledge from the previous aim, will help identify the key perturbations at molecular and higher levels to infer adverse outcomes at higher biological hierarchies.

Aim 3: Relate *in vitro* results to an adverse outcome at the organism level

The overall goal of Aim #3 is to connect the identified responses from Aim #1 and #2 to an adverse outcome at the organism level of public health concern. The disorder investigated in this study is cow milk allergy using a transwell culture system that comprises epithelial cell Caco-2 and mast cell LAD2. The specific objectives are to:

- examine the changes in milk allergen delivery and mast cell degranulation level after pre-treating particles to the model system.

- examine the changes in milk allergen delivery and mast cell degranulation level after simultaneous exposure to NPs and milk to the model system.
- identify potential changes in the mechanisms of allergy triggered by the co-exposure of NPs and milk.

The specific hypotheses are 3A: that the responses after co-exposure of particles and milk will be different from the responses to milk exposure after particle pre-treatment; 3B: that the simultaneous exposure of milk and particles may change allergen delivery across the intestinal epithelium; 3C: that the co-exposure can change the mechanisms of downstream immune responses. The rationale for this proposed aim is that the responses at lower biological levels identified in the previous chapters can be organized and related to immune responses and adverse outcomes at higher biological levels.

Aim 4: Apply the developed model to High-Throughput Screening (HTS) platforms for toxicity screening of selected chemicals.

The overall goal of Aim #4 is to apply the targeted bioassays developed in previous chapters to toxicity screening of a model multilayered NP (QD) and probe the effects of surface transformation on toxicity. Specifically, the objectives are to:

- examine the contribution of individual components to the overall toxicity of QD quantitatively using a mathematical model
- identify the primary toxicity mechanism of the QDs using the panel of bioassays identified in previous aims.

- characterize the toxicity of ingested NPs before and after each stage of the three-phase simulated GI digestion

The specific hypotheses are 4A: that the complete QDs will induce higher cytotoxicity responses than each of its components; 4B: that surface chemistry is a critical factor affecting the overall toxicity of the QDs; and 4C: that the digestion of QDs along the gastrointestinal tract changes the toxicity of the QDs. The rationale for this proposed Aim is to probe the transformation of the NPs after ingestion and apply the developed bioassays for toxicity screening of ingested NPs.

Chapter 2

2. Literature review

2.1. Food Intake, Dietary NPs, and GI Disorders

Food intake and the function of the GI system are closely interrelated in the induction and progression of certain disorders affecting the GI system.[2] Dietary components may modulate gut microbial composition, act as allergens to trigger immune responses in susceptible individuals, and cause or worsen inflammation.[8, 9] In addition to natural food materials, food additives might stimulate changes in the GI system and influence the overall wellbeing.[10, 11] However, their innate complexities and interactions with natural food ingredients complicate the identification of the role of non-dietary components in disease progression. One pilot study compared a controlled diet to a diet with reduced micron and submicron particles of titanium dioxide (TiO_2) and aluminosilicates, finding improvement of Crohn's disease upon the reduction of particles.[12] Dietary TiO_2, a well-known food colorant, was also documented to exacerbate dextran sodium sulfate-induced colitis and contribute to pathways that led to intestinal fibrosis, but the later effect had not been proved.[13] These studies lead to the concern about the synthesized submicron materials added to the food products regarding their safe doses and potential health effects.

Although natural NPs, such as casein micelles and starch particles, can be present in food products as original components or generated during food processing, the food industry has witnessed a dramatically increased application of engineered NPs in recent years.[14-16] These NPs are artificially synthesized materials with at least one dimension in nano-scale (1-100 nm), and functionalized to attain specific physicochemical properties in improving the texture, taste, nutrient absorption, and

shelf life of food products.[17] Advances in the fields of nanotechnology have resulted in widespread application in consumer products. The nanomaterial consumer products inventory (CPI) project reported 54 commercial products in 2005, which increased to 1,814 by 2013 with 119 products under the category of food and beverage.[18] The number of commercial products became 9,562 in 2021 based on the data in another updated nanotechnology products database (StatNano), including 363 products in the food sector.[19] As common NPs in the food sector, engineered NPs have found their roles as food ingredients or additives, in food processing, and as food packaging materials (Table 2.1).[1, 20] A lot of particles listed in the table, however, were not intentionally produced as NPs. Under the category of food additives, SiO_2 (E551) [21] and TiO_2 (E171) [22] contain both micro- and nano-sized particles due to production. Silver (E174) is usually presented in its elemental form, but 20% of the Ag was found to be released as NPs from confectionary pearls.[21] The usage of some additives dates back to the beginning of the 20th century, but the presence of the NPs was only recognized and verified in the past few years due to technology advancement.[22]

Table 2.1 Application of engineered nanoparticles in the food sector.

Categories	Types of NPs	Applications	Reference
Food additives & ingredients	SiO_2 (E551)	Anti-caking/ anti-clumping agent	23, 24
	TiO_2 (E171)	Colorant	25
	Ag (E174)	Confectionary	26
	Al_2O_3 (E554)	Medicine/ personal care	27, 28
Food processing	Polymeric NPs (e.g. Polyamide hydrochloride, poly(styrenesulfonate))	Nanofiltration	29
	Nanoliposomes, solid lipid NPs & nanostructure lipid carriers	Nanoencapsulation	30
Food Packaging	ZnO, AgNP	Anti-microbial packing agent	31, 32
	Biopolymer-based nanocomposite (Organoclay NPs)	Reinforced food packaging material	33
	Carbon nanotubes	Gas sensors in food packaging	34

The commercialization of nanotechnology products and the anticipated applications of NPs in food products raise concerns about their safety aspects to human health. The toxicological features of these dietary NPs require extensive evaluations for potentially unexpected biological consequences due to their unique physicochemical properties compared to their bulk counterparts. Safety assessment of NPs emphasizing the transformation and toxicokinetics of NPs entering the human body through food is also critical for the sustainable deployment of nanotechnology in the food and agriculture sector.

2.2. Toxicokinetics of NPs

A person could be exposed to NPs through inhalation, dermal contact, or ingestion, among which oral ingestion of NPs-containing food or beverage takes up 16% of total exposure.[18, 35] It is estimated that ingestion of fine (100 nm -1 μm) and ultrafine (<100 nm) particles of an average person under a typical western diet ranges from 10^{12}- 10^{14} for a person per day, with the major sources being TiO_2 and silicates.[36] Specific intake of TiO_2 from food sources is estimated to be 1-3 mg/kg_{bw}/day, with about 36% being nano-sized particles.[25] Nano silica's daily intake is estimated to be about 124 mg based on the worst-case scenario.[23] Bio-accumulation of NPs can also occur along the food chain and potentially lead to higher doses of chronic exposure.[37] In addition, unintentional exposure can happen when food products contain residual NPs of pesticides and veterinary drugs or migrated NPs from food contacting packaging materials.[38]

Orally administered NPs interact with different biological milieu during their journey through the GI tract. Various digestion compartments along the GI tract, including the mouth, stomach, and intestine, can secrete digestive fluid of distinct compositions to digest food components.[39] The interactions between ingested NPs and the digestive fluid could affect the physicochemical properties of the NPs and downstream effects on bioavailabilities and potential toxicities.[40, 41] The transformation may be further complicated by possible synergic effects due to the co-exposure of different NPs and the food matrix. As a result, pristine NPs generally used in toxicological studies could give rise to outcomes of less relevance to the real-world exposure scenario. It is thus important to understand the toxicokinetics of the NPs after ingestion.

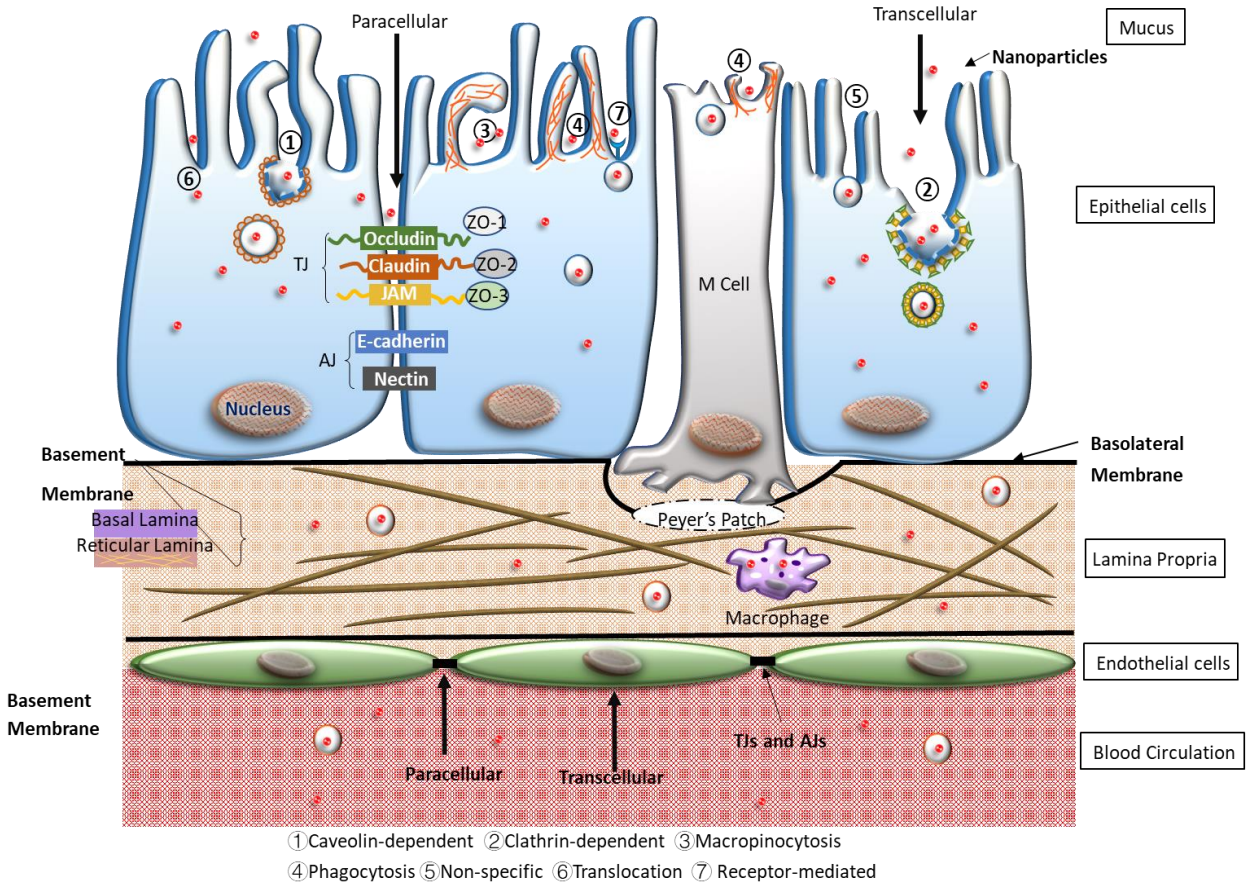

Figure 2.1 Endocytosis pathways of nanomaterials in the intestinal epithelial layer and the subsequent absorption into the circulatory system.

The absorption of NPs mainly occurs at the intestinal surface, the body's largest external surface contacting with food ingredients, microorganisms, and toxic substances.[42] The intestinal epithelial layer is well known for its "gate and fence" function.[43] It uses the lipid membrane and semipermeable junction complex to prevent hazardous substances from entering while allowing nutrients uptake (Figure 2.1).[42, 43] The primary mechanism of cellular uptake of NPs is endocytosis, which refers to the membrane engulfment of NPs (<50-100 nm) followed by the formation of vesicles and transportation to specialized intracellular compartments).[44-46] Paracellular uptake is another major uptake mechanism where materials pass through the membrane boundary *via* the gap between neighboring cells.[47] The sizes and surface charges of NPs greatly influence bioavailability. Generally, smaller particles and positively charged metal and polymeric particles are preferred in cellular uptake.[48-52] However, special cases do occur as phagocytotic cells would preferentially choose to absorb anionic particles over cationic particles.[53]

NPs may not retain their original size, structure, and composition during metabolism, and can undergo transformation and degradation throughout the GI systems. Upon entering a complex biological system, NPs may interact with the surrounding biomolecules to form a dynamic "biocorona" on their surfaces.[54] Digestive fluids in the mouth (saliva), stomach, pancreas, and intestine contain different biomolecules and can distinctively modify the surface of NPs with variations in pH, digestive enzyme, and ionic strength.[39, 55] The interactions can also affect the function of the biomolecules. For example, the interaction between SiO_2 NP and trypsin, a protease enzyme in the intestinal fluid, may alter the enzyme structure and affect its function in protein digestion.[56] In addition to the digestive fluids, the interactions between the food matrix and the NPs can also modify the composition of the biocorona and change the functions of the

biomolecules. Past studies have identified changes in the composition of NP surface biocorona after interacting with milk and changes in the allergenicity of milk proteins.[57, 58] The interactions between the NPs and the surrounding bio-environment thus warrant detailed studies to characterize the changes of the NPs and identify the subsequent effects on the GI system.

The bodily distribution patterns of several commonly used NPs have been studied using animal models, suggesting increased accumulation in the kidney, liver, brain, lung, stomach, and blood in a dose-related manner with typically higher concentrations in the kidney and liver.[59, 60] Factors influencing NPs' distribution throughout the body include size and shape, where smaller and spherical NPs are preferred in the uptake.[61-63] Excretion and clearance of NPs usually occur *via* urine excretion after renal filtration and bile excretion following hepatobiliary processing.[64] Liver is the predominant organ for detoxication and thus becomes the major accumulation site for NPs.[65, 66] The clearance of particles is also closely related to the shape and size of the particles. Renal clearance of quantum dots smaller than 5.5 nm is mostly mediated by excretion into urine rapidly and eliminated much faster than the rate of clearance for larger quantum dots (>15 nm).[67]

The transportation of the ingested particles in the GI tract results in interactions between the particles and the biological environment, which may potentially lead to hazardous outcome.[68] Although various studies focused on orally administered NPs have not identified acute cytotoxic effects, the field is still needing knowledge for sublethal and chronic effects at various biological level.[3] The next section briefly introduces examples of identified adverse effects of ingested NPs on the human GI tract from the literature.

2.3. Potential Adverse Effects of NPs on the GI System

Although no disease condition has been directly associated with the exposure to ingested dietary NPs, it is evidenced from inhalation toxicology that nanosized materials could elicit severe adverse health effects such as pulmonary fibrosis, inflammation, and cardiovascular diseases.[69, 70] Since engineered NPs have shown similarities to ultrafine particles in inducing potential adverse health effects, it is possible that ingested NPs may share similar effects in the GI tract as inhaled particles in the respiratory system.[71-73]

2.3.1. NPs induce reactive oxygen species (ROS) generation

Reactive oxygen species (ROS) are molecular oxygen-derived molecules and free radicals, including superoxide anion radicals, hydroxyl radicals, singlet oxygen, hydrogen peroxide (H_2O_2), and other oxygen-containing radicals.[74] ROS generation is a regular cellular process, especially in mitochondria, and can stimulate immune responses against pathogens while participating in various cellular signaling pathways.[75] However, excess ROS production will result in oxidative stress and a series of cellular damage so that cells fail to maintain their physiological functions.[76] Such damage includes oxidative modification of proteins, nucleic acids, gene expression, and inflammatory responses, leading to cell death and other genotoxic effects.[77]

ROS formation can happen directly abiotically at the reactive surface of NPs, which is the interface between the NPs' surface and the contacting biological systems.[78] For NPs containing transitional metals on the surface or made of single components, the electron-hole pairs formed on the material surface could lead to the generation of ROS, changes in free energy, and conformational changes with the presence of oxygen (O_2) by dismutation or Fenton chemistry, which is the primary

reaction that breaks down hydrogen peroxide and generates hydroxyl radicals.[79-83] NPs with smaller sizes will lead to higher ROS levels due to higher surface area to volume ratio and surface charge.[84-87] Generation of ROS can also happen biotically inside the cells as byproducts during oxidative phosphorylation in mitochondria, where electrons escape from the electron transport chain and form superoxides with molecular oxygen.[88] The generated superoxide can be subsequently converted to hydrogen peroxide from dismutation and other ROS.[89] The accumulation and overload of ROS can disrupt cellular homeostasis and induce oxidative stress, which is known to cause various injuries to the cells.[90] The release of oxidative products into the blood and persistent oxidative stress have also been characterized as critical signatures for cancer.[91] Studies have found that metal and metal oxide NPs can induce ROS generation and subsequent oxidative stress and DNA damage in intestinal epithelium cell models, indicating that this can be a potential adverse effect induced by ingested NPs.[92-94]

2.3.2. NPs elicit pro-inflammatory responses

Inflammation is a protective response to stress, pathogens, infection, or tissue damage, which involves the coordination between immune cells and blood transportation by various molecular signaling pathways.[95, 96] Inflammation process starts with an inducer (oxidative stress, infection, or tissue damage), which results in the activation and recruit of immune cells like mast cells and macrophages to the site of inflammation, followed by the release of cytokines, chemokines, free radicals and lipid mediators (Figure 2.2).[97, 98] Pro-inflammatory responses can stimulate both tissue repair and chronic inflammatory conditions.[99] The chronic inflammation localized in the GI tract is termed inflammatory bowel disease (IBD), a common idiopathic disorder that comprises two major types: Ulcerative colitis (UC) and Crohn's disease (CD).[100] The disease can be induced by

genetic, environmental, and immunoregulatory factors.[101] Symptoms of IBD are characterized by mucosal ulceration, which can induce a series of downstream effects ranging from chronic diarrhea and abdominal pain to systematic effects like weight loss, fever, fatigue, skin ulcers, arthritis, and bile-duct inflammation.[102]

Several studies have reported that NPs can activate inflammatory signaling pathways and induce pro-inflammatory cytokines in human intestinal epithelial cell models.[36, 103, 104] *In vivo* studies have also found that NPs can exacerbate dextran sodium sulfate-induced colitis *via* activating NLRP3

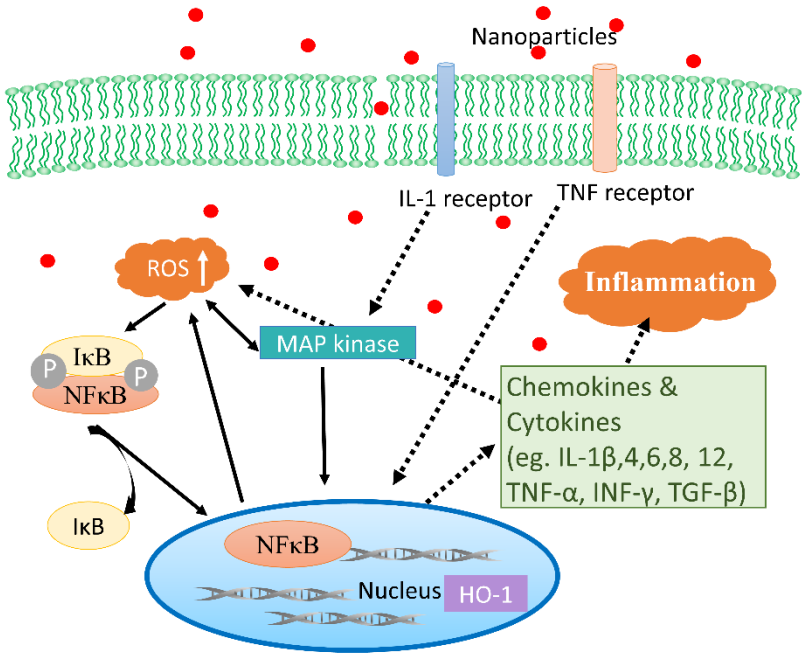

Figure 2.2 Signaling pathways of nanomaterials-induced inflammation and ROS generation. The two adverse outcomes are inter-related to each other by sharing signaling pathways and inducing similar downstream cytokines and chemokines.

inflammasome and initiating pro-inflammatory responses.[13] Furthermore, the ability of particles to induce oxidative stress has been proposed to associate with the activation of inflammatory mediators closely.[105] This close relationship also suggests that pro-inflammatory responses should be evaluated as potential adverse effects caused by ingested NPs that warrant future research.

2.3.3. NPs cause intestinal epithelial layer disruption

The intestinal epithelium functions as a barrier to protect the intestinal lumen and regulate molecular trafficking from the external environment.[42, 106] The integrity of the epithelial layer is crucial to nutrient absorption and the overall health of the GI systems. Disruption of the intestinal mucosa will result in abnormalities in permeability and higher risks of introducing toxins and pathogens to the intestine.[42] Clinically, this dysfunction of the epithelial layer is implicated as hyperpermeability or "leaky gut", thereby leading to several acute and chronic intestinal diseases.[42, 107]

The intestinal epithelial layer is joined by epithelial cells that form selective barriers by connecting adjacent cells through junctional complexes.[107] There are three major components of the junction complexes: tight junctions (TJs), adherens junctions (AJs), and desmosomes, where the first two are major types of cell junctions.[107, 108] Tight junctions are the primary regulators for the epithelial layer's permeability by controlling the ions and molecules' movement *via* paracellular and transcellular pathways.[42, 109] TJs consist of the transmembrane protein claudin family, occludin, JAM, and the cytoplasmic protein zonulin.[110] Among these proteins, the claudin family has the greatest number of protein types and is the essential protein family for tight junction selectivity.[111] AJs comprise the transmembrane protein cadherin and the cytoplasmic protein catenin.[108] This cadherin–catenin complex can bridge adjacent cells *via* homophilic interactions while attaching to the intracellular actin filaments and other cytoskeletal components.[112, 113] Mature adherens junction can induce the formation of tight junction, but tight junction stabilization does not require adherens junction protein (cadherin).[114]

Cell junction complex disruption is closely related to the induction and release of cytokines and chemokines. Pro-inflammatory cytokines can cause damage in the intestinal epithelium tight junction, while the disruption of junctional complexes will also lead to the increased influx of potentially hazardous materials.[115-117] The small size of NPs allows them to cross the 20 nm interface between neighboring cells.[118] The passage of NPs may disrupt the junction complexes and thus introduce more pathogenic or toxic materials to enter the circulation system and translocate to various organs. Studies have reported that TiO_2 NPs and AgNPs can cause loss of VE-cadherin and increased endothelial permeability without inducing oxidative stress and apoptosis.[119-121] However, the composition of the AJ is not the same in endothelial layers from epithelial layers, and thus the effect of NPs on the adherens junction will vary. As for epithelial cells in the GI tract, studies have also reported possible disruption in membrane integrity after exposure to α-Fe_2O_3 NPs.[122] SiO_2, TiO_2, and hydroxyapatite NPs were also reported to disrupt the membrane structure by inducing epithelial-mesenchymal transition, a process in which epithelial cells lose the adjacent cell junctions and epithelial properties and acquire mesenchymal markers.[123] Thus, the disruption of epithelial function and the integrity of the cellular junction should also be evaluated as potential adverse effects caused by ingested NPs.

2.3.4. NPs affect immune responses-a food allergy investigation

In addition to the inflammatory responses and oxidative stress, NPs may also affect the immune system responses. One of the most closely related immune responses to the GI tract is food allergy, which is the adverse immune response to food ingestion responsible for various symptoms and disorders in GI tracts.[124] The food-induced allergic reactions can be primarily mediated by immunoglobulin E (IgE)-dependent and IgE-independent mechanisms.[125] The majority of the

allergic responses are IgE mediated hypersensitivity reactions (type I reaction) and can occur within minutes to hours after food ingestion in susceptible individuals.[126] IgE is a primary immunoglobulin produced by the immune system in elevated concentrations for individuals with allergic diseases. The common IgE-mediated allergy mechanism has been well-characterized in the literature.[127, 128] Briefly, ingested allergens will be sampled by antigen-presenting cells (e.g., epithelial cells and dendritic cells) in the GI tract before entering tissues. Allergens transported and processed in regional lymph nodes or local mucosa will trigger the transformation of naive T cells into T helper 2 (TH2) cells and the production of IgE from B cells.[127, 128] The produced IgE will then diffuse into lymphatic and blood vessels to be distributed systemically.[127, 128] Reintroducing the allergen-specific or non-specific IgE into the interstitial fluid allowed their binding to the high-affinity receptor for IgE (FcεRI) and a low-affinity receptor for IgE (CD23) on tissue-resident mast cells.[127, 128] The bounded IgE resulted in the sensitization of the mast cells and prepared them to respond upon the subsequent allergen exposure.[127, 128] When the susceptible individual is exposed to the allergens again, sensitized mast cells will be degranulated and release a variety of inflammatory mediators, including histamine, β-hexosaminidase, and various cytokines and chemokines that can regulate innate and adaptive immune responses.[127] In addition to the common IgE-dependent mechanism, allergic reactions can also happen in an IgE-independent manner *via* IgG mechanism, external stimuli, and infection.[129, 130] Cow milk protein (CMP) is the most common allergen that can induce both types of allergy in early childhood. In developed countries, allergy to milk protein affects approximately 2 to 3% of the population in the first year of life and often persists to school age.[131, 132] As a population group more susceptible to milk allergy, the relatively higher intake of sugar-containing products also suggests higher risks of

exposure to food additives potentially containing dietary NPs as colorants and anticaking agents (e.g., dietary TiO_2 exposure for children is 2-3 times higher than in other age groups).[12]

The effect of NPs on allergy is still an emerging field. Most studies report that NPs are inducing mast cell degranulation in unknown IgE-independent pathways without the participation of specific allergens.[133, 134] However, much less is known about the effects of simultaneous exposure to food allergens and NPs due to the possibility of biocorona formation on the particle surface in complex biological systems.[135] Based on a recent study from our group, dietary NPs can alter the structure of the milk proteins, increase the allergenicity, and directly cause mast cell degranulation when mixed with milk.[58] However, food allergens cannot be exposed to immune cells directly before migration across the intestinal epithelial layer. As such, the co-exposure of NPs with milk allergen to more complex *in vitro* models warrant further analysis.

The potential adverse effects discussed in this section represented individually studied effects at the cellular level (ROS generation, pro-inflammatory response), tissue level (epithelial layer disruption), and organism level (food allergy). In order to infer the potential effects of NPs exposure on the GI tract in disease progression, the perturbations at various biological levels need to be organized logically. In this thesis work, we chose the AOP pathway as a framework to probe the toxicity of NPs from molecular to organism level.

2.4. Adverse Outcome Pathway as a Framework for Organizing Knowledge in Toxicology

Human epidemiological studies can be regarded as the epitome in the hierarchy of risk assessment since the data provides the most relevant link between health risks and diet patterns of a population. However, epidemiology studies mainly examine the outcomes related to the exposures to

suspected risks after an outbreak, limiting its use for risk analysis of a dietary component before it is introduced into the market for mass consumption. Human clinical trials are essential in drug development but are not required for food additives and functional food ingredients due to a lack of a specific regulatory framework.[136, 137] *In vivo* animal tests have been considered the 'gold standard' for toxicity studies and are used on the premise that adverse health outcomes observed in response to a chemical in a vertebrate can be reasonably well extrapolated to humans.[138] Although these traditional toxicology tests are routinely performed by standardized protocols and have regulatory significance, these approaches still suffer from high costs, time, and ethical issues.[4]

Recent advances in system and computational biology, bioinformatics, and toxicogenomics call for transforming toxicity testing from the traditional approach of observational studies in animals to mechanistic toxicology using *in vitro* and small organism models with high throughput capabilities.[139, 140] In 2007, the National Research Council (NRC) in the U.S. issued a report titled "Toxicity Testing in the 21st Century-a Vision and Strategy" which emphasized the need for "new toxicity-testing paradigm" and suggested the potential use of cellular response pathways to evaluate and predict toxicity.[4] The envisioned next-generation toxicity approach requires utilizing systematic knowledge of biologically significant perturbations in key toxicity pathways that entails human disease conditions to perform comprehensive arrays of *in vitro* tests and computational biology. [4] In accordance with the vision, one of the tools proposed to facilitate the development of the novel toxicology platform is the use of AOP to identify and relate significant perturbations as earlier triggers of disease conditions for predictive toxicity.

The AOP represents a framework that systematically organizes existing toxicological knowledge into sequential relationships that can link endpoints at all levels in an organism in a causal

manner.[141] Practically, the AOP framework can relate and organize data from *in vitro*, *in vivo* and *in silico* studies into models to explain or predict potential adverse effects of the target material.[142] Since this method of toxicity assessment yields answers on the pathways elicited by a chemical, it can be useful for predicting the likelihood of adverse effects in animals and humans. The AOP Wiki is currently the primary repository of AOP development that contains qualitative information for both developed and ongoing AOPs studies coordinated by the OECD.[143] According to the website, AOPs that organize the mechanistic information available for gastrointestinal injury are grossly underdeveloped.[143]

Structurally, an AOP regards disease as a culmination of perturbations. The process starts with a molecular initiating event (MIE) and leads to key events (KE) that culminate in adverse outcomes (disease condition).[144] The definition of MIE has seen different variations due to the field of application, but it signifies the initial interaction between the chemical and biosystem at the most basic biological level (Figure *2.3*). Such interaction will lead to sequential key events (KEs), which are alterations that perpetuate through the succeeding hierarchy of organisms such as tissue and organ**.** The culmination of the KEs results in adverse outcomes (AOs), yielding disease conditions of an organism on the individual or population level.[144] Key event relationships (KERs) relate KEs in downstream reactions and form the AOP networks.[141] The fact that AOPs are not limited or

specific to any chemicals but instead focus more on the biological responses at different levels (cellular, tissue, organ) provides a much broader platform to evaluate toxicity comprehensively.

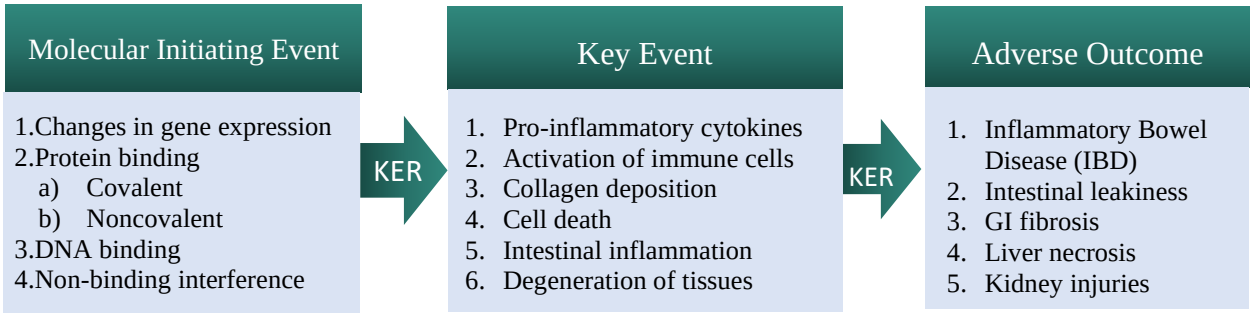

Figure 2.3 Example of adverse outcome pathway (AOP)

2.5. Knowledge Gaps

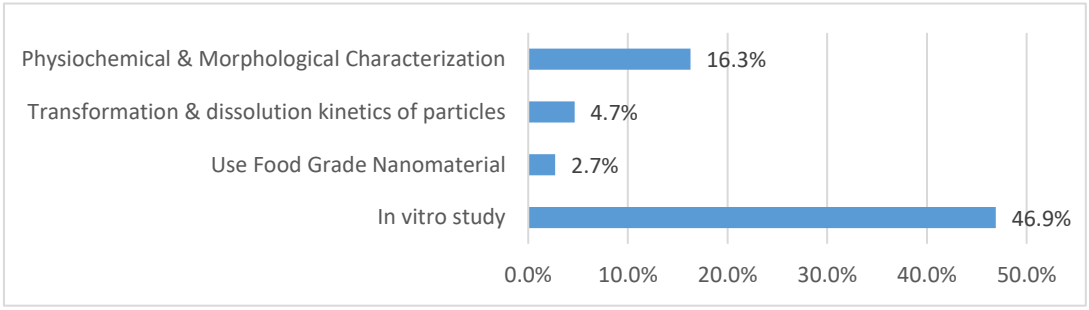

Figure 2.4 Literature screening results for knowledge gaps.

A bibliometric search was performed in January 2018 (updated in April 2020 and February 2022) with three databases, including PubMed, Web of Science, and Scopus using the Boolean operators "(food OR dietary OR ingested OR oral) AND nanoparticle AND (gut OR gastrointestinal OR intestine) AND (toxicity OR toxic)". A total of 1043 peer-reviewed publications were identified, and 258 were primary research papers focusing on human toxicological effects, which were deemed relevant studies. Out of the relevant studies, almost half of the tests are *in vivo* animal studies, and 16.3% of the papers have conducted proper characterization for NPs (Figure *2.4*). Only 2.7% of the studies used food-grade NPs, suggesting a significant knowledge gap in picturing

the actual exposure scenario of dietary NPs.[145, 146] In addition, very few of the published papers studied the dissolution kinetics of the NPs in the gastrointestinal system, indicating a lack of transformation of NPs in the GI tract during metabolism.

Another knowledge gap identified is that most studies focused on single adverse endpoints in response to NP exposure. As mentioned in previous sections, these measurable adverse effects were well documented to be related to each other either by causal relationship or by sharing common signaling pathways and metabolisms.[98, 147, 148] Furthermore, these adverse effects are all well evidenced to be factors in GI disease progression.[149-152] Hypothetically, there could be a potential relationship between the exposure to NPs from dietary sources to onset or early triggers of gastrointestinal disorders. Yet, there is no systematic study to justify the validity of such relationships in a logically causal manner.

As a result, a more comprehensive and predictive analytical study is needed to assess the potential toxic properties of ingested NPs in the GI tract. The AOP approach facilitates the organization of the sequence of adverse effects from the molecular level to the organism level, so that conducting *in vitro* assays evaluating molecular or cellular effects can be used to predict the hazards of exposure in the disease progression of GI disorders.

Preface to Chapter 3

From the literature review, I understood the importance of identifying molecular level perturbations in the adverse outcome approach. Chapter 3 presents the study of transcriptomic changes using RNA sequencing for two intestinal cell models (Caco-2 and HIEC-6) after exposure to a reference library of common dietary nanomaterials of various concentrations. From this study, lists of differentially expressed genes, perturbed biological pathways, and transcriptomic point of departure (tPODs) values were identified. This work lays many important foundations. First, it provides mechanistic insights into how these NPs may perturb intestinal cells. It achieves this by taking a transcriptomic approach in which 989 hallmark genes are studied (from the L-1000 project), as well as a comparative approach that entails studying multiple cell lines (n=2), NPs and forms (n=9), and concentrations (n=11). The results emphasize the importance of chemical-specific and size-dependent responses. Second, the work demonstrates the potential of a novel high-throughput toxicogenomic testing platform that derives tPOD values that are gaining regulatory interest.

This chapter is authored by the candidate and coauthored by Dr. Krittika Mittal, Jessica Ewald, and Qiagen specialists Dr. Samuel J. Rulli and Jennifer Jakubowski and the candidate's supervisors Dr. Niladri Basu and Dr. Saji George. The study design was developed by the candidate, along with supervisors and collaborators at Qiagen. The candidate and Dr. Mittal shared the responsibility of performing all the experiments. In addition to performing the laboratory research, the candidate led the statistical analysis, interpretation of the data, discussion of the results, and preparation of the manuscript, with the help of Dr. Mittal and Jessica Ewald and was advised by

the candidate's supervisor Dr. Niladri Basu. The manuscript has been submitted to *Food and Chemical Toxicology* in June 2022.

Chapter 3

3. Transcriptomic point of departure calculated from human intestinal lines exposed to dietary nanoparticles

3.1. Abstract

Use of nanoparticles (NPs) in the food industry raises health concerns particularly in the gastrointestinal system. Assessing dietary NPs remains challenged due the vast number of products and the resource-intensive nature of traditional toxicity testing. Recent advancements in high-throughput transcriptomics, coupled with benchmark dose (BMD) analysis are poised to modernize chemical safety assessments. The objective of this study was to derive transcriptomic point of departure (tPOD) values for common dietary NPs through dose-response analysis of 3' RNA-sequencing data. Two intestinal cell lines (Caco-2, HIEC-6) were exposed to 9 forms of Ag, SiO_2, and TiO_2, and expression of L1000 landmark genes was characterized. In Caco-2 cells, $tPOD_{mode}$ concentrations were 0.4-0.6, 21-32, and 17-59ppm for NPs of Ag, SiO_2, and TiO_2, respectively; in HIEC-6 cells, the respective tPOD values were 6-7, 7-9, and 3-13ppm. Pathway BMDs across cases identified, for example, osteoclast and Th1/Th2 cell differentiation, and cell cycle, signaling, and senescence pathways. In all cases, the tPOD and pathway BMD values were lower than concentrations associated with cellular changes These results demonstrate that transcriptomics dose-response analysis using *in vitro* models can help to increase understanding of a NP's mechanisms of action and derive quantitative information for dietary risk assessment purposes.

3.2. Introduction

Nanoparticles (NPs) are commonly used to improve food quality attributes such as taste, appearance, and shelf life.[1] However, with increasing use of NPs in the food industry, concerns are growing about potential human exposures to NPs and associated health risks.[2, 3] Once ingested, food products can release NPs [4, 5] into the gastrointestinal environment.[6] Previous *in vitro* studies have reported that non-food grade (NFG) titanium dioxide (TiO_2) NPs [7] and silver (Ag) NPs[8] may impair the function of apical intestinal epithelial cells. Further, a limited number of studies have also demonstrated that such NPs, including food grade (FG) particles, may cause inflammatory changes and oxidative stress to intestinal cells.[9-11]

The rapid growth in consumer products containing NPs poses a dilemma for regulatory risk assessment. For example, in 2005 the Consumer Products Inventory (CPI) identified 54 commercial products containing NPs, and this increased to 1,814 by the year 2013 with 119 of these products falling in the 'food and beverage' category.[12] In a different nanotechnology products database (StatNano), the number of commercial products totaled 9,562 in 2021, including 363 products in the food sector.[13] Evaluating the potential toxicity of a chemical product using traditional approaches is a resource intensive activity that can take several years, require thousands of animals, and cost millions of dollars.[14] Given the inefficiencies and ethical concerns with traditional testing approaches, regulatory agencies, the scientific community, and stakeholder groups are moving towards the development and validation of alternative, mechanism-based approaches to support risk assessments.[15]

Under the banner of New Approach Methods (NAMs), there is increasing interest in the potential for toxicogenomic-based approaches to help modernize chemical product safety assessments.[16, 17] First, transcriptomic analysis using RNA sequencing (RNA-seq) is a powerful tool that can be used to characterize the expression of thousands of genes simultaneously.[18, 19] Second, gene panels of ~1,000-3,000 targets (e.g., S1500+ by the US National Toxicology Program [20], T1000 by the Basu group [21], or L1000 by the Broad Institute [22]) have been developed to enable researchers to study a much larger biological space compared to traditional approaches (e.g., LC50 studies that focus on few apical measures, or even qPCR studies of a few genes) while reducing costs and maintaining focus (compared to whole transcriptome screening). Third, papers published in recent years have demonstrated that the benchmark dose (BMD) concentrations derived from chronic animal bioassays, that regulators and risk assessors depend upon and trust, correlate well with transcriptomic point of departure (tPOD) concentrations calculated from short-term animal [23, 24] and *in vitro*[25] studies. The convergence of these transcriptomic advances are now being applied to studies of industrial chemicals like PFOS (perfluorooctane sulfonate) [26], benzo[*a*]pyrene [27], and mercury [25], though to our knowledge these approaches have yet to be applied to the investigation of NPs in the food industry.

The overall objective of this study was to derive tPOD values for common NPs used in the food industry. In doing so, these tPODs can help increase understanding of a NP's mechanism of action and to derive quantitative dose-response relationships for dietary risk assessment purposes. The objective was addressed through a comparative study involving two intestinal cell lines; human colon adenocarcinoma cell (Caco-2) and human intestinal epithelial cell (HIEC-6), which are common *in vitro* models for enterocyte and crypt cell function, respectively.[28] These two cell lines

were exposed to a reference library of nine different forms of Ag, SiO_2, and TiO_2 including FG and NFG particles as well as NPs and microparticles (MPs), and cellular transcriptomic responses were queried through the characterization of the L1000 "landmark genes". Through this study design we were also able to investigate molecular effects associated with NP surface chemistry by comparing responses between positively charged polyethyleneimine (PEI)-AgNP and negatively charged Citrate-AgNPs, and the effects associated with particle size by comparing responses between MPs and NPs of SiO_2 and TiO_2.

3.3. Materials and Methods

3.3.1. Materials

Table 3.1 Key information concerning the reference library of particles tested in this study. FG = Food Grade, NFG = Non-Food Grade, MP = microparticle, NP = nanoparticle

Particles		**Supplier**	**Catalog #**	**Lot #**	**Purity**	**Concentration range** (ppm)
SiO_2	FG MP	Evonik Industries	SIPERNAT 22	316120711	97%	0.005, 0.01, 0.05, 0.1, 0.5, 1, 5, 10, 50, 100
	FG NP	Evonik Industries	AEROSIL 200F	135040620	99.8%	
	NFG NP	Sigma	637238	MKBV0453V	99.5%	
TiO_2	FG MP	Pure Organics	NA	NA	NA	
	FG NP	CNMI Industry Cooperation	A020-II	285821	99%	
	NFG NP	Sigma	634662	NA	99.5%	
Ag	Citrate-AgNP	Synthesized in lab				
	PEI-AgNP	Synthesized in lab				
Positive Control	$AgNO_3$	Sigma	209139	MKCK055	99%	0.781, 1.56, 3.13, 6.25, 12.5, 25, 50

The test chemicals were previously detailed[11] and summarized Table 3.1. In brief, SiO_2-FG-NPs and -MPs were purchased from Evonik Industries (Essen, Germany). TiO_2-FG-NPs were acquired from CNMI industry cooperation (Beijing, China), and -MPs were obtained from Pure Organic™ (Toronto, Canada). SiO_2-NFG-NPs and TiO_2-NFG-NPs were purchased from Sigma-Aldrich (St. Louis, USA). Citrate-coated AgNPs were synthesized in the lab based on a past study with minor modifications.[29] Briefly, 1 mM silver nitrate ($AgNO_3$) and 10 mM trisodium citrate solution were dissolved in Millipore type-1 ultrapure water (Millipore Sigma), and mixed at a 2:1 v:v ratio for 3 hours (h) in a 70 °C water bath. The resulting product solution (green-yellow in color) was eluted twice with water for 30 minutes (min) at 16,000 g (Eppendorf 5430R refrigerated centrifuge, Eppendorf Canada, Ontario, Canada) and resuspended in water for use. PEI-coated AgNPs were prepared using a modified light-assisted synthesis method.[30] Briefly, 1% w/v $AgNO_3$ and 1% w/v branched-PEI solution were first dissolved in water and mixed at a 2:1 ratio. The tube containing the mixture was then covered with aluminum foil and sonicated for 30 min. Next, the mixture was exposed directly to a light source (120 V, 160 W) for 4 min until the color of the solution turned amber red. The product solution was washed twice with water for 30 min at 16,000 g (Eppendorf 5430R) and resuspended in water for use.

3.3.2. Cell culture

Caco-2 cells were purchased from ATCC (ATCC, Virginia, USA), and cells from passage 6 were used. Cells were seeded in 100 mm petri dishes (Thermo Fisher Scientific, New York, USA) and supplemented with 10 mL of complete culture media that contained Gibco Dulbecco's Modified Eagle Medium (DMEM) (Thermo Fisher Scientific), 10% fetal bovine serum (FBS) (WISENT, Quebec, Canada), and 1% Penicillin-Streptavidin (PEN-STREP). HIEC-6 cells were purchased

from ATCC, and cells from passage 6 were used. The cells were cultured in 100 mm petri dishes supplemented with 10 mL media that contained OptiMEM 1 Reduced Serum Medium (Thermo Fisher Scientific), 4% fetal FBS (WISENT), 1% PEN-STREP (WISENT) 20 mM HEPES (Thermo Fisher Scientific), 10 mM GlutaMAX (Thermo Fisher Scientific), and 10 ng/mL Epidermal Growth Factor (EGF) (Thermo Fisher Scientific). Both cell lines were maintained in a CO_2 incubator (Caron Oasis™ Benchtop IR CO_2 Incubator, VWR, Canada) at 37 °C and 5% CO_2 with 95% humidity, and the media was changed every two days. Upon reaching 90% confluency, cells were harvested using 0.25% Trypsin/EDTA (WISENT) and sub-cultured or seeded for subsequent experiments.

3.3.3. Particle exposure and cell lysis

On day 1, both cell lines were seeded at a density of 1,000 cells per well in 96 well plates (volume 100 µL) and incubated overnight. Two wells were left empty for reference RNA controls (Human XpressRef Universal Total RNA, QIAGEN). On day 2, the culture media was aspirated from each well and replaced with prepared particle suspensions (see Table 3.1 for the 9 different forms of tested Ag, SiO_2, and TiO_2) that were constituted in sera-free media. For the NPs exposures, 10 concentrations of each particle were tested, ranging from 0.005 to 100 ppm (Table 3.1). Cells incubated in sera-free media without particles were considered as negative controls (7 wells per plate). Three plate replicates were performed for each cell model and each of the studied particles.

Following a 24 h exposure period, cells were lysed (QIAseq UPX cell lysis kit, QIAGEN). Briefly, the exposure media was aspirated, the cells were washed 3 times with phosphate-buffered saline (PBS) and then lysed with a premix containing cell lysis buffer, RNase inhibitor, and nuclease-

free water, while incubated on ice for 15 min with gentle shaking. The plates were then stored in a -80 ºC freezer until library preparation.

3.3.4. Library preparation and RNA sequencing

3.3.4.1. Reverse Transcription (RT) and single primer extension

Reverse transcription, single primer extension, and PCR amplification were carried out with the QIAseq UPX 3' targeted RNA panel kit catalog number 333041 / CSHS-10608Z-990 (QIAGEN, Frederick, MD, USA) following the manufacturer's protocol. This particular kit (L1000) was designed to measure 989 genes representative of the entire transcriptome.[22] Each transcript in each well of the RT plate was labeled with a unique molecular index (UMI) for each cDNA molecule, and samples in a given microplate well were labeled with a cell ID. Briefly, the cell lysate (3 µL) was transferred to its corresponding well in the reverse transcription (RT) plate and combined with 2 µL RT premix (containing RT buffer, EZ reverse transcriptase, and nuclease-free water). The RT plate was then incubated in the Biorad CFX96 Touch Real-Time PCR Detection System (Biorad, Hercules, CA, USA) at 25 ℃ for 5 minutes (min), 42 ℃ for 1 h, 95 ℃ for 5 min, and finally an infinite 4 ℃ incubation. Next, the cDNA generated from 94 wells of each RT plate was pooled into respective microcentrifuge tubes (6 plates into 6 tubes). Two wells containing the XpressRef genes from all 6 plates were combined into 1 tube (12 wells into 1 tube). The combined products in the 7 tubes were isolated using magnetic beads and eluted twice with water.

Following reverse transcription, a single primer extension step was performed. The product from the previous step (10 µL) was added to the premix (30 µL) containing HotStarTaq DNA polymerase, UPX AMP Primer, UPX 3' targeted panel pool (L1000), SPE buffer, and water. The

mixture was incubated in the Biorad CFX96 thermocycler with a 2-step cycling protocol (95°C for 15s and 68°C for 10 min) for 10 cycles. After a final holding step at 72°C for 5 min, the products were cooled to 4°C and washed with the magnetic beads.

3.3.4.2. PCR amplification and indexing

A universal PCR step was conducted by mixing the product from the single primer extension (1 μL) with 24 μL PCR premix that contained HotStarTaq DNA polymerase, UPX 3' targeted index, UPX3' uPCR buffer, and water. The PCR products for each plate were combined into a single library. The mixture was incubated in the Biorad CFX96 thermocycler with a 2-step cycling protocol (95°C for 15s and 65°C for 2 min). After 18 cycles, the products were cooled to 4°C. A magnetic bead step was used to concentrate and enrich for the library. Next library quality control assays were performed with the seven prepared libraries and subsequently sequenced on an Illumina NextSeq500.

3.3.5. Data Analysis

First, raw data was demultiplexed according to the various indexes used (i.e., cell ID and UMI) by the GeneGlobe analysis hub (https://geneglobe.qiagen.com/) to yield UMI count matrices. Next, basic features of the transcriptomic analysis were characterized (e.g., reads per sample), and then differences in raw counts across cell lines, chemicals, and test concentrations were characterized using PCA in the R software and Bioconductor packages.[31] The counts were then submitted to FastBMD (https://www.fastbmd.ca/FastBMD/) to identify lists of gene BMDs and to calculate the transcriptomic point of departure (tPOD) and pathway BMD values. The data uploaded to FastBMD were summarized by the sum without filtering for low variance and low abundance due

to the limited number of genes in the L1000 panel. The counts were transformed by log2-counts per million (log-CPM), and differential expression analysis of each concentration group versus control was performed with the limma R package to filter out genes that did not respond to NP exposure. Genes were kept if the false discovery rate (FDR) was <0.05, and the abs(log2FC) was >1 for at least one concentration versus control comparison. Curve fitting was performed on the differentially expressed genes (DEGs) with all models except for Poly3 and Poly4, and models were kept that passed the lack-of-fit p-value threshold of 0.1. A BMR factor of 1 was used to calculate gene BMDs from the fitted curves. Enrichment analysis using Gene Ontology (GO) and KEGG pathways were performed using the clusterProfiler package in R software (ver.4.0).[32] The statistical significance threshold for all enrichment analyses was FDR < 0.05. All figures were plotted with the R software (R v4.1.2, RStudio, v2021.09.02).

3.4. Results and Discussion

3.4.1. Transcriptome characterization of all samples

Sequencing reads information is summarized in Table 3.5. In brief, the raw reads per sample ranged from 63.8-85.8 million for HIEC-6 and 50.0-65.4 million for Caco-2, and 80-83% of these were mapped to gene IDs for downstream analysis. In total, 989 genes were measured across all samples from both cell lines. Of the measured genes, 60.4% of HIEC-6 cells and 58.3% of Caco-2 cells have counts over 100, and about 9.4% of HIEC-6 cells and 4.9% of Caco-2 cells had counts over 1000.

To help increase understanding of the biological differences and similarities between the two cell lines, we compared the lists of expressed genes between the control samples (Figure 3.5A). More

than 91% of the genes (903 out of 989) were commonly expressed in both cell lines. The correlation of expressed genes between the two cell lines in the control samples had a moderate to a strong relationship (R=0.68; Figure 3.5B). Pathway enrichment analysis of the genes unique to control samples from each cell line identified one signaling pathway involved in immune responses as being unique to the Caco-2 cells (T cell receptor pathway), and one pathway involved in cancer being unique to the HIEC-6 cells (Table 3.6).

Next, we examined transcriptomic variation across the entire dataset (i.e., 10 concentrations tested of nine chemicals in both cell lines) through PCA plots. Across the top 4 components, there were no particle-associated discrete clusters in either cell line (Figure 3.6). Though, at higher concentrations of exposure, PEI-AgNPs and $AgNO_3$ showed some separation in the PCA plots of Caco-2 cells (Figure 3.6A). Similarly in HIEC-6 cells, at higher concentrations of exposure there was some separation of samples exposed to PEI-AgNPs and $AgNO_3$ along with Citrate-AgNP and SiO_2 NPs (Figure 3.6B).

3.4.2. Comparison of Differentially Expressed Genes (DEGs)

We purposefully used $AgNO_3$ as a positive control based on the cytotoxicity data in our published study (Chapter 4).[11] In the current study, this chemical induced expression of several hundred genes in both cell lines (Table 3.2), and these genes enriched pathways concerning cellular responses to external stress, oxidative stress, and cell cycle regulation (Table 3.7). The affected biological pathways were identified in a previous study of $AgNO_3$ in Caco-2 cells [33], as well as in a review of data for $AgNO_3$ in the Comparative Toxicogenomics Database (ctdbase.org). Although the total number of DEGs following $AgNO_3$ treatment in HIEC-6 cells was lower than measured

in Caco-2 cells, there was overlap in the enriched pathways (Figure 3.1) as well as similarity between the tPOD results as discussed further below (Table 3.2). We also note that GO (Biological Processes) enrichment analysis of the top 50 DEGs (Table 3.7) following $AgNO_3$ exposure in Caco-2 cells returns "programmed cell death" and "regulation of apoptotic processes" (versus "response to hormone stimulus and "DNA replication initiation" in the HIEC-6 cells) thus suggesting possible inter-cell line sensitivities.

Table 3.2. Summary of the number of differentially expressed genes (DEGs) and transcriptomic point of departure (tPODs) in both cells exposed to the reference library of particles

Cell	Caco-2					HIEC-6				
Particle	# of DEGs	# of Gene BMDs	tPODs (ppm)			# of DEGs	# of Gene BMDs	tPODs (ppm)		
			20th gene	**Mode**	**10th percentile**			**20th gene**	**Mode**	**10th percentile**
SiO_2-FG-micro	4	4	NA	3.99	0.93	11	9	NA	17.92	9.94
SiO_2-FG-nano	50	50	26.91	31.56	22.95	427	425	1.74	7.15	3.59
SiO_2-NFG-nano	261	261	6.91	20.72	11.07	308	306	1.91	8.71	4.96
TiO_2-FG-micro	4	4	NA	35.52	34.66	10	10	NA	4.3	2.5
TiO_2-FG-nano	5	5	NA	58.85	10.48	4	4	NA	13.18	12.02
TiO_2-NFG-nano	5	4	NA	16.98	10.02	8	7	NA	3.37	0.67
Citrate-AgNP	187	183	1.32	0.66	0.8	380	378	1.89	6.28	3.33
PEI-AgNP	217	216	0.9	0.42	0.54	537	537	1.59	7.02	3.88
$AgNO_3$	604	601	1.79	7.33	3.4	187	186	2.96	4.13	3.15

In general, more DEGs were found in HIEC-6 cells *vs*. Caco-2 cells for a given treatment group though overall patterns were similar (Table 3.2; Table 3.7-Table 3.9). The most and least DEGs were found in cells exposed to Ag and TiO_2 compounds, respectively. Within the Ag group, we observed slight differences according to surface charge. Specifically, in both cell lines, positively charged PEI-AgNP induced more DEGs than the negatively charged Citrate-AgNP. For SiO_2 particles, we observed that the number of DEGs varied according to particle size, with more DEGs (i.e., 12-65x more) in cells exposed to the NP *vs.* the MP forms. Within the TiO_2 group, relatively

few (i.e., 3-10) DEGs were found, and no common or unique patterns of expression dependent on particle size and crystal form were identified (Table 3.9).

3.4.3. Pathway enrichment analysis

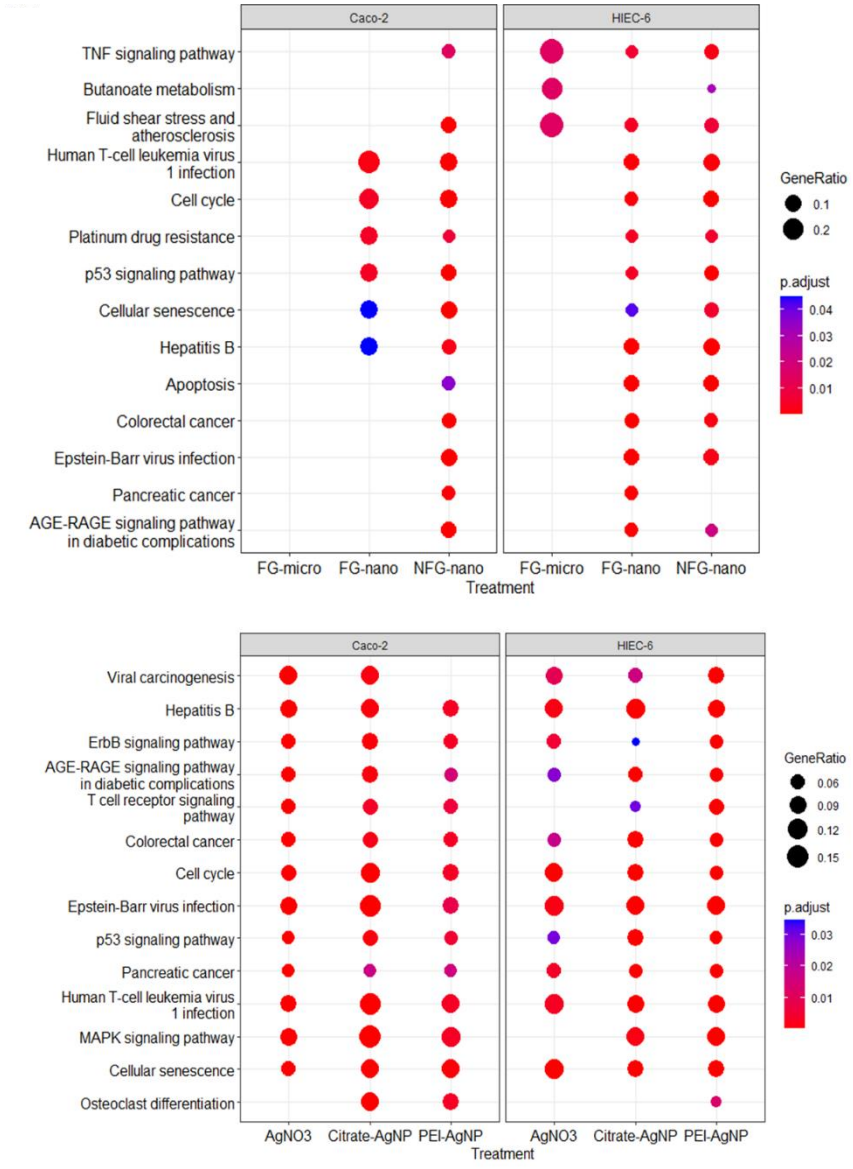

Figure 3.1 Clustered KEGG pathway enrichment analysis comparing transcriptomic responses between Caco-2 (left side) and HIEC-6 (right side) cells following exposure to: A (top panel) SiO_2 particles; and B (bottom panel) Ag compounds. The size of the dots represents a gene ratio, which is the percentage of identified genes for the given KEGG pathway based on the input DEG list. The colors of the dots correspond to the false discovery rate (FDR) adjusted p-value based on the Benjamini-Hochberg method.

To further investigate differences between (and within) the particle groups and the two cell lines, we performed enrichment analysis on the DEG lists. We excluded TiO_2 owing to the limited transcriptomic changes measured, and thus focused this analysis on SiO_2 and AgNPs (Figure 3.1;Table 3.10).

Compared to their nano counterparts, fewer pathways were affected by SiO_2 MPs in both cells lines (Figure 3.1A). This observation aligns with the relatively lower toxicity than NPs in the published study, where no phenotypic changes were observed in Caco-2 cells exposed to both SiO_2 and TiO_2.[11] For SiO_2 NPs, signaling and cell cycle pathways were commonly expressed across the two forms of particles studied, while cancer and apoptosis pathways were uniquely induced by the NFG-NP form. Fewer pathways were identified in Caco-2 cells exposed to SiO_2 FG-NPs versus NFG-NPs, which aligned with our published study which also demonstrated fewer apical changes in the SiO_2 FG-NPs treated cells versus those exposed to NFG-NPs.[11] However, in HIEC-6 cells the responses between the two SiO_2 NPs seemed similar.

For AgNPs, the identified pathways were similar between both cell lines and among the different particle exposure groups (Figure 3.1B). In addition, the identified pathways in the NP groups were in good agreement with data from the $AgNO_3$ exposed cells, suggesting a close relationship between the mechanisms in which Ag^+ ion and AgNP exert adverse effects. Previous studies have reported that AgNPs taken up by cells are localized in lysosomes, where Ag^+ ions can be released from the AgNPs due to the acidic lysosomal environment.[34, 35] According to the proton sponge theory, the intracellular dissolution of Ag^+ ions causes excess chloride influx leading to osmotic swelling, lysosome rupture, and downstream responses such as reactive oxygen species (ROS) production.[36, 37] In our published work, we identified lysosome acidification and ROS generation

in cells treated with PEI-AgNP and $AgNO_3$.[11] Such observations on Ag-mediated cellular responses largely aligned with the transcriptomic changes observed in this study and elsewhere [38-41] in which pathways associated with oxidative stress, inflammation, and immune response are overrepresented.

3.4.4. Transcriptomic benchmark dose-response analysis

3.4.4.1. Caco-2 cells

Curve fitting resulted in gene BMDs for nearly all of the DEGs, and from this tPOD values were calculated that ranged from 0.4 to 59 ppm (Table 3.2). Across all the treatment groups, the $tPOD_{10th\ percentile}$ values were less than the $tPOD_{mode}$ values by an overall factor of 2. Based on the tPOD values, the TiO_2 exposed cells were least responsive (e.g., $tPOD_{mode}$ was 17 to 59 ppm). While we express caution with this observation as there were few DEGs, such a result may be expected as few biochemical and cellular effects were observed in a published study where the same TiO_2 particles were tested under similar conditions.[11] AgNP exposed cells had the lowest tPOD values ($tPOD_{mode}$ was 0.4 to 0.7 ppm), about 30-80x lower than the tPOD values of SiO_2 NPs treated cells ($tPOD_{mode}$ was 21 to 32 ppm) (Figure 3.2A). In general, there was little overlap across the treatment groups in terms of identified DEGs from which gene BMDs were calculated based on the upset plot results (Figure 3.2B). Caco-2 cells exposed to SiO_2-NFG-nano had the highest number of unique gene BMDs, followed by cells exposed to PEI-AgNP and Citrate-AgNP. For both SiO_2 NP treated cells, gene BMD values spanned a test concentration that ranged between 10 and 100ppm (Figure 3.2C). The gene BMD values for both types of AgNP treated cells were similar in distribution and centered around 1 ppm (Figure 3.2D).

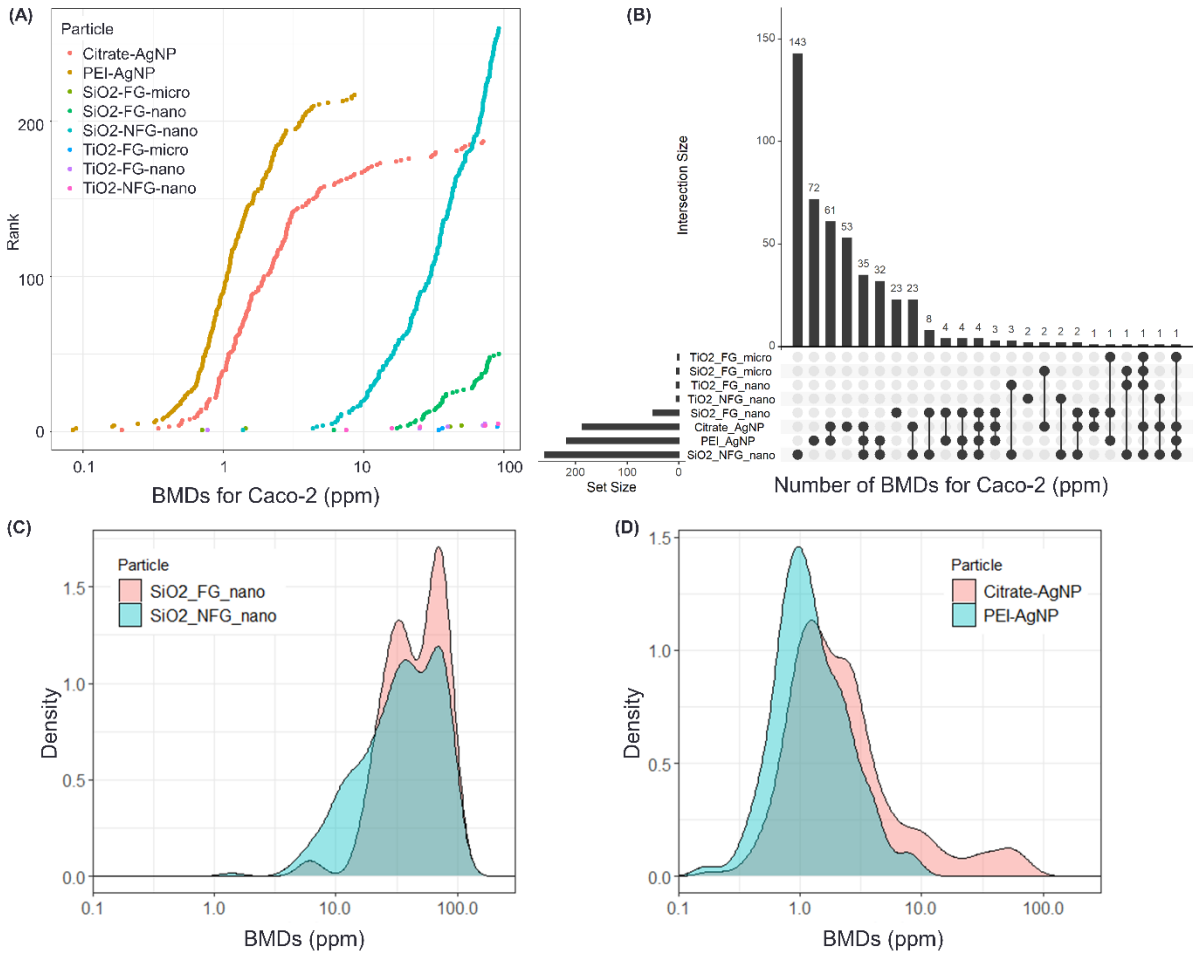

Figure 3.2 Summary of transcriptomic benchmark dose (BMD) responses in Caco-2 cells exposed to the chemical particles studied. A) Gene-level accumulation plot following exposure to the nine different chemical particles; B) Upset plot showing the number of BMDs commonly found across the different test chemicals; Density plots of gene BMDs for: C) SiO_2 nanoparticles, and D) Ag nanoparticles.

In addition to the gene-level BMD analysis, we performed pathway-level BMD analysis to help increase understanding of a particle's mechanism of action in Caco-2 cells. No biological pathway was significantly enriched using our *a priori* statistical plan (i.e., adjusted *p*-value < 0.05), and this was possibly due to the size of the gene set. Hence, to further explore this dataset, we relaxed the threshold to consider pathways with an unadjusted *p*-value < 0.05 and present these results with caution. The enriched pathways for TiO_2 treated cells are reserved for the supplemental materials

(Table 3.11) due to the low number of hits (n=2) and the relatively low percentage pathway coverage (< 10%).

Similar to the gene BMD data, the pathway BMDs for AgNP treated cells (i.e., most sensitive pathway BMDs were 1 to 2 ppm; Table 3.3) were lower than those for SiO_2 treated cells (i.e., most sensitive pathway BMDs were 14 to 27 ppm; Table 3.3) and TiO_2 treated cells (Table 3.11). Osteoclast differentiation was the only pathway common between cells treated with both AgNP types. This pathway contains genes responsible for pro-inflammatory cytokines such as TNF-α and IL-1, and signaling pathways such as NF-κB; these are all molecules that we have found to be affected by AgNPs in a published study.[11]

Table 3.3. Enriched KEGG Pathway in Caco-2 cells with pathway BMD identified due to the treatment of AgNP and SiO_2 particles. The enriched pathways for TiO_2 are listed in Table 3.11.

Sample	Name of pathway	Pathway BMD (ppm)	*p*-value	Adjusted *p*-value	Percentage pathway	Number of hits
PEI-AgNP	Osteoclast differentiation	1.08	0.014	0.927	45.5%	10
Citrate-AgNP	Osteoclast differentiation	2.23	0.001	0.152	47.8%	11
	Th1 and Th2 cell differentiation	2.90	0.029	0.778	41.2%	7
SiO_2-FG-NP	HTLV-I infection	26.69	0.013	0.919	13.7%	7
	Platinum drug resistance	50.86	0.020	0.919	19.0%	4
	Necroptosis	53.72	0.037	0.919	16%	4
SiO_2-NFG-NP	p53 signaling pathway	14.41	0.015	0.403	48.1%	13
	cGMP-PKG signaling pathway	16.84	0.031	0.403	50.0%	9
	Cell cycle	20.92	0.001	0.072	51.2%	21
	HTLV-I infection	21.20	0.023	0.4039	40.8%	20
	Cellular senescence	28.94	0.030	0.403	40.9%	18
	B cell receptor signaling pathway	29.7	0.020	0.403	52.9%	9
	HIF-1 signaling pathway	32.70	0.026	0.403	47.8%	11
	NF-kappa B signaling pathway	40.13	0.002	0.094	60.0%	12

For SiO_2, the identified pathways were focused on stress responses, cell cycle and signaling pathway (Table 3.10). HTLV-1 infection was the pathway commonly shared between NP exposed

cells (Table 3.3), and TNF-α is a critical initiating factor in this pathway.[11] We note that the lowest pathway BMD for SiO_2-NFG-NP was associated with p53 signaling (14.4 ppm), and that cell cycle (20.9 ppm) and cellular senescence (28.9 ppm) were induced at higher concentrations of SiO_2 exposure. For FG-NP, HTLV-I infection pathway had the lowest BMD (21.2 ppm), and this value was close to the BMD for the same pathway in NFG-NP (26.7 ppm). Together, these differences in pathway BMD values make temporal sense as cell cycle changes and cellular senescence are the consequences of p53 signaling pathway activation.[40, 42] Further, cellular senescence can be a precursor of pro-inflammatory responses like NF-κB signaling pathway activation, and so it is not surprising that the pathway BMD value for NF-κB signaling pathway (40.1 ppm) was relatively high.[43] NF-κB signaling can ultimately initiate downstream immune responses, inflammation, and oxidative stress.[38, 39] In the published work with Caco-2 cells (Table 3.12), we identified that NP exposure significantly enhanced ROS generation as well as pro-inflammatory cytokine release of IL-8 (18-20 fold by AgNPs, 5-11 fold by SiO_2 and TiO_2) and TNF-α (2-4 fold by AgNPs and SiO_2).[11] The increased release of IL-8 and TNF-α was closely related to NF-κB activation, which can induce the expression of genes of various pro-inflammatory cytokines and chemokines (including TNF-α and IL-8).[44, 45] Taken together, the findings suggest mechanisms by which the studied NPs can impair cellular homeostasis in Caco-2 cells and activate downstream pathways leading to adverse outcomes relevant to gastrointestinal health.[39-41]

3.4.4.2. HIEC-6 cells

Similar to the results for the Caco-2 cells, curve fitting of transcriptomics data from HIEC-6 cells resulted in gene BMDs for nearly all DEGs, and from this tPOD values ranging from 3.4 to 17.9 ppm were calculated for the particles studied (Table 3.2). Like with the Caco-2 cells, in HIEC-6

cells, $tPOD_{10th\ percentile}$ values were less than the $tPOD_{mode}$ values by an overall factor of 2. The tPOD values for TiO_2 exposed HIEC-6 cells (3.4 – 13.2 ppm), like with the Caco-2 cells, should again be evaluated with caution because of the low number of DEGs identified (Table 3.9). However, in contrast to our findings from the Caco-2 cells, the tPOD values from HIEC-6 cells exposed to NPs of SiO_2 ($tPOD_{mode}$ was 7.2-8.7 ppm) and Ag ($tPOD_{mode}$ was 7.2-8.7 ppm) were not different from each other (Table 3.2). Interestingly, we also note that the tPODs for the AgNP exposed HIEC-6 cells were about 10-fold higher than those calculated from the Caco-2 cells, and that this was reversed for the SiO_2 NPs in which the tPODs were higher in the HIEC-6 cells versus the Caco-2 cells.

In HIEC-6 cells, the accumulation plots show that robust gene BMDs were only found for AgNPs and SiO_2 NPs, and that the responses across all four particles were similar and in the 1 to 100 ppm range (Figure 3.3A). Based on an inspection of the upset plot, the highest number of gene BMDs were uniquely linked with exposure to PEI-AgNP, followed by common genes shared between various combinations of Ag and SiO_2 NP treated cells (Figure 3.3B). Common genes shared by different groupings of SiO_2 and AgNPs (versus the MPs) suggest that particle size is important. The distribution of gene BMDs for the two SiO_2 NPs (Figure 3.3C) and Citrate-AgNP (Figure 3.3D) were similar and centered around 10 ppm. However, the distribution of the gene BMDs for PEI-AgNP treated cells showed more of a bimodal pattern with two peaks centered at 5 ppm and 80 ppm (Figure 3.3D). Based on a published study from our group with the same reference library of particles and cell models, we observed that PEI-AgNPs induced cytotoxic effects at concentrations greater than 25 ppm.[11] Thus, the two peaks in the distribution plot (Figure 3.3D) and the two inflections in the accumulation plot (Figure 3.3A) may correspond to gene BMDs that

are linked to sub-lethal and lethal responses. The GO annotation of biological process for the gene BMDs near the two peaks (1-10 ppm and 70-90 ppm) demonstrates that genes related to mitosis, cell cycle and cell division were clustered at higher concentration, while at the lower concentration the only biological process identified was sugar transport (Table 3.13).

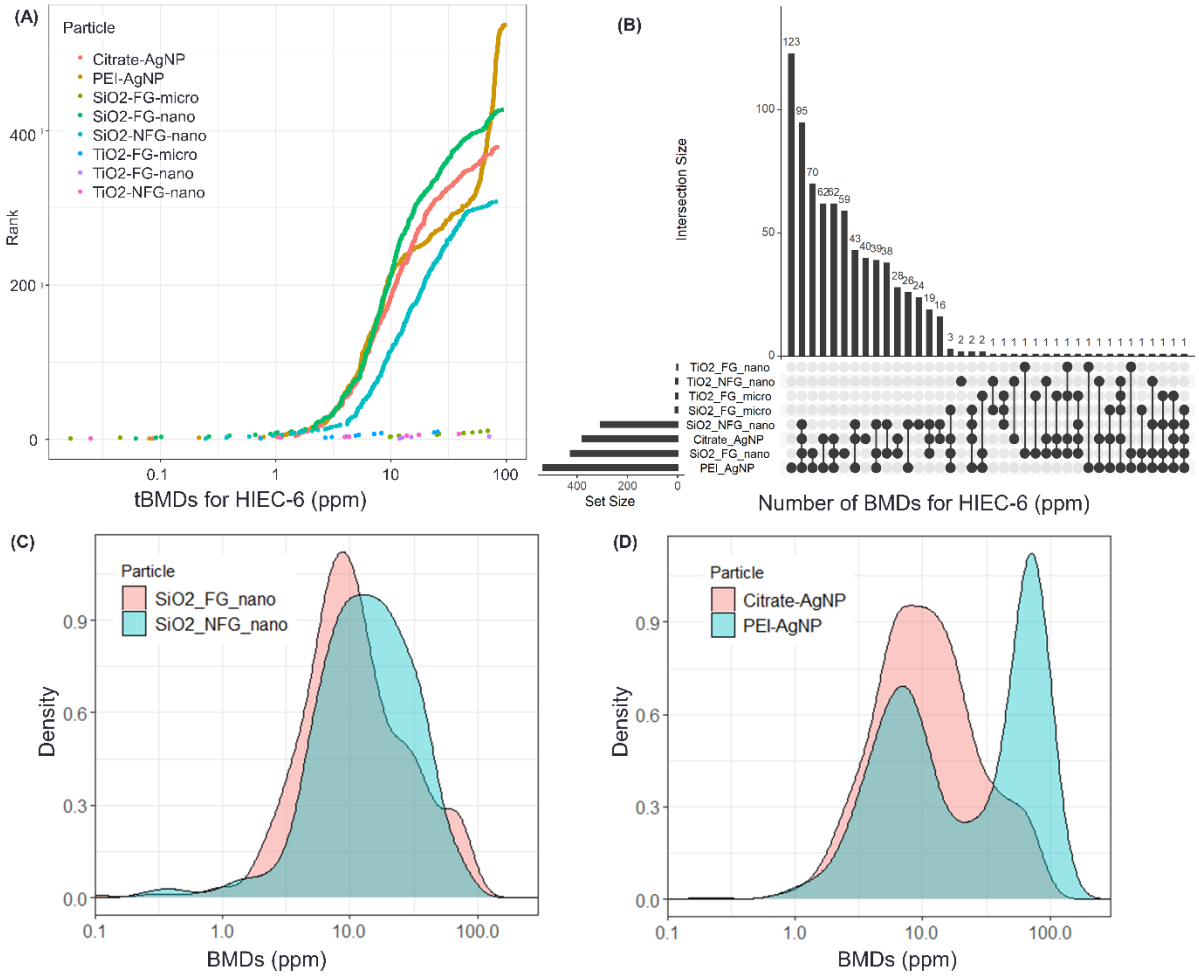

Figure 3.3 Cell specific benchmark doses (BMDs) for HIEC-6 cells displayed in density plots for exposure of (A) SiO_2 and (B) AgNP and (C)accumulation plot based on BMD value ranking. Upset plots showed differentially expressed genes (DEGs) with tPODs showing shared and unique genes between exposure treatments.

Similar to the Caco-2 cells, the pathway-level BMD results are presented cautiously (i.e., unadjusted *p*-value <0.05 was considered). Further, pathway BMD results for SiO_2 MP and TiO_2

treated cells are reserved for the supplemental materials due to the comparatively low number of hits (<5) and the relatively low percentage pathway coverage (<15 %) (Table 3.14). Similar to the gene BMD data, the pathway BMD values for the Ag and SiO_2 NPs were similar (Table 3.4). In general, identified pathways were related to activation of signaling pathways critical to stress response, inflammation, and immune regulation.[38, 40, 46, 47] The most pathway BMDs were found in the PEI-AgNP treatment group, and these were not identified in the other treatment groups. The lowest pathway BMD (10.2 ppm) for PEI-AgNP treated cells was identified as "epithelial cell signaling in Helicobacter pylori infection" pathway. Based on the pathway's description in KEGG, disruption of the apical junctional complex is one of the downstream activities in the epithelial cell signaling after Helicobacter pylori infection.[42] Previous studies have also demonstrated that apical junctional complex was regulated by the actin cytoskeleton and can be disrupted after Helicobacter pylori infection.[47, 48] In our published study, we observed the contraction of the actin filaments and formation of stress fiber bundles in cells following exposure to 25 ppm PEI-AgNP, a concentration similar to the pathway BMD for "Regulation of actin cytoskeleton" (27.4 ppm) in this study.

Table 3.4. Pathway BMD concentrations in HIEC-6 cells exposed to Ag and SiO2 NPs. The enriched pathways for SiO_2 MPs and TiO_2 are listed in Table 3.14. The 'percentage pathway' and 'number of hits' refers to the genes annotated in the L1000 gene set versus the entire transcriptome.

Sample	Name of pathway	Pathway BMD(ppm)	*p*-value	Adjusted *p*-value	Percentage pathway	Number of hits
PEI-AgNP	Epithelial cell signaling in Helicobacter pylori infection	10.19	0.035	0.588	81.3%	13
	Th1 and Th2 cell differentiation	10.23	0.035	0.588	81.3%	13
	Axon guidance	15.60	0.033	0.588	76.0%	19
	Regulation of actin cytoskeleton	27.36	0.023	0.588	75.9%	22
	T cell receptor signaling pathway	32.40	0.008	0.392	80.8%	21

	B cell receptor signaling pathway	33.99	0.002	0.222	93.3%	14
Citrate-AgNP	p53 signaling pathway	7.84	0.028	1.000	59.3%	16
FG-SiO_2-NP	Calcium signaling pathway	7.43	0.027	0.990	70.6%	12
NFG-SiO_2-NP	TNF signaling pathway	8.18	0.042	1.000	52.4%	11

3.4.5. Benchmarking tPOD and pathway BMD values

To benchmark our results, we compared the tPOD and pathway BMD values derived here with a published study of ours [11] in which we measured responses at higher biological levels (e.g., cellular ROS generation and calcium influx) following exposure of the same cell lines to the same reference library of particles (Figure 3.4). Most of the tested particles did not induce cell death at the concentrations tested, and in cases where cytotoxicity was measured, we calculated LC20 values (concentration that causes 20% cell death) (Table 3.12;Table 3.15). Microparticles of SiO_2 and TiO_2 were not compared in this discussion due to the low number of identified BMDs and absence of phenotypic responses in the published study.[11] Further, exposure of both cells to TiO_2 compounds induced few DEGs in this study, and thus the tPOD values and pathway BMDs were not considered robust enough to be compared with the cellular results. In the current and previous study, TiO_2 particles were consistently the least toxic among the ones tested.

For SiO_2 particles, cytotoxicity was only measured in Caco-2 cells exposed to SiO_2-FG-NPs in which a LC20 value of 62.8 ppm calculated. In Caco-2 cells, the tPOD and pathway BMD values were at least 2.5-fold lower than concentrations associated with cellular responses (Figure 3.4). In HIEC-6 cells, the tPOD and pathway BMD values were similar to concentrations that caused ROS generation though 6-times lower than concentrations that caused calcium flux changes.

For Ag compounds, LC20s were calculated for $AgNO_3$ (4.5 ppm) and PEI-AgNP (28.1 ppm) in Caco-2 cells, with no cytotoxic response measured for Citrate-AgNP at the concentrations tested. In HIEC-6 cells LC20 values were calculated for all three forms of Ag i.e., $AgNO_3$ (12.9 ppm), PEI-AgNP (28.1 ppm), and Citrate-AgNP (84.7 ppm). In addition to these cytotoxic responses, cellular responses were found at lower exposure ranges for both cells (Caco-2 cells = 6.25-50 ppm; HIEC-6 cells = 3.13-12.5 ppm)[11], and in general these concentrations were 5 times higher than most gene tPODs calculated in the current study (about 1 ppm) (Figure 3.4).

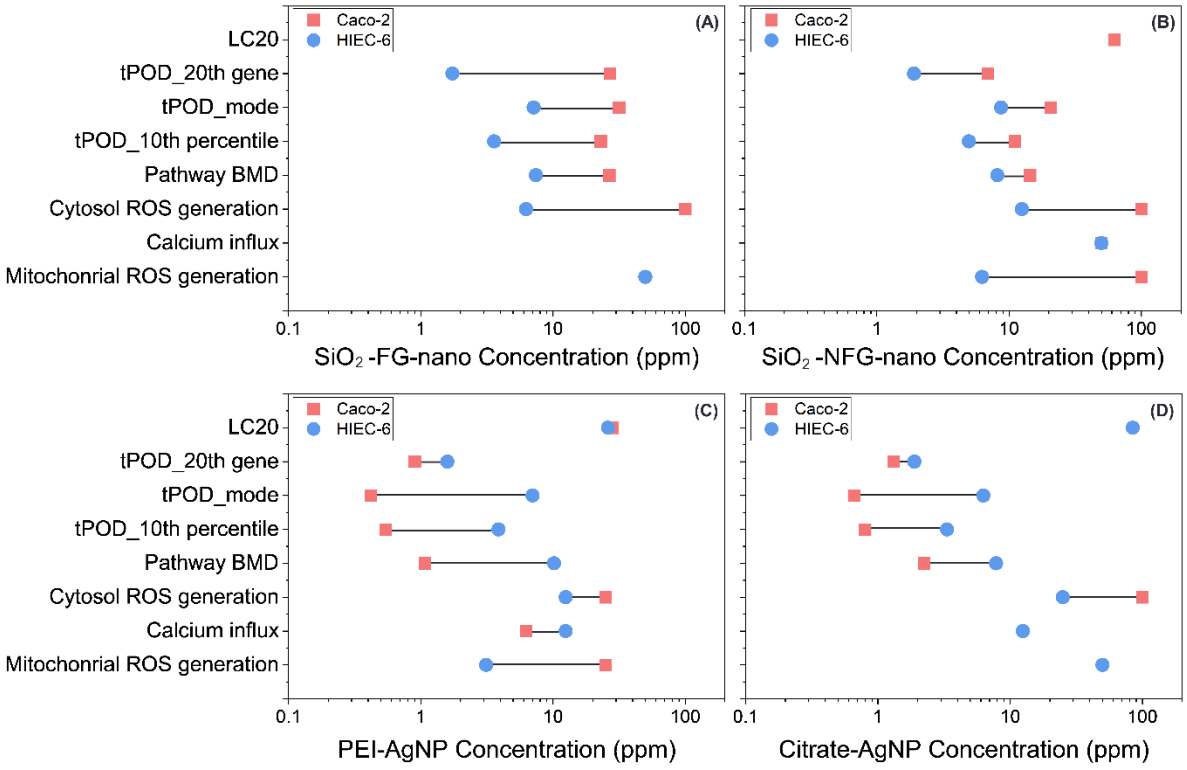

Figure 3.4 Comparison of *in vitro* t-POD, and pathway BMD values (ppm) for (A) SiO_2-FG-nano particles, (B)SiO_2-NFG-nano particles, (C)PEI-AgNP and (D) Citrate-AgNP from this study with lowest concentration of time-dependent phenotypic results of LC20 (24 h), cytosol reactive oxygen species (ROS) generation (6 h), calcium influx (10 h), and mitochondrial ROS generation (6 h) from Chapter 4. For each of the chemicals, the values are provided for both Caco-2 and HIEC-6 cells

3.5. Study Limitations

A key finding is that the tPOD and pathway BMD values were lower than concentrations associated with cellular and cytotoxic changes, though we need to remember that biological responses are time dependent. Based on the study in Chapter 4, not all biological changes could be captured optimally at 24 h in HIEC-6 cells with the generation of cytosolic and mitochondrial ROS (6 h) and calcium influx (10 h) serving as examples.[11] Here we characterized tPODs after 24 h of exposure, and it is not clear how these values (as well as the identified genes and pathways) would vary with shorter or longer exposure periods. The assumed variability likely affects the ability to properly benchmark tPOD values with other biological measures, which themselves also vary with time.

We focused our analysis on a 989 "landmark" genes (L1000)[22], and while this was to be representative of the entire transcriptome, it was a reduced gene set and some of our statistical thresholds had to be relaxed to help ensure that sufficient genes would be captured for transcriptomic dose-response modeling. While quantitative gene BMD and tPOD data were obtained that seemed to line-up with expectations (i.e., rank-order of NP potencies), there were some challenges with functional interpretation of the pathway-level results. For example, the pathways identified following exposure to SiO_2-FG-NP (HTLV-I infection and platinum drug resistance) had 7 and 4 hits respectively, and these were difficult to functionally interpret. Across all the pathway BMD analyses, none of the adjusted p-values were below the 0.05 a priori cut off.

To our knowledge there is no adequate data from human populations that could be used for benchmarking purposes, and thus we had to compare the tPOD data from the current study with a

previous *in vitro* one. However, the *in vitro* models are limited to a few types of cells which cannot represent the complicated multi-cell environment in the small intestine let alone the whole organism.[49] To improve the bio-relevancy of the results, more realistic models like *ex vivo* culture model developed from human tissue (intestinal) biopsies can be considered.[50] Also, the *in vitro* results may be converted to equivalent doses ($POD_{Bioactivity}$) through reverse dosimetry by toxicokinetic models from which bioactivity-to-exposure ratios (BER) may be derived to support risk-based ranking activities.[51]

3.6. Conclusion

To our knowledge, this study is the first to derive tPODs in intestinal cell models for dietary nanomaterials used in the food industry. In general, the calculated tPODs were lower than concentrations associated with changes in calcium channeling, oxidative stress, and membrane potential. This finding is not surprising given that stressor-mediated changes at the transcriptional level occur before responses at higher tiers of biological organization as part of a coordinated stress response used by cells to maintain homeostasis.[52] Further, the work here supports the idea that tPODs derived from *in vitro* studies may provide meaningful and rich data on a chemical's mechanism of action as well as quantitative data that may be used in risk assessments.

3.7. Supplemental Information

3.7.1. Tables

Table 3.5 The raw reads summary of the sequencing data.

Samples	**HIEC6-1**	**HIEC6-2-**	**HIEC6-3**	**Caco2-1**	**Caco2-2**	**Caco2-3**
Reads total	63802359	85815776	77784757	50033483	65399065	51571751

Reads dropped	all NNNNNN sequence	7486956	10349822	8643791	5397492	7099181	5563871
	cell id not extracted	17	19	17	7	8	5
	cell id not matching a used oligo within hamming distance 1	1785035	2359361	2005895	1362950	2136359	1344617
	less than 25 bp	0	0	0	0	0	0
	not mapped to genome	731669	958728	867067	741527	1009445	819754
	off target	721875	962346	888820	477124	622151	490869
	primer not identified at read start	180245	249096	224619	151998	195792	153964
	less than 25 bp endogenous seq after primer	345492	442976	416041	375765	541856	436974
	cell has no genes with more than 5 UMIs	39	0	123	94	16	0
Reads used	aligned to genome, multiple loci	315269	427989	385455	226153	303704	229188
	aligned to genome, unique loci	52235762	70065439	64352929	41300373	53490553	42532509
	aligned to ERCC, multiple loci	0	0	0	0	0	0
	aligned to ERCC, unique loci	0	0	0	0	0	0

Table 3.6 Enriched pathway for control samples of HIEC-6 and Caco-2 cells.

Pathway (Caco-2)	**Total**	**Expected**	**Hits**	**P.Value**	**FDR**
T cell receptor signaling pathway	101	0.261	4	0.000113	0.0359
Pathway (HIEC-6)	**Total**	**Expected**	**Hits**	**P.Value**	**FDR**
Pathways in cancer	530	1.3	7	0.000166	0.0527

Table 3.7 Top 50 differentially expressed genes (sorted by increasing gene BMD value) for Ag treated cells. NP = nanoparticle.

$AgNO_3$		**Citrate-AgNP**		**PEI-AgNP**	
Caco-2	HIEC-6	Caco-2	HIEC-6	Caco-2	HIEC-6
TFAP2A	TMEM97	PTPRF	TMEM97	FYN	MYLK
SERPINE1	CEBPD	NCK2	FAT1	PFKL	PYCR1
TSC22D3	NIPSNAP1	SQSTM1	CTNNAL1	SPP1	EPB41L2
RNMT	CD58	EPHB2	DDIT4	HSPA1A	HES1
SPDEF	ADO	PROS1	UBE2C	TXNRD1	CCDC86
CDKN1A	GFPT1	ZNF395	MYLK	EBP	HIST2H2BE
TIMM22	FCHO1	HS2ST1	ERBB2	DNTTIP2	DUSP4

EGR1	FAT1	MPC2	TSPAN4	PXMP2	WFS1
MLLT11	TP53BP2	IARS2	ARID5B	ACAT2	TSPAN4
ALAS1	FZD7	AARS	CCDC86	ME2	CEBPD
ZNF589	CAT	TSPAN6	BAG3	ILK	KLHL21
SUV39H1	SPDEF	FGFR4	MFSD10	S100A13	GNAI1
FKBP4	BRCA1	MFSD10	FZD7	ITGAE	ARID5B
ICAM1	NPDC1	TBC1D9B	CDK1	DERA	PHGDH
RAB21	KDM3A	LSR	PIK3R4	TIMM9	IARS2
HOXA5	EGF	GRB7	SMAD3	PECR	FAT1
DRAP1	PAX8	SCARB1	KLHL21	SQSTM1	PNP
PPARD	SLC25A13	DNA	DYRK3	MYC	ST3GAL5
NFKBIE	PRKCH	NENF	APOE	CXCL2	MEST
VAV3	FBXO21	LAMA3	KCTD5	Hsp40	HACD3
FOS	GNA11	NNT	ABCF1	COG2	PRSS23
STX4	ORC1	CDC25B	ATP6V0B	MRPS2	MCOLN1
MOK	PPIC	PYGL	DDR1	TSPAN3	NISCH
TBP	MFSD10	PRSS23	TEX10	PGM1	SLC27A3
E2F2	APOE	GNA11	GDPD5	TGFBR2	ACAT2
GATA2	WFS1	CLSTN1	IER3	CDCA4	HSPA1A
KLHL21	EPB41L2	DAG1	KIF20A	NCK2	MACF1
UFM1	CDCA4	MAPKAPK2	BCL2	MLLT11	JUN
KIAA0586	ETS1	MYC	NCK2	SCARB1	FBXO21
TBC1D31	PIK3C2B	PSRC1	PRSS23	HMOX1	CPNE3
PEX11A	BACE2	SENP6	IARS2	DYRK3	NNT
DFFB	SPP1	C2CD5	SLC27A3	NT5DC2	DDIT4
PIK3R3	RNPS1	MLLT11	MEST	MPC2	MBTPS1
CDK5R1	ADGRG1	PFKL	SNX7	CDK1	EXT1
NOS3	PRKCQ	IL13RA1	HACD3	USP6NL	ADP-ribose
PRKCH	POLE2	SERPINE1	TFDP1	ATF5	FZD7
PSMB8	PLS1	CDKN1A	DSG2	INPP1	HN1L
CBR1	CGRRF1	SLC11A2	EVL	CCDC85B	TMED10
ZNF586	CDC45	MBTPS1	ATF6	FAM57A	AMDHD2
PTPN6	EIF4EBP1	SYNE2	TNFRSF21	PRCP	PIK3R4
RAB27A	KIF14	ACAA1	SORBS3	MAST2	TBC1D9B
IGFBP3	EPHB2	SLC1A4	HADH	DNAJB6	CCDC85B
KCTD5	ERBB3	PRCP	KIT	ADAM10	CAT
TM9SF2	LPAR2	SLC35A3	CSK	IARS2	MFSD10
KIAA0753	KCTD5	CAT	PPIC	NRIP1	ERBB2
PAX8	JMJD6	GDPD5	IL13RA1	TBC1D9B	SMAD3
CCNE2	CCNB2	SPTAN1	MACF1	CEBPD	ATF6
ADO	ICAM1	DSG2	FASTKD5	TSPAN6	IGFBP3
DAXX	MOK	NR2F6	PXMP2	NNT	DSG2
CBR3	CCNF	Hsp40	MEF2C	GADD45B	APOE

Table 3.8 Top 50 differentially expressed genes (sorted by increasing gene BMD value) for SiO_2 particle treated cells. FG = Food Grade, NFG = Non-Food Grade, MP = microparticle, NP = nanoparticle.

SiO_2-FG-MP		**SiO_2-FG-NP**		**SiO_2-NFG-NP**	
Caco-2	HIEC-6	Caco-2	HIEC-6	Caco-2	HIEC-6
COQ8A	HMOX1	SLC25A4	EPHB2	CORO1A	EPB41L2
EDN1	KDM5A	BUB1B	MEST	RAB4A	ATP1B1
CCP110	HMGCS1	CTNNAL1	PYCR1	KCNK1	DDIT4
ST6GALNAC2	BDH1	DNA	DNA	IL1B	DYRK3
	PPP1R13B	STAMBP	ATP6V0B	DYRK3	TRIB3
	HES1	FOSL1	NNT	DNTTIP2	MFSD10
	FOS	PPP2R5A	MYLK	NFATC4	PMAIP1
	GDPD5	DSG2	KIT	BTK	APOE
	CDK5R1	PRSS23	PMAIP1	LRPAP1	HIST2H2BE
	PTGS2	CCNA2	IARS2	SYK	RASA1
	SPTLC2	MCM3	TSKU	EGF	DDR1
		MSH6	NFKBIE	GLI2	TNFRSF21
		RAE1	PSRC1	ABHD4	FOS
		TMEM2	CCDC85B	TBX2	RELB
		ATP2C1	EDN1	HTRA1	NFKBIB
		PARP1	NFKBIB	KLHL9	KLHL21
		MRPS16	ADGRG1	IGFBP3	CDK7
		PLEKHM1	HERPUD1	LOXL1	ACAT2
		MBTPS1	TNFRSF21	HOMER2	DNAJB1
		TSPAN4	MFSD10	PRKCQ	MAT2A
		HIV-1	FAM69A	MMP2	TEX10
		ERO1A	DNAJB1	INTS3	CTSL
		CLTC	UFM1	NUDCD3	EFCAB14
		CCNE2	AGL	FKBP4	HERPUD1
		POLE2	ERBB2	DNM1	BMP4
		KIF20A	FOS	TIAM1	CDC45
		PXMP2	PLCB3	GFOD1	TOP2A
		ATF5	GATA2	SPDEF	IKBKE
		TBP	CDK5R1	BACE2	MCM3
		DCK	PAX8	KIT	CHN1
		NOSIP	NPDC1	RBM34	CCDC86
		USP14	TJP1	GHR	JUN
		TBC1D9B	TSPAN4	TGFB3	PPIC
		PKIG	PPIC	CBR3	CCNB2
		CEP57	ANKRD10	RPA1	ZFP36
		USP1	RASA1	RBKS	HN1L
		PSMD10	ISOC1	KIF5C	AGL
		BID	MSH6	P3R3URF-PIK3R3	LOXL1
		ILK	POLG2	NUP133	FAM69A
		RFX5	APOE	CHN1	LSM5

		UFM1	ARID5B	GPER1	PDIA5
		CLSTN1	ID2	RAB21	CCDC85B
		HPRT1	STAT1	ITGB5	CCNB1
		DCTD	MBTPS1	SNCA	WDR61
		SFN	DECR1	SSBP2	EGR1
		ETS1	CANT1	SMARCC1	NNT
		RNF167	FZD7	HK1	POLG2
		ECD	MAT2A	DNAJC15	DNMT1
		FAS	SNX6	ZNF586	STAT1
		TM9SF2	DAG1	DUSP6	PARP1

Table 3.9 Top differentially expressed genes for TiO_2 treated cells. FG = Food Grade, NFG = Non-Food Grade, MP = microparticle, NP = nanoparticle.

TiO_2-FG-MP		**TiO_2-FG-NP**		**TiO_2-NFG-NP**	
Caco-2	HIEC-6	Caco-2	HIEC-6	Caco-2	HIEC-6
EDN1	KIF2C	EDN1	EZH2	RBM15B	MAMLD1
TARBP1	JUN	UBQLN2	PLA2G4A	HLA-DMA	HMOX1
BTK	UFM1	ICAM1	SPP1	SCCPDH	KIT
	PTGS2	NUP133	CCNE2	CCL2	BCL2
	SNAP25	CCP110			BUB1B
	SPP1				GDPD5
	TOP2A				SMC1A
	PAX8				
	GDPD5				
	ADGRG1				

Table 3.10 Top 5 gene ontology (GO) annotation of enriched biological process for the genes with the lowest 50 BMDs. The particles not listed did not yield significant results.

Cell	Sample	Name of Pathway	*p*-value	Adjusted *p*-value	Number of hits
Caco-2	$AgNO_3$	Regulation of cell death	3.51E-09	5.51E-05	19
		Regulation of apoptotic process	4.20E-09	3.29E-05	18
		Regulation of programmed cell death	5.65E-09	2.95E-05	18
		Regulation of miRNA transcription	5.86E-07	2.30E-03	5
		Positive regulation of cellular process	5.94E-07	1.86E-03	31
HIEC-6	$AgNO_3$	Positive regulation of protein localization to membrane	6.23E-07	9.76E-03	35

		Endocytosis	3.94E-06	3.09E-02	34
		Regulation of cell population proliferation	4.23E-06	2.21E-02	32
		Intracellular signal transduction	4.89E-06	1.91E-02	10
		Signaling	8.15E-06	2.56E-02	35
Caco-2	PEI-AgNP	Animal organ regeneration	2.69E-06	2.11E-02	5
		Response to organic substance	2.17E-06	3.40E-02	23
HIEC-6	Citrate-AgNP	Regulation of cell population proliferation	2.39E-07	3.74E-03	18
		Negative regulation of cell population proliferation	3.14E-06	2.46E-02	11
		System development	4.26E-06	2.23E-02	25
		Negative regulation of programmed cell death	5.03E-06	1.97E-02	12
		Positive regulation of transport	5.32E-06	1.67E-02	12
Caco-2	SiO_2-FG-NP	Regulation of cell cycle	4.11E-07	0.006	14
Caco-2	SiO_2-NFG-NP	Regulation of cell death	5.18E-09	8.11E-05	19
		Transmembrane receptor protein tyrosine kinase signaling pathway	6.35E-08	1.66E-04	10
		Positive regulation of multicellular organismal process	5.96E-08	1.87E-04	17
		Enzyme-linked receptor protein signaling pathway	2.64E-08	2.07E-04	12
		Regulation of programmed cell death	5.57E-08	2.18E-04	17
HIEC-6	SiO_2-FG-NP	Response to organic substance	4.96E-08	3.89E-04	22
		Cellular response to chemical stimulus	2.78E-08	4.36E-04	22
		Response to chemical	9.07E-07	3.55E-03	25
		Tube development	6.86E-07	3.58E-03	12
		Regulation of anatomical structure morphogenesis	1.44E-06	4.52E-03	12
HIEC-6	SiO_2-NFG-NP	Cellular response to stress	1.08E-07	1.69E-03	17
		Response to organic substance	5.92E-07	4.64E-03	21
		Cellular response to chemical stimulus	7.25E-06	1.42E-02	19
		Cell proliferation involved in kidney development	3.99E-06	1.57E-02	3
		Response to stress	7.07E-06	1.58E-02	22

Table 3.11 Pathway BMD in Caco-2 cells exposed to TiO_2 particles. FG = Food Grade, NFG = Non-Food Grade, NP = nanoparticle.

Sample	Name of pathway	Pathway BMD	*p*-value	Adjusted *p*-value	Percentage pathway	Number of hits
TiO_2-FG-NP	TNF signaling pathway	32.45	0.005	0.351	8.7%	2
	AGE-RAGE signaling pathway in diabetic complications	32.45	0.010	0.351	6.5%	2

	Fluid shear stress and atherosclerosis	32.45	0.010	0.351	6.3%	2
TiO_2-NFG-NP	Influenza A	44.68	0.005	0.264	7.1%	2
	Herpes simplex infection	44.68	0.005	0.264	6.9%	2

Table 3.12 Summary of the transcriptomic point of departure (tPODs) in this study and the lowest concentration of significant apical results in our published study of Caco-2 cells after 24 h exposure to chemicals.

Particle	tPODs (ppm)			Apical phenotypic assays (ppm)			
	20th gene	Mode	10th percentile	LC20	Cytosol ROS generation	Mitochondrial ROS generation	Calcium flux
SiO_2-FG-micro	NA	3.99	0.93	NA	NA	NA	NA
SiO_2-FG-nano	26.91	31.56	22.95	NA	100	NA	NA
SiO_2-NFG-nano	6.91	20.72	11.07	62.78	100	100	50
TiO_2-FG-micro	NA	35.52	34.66	NA	NA	NA	NA
TiO_2-FG-nano	NA	58.85	10.48	NA	NA	NA	NA
TiO_2-NFG-nano	NA	16.98	10.02	NA	NA	100	NA
Citrate-AgNP	1.32	0.66	0.8	NA	100	NA	NA
PEI-AgNP	0.9	0.42	0.54	28.14	50	12.5	6.25
$AgNO_3$	1.79	7.33	3.4	4.46	NA	100	100

Table 3.13 Gene ontology (GO) annotation for enriched biological process for the genes that have BMDs clustered in the first peak (1-10 ppm) and second peak (70-90 ppm) in HIEC-6 cells treated with PEI-AgNPs.

BMD range	Name of Pathway	*p*-value	Adjusted *p*-value	Percentage pathway	Number of hits
First peak (1-10 ppm)	Sugar transport	0.001	0.040	2.7	6
Second peak (70-90 ppm)	Cell division	5.00E-06	2.10E-04	10.7	15
	Cell cycle	6.60E-06	2.10E-04	13.6	19
	Mitosis	1.90E-05	4.00E-04	8.6	12

Table 3.14 Enriched KEGG Pathway in HIEC-6 cells with pathway BMD identified due to the treatment of different particles.

Sample	Name of pathway	Pathway BMD	*p*-value	Adjusted *p*-value	Percentage pathway	Number of hits
SiO_2- FG-MP	Breast cancer	25.60	0.036	0.914	6.1%	2
	Metabolic pathways	34.86	0.011	0.613	3.8%	4

	TNF signaling pathway	42.94	0.015	0.613	9.5%	2
	Oxytocin signaling pathway	42.94	0.018	0.613	8.7%	2
TiO_2- FG-MP	Oxytocin signaling pathway	4.01	0.024	0.824	8.3%	2
	TNF signaling pathway	4.01	0.017	0.824	10.0%	2
	Toll-like receptor signaling pathway	5.66	0.010	0.824	13.3%	2
TiO_2- FG-NP	MicroRNAs in cancer	13.71	0.010	0.660	5.0%	2
	PI3K-Akt signaling pathway	41.70	0.013	0.660	4.3%	2
TiO_2- NFG-NP	Pathways in cancer	3.965	0.030	0.643	2.9%	3
	Cell cycle	15.53	0.030	0.643	5.1%	2
	Fluid shear stress and atherosclerosis	19.31	0.019	0.643	6.5%	2
	HIF-1 signaling pathway	19.31	0.010	0.643	9.1%	2
	MicroRNAs in cancer	19.31	0.032	0.643	5.0%	2
	PI3K-Akt signaling pathway	21.28	0.041	0.657	4.3%	2

Table 3.15 Summary of the transcriptomic point of departure (tPODs) in this study and the lowest concentration of significant apical results in our published study of HIEC-6 cells after exposure to chemicals.

Particle	tPODs (ppm)			Apical phenotypic assays (ppm)			
	20th gene	Mode	10th percentile	LC20	Cytosol ROS generation (6 h)	Mitochondrial ROS generation (6 h)	Calcium flux (10 h)
SiO_2-FG-micro	NA	17.92	9.94	NA	NA	NA	50
SiO_2-FG-nano	1.74	7.15	3.59	NA	6.25	12.5	NA
SiO_2-NFG-nano	1.91	8.71	4.96	NA	12.5	6.25	50
TiO_2-FG-micro	NA	4.3	2.5	NA	NA	NA	NA
TiO_2-FG-nano	NA	13.18	12.02	NA	50	6.25	NA
TiO_2-NFG-nano	NA	3.37	0.67	NA	50	25	NA
Citrate-AgNP	1.89	6.28	3.33	84.68	25	50	12.5
PEI-AgNP	1.59	7.02	3.88	28.11	12.5	3.13	12.5
$AgNO_3$	2.96	4.13	3.15	12.88	1.56	6.25	50

3.7.2. Figures and discussion

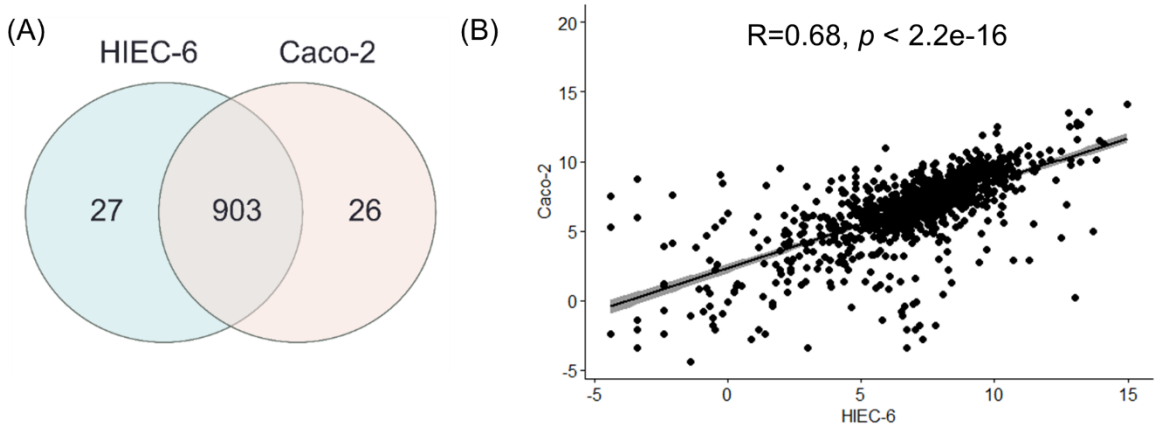

Figure 3.5 Characterization of the control samples (Dose 0) in Caco-2 cells and HIEC-6 cell by (A)Venn diagram showing the shared and unique genes and (B) scatter plot with correlation calculated between two cell lines.

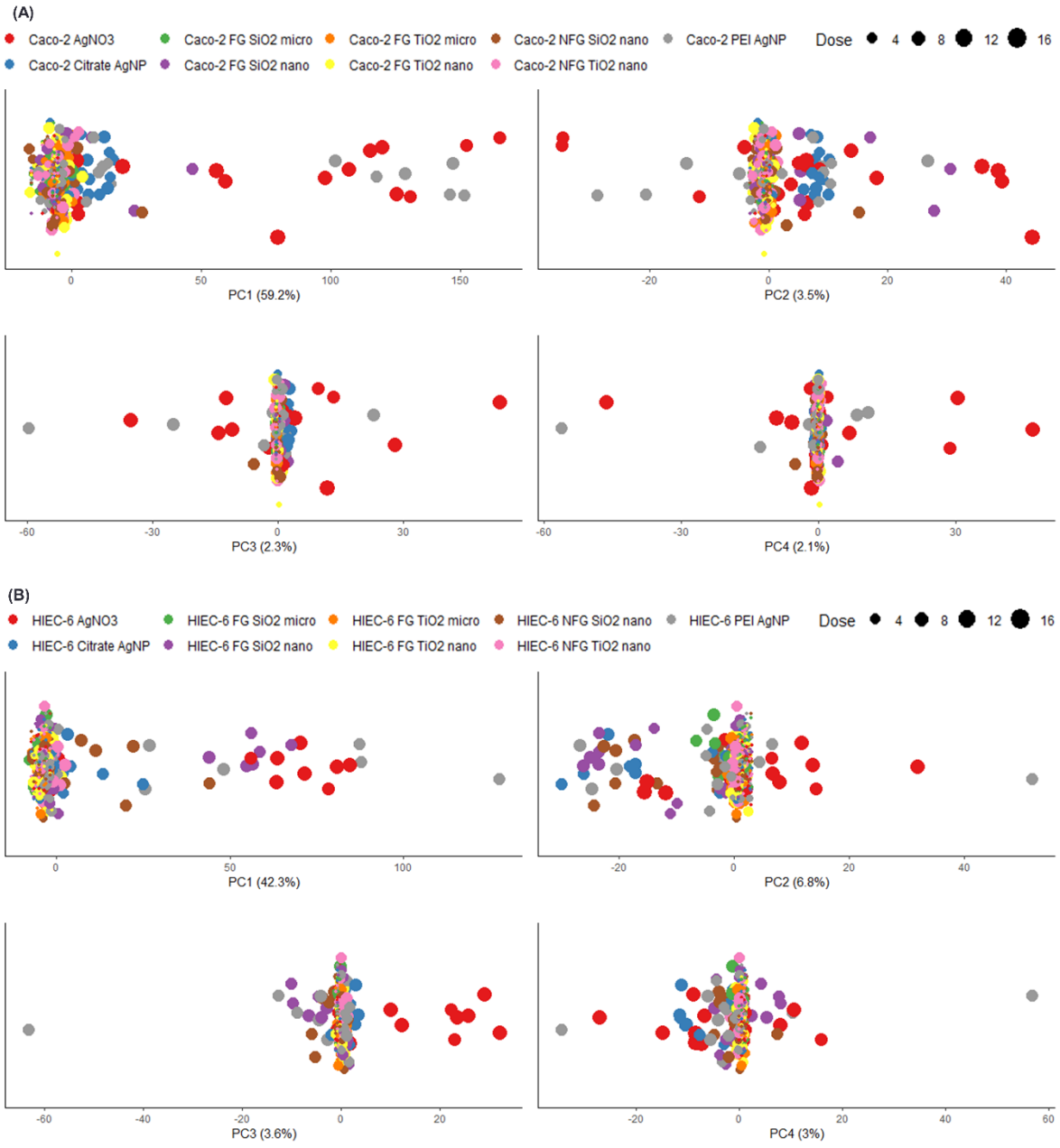

Figure 3.6 PCA plots for the first four principal components (PC1-PC4) for (A) Caco-2 and (B) HIEC-6 cell lines based on raw counts from all samples.

3.8. References

1. Sekhon, B. S., Food nanotechnology - an overview. *Nanotechnol Sci Appl* **2010,** *3*, 1-15.

2. Lomer, M. C. E.; Thompson, R. P. H.; Powell, J. J., Fine and ultrafine particles of the diet: influence on the mucosal immune response and association with Crohn's disease. *Proceedings of the Nutrition Society* **2002,** *61* (1), 123-130.

3. George, S.; Kaptan, G.; Lee, J.; Frewer, L., Awareness on adverse effects of nanotechnology increases negative perception among public: survey study from Singapore. *Journal of nanoparticle research* **2014,** *16* (12), 1-11.

4. Weir, A.; Westerhoff, P.; Fabricius, L.; Hristovski, K.; von Goetz, N., Titanium Dioxide Nanoparticles in Food and Personal Care Products. *Environmental Science & Technology* **2012,** *46* (4), 2242-2250.

5. Liu, Y.; Huang, Y.; Mou, Z.; Li, R.; Hossen, M. A.; Dai, J.; Qin, W.; Lee, K., Characterization and preliminary safety evaluation of nano-SiO2 isolated from instant coffee. *Ecotoxicology and Environmental Safety* **2021,** *224*, 112694.

6. Wershil, B. K.; Furuta, G. T., 4. Gastrointestinal mucosal immunity. *Journal of Allergy and Clinical Immunology* **2008,** *121* (2), S380-S383.

7. Koeneman, B. A.; Zhang, Y.; Westerhoff, P.; Chen, Y.; Crittenden, J. C.; Capco, D. G., Toxicity and cellular responses of intestinal cells exposed to titanium dioxide. *Cell Biology and Toxicology* **2010,** *26* (3), 225-238.

8. Williams, K. M.; Gokulan, K.; Cerniglia, C. E.; Khare, S., Size and dose dependent effects of silver nanoparticle exposure on intestinal permeability in an in vitro model of the human gut epithelium. *Journal of Nanobiotechnology* **2016,** *14* (1), 62.

9. Dorier, M.; Béal, D.; Tisseyre, C.; Marie-Desvergne, C.; Dubosson, M.; Barreau, F.; Houdeau, E.; Herlin-Boime, N.; Rabilloud, T.; Carriere, M., The food additive E171 and titanium dioxide nanoparticles indirectly alter the homeostasis of human intestinal epithelial cells in vitro. *Environmental Science: Nano* **2019,** *6* (5), 1549-1561.

10. Cornu, R.; Chrétien, C.; Pellequer, Y.; Martin, H.; Béduneau, A., Small silica nanoparticles transiently modulate the intestinal permeability by actin cytoskeleton disruption in both Caco-2 and Caco-2/HT29-MTX models. *Arch Toxicol* **2020,** *94* (4), 1191-1202.

11. Xu, K.; Basu, N.; George, S., Dietary nanoparticles compromise epithelial integrity and enhance translocation and antigenicity of milk proteins: An in vitro investigation. *NanoImpact* **2021,** *24*, 100369.

12. Vance, M. E.; Kuiken, T.; Vejerano, E. P.; McGinnis, S. P.; Hochella, M. F., Jr.; Rejeski, D.; Hull, M. S., Nanotechnology in the real world: Redeveloping the nanomaterial consumer products inventory. *Beilstein Journal of Nanotechnology* **2015,** *6*, 1769-1780.

13. Philpott, H. L.; Nandurkar, S.; Lubel, J.; Gibson, P. R., Drug-induced gastrointestinal disorders. *Frontline Gastroenterol* **2014,** *5* (1), 49-57.

14. Mittal, K.; Crump, D.; Head, J. A.; Hecker, M.; Hickey, G.; Maguire, S.; Hogan, N.; Xia, J.; Basu, N., Resource requirements for ecotoxicity testing: A comparison of traditional and new approach methods. *bioRxiv* **2022**.

15. European Chemicals, A., *New approach methodologies in regulatory science : proceedings of a scientific workshop : Helsinki, 19-20 April 2016*. European Chemicals Agency: 2016.

16. Thomas, R. S.; Bahadori, T.; Buckley, T. J.; Cowden, J.; Deisenroth, C.; Dionisio, K. L.; Frithsen, J. B.; Grulke, C. M.; Gwinn, M. R.; Harrill, J. A., The next generation blueprint of computational toxicology at the US Environmental Protection Agency. *Toxicological Sciences* **2019,** *169* (2), 317-332.

17. Harrill, J.; Shah, I.; Setzer, R. W.; Haggard, D.; Auerbach, S.; Judson, R.; Thomas, R. S., Considerations for Strategic Use of High-Throughput Transcriptomics Chemical Screening Data in Regulatory Decisions. *Curr Opin Toxicol* **2019,** *15*, 64-75.

18. Kukurba, K. R.; Montgomery, S. B., RNA Sequencing and Analysis. *Cold Spring Harb Protoc* **2015,** *2015* (11), 951-969.

19. Ozsolak, F.; Milos, P. M., RNA sequencing: advances, challenges and opportunities. *Nature Reviews Genetics* **2011,** *12* (2), 87-98.

20. Mav, D.; Shah, R. R.; Howard, B. E.; Auerbach, S. S.; Bushel, P. R.; Collins, J. B.; Gerhold, D. L.; Judson, R. S.; Karmaus, A. L.; Maull, E. A., A hybrid gene selection approach to create the S1500+ targeted gene sets for use in high-throughput transcriptomics. *PloS one* **2018,** *13* (2), e0191105.

21. Soufan, O.; Ewald, J.; Viau, C.; Crump, D.; Hecker, M.; Basu, N.; Xia, J., T1000: a reduced gene set prioritized for toxicogenomic studies. *PeerJ* **2019,** *7*, e7975.

22. Subramanian, A.; Narayan, R.; Corsello, S. M.; Peck, D. D.; Natoli, T. E.; Lu, X.; Gould, J.; Davis, J. F.; Tubelli, A. A.; Asiedu, J. K.; Lahr, D. L.; Hirschman, J. E.; Liu, Z.; Donahue, M.; Julian, B.; Khan, M.; Wadden, D.; Smith, I. C.; Lam, D.; Liberzon, A.; Toder, C.; Bagul, M.; Orzechowski, M.; Enache, O. M.; Piccioni, F.; Johnson, S. A.; Lyons, N. J.; Berger, A. H.; Shamji, A. F.; Brooks, A. N.; Vrcic, A.; Flynn, C.; Rosains, J.; Takeda, D. Y.; Hu, R.; Davison, D.; Lamb, J.; Ardlie, K.; Hogstrom, L.; Greenside, P.; Gray, N. S.; Clemons, P. A.; Silver, S.; Wu, X.; Zhao, W.-N.; Read-Button, W.; Wu, X.; Haggarty, S. J.; Ronco, L. V.; Boehm, J. S.;

Schreiber, S. L.; Doench, J. G.; Bittker, J. A.; Root, D. E.; Wong, B.; Golub, T. R., A Next Generation Connectivity Map: L1000 Platform and the First 1,000,000 Profiles. *Cell* **2017,** *171* (6), 1437-1452.e17.

23. LaRocca, J.; Costa, E.; Sriram, S.; Hannas, B. R.; Johnson, K. J., Short-term toxicogenomics as an alternative approach to chronic in vivo studies for derivation of points of departure: A case study in the rat with a triazole fungicide. *Regulatory Toxicology and Pharmacology* **2020,** *113*, 104655.

24. Thomas, R. S.; Wesselkamper, S. C.; Wang, N. C. Y.; Zhao, Q. J.; Petersen, D. D.; Lambert, J. C.; Cote, I.; Yang, L.; Healy, E.; Black, M. B., Temporal concordance between apical and transcriptional points of departure for chemical risk assessment. *Toxicological Sciences* **2013,** *134* (1), 180-194.

25. Mittal, K.; Ewald, J.; Basu, N., Transcriptomic Points of Departure Calculated from Rainbow Trout Gill, Liver, and Gut Cell Lines Exposed to Methylmercury and Fluoxetine. *Environmental Toxicology and Chemistry* **2022,** *41* (8), 1982-1992.

26. Martínez, R.; Navarro-Martín, L.; Luccarelli, C.; Codina, A. E.; Raldúa, D.; Barata, C.; Tauler, R.; Piña, B., Unravelling the mechanisms of PFOS toxicity by combining morphological and transcriptomic analyses in zebrafish embryos. *Science of The Total Environment* **2019,** *674*, 462-471.

27. Moffat, I.; Chepelev, N. L.; Labib, S.; Bourdon-Lacombe, J.; Kuo, B.; Buick, J. K.; Lemieux, F.; Williams, A.; Halappanavar, S.; Malik, A. I.; Luijten, M.; Aubrecht, J.; Hyduke, D. R.; Fornace, A. J.; Swartz, C. D.; Recio, L.; Yauk, C. L., Comparison of toxicogenomics and traditional approaches to inform mode of action and points of departure in human health risk assessment of benzo[a]pyrene in drinking water. *Critical Reviews in Toxicology* **2015,** *45* (1), 1-43.

28. Pageot, L. P.; Perreault, N.; Basora, N.; Francoeur, C.; Magny, P.; Beaulieu, J. F., Human cell models to study small intestinal functions: Recapitulation of the crypt-villus axis. *Microscopy Research and Technique* **2000,** *49* (4), 394-406.

29. Wan, Y.; Guo, Z.; Jiang, X.; Fang, K.; Lu, X.; Zhang, Y.; Gu, N., Quasi-spherical silver nanoparticles: Aqueous synthesis and size control by the seed-mediated Lee–Meisel method. *Journal of Colloid and Interface Science* **2013,** *394*, 263-268.

30. Toh, H. S.; Faure, R. L.; Mohd Amin, L. B.; Hay, C. Y. F.; George, S., A light-assisted in situ embedment of silver nanoparticles to prepare functionalized fabrics. *Nanotechnol Sci Appl* **2017,** *10*, 147-162.

31. Jolliffe, I. T.; Cadima, J., Principal component analysis: a review and recent developments. *Philosophical Transactions of the Royal Society A: Mathematical, Physical and Engineering Sciences* **2016,** *374* (2065), 20150202.

32. Wu, T.; Hu, E.; Xu, S.; Chen, M.; Guo, P.; Dai, Z.; Feng, T.; Zhou, L.; Tang, W.; Zhan, L., clusterProfiler 4.0: A universal enrichment tool for interpreting omics data. *The Innovation* **2021,** *2* (3), 100141.

33. van der Zande, M.; Undas, A. K.; Kramer, E.; Monopoli, M. P.; Peters, R. J.; Garry, D.; Antunes Fernandes, E. C.; Hendriksen, P. J.; Marvin, H. J. P.; Peijnenburg, A. A.; Bouwmeester, H., Different responses of Caco-2 and MCF-7 cells to silver nanoparticles are based on highly similar mechanisms of action. *Nanotoxicology* **2016,** *10* (10), 1431-1441.

34. Miyayama, T.; Matsuoka, M., Involvement of lysosomal dysfunction in silver nanoparticle-induced cellular damage in A549 human lung alveolar epithelial cells. *Journal of Occupational Medicine and Toxicology* **2016,** *11* (1), 1.

35. De Matteis, V.; Malvindi, M. A.; Galeone, A.; Brunetti, V.; De Luca, E.; Kote, S.; Kshirsagar, P.; Sabella, S.; Bardi, G.; Pompa, P. P., Negligible particle-specific toxicity mechanism of silver nanoparticles: the role of Ag+ ion release in the cytosol. *Nanomedicine* **2015,** *11* (3), 731-9.

36. Akinc, A.; Thomas, M.; Klibanov, A. M.; Langer, R., Exploring polyethylenimine-mediated DNA transfection and the proton sponge hypothesis. *The Journal of Gene Medicine: A cross-disciplinary journal for research on the science of gene transfer and its clinical applications* **2005,** *7* (5), 657-663.

37. Xia, T.; Kovochich, M.; Liong, M.; Meng, H.; Kabehie, S.; George, S.; Zink, J. I.; Nel, A. E., Polyethyleneimine coating enhances the cellular uptake of mesoporous silica nanoparticles and allows safe delivery of siRNA and DNA constructs. *ACS nano* **2009,** *3* (10), 3273-3286.

38. Onizawa, M.; Nagaishi, T.; Kanai, T.; Nagano, K.-i.; Oshima, S.; Nemoto, Y.; Yoshioka, A.; Totsuka, T.; Okamoto, R.; Nakamura, T., Signaling pathway via TNF-α/NF-κB in intestinal epithelial cells may be directly involved in colitis-associated carcinogenesis. *American Journal of Physiology-Gastrointestinal and Liver Physiology* **2009,** *296* (4), G850-G859.

39. Wullaert, A.; Bonnet, M. C.; Pasparakis, M., NF-κB in the regulation of epithelial homeostasis and inflammation. *Cell research* **2011,** *21* (1), 146-158.

40. Harris, S. L.; Levine, A. J., The p53 pathway: positive and negative feedback loops. *Oncogene* **2005,** *24* (17), 2899-2908.

41. Babykutty, S.; Suboj, P.; Srinivas, P.; Nair, A. S.; Chandramohan, K.; Gopala, S., Insidious role of nitric oxide in migration/invasion of colon cancer cells by upregulating MMP-2/9 via activation of cGMP-PKG-ERK signaling pathways. *Clinical & Experimental Metastasis* **2012,** *29* (5), 471-492.

42. Kanehisa, M.; Goto, S., KEGG: kyoto encyclopedia of genes and genomes. *Nucleic Acids Res* **2000,** *28* (1), 27-30.

43. Kirkland, J. L.; Tchkonia, T., Cellular senescence: a translational perspective. *EBioMedicine* **2017,** *21*, 21-28.

44. Manna, S. K.; Ramesh, G. T., Interleukin-8 induces nuclear transcription factor-kappaB through a TRAF6-dependent pathway. *J Biol Chem* **2005,** *280* (8), 7010-21.

45. Fantini, M. C.; Pallone, F., Cytokines: from gut inflammation to colorectal cancer. *Current drug targets* **2008,** *9* (5), 375-380.

46. Clapham, D. E., Calcium Signaling. *Cell* **2007,** *131* (6), 1047-1058.

47. Ivanov, A. I.; Parkos, C. A.; Nusrat, A., Cytoskeletal Regulation of Epithelial Barrier Function During Inflammation. *The American Journal of Pathology* **2010,** *177* (2), 512-524.

48. Ivanov, A. I.; McCall, I. C.; Parkos, C. A.; Nusrat, A., Role for actin filament turnover and a myosin II motor in cytoskeleton-driven disassembly of the epithelial apical junctional complex. *Molecular biology of the cell* **2004,** *15* (6), 2639-2651.

49. Brittan, M.; Wright, N. A., Gastrointestinal stem cells. *The Journal of Pathology: A Journal of the Pathological Society of Great Britain and Ireland* **2002,** *197* (4), 492-509.

50. Foulke-Abel, J.; In, J.; Kovbasnjuk, O.; Zachos, N. C.; Ettayebi, K.; Blutt, S. E.; Hyser, J. M.; Zeng, X.-L.; Crawford, S. E.; Broughman, J. R., Human enteroids as an ex-vivo model of host–pathogen interactions in the gastrointestinal tract. *Experimental Biology and Medicine* **2014,** *239* (9), 1124-1134.

51. Canada, H., Science Approach Document–Bioactivity Exposure Ratio: Application in Priority Setting and Risk Assessment. Existing Substance Risk Assessment Bureau Canada: 2021.

52. Calabrese, E. J.; Bachmann, K. A.; Bailer, A. J.; Bolger, P. M.; Borak, J.; Cai, L.; Cedergreen, N.; Cherian, M. G.; Chiueh, C. C.; Clarkson, T. W., Biological stress response terminology: integrating the concepts of adaptive response and preconditioning stress within a hormetic dose–response framework. *Toxicology and applied pharmacology* **2007,** *222* (1), 122-128.

Preface to Chapter 4

The previous chapter studied the effects of dietary NPs exposure on the gene expression of intestinal model cells and derived tPODs to rank the toxicity of the particles based on chemical types and particle sizes. Functional pathway enrichment analysis suggested potential downstream responses, including oxidative stress, inflammation, and immune responses. Since the adverse outcome pathway approach emphasizes the relationships between key events at different biological levels, the changes observed at the molecular level shall be compared and related to apical responses at higher biological hierarchies.

In this chapter, the reference library identical to the previous chapter was exposed to the same cell model and is characterized for cellular and intracellular effects suggested in Chapter 3. This study used a panel of bioassays that use fluorescence markers to probe the changes in cell membrane integrity, organelle acidity, ROS generation, mitochondria function, and calcium influx using a high-content screening instrument. Inter-cellular changes were also investigated for the integrity of the cellular junction complex, the barrier function of the intestinal epithelium, and the release of inflammatory cytokines after particle exposure. Based on the responses, I proposed the mechanism of toxicity for the dietary particles in affecting the intestinal cell homeostasis and the epithelial barrier function and suggested the possible connection to cow's milk allergy progression.

This chapter is authored by the candidate and coauthored by the candidate's supervisors, Dr. Saji George, and Dr. Niladri Basu. The study design was developed by the candidate and supervisors. The candidate was responsible for performing all experiments, data analysis and interpretation, discussion of the results, and preparation of the manuscript under the supervision of Dr. Saji

George and Dr. Niladri Basu. The manuscript titled “Dietary nanoparticles compromise epithelial integrity and enhance translocation and antigenicity of milk proteins: An *in vitro* investigation” was published in *NanoImpact* in 2021.

Chapter 4

4. Dietary nanoparticles compromise epithelial integrity and enhance translocation and antigenicity of milk proteins: An *in vitro* investigation

4.1. Abstract

Nanoparticles (NPs) are increasingly being used in the food sector, yet little is known about the potential health risks associated with oral exposure to dietary NPs. In this study, the most widely used NPs in food industry including food grade silicon dioxide (SiO_2), titanium dioxide (TiO_2) and silver (Ag), along with their non-food grade and bulk counterparts, are characterized for physicochemical properties and molecular, cellular, and intracellular effects on human intestinal epithelial cells (Caco-2 and HIEC-6). Silver NPs are the most cytotoxic and induce significant cellular changes in oxidative stress, Ca^{2+} flux and mitochondria function, leading to cellular junction disruption at the lowest exposure concentration. At higher testing concentrations, NPs but not microparticles of SiO_2 and TiO_2 cause sublethal cellular responses and remodel tight junctions without impairing epithelial integrity. To relate the cellular results to key events in GI disorder progression, NPs are exposed to an *in vitro* co-culture model for cow's milk allergy comprised of Caco-2 and allergy sera-primed mast cells (LUVA). All particle treatments increase the allergen delivery across intestinal epithelium and subsequent allergy responses. Overall, the study has identified a particle-dependent alteration in intestinal epithelium and highlighted potential safety concerns of dietary NPs.

4.2. Introduction

Consumers of typical western diet are exposed to approximately 10^{12}-10^{14} nanoparticles (NPs) per day largely due to the extensive use of NPs in the food industry.[1] The most common NPs used in food additive include titanium dioxide (TiO_2) or silica (SiO_2).[2] Uncertainty over health risks associated with dietary exposure to NPs is a major cause of concern for consumers and public health officials.[3] Previous studies using human cell line models have demonstrated that non-food grade (NFG) TiO_2 NPs[4] may modify the microvilli organization on the apical intestinal epithelium and AgNPs[5] may disrupt intestinal permeability. Compared to NFG particles, there are fewer studies concerning food grade (FG) particles. Two *in vitro* studies with FG TiO_2 NPs[6] and FG SiO_2 NPs[7] reported inflammatory responses and oxidative stress effects in intestinal cell models. While these studies suggest possible adverse effects of ingested NPs, our knowledge of the mechanisms that underpin the progression from NP exposure to potential GI disorders is far from resolved.

The integrity of intestinal epithelium is critical for preventing undesired trespass of xenobiotics, and this function is maintained by adherens junctions (AJ) and tight junction (TJ) proteins, including occludin, claudins, and zonula occludens (ZO).[8] Disruption of AJ and TJ mediated by NFG NPs have been reported in endothelial cells. For example, Setyawati *et al.* reported the potential of NFG TiO_2 NPs to enter the paracellular space and interact with vascular endothelial cadherins (VE-cadherins) ultimately causing endothelial leakage.[9] Another study by Cornu *et al.* showed relaxation of cell junction complexes due to FG SiO_2 treatment in intestinal epithelium without changing permeability.[7] The mechanisms by which NPs exposure may disrupt the

intestinal epithelium deserve further investigation due to the close relationship between the increased intestinal permeability (leaky gut) and various GI disorders.

Compromised barrier function of the intestinal epithelium allows easier access of dietary antigens to the immune system, and this has commonly been reported in patients with food allergies and inflammatory bowel disease (IBD).[10] Cow's milk allergy, in particular, refers to an individual's immune response following exposure to proteins in cow's milk (mainly casein and β-lactoglobulin), and is prevalent in youth populations (e.g., affects 0.5% - 3% of children in high-income countries).[11] Interestingly, SiO_2 and TiO_2 NPs are used in various sugary products as anti-caking agents and colorants.[2] For children, this is particularly noteworthy given their relatively high intake of sugar containing products (e.g., dietary TiO_2 exposure for children is 2-3 times higher than in other age groups).[12] However, the possibility of enhanced delivery and increased antigenicity of food allergens due to NPs mediated changes in the intestinal epithelium function has not been verified.

The objective of the current study is to use cellular GI models to probe the effects of common dietary NPs on molecular, biochemical, cellular, and immune responses significant to epithelial integrity, and the implications of such changes to allergen seepage that may underlie allergic responses. We used human colon adenocarcinoma cell (Caco-2) as enterocyte model and human intestinal epithelial cell (HIEC-6) as crypt cell model.[13] These cell lines were exposed to different forms of SiO_2 NPs (FG NPs, and NFG NPs), TiO_2 NPs (FG NPs and NFG NPs), and AgNPs (citrate coated AgNP (Citrate-AgNP) and polyethylenimine coated AgNP (PEI-AgNP)). Non-food grade NPs were compared to their food grade counterparts given potential compositional differences according to food regulations.[12] The effect of surface chemistry was also compared for

AgNPs (i.e., between positively charged PEI-AgNP and negatively charged Citrate-AgNPs). In addition to NPs, we also studied microparticles (MPs) of SiO_2 and TiO_2 given that food products contain particles of variable sizes.[12] Using the *in vitro* models, we addressed the potential of these dietary NPs to induce oxidative stress and inflammatory responses, and also how such exposures could modulate junction proteins and affect epithelial permeability. Subsequently, we tested the effects of NP-mediated compromise in epithelial integrity on the milk allergen (β-lactoglobulin) delivery and hypersensitivity reactions against milk proteins using a co-culture model (Caco-2 and sensitized LUVA cell).

4.3. Materials and Methods

4.3.1. Materials

Food-grade silica nano (AEROSIL 200F, lot # 625010907) and micron size particles (SIPERNAT 22, lot# 156032047) were obtained from Evonik Industries (Essen, Germany). Nonfood-grade silica NPs (cat# 637238, 10−20 nm particle size (BET), 99.5% trace metals basis) were purchased from Sigma-Aldrich (St. Louis, USA). Food grade titanium NPs were acquired from CNMI industry cooperation (Beijing, China) and MPs were purchased from Pure Organic™ (Toronto, Canada). Non-food grade NPs were obtained from Sigma.

Citrate coated AgNPs were synthesized based on a previously reported method with minor modifications.[14] Briefly, 1 mM aqueous solution of silver nitrate and 10 mM trisodium citrate solution were mixed at a 2:1 volume ratio and incubated in 70 °C water bath for 3 hours (h). The resulting product (greenish yellow in color) solution was eluted twice with water for 30 minutes

(min) at 16,000 g (Eppendorf 5430R refrigerated centrifuge, Eppendorf Canada, Ontario, Canada) and resuspend in water for future use.

PEI coated AgNPs were prepared using light-assisted synthesis method.[15] Briefly, 1%, w/v aqueous solution of silver nitrate and 1% w/v branched-PEI solution were mixed at a 2:1 ratio and sonicated in a water bath. The falcon tube containing the mixture was covered with aluminum foil to avoid light. After 30 min of sonication, the mixture was exposed directly to a light source (120 V, 160 W) for 4 min until the color of the solution turned to amber red. The product solution was washed twice with water for 30 min at 16,000 g with the Eppendorf 5430R refrigerated centrifuge (Eppendorf) and resuspended in water.

4.3.2. Particle characterization

The size and morphology of the particles were characterized by scanning electron microscopy (SEM) (HITACHI FE-SEM SU8000, Japan) at 5 kV and 7 kV. Water suspension of 50 µg/mL particles were freshly prepared and 10 µL was dropped on to the SEM sample stub. Samples were air dried at room temperature (RT) and were imaged without coating.

The hydrodynamic size, polydispersity index (PDI) and surface charges of particles were characterized by dynamic light scattering (DLS) and zeta potential measurement. For this, 2 mL of 50 µg/mL NPs dispersed in deionized water or cell culture media (incubated for 24 h at 37 °C) were added to a pre-rinsed DLS cuvette and analyzed using DLS (Nanobrook Omni instrument, Brookhaven's, New York, USA) at 25 °C. Samples were then loaded into a pre-rinsed folded capillary cell for zeta potential measurement with an applied voltage of 100 V.

The crystal structure of the particles was characterized with X-ray diffraction (XRD). All particles (in powdered form) were placed on the XRD specimen holder and pressed with a glass slide to ensure uniform sample thickness. Samples were then analyzed using Bruker D8 Discover diffractometer with VANTEC-2000 detector system and Cu Kα radiation (λ = 0.1542) (Bruker, USA). The diffraction angle ranged between 4°−104°. The results were analyzed using the software Diffrac Eva 4.0.

4.3.3. Cell culture

Caco-2 was selected as one of the *in vitro* models of intestinal epithelium due to their morphological and functional similarities to mature human enterocytes. Caco-2 cell lines (ATCC# HTB37, passage between 10-35) originally obtained from ATCC (ATCC, Virginia, USA) were seeded in 100 mm petri dish (Thermofisher, New York, USA). The cells were supplemented with 10 mL of complete culture media that contained Gibco Dulbecco's Modified Eagle Medium (DMEM) (Thermofisher), 10% fetal bovine serum (FBS) (WISENT, Quebec, Canada) and 1% PEN-STREP (WISENT). Cells were cultured at 37 °C and 5% CO_2 with 95% humidity with media changed every two days. Upon reaching 90% confluency, cells were harvested using 0.25% Trypsin/EDTA (WISENT) and sub-cultured or seeded for subsequent experiments.

HIEC-6 was selected as a normal human cell line that does not differentiate upon confluency. This cell line exhibits markers that resemble the function of undifferentiated lower crypt cells, allowing comparison between different cell types with variable functions.[13] HIEC-6 cells (ATCC# CRL-3266) were purchased from ATCC (ATCC, Virginia, USA) between passage 7 and 15 were cultured in 100 mm petri dish supplemented with 10 mL media that contained OptiMEM 1

Reduced Serum Medium (Thermofisher), 4% fetal FBS (WISENT), 1% PEN-STREP (WISENT) 20 mM HEPES (Thermofisher), 10 mM GlutaMAX (Thermofisher) and 10 ng/mL Epidermal Growth Factor (EGF) (Thermofisher). Similarly, cells were incubated at 37 °C and 5% CO_2 with 95% humidity with media changed every two days. Upon reaching 90% confluency, cells were harvested using Trypsin/EDTA (WISENT) and sub-cultured or seeded into multiwell plates for future experiments.

4.3.4. Cell viability

Caco-2 and HIEC-6 cells were seeded at a density of 1×10^4 in each well of 96 well plates overnight before the assay. To prepare the particle samples for exposure, 100 µg/mL particle suspensions were prepared for each type of particle in serum free culture media. Subsequently, two-fold serial dilutions were performed until concentrations of 1.5625 µg/mL were reached for all particle samples. The original culture media in each 96 wells were aspirated and cells were exposed to 100 µL media containing incremental concentrations (1-100 µg/mL) of particles and kept incubated for another 24 h. After exposure, cells were washed three times with fresh serum free media followed by the addition of 50 µg/mL resazurin (Abcam, USA) suspended in serum free media.[16] Viable cells irreversibly reduced resazurin to highly fluorescent resorufin, whose fluorescence intensity could be measured at 530 nm excitation and 590 nm emission with the BioTek Synergy HT plate reader (BioTek instrument, Vermont, USA) after 4 h of incubation. Silver nitrate (Sigma) solutions with the same concentration range were used as positive controls. The percentage viability was analyzed based on non-exposed cells (100% viable) and the statistics were calculated using student t test (n=3, $*p<0.05$).

4.3.5. Cellular uptake of AgNPs

Bioavailability of AgNPs was measured using ICP-MS in Caco-2 cell digests to assess the difference in cellular uptake between 25 μg/mL Citrate-AgNPs and 25 μg/mL PEI-AgNPs. After 24 h particle exposure, the particle suspensions were aspirated and cells in 24 wells plates were washed three times with fresh serum free culture media. The cells were then trypsinized and harvested by centrifugation (Eppendorf 5430R refrigerated centrifuge, 255×g, 5 min). In each case, cells pellet was mixed with 400 μL 70 % (v/v) HNO_3 in open 15 mL Digitubes (SCP Science, Quebec, Canada) at 90 °C using a heating block for 1 h, followed by 400 μL H_2O_2 digestion in the same condition. The digestion product was diluted with Milli-Q water to 1.3% (v/v) HNO_3 acid for ICP-MS analysis. One well from each treatment was used to count the cells. Perkin Elmer NexION 300X ICP-MS measuring Ag 109. The data was presented as the mass of Ag in microgram per 100,000 cells. Results for ICP-MS analysis were given in the supporting information (SI).

4.3.6. Effect of NPs on cell junction complex and change in membrane permeability

The effects of the NPs on the intestinal barrier were assessed in differentiated Caco-2 cells and HIEC-6 cells using transwell cell culture inserts. The changes in transepithelial electrical resistance (TEER) were monitored to assess the epithelial barrier integrity. Caco-2 cells and HIEC-6 cells were cultured on transwell inserts (polycarbonate membrane filters, 0.4 um pore size, 1×10^8 pores/cm) (Corning Incorporated, Maine, USA) at 5×10^4 cells/cm^2. The inserts were placed in 6-well plates, resulting in apical (upper) and basolateral (lower) chambers. Complete

DMEM was added to apical chambers (1.5 mL) and basolateral chambers (2.6 mL). Media were refreshed every two days until 21-25 days when Caco-2 cells were differentiated into polarized intestinal cells (TEER>250 Ω/cm^2). HIEC-6 cells were maintained for 7 days after confluency until TEER>150 Ω/cm^2. After achieving the targeted resistance level, the cells in the apical compartment with well-formed epithelial barriers were exposed to media containing 100 µg/mL particle suspensions (25 µg/mL for AgNPs) for 24 h, while the media in the basolateral compartment were replaced with fresh media. TEER measurements were taken at 2, 4, 6, 8,10 and 24 h after the addition of particles by the Millicell-ERS system (ERS-2 Epithelial Volt-Ohm Meter, Millicell). Changes in TEER values of cells were recorded in duplicates. Each experiment included a negative control (cells in culture media), and a positive control (cells exposed to 25 mM EDTA). A rescue experiment was performed in parallel to the treatment after 2 h exposure by adding 10mM of N-Acetyl Cysteine (NAC) (Sigma) dissolved in serum free media.

Permeability of the Caco-2 cell monolayer was measured by the transport of fluorescein isothiocyanate dextran 4,400 (FD-4) (Sigma).[17] After TEER measurements, the particle suspension in the apical compartment was removed and cells were washed twice with serum free media. FD-4 suspended in serum free media (1 mg/mL) was then added to the apical compartment and incubated for 1 h with the cells. Samples were taken from the basal compartment into 96 well plates for fluorescence measurement with a Spectramax i3x plate reader at excitation 490 nm and emission 535 nm (Molecular Devices, San Jose, USA). Localization of FD-4 was visualized with LSM 710 confocal laser scanning microscopy (Carl Zeiss, Oberkochen, Germany) with Argon ion laser at 488nm.

4.3.7. Change in inflammatory cytokines level

Confluent cells seeded in 96 well plates were exposed to 100 µg/mL particle suspensions (25 µg/mL for PEI-AgNP) prepared in serum free media. After 24h incubation, the media from each well were collected and centrifuged at 255×g, 4 ºC for 5 min with Eppendorf 5430R refrigerated centrifuge (Eppendorf) to remove cell debris, and the resulting supernatant was used to measure cytokines. Interleukin (IL-8) and tumor necrosis factor alpha (TNF-α) enzyme-linked immunosorbent assay (ELISA) kits (Sigma) and IL-10 ELISA kit (BD Bioscience, California, USA) were used following the instructions provided by the manufacturer for assessing the generation of IL-8, TNF-α and IL-10, respectively. For IL-8 and TNF- α kits, supernatants of cell culture media after exposing to incremental concentrations of NPs were aliquoted (100 µl) into wells of ELISA plates and incubated for 2.5 h at room temperature. The solutions were discarded and wash 4 times with 1x washing solution after incubation. Subsequently, 100 µL of 1x prepared detection antibody were added to each well and incubate for 1 h at RT with gentle shaking. The incubation was followed by 4 times washing with 1x washing solution. After washing, 100 µL of prepared streptavidin solution were added to each well and incubated for 45 minutes at RT, with plates covered and gentle shaking. The wells were washed four times before adding 100 µL of TMB substrate reagent to each well, followed by incubation for 30 min at RT in the dark with gentle shaking. For IL-10 kit, 50 µL of ELISA diluent were loaded into appropriate wells and mixed with 100 µL of samples before incubating for 2 h at RT. Working detector was prepared by mixing detection antibody with required quantity of enzyme concentrate, and 100 µL was added to each well for 1 h incubation at RT after four times washing with washing buffer. After the incubation, the wells were washed for seven times before adding 100 µL of TMB substrate reagent

to each well, followed by incubation for 30 min at RT in the dark with gentle shaking. The absorbance intensity was measured using a Spectramax i3x plate reader (Molecular Devices) at 450 nm immediately after adding 50 µL of stop solution for all kits. The results for each sample were calculated using a standard curve of provided recombinant proteins. Lipopolysaccharides (LPS) (5 ng/mL; Sigma) exposed samples were used as positive controls for cytokine release. All experiments were performed in triplicates and the resulting fold changes were calculated based on the negative controls of cells exposed to serum free media.

4.3.8. Localization of junction protein complex

Confluent Caco-2 and HIEC-6 cells were seeded in 96 well clear bottom black culture plates and were exposed to 100 µg/mL particle suspensions (25 µg/mL for PEI-AgNP) for 24 h. After exposure, cells were washed three times with phosphate-buffered saline (PBS) buffer (pH =7.4), fixed with 4% formaldehyde (Sigma) for 15 min, and permeabilized with 0.25% Triton X-100 (Sigma) in PBS (PBST) for 10 min. After permeabilization, 1% bovine serum albumin (BSA) in PBST was added for 30 min to block unspecific binding of the antibodies. The cells were then incubated wit primary antibodies of anti Zonula Occludens-1 (ZO)-1, anti Claudin-1 and anti E-cadherin (Abcam) in 1% BSA in PBST overnight at 4 °C. After incubation, primary antibodies were decanted, and secondary antibodies conjugated with fluorophores (in PBST containing 1% BSA) were added for 1 h at RT in dark. Each of the steps was followed by washing with PBS buffer for 5 min. F-actin filaments were stained by Phalloidin conjugated with Alexa 488 (Sigma) and cell nuclei were stained by Hoechst 33342 (Thermofisher). All dyes were incubated at RT in dark for 10 min. The cells were then imaged by LSM 710 confocal laser scanning microscopy (Carl Zeiss).

4.3.9. Change in gene expression

The differential expressions of 5 genes involved in inflammation (TNF-α, IL-1β, IL-6, IL-8 and IL-15), 3 genes for oxidative stress (GSTP1, HO-1 and Catalase) and 5 markers of epithelial mesenchymal transition (Claudin-1, Zonula occludens-1, E-cadherin, α-SMA and Vimentin) were assessed by quantifying respective mRNA expression. For this, confluent Caco-2 cells seeded in 96-well culture plates were exposed to 100 µg/mL particles suspensions (25 µg/mL for PEI-AgNP). After 24 h, the cells were washed twice with PBS following which RNA was extracted using the RNeasy Mini Kit (Qiagen, Maryland, USA) as described by the manufacturer. Total RNA was reverse transcribed onto cDNA using Omniscript RT Kit (Qiagen) following the manufacturer's protocol. Primers of selected genes (IDT, Iowa, USA) are given in Table 4.1 (supplementary information). Real-time PCR was performed on a CFX384 Touch Real-Time PCR Detection Systems (Biorad, Hercules, CA, USA) using RT2 SYBR® Green qPCR Mastermix (Qiagen). Amplification was carried out in a 10 µL reaction containing 4 µL of cell suspension, 0.5 µL of each primer and 5 µL of SYBR® Green dye (Qiagen). The mixture was incubated under the experimental protocol consisted of the following program: (i) preincubation step for 10 min at 95 ºC; (ii) amplification step including 40 cycles of denaturation at 95 ºC for 15 s followed by annealing at and extension at 60 ºC for 1 min, with fluorescence acquisition performed after each cycle; (iii) melt curve analysis: holding at 65 ºC for 31s followed 60 cycles of 5s heating at 0.5 ºC /s, with temperature increment of 0.5 ºC/cycle to 95 ºC; (iv) cooling to 4 ºC. The relative gene expression levels were calculated using the ΔΔCq method, and we note that reference gene (GAPDH and β-actin) expression was constant among exposure groups

4.3.10. Cellular staining with fluorescent probes and high-content epifluorescence microscopy

High-content screening (HCS) for oxidative stress-dependent cytotoxicity in particle exposed cells was conducted according to a previously detailed protocol.[18] Briefly, cells were seeded in each well of the clear bottom 384 well black plate (Thermofisher) at a density of 2000 cells/well overnight for attachment. On the second day, 100 µg/mL particle suspensions were suspended in serum free culture media to perform two-fold serial dilutions until concentrations of 1.5625 µg/mL were reached for all particle samples. The cells were then exposed to 30 µL of media containing incremental concentrations (1.5625 -100 µg/mL) of particles and kept incubated for another 24 h. The positive control was $AgNO_3$ solution prepared the same way as the other particles with the same concentration range. After 24 h of incubation, four fluorescent dye mixtures (cocktails) were prepared and added to different wells by mixing wavelength-compatible dyes (Molecular probes, Invitrogen, Carlsbad, CA, USA) in DPBS buffer for both types of cells. The first cocktail consisted of Hoechst 33342 (1 µM), 2',7'-dichlorodihydrofluorescein diacetate (DCF) (10 µM), and LysoTracker (75 nM); the second cocktail was comprised of Hoechst 33342 (1 µM), Fluo-4 (5 µM) and propidium iodide (PI) (5 µM); the third cocktail contained Hoechst 33342 (1 µM) and MitoSox Red (5 µM); and the last cocktail included Hoechst 33342 (1 µM) and JC-1 (1 µM). Thirty microliter (cocktail 1 and 2) or 20 µL (cocktail 3 and 4) of dye mixture was added to each well in the 384 well plate incubated for 30 min under standard culture conditions in the dark. Fluorescence images of the cells from each microplate well were captured with a Zeiss Cell Discoverer 7 (Carl Zeiss). Three pictures were collected from each well in three different positions (upper middle, middle, and lower middle section of the well) under 10x magnification.

The captured images were processed with the Zeiss ZEN software. The number of cells in each picture was counted based on morphological features of the nucleus stain. For data analysis, the sum of intensity of each channel from each well was normalized by the number of cells. A heatmap was constructed for each dye corresponding to its respective assay by calculating strictly standardized mean difference (SSMD) with respect to negative control (cells exposed to serum free media).[19] Samples with a SSMD score below 1 signified weak difference from the control and were colored green, SSMD scores between 1 and 2 denoted moderate difference from the control and the samples were colored yellow, SSMD scores between 2 and 3 indicated fairly strong differences and were colored orange, and SSMD scores above 3 represented samples that were strongly different from the control and were colored red. The average of the three pictures were used as the result per well, and the average of the four replicates was used as the result for each sample.

4.3.11. Effect of NPs on allergen delivery and allergen responses in model GI epithelium

The effects of the NPs on antigen delivery and allergy response in the intestinal barrier were assessed by a co-culture system that consisted of differentiated Caco-2 cells and mast cells (LUVA) using transwell cell culture inserts. Caco-2 cells were cultured on transwell inserts (polycarbonate membrane filters, 0.4 μm pore size, 1×10^8 pores/cm) (Corning Incorporated) at 5×10^4 cells/cm^2. The inserts were placed in 24 well plates and 600 μL complete DMEM culture media was added to the basolateral chambers. Media were refreshed every two to three days until 21-25 days for differentiated and complete formation of cellular junction complex.

LUVA cells purchased from Kerafast (Massachusetts, USA) were used as human mast cell model as they are used routinely for allergy related studies.[20] The cells were cultured using StemPro®-34 SFM serum free medium for hematopoeitic stem cells (Thermofisher) supplemented with StemPro®-34 SFM nutrient supplement (Thermofisher), 1% PEN-STREP (WISENT), 2 mM L-glutamine (Thermofisher) and 100 µg/mL Primocin (Thermofisher). The cells were incubated at 37 °C and 5% CO_2 with 95% humidity. The cells were harvested with gentle pipetting and sub-cultured or seeded into multiwell plates for future experiments.

Two days before the assay, LUVA cells were seeded at a density of 200,000 cells/well in empty wells of the 24 wells plate (37°C at 5% CO_2) and were kept separate from the Caco-2 cells. One day before the assay, the Caco-2 cells in the apical compartment were exposed to 100 µg/mL particle suspensions in serum free media (25 µg/mL for AgNPs) for 24 h. The cells used as positive controls were exposed to 25 mM EDTA and the cells used as negative controls were exposed to serum free media. The mast cells were sensitized overnight with milk allergy patients' sera diluted in Tyrode buffer (135 mM NaCl, 5 mM KCl, 1.8 mM $CaCl_2$, 1 mM $MgCl_2$, 5.6 mM glucose, 20 mM HEPES) in the ratio of 1:50.

On the day of exposure, the particle suspensions in the apical compartment were replaced with commercial skim milk (centrifuged at 15,000 g for 10 min before sampling the supernatant). For LUVA cells, the sensitization solution was aspirated and replaced with 600 µL of culture media mixture (the ratio of serum free DMEM media to StemPro®-34 SFM complete media was 1:3). Then the inserts containing milk exposed Caco-2 cells were transferred to the wells that seeded with mast cells and incubated for 6 h at 37 °C and 5% CO_2 before sampling.

In order to measure the amount of milk allergens delivered to the basal compartment during the exposure, ELISA assays targeting one of the major milk allergens β-lactoglobulin were performed. Supernatant from each basal compartment of the transwell plate was sampled 6 h after milk exposure and diluted 3 in 2 with 0.1 M Na_2HPO_4 coating buffer (Sigma), and 100µL of the resulting mixture was added to 96 well plates and kept at 4 ºC overnight. The next day, the solution was discarded from the plate and the wells were filled with 100µL blocking buffer that contained 2% BSA (Thermofisher) in 1X Tris-buffered saline (TBS) buffer. The buffer was prepared as 10 mM Tris (Sigma) and 150 mM NaCl (Bishop, Canada) in deionized water with pH adjusted to 7.5 with HCl (Sigma). After 1 h incubation, the blocking buffer was discarded and replaced with 100 µL primary antibodies diluted in blocking buffer (1:5000) and incubated for 1 h at RT. The primary antibody solution was aspirated, and the wells were washed with washing buffer (0.05% Tween-20 in TBS) for 4 times before adding 100 µL secondary antibody (Abcam, USA) diluted 1:10000 in blocking buffer for 1 h at RT. The wells were washed again for 4 times with washing buffer after discarding the secondary antibody solution. The substrate solution of 0.25 mg/mL 3,3',5,5'-tetramethylbenzidine (TMB) (Sigma) dissolved in 0.1 M citric acid buffer (pH 5) that also contained 0.625% of acetone, 5% methanol and 0.009% H_2O_2 was prepared and 100 µL was added to each well for 3 min before adding 100µL 0.2 M H_2SO_4 stop solution. The absorbance was read at 450 nm by Spectramax i3x plate reader (Molecular Devices).

TEER measurements were taken at 2, 4, 6, 8,10 and 24 h after the addition of NMs by the Millicell-ERS system (ERS-2 Epithelial Volt-Ohm Meter, Millicell). Changes in TEER values of samples was recorded in duplicates. On the next day of exposure, 50 µL of supernatant was taken from the basal compartment after milk exposure and mix with 50 µL substrate solution (1 mM p-nitrophenyl-N-acetyl-b-D-glucopyranoside (PNAG) in 50 mM citric buffer) and incubated for 90

min at 37 °C. For the positive controls of degranulation assay, 0.1% Triton X-100 in Tyrode buffer was added to the basal compartment for 1 h. The reaction was stopped with 100 µL glycine solution (0.1M) and absorbance was read at 405 nm using Spectramax i3x plate reader (Molecular Devices). β-hexosaminidase release was expressed as the percentage of total cell content after subtracting background release from unstimulated cells. All experiments were performed in triplicates.

4.4. Results

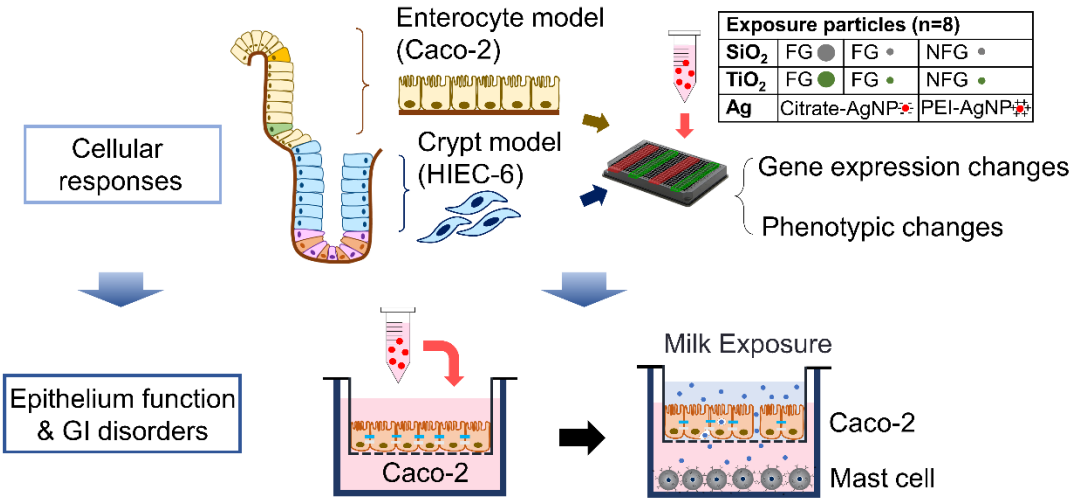

Figure 4.1 Conceptual diagram of the experimental design

4.4.1. Particle characterization

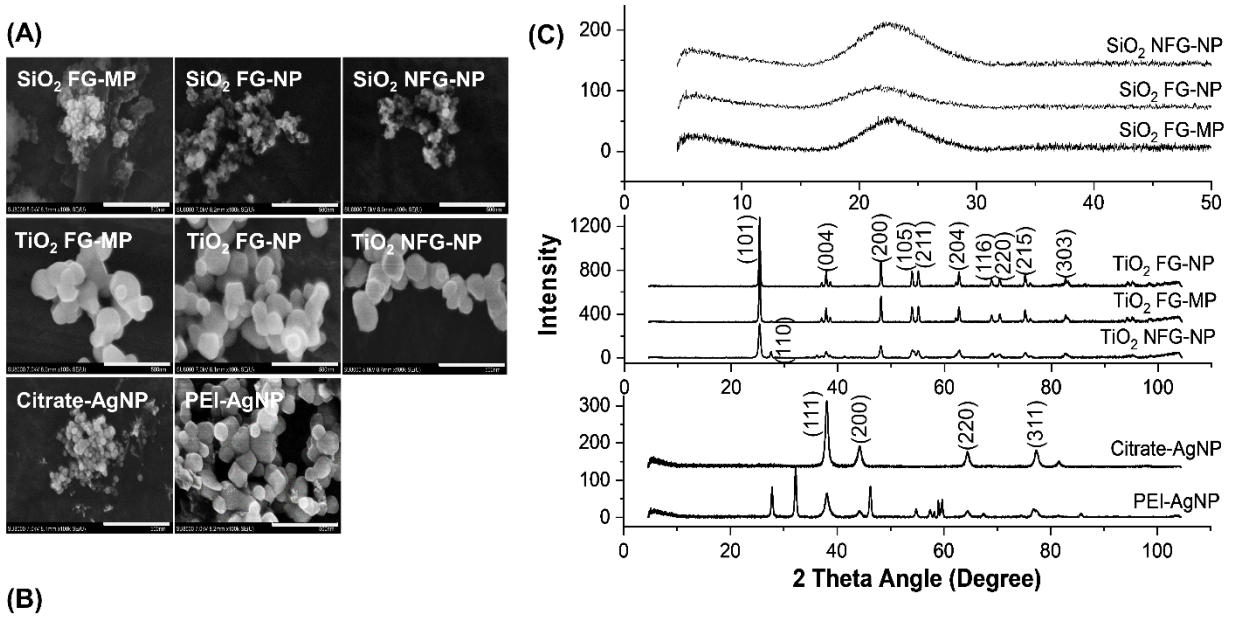

(B)

Sample		SiO_2 FG-MP	SiO_2 FG-NP	SiO_2 NFG-NP	TiO_2 FG-MP	TiO_2 FG-NP	TiO_2 NFG-NP	Citrate-AgNP	PEI-AgNP
Zeta potential [mV]		-39.26 ± 8.252	-29.15 ± 4.688	-33.67 ± 2.086	-27.72 ± 0.347	-35.49 ± 1.633	-13.50 ± 0.771	-33.82 ± 2.30	21.87 ± 0.686
Dynamic Size [nm]	Water	527.7 ± 117.9	361.5 ± 8.75	352.8 ± 18.9	343.9 ± 13.25	350.6 ± 15.91	330.6 ± 18.5	54 ±22.04	69.4 ± 11.31
	Media	929.6 ± 20.51	317.9 ± 19.72	340.1 ± 5.34	948.4 ±11.31	776.7 ± 172.5	572.8 ± 27.9	108.4 ±1.48	269.9 ± 35.65

Figure 4.2 Characterizations of the particles including: (A) Representative Scanning Electron Microscopy (SEM) images (scale bar=500 nm); (B) hydrodynamic diameter and zeta potential of particles suspended in water and in serum free culture media measured by dynamic light scattering; and (C) X-ray diffraction spectra of studied particles provided for dry particles.

In this study, we used FG and NFG SiO_2 and TiO_2 acquired from commercial suppliers, while AgNPs of positive and negative surface charges were synthesized in our laboratory. Primary particle size and morphology were characterized by SEM (Figure 4.2A), agglomeration sizes and zeta potential in water and cell culture media were measured by DLS (Figure 4.2B), and crystalline structures by XRD (Figure 4.2C). Representative Transmission Electron Microscopy (TEM)

images and DLS graphs for selected NPs were presented in SI (Figure 4.9). All types of silica particles were constituted by agglomerates of spherically shaped particles with a primary diameter of about 30 nm. Food-grade microparticles of SiO_2 also contained aggregated primary particles of size ~30 nm that yield MPs of size 1 μm. TiO_2 NPs were about 100 nm in dry state (from SEM images in Figure 4.2A), but their hydrodynamic diameter increased significantly when these particles were suspended in water and cell culture media. Citrate-AgNPs were smaller (25-50 nm) with uniformed size in dry state compared to PEI-AgNP (50-100nm), but larger particles for both were detected when suspended in cell culture media (>100 nm). The zeta potentials of all particles suspended in water and culture media were negative except PEI-AgNP (with cationic surface coating) (Figure 4.2B). We confirmed that SiO_2 particles were amorphous (broad peak from the XRD spectra) (Figure 4.2C). The major constituent of the three tested TiO_2 particles was anatase TiO_2, but NFG also contained rutile phase TiO_2. Signature peaks corresponding to Ag were found in both AgNPs with identified face-centered cubic structure.

4.4.2. Cellular responses

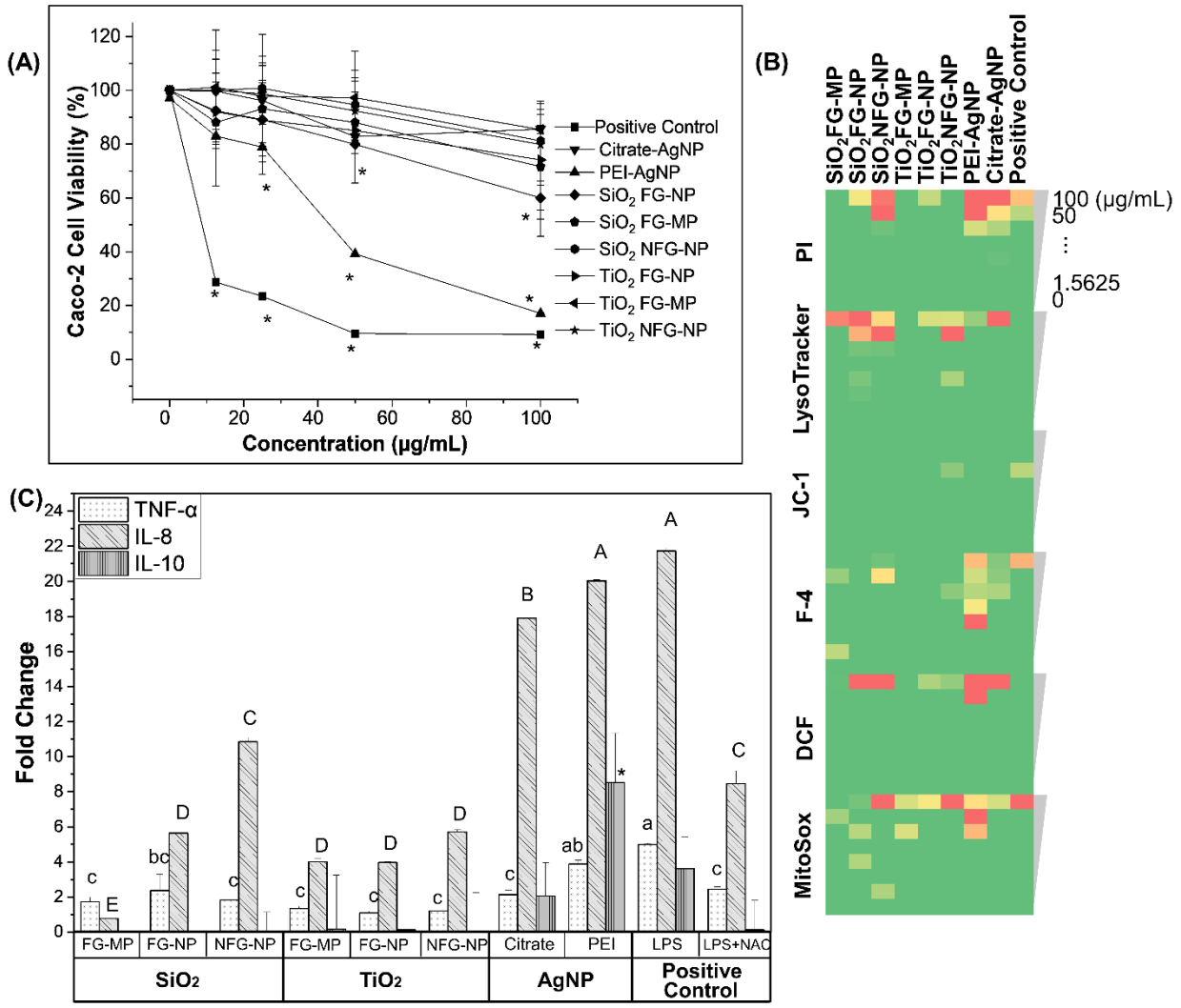

Figure 4.3 Concentration dependent cellular responses after 24 h exposure to incremental concentrations of particles. (A) Resazurin assay was conducted on confluent Caco-2 cells exposed to tested particles. Cell viability is expressed as % change relative to negative control (blank, no particle exposure) (n=3, *p<0.05). (B) Heatmap summarizing strictly standardized mean difference values was calculated from high-content screening (HCS) results for cellular responses in Caco-2 exposed to of tested particles. Green colors indicate no significant toxic effects compared to the negative control (blank) while red indicates significant differences in cellular responses. The measured cellular responses are designated with the fluorophores used in the respective assays as: (i) PI = cell membrane permeability *via* propidium iodide uptake. (ii) LysoTracker = acidic organelles (iii) JC-1 = perturbation of mitochondrial membrane potential measured by JC-1. (iv) F4 = intracellular Ca^{2+} flux measured by Fluo-4. (v) DCF = intracellular reactive oxygen species measured by DCF. (vi) MitoSox = mitochondrial superoxide generation measured by MitoSox Red. Representative pictures from HCS of selected NPs are displayed in Figure 4.14. (C) The release of TNF-α, IL-8 and IL-10 in Caco-2 monocultures after 100 µg/mL particle exposure (25 µg/mL for PEI-AgNP) was measured by ELISA. The results are expressed as fold change relative to negative control (bars represent the mean ±SD values, n=3/bar). Statistical significance was analyzed by one-way ANOVA test (Tukey, p<0.05). The results are presented using asterisk for IL-10 with it indicating significant difference from negative control. Lower case letter was used for TNF-α and upper-case letter for IL-8, with different letters representing significant differences from each other.

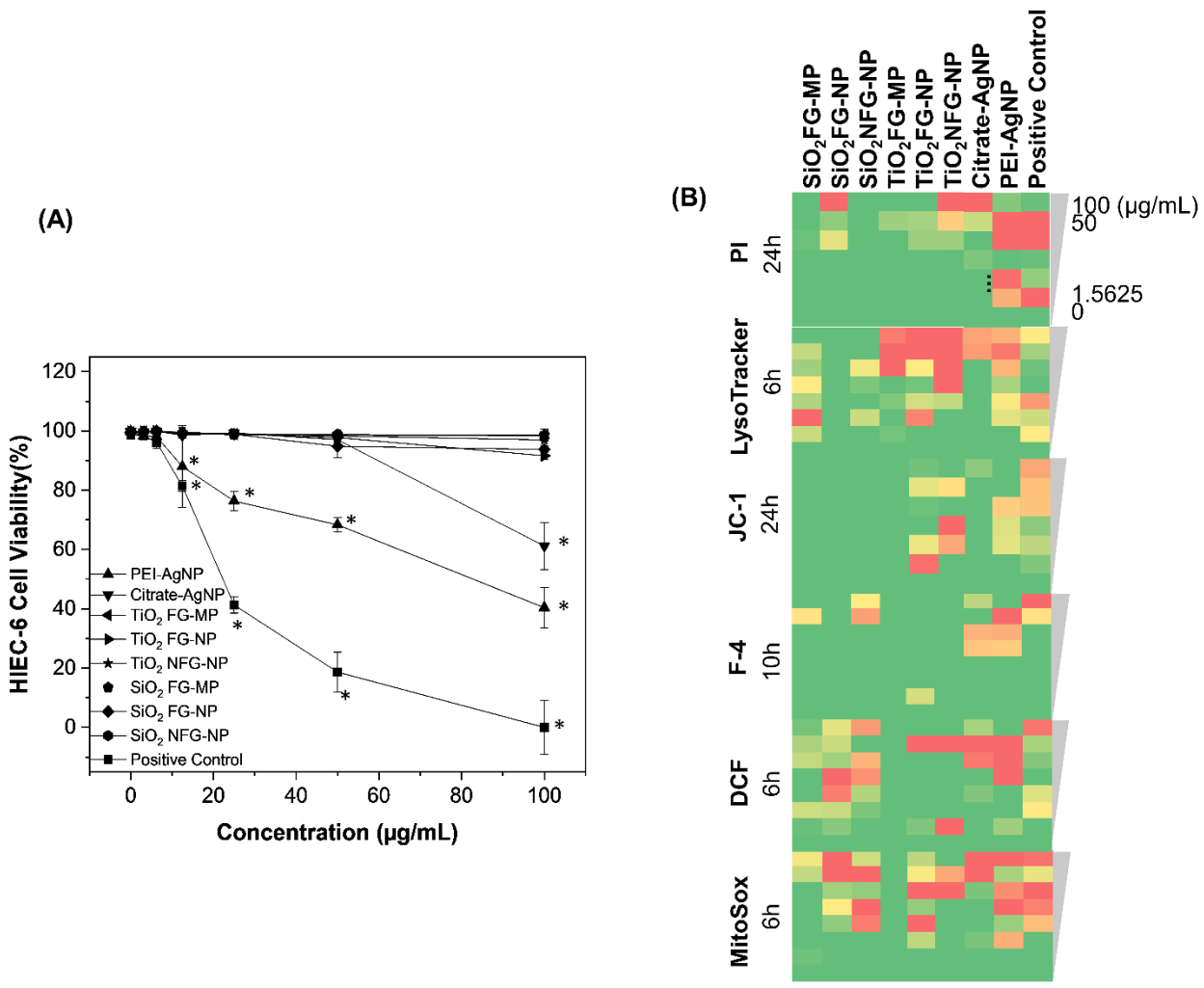

Figure 4.4 Concentration dependent cellular responses following 24 h exposure to incremental concentrations of particles. (A)Resazurin assay was conducted on confluent HIEC-6 cells exposed to tested particles. Cell viability is expressed as % change relative to negative control with no particle exposure (n=3, *p<0.05). (B) Heatmap summarizing strictly standardized mean difference values was calculated from high-content screening (HCS) results for cellular responses in HIEC-6 cells exposed to tested particles. The rows and columns in the heat map correspond to the concentration range and sample types, respectively. Green colors indicate no significant toxic effects compared to the negative control (blank) while red indicates significant differences in cellular responses. The measured cellular responses are designated with the fluorophores used in the respective assays as: (i) PI = cell membrane permeability *via* propidium iodide uptake. (ii) LysoTracker = acidic organelles (iii) JC-1 = perturbation of mitochondrial membrane potential measured by JC-1. (iv) F4 = increased intracellular Ca^{2+} flux measured by Fluo-4. (v) DCF = intracellular reactive oxygen species measured by DCF. (vi) MitoSox = mitochondrial superoxide generation measured by MitoSox Red. Representative pictures from HCS of selected NPs are displayed in Figure 4.14.

4.4.3. AgNPs but not SiO_2 and TiO_2 particles reduced cell viability

In order to investigate the different mechanisms mediating NP-induced responses, treatment-related cellular and sub-cellular effects were investigated. Of the eight different types of particles investigated, PEI-AgNPs were the most potent and caused no less than 20% loss of cell viability at a concentration of 25 µg/mL (Figure 4.3A and Figure 4.4A). Although SiO_2 FG-NPs and MPs at 100 µg/mL also showed statistically significant cytotoxic effects, neither particle induced more than 20% reduction in cell viability. For the remaining five tested particles, we found no evidence of cytotoxicity at any of the test concentrations.

4.4.4. Sub-lethal effects after particles treatment

Oxidative stress has been recognized as a key mechanism underlying NP toxicity. This study confirmed that SiO_2, TiO_2 and AgNPs may induce intracellular reactive oxygen species (ROS) production from DCF assay (Figure 4.3B, Figure 4.4B). Specifically, PEI-AgNPs induced a significant increase (strictly standardized mean difference (SSMD) ≥2) in mitochondrial ROS (Mitosox Red assay) at concentrations of 3.125 µg/mL for HIEC-6 cells and 25 µg/mL for Caco-2 cells, respectively. Comparatively, HIEC-6 cells were more sensitive than Caco-2 cells as evidenced in the heatmap with more red colors in lower exposure concentrations (Figure 4.3B *vs.* Figure 4.4B). The measured changes in the cellular oxidative stress level were also supported by gene expression data for Caco-2 cells, where exposure of cells to AgNP resulted in the highest fold changes in the expression of all three key oxidative stress genes (catalase, HO-1 and GST) (Figure 4.11). Exposure of cells to SiO_2 NPs resulted in the formation of intracellular ROS only at the highest test concentration (Figure 4.3B), and this response was supported by changes in the

expression of catalase and GST genes (Figure 4.11). TiO_2 NPs exposure did not result in changes in ROS levels, though an increase in GST expression was observed. In addition to these findings, the HCS data for HIEC-6 cells (Figure 4.4B) revealed time dependent responses for lysosome destabilization, ROS production, followed by Ca^{2+} flux changes, mitochondrial depolarization. However, Caco-2 cells were less sensitive to particle treatments for the previously mentioned responses and only measured difference from 25 μg/mL and above (except for Ca^{2+} flux changes at 6.25 μg/mL) after 24 h exposure.

To characterize cellular inflammatory responses following particle exposure, cytokines were measured using ELISA assays. For both pro-inflammatory markers (IL-8 and TNF-α), significant increases from negative control were observed following AgNP exposures (Figure 4.3C). PEI-AgNPs treated cells measured 2 times higher IL-8 release than SiO_2 NPs treated cells and 3 times higher than TiO_2 NPs exposed cells. For various forms of each particle, the amount of IL-8 and TNF-α produced by SiO_2 NPs exposed cells were higher than those treated with MPs, but such difference was not observed in TiO_2 treated cells. Significant increase in anti-inflammatory cytokines IL-10 was observed only after AgNPs exposure.

4.4.5. Junctional protein distribution and epithelial barrier function

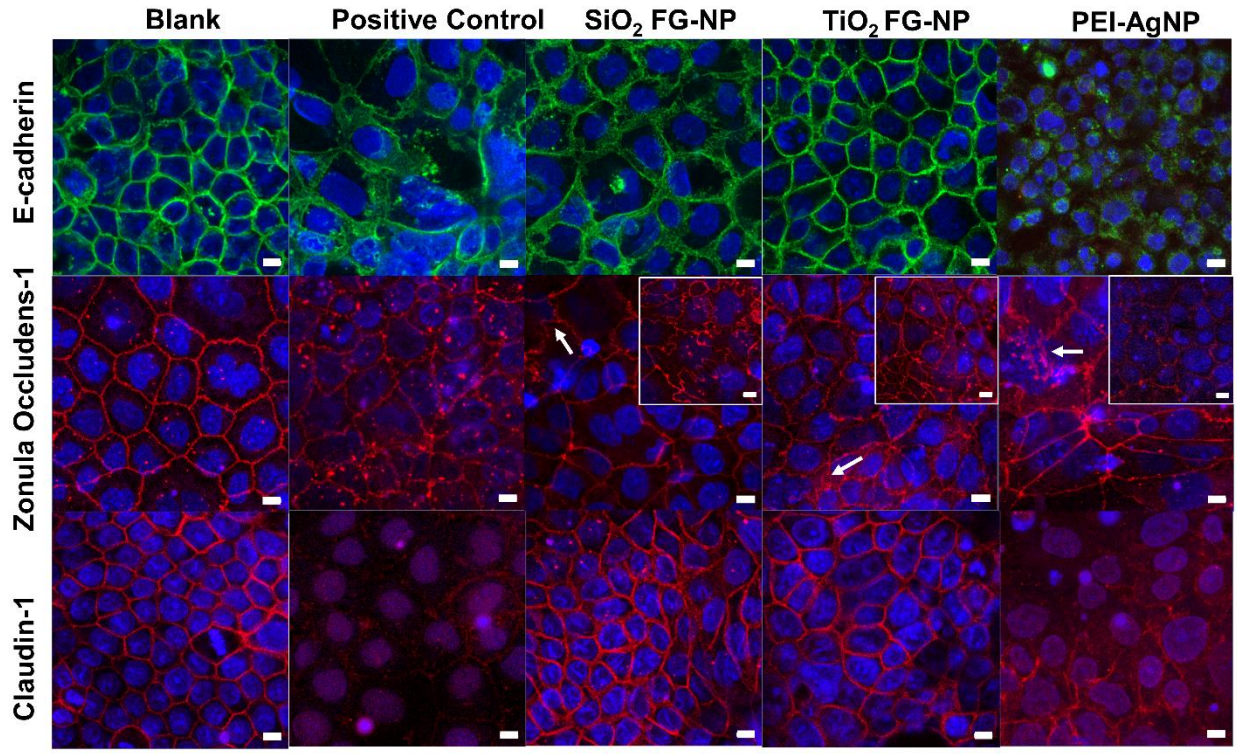

Figure 4.5 Representative confocal microscopy images of Caco-2 cells with and without 24 h exposure to 100 µg/mL NPs (25 µg/mL for PEI-AgNPs) after staining for junction protein complexes (Claudin-1, Zonula Occludens-1, E-cadherin). Nucleus was stained by Hoechst 33342 (blue), E-cadherin was conjugated with anti-E-cadherin antibody and stained by Alexa-488(green). ZO-1 and Claudin-1 were conjugated with specific antibodies and stained by Alexa-594(red). Arrows indicated the change in pattern of ZO-1. Inlet images captured more prominent effect after 4 days exposure. Scale bar=10 µm. Images for other particle treatments are presented in Figure 4.15.

Analysis of laser scanning confocal microscopy images of cellular components and junction proteins stained with fluorophores identified changes at the cellular junction complexes after particle exposure. In media control cells (blank), E-cadherin, ZO-1 and Claudin-1 were seen at cell–cell contact zones forming distinct and intact rings around the periphery of individual cells (Figure 4.5). We did not observe changes in E-cadherin staining pattern in cells treated with TiO_2 NPs. Cells treated with SiO_2 FG-NP shared widened and diffused E-cadherin staining pattern

while those exposed to AgNP showed discontinuous staining at cell junctions (Figure 4.5). For TJ proteins, the fluorescence intensity of Claudin-1 decreased significantly at cell junctions of AgNPs treated cells compared to the negative control. Images of cells exposed to all NPs treatment showed a similar decrease in fluorescence intensity and Claudin-1 distribution. Interestingly, there was also an irregular, zig-zag shaped pattern (Figure 4.5, shown by arrow) observed in ZO-1 staining for all NPs. Such effects were more prominent for cells exposed to NPs for 4 days (inlet images). All in all, the imaging results for the three junction proteins suggested alteration of the apical TJ complex (ZO-1 and Claudin-1) and AJ complex (E-cadherin) in the case of SiO_2 FG-NP but not TiO_2 FG-NP.

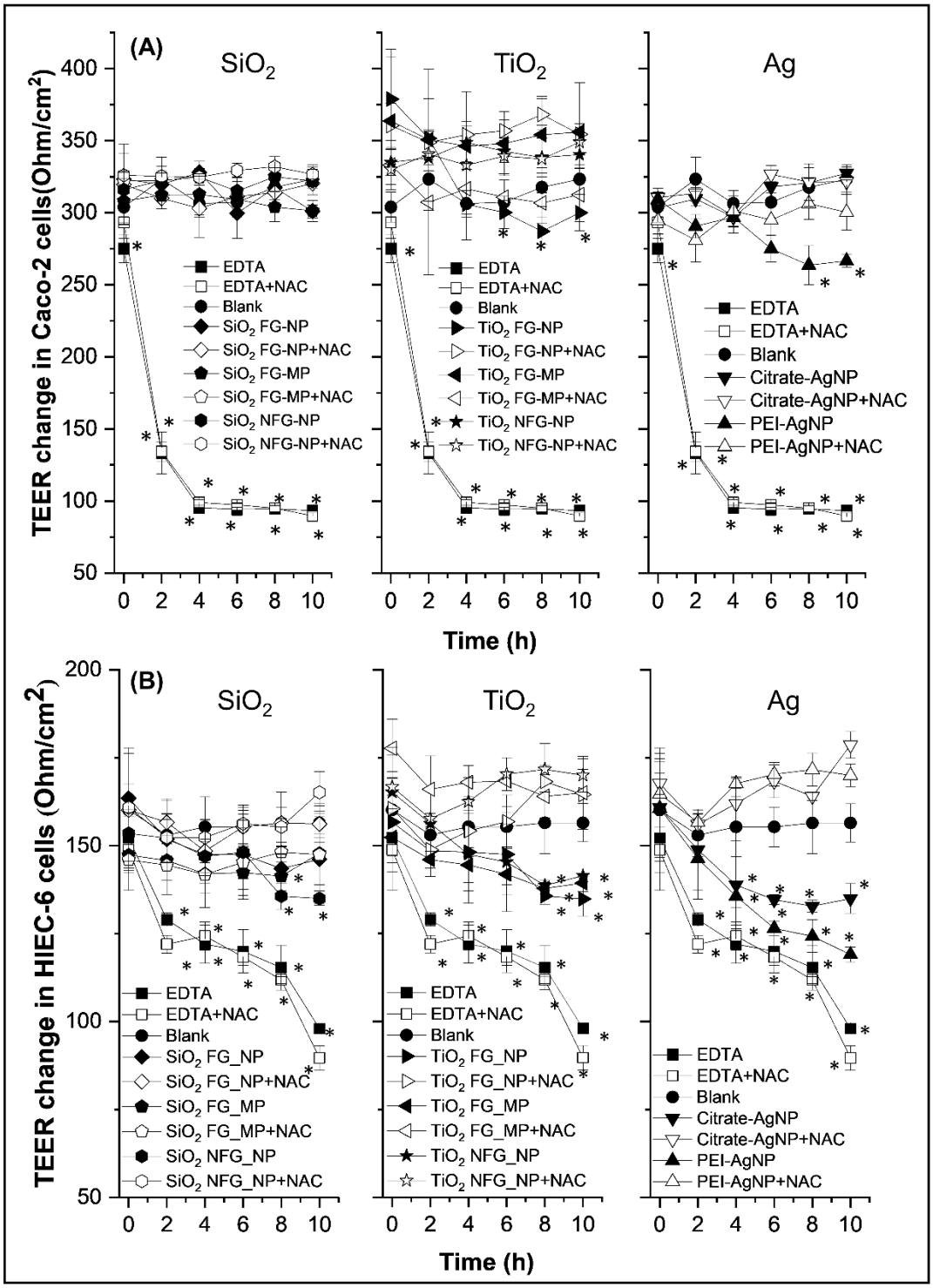

Figure 4.6 Results of the transepithelial electric resistant assay to detect epithelial layer leakage in (A) Caco-2 cell and (B) HIEC-6 cells. Mean values were calculated from at least two independent experiments having duplicate samples (data presented as mean±SD, n=2, *p<0.05).

After probing the changes in the junctional protein complex, we further explored the functional changes for the epithelial layer by measuring TEER. Exposure of the differentiated Caco-2 cells to NPs did not trigger significant changes in TEER except in the case of PEI-AgNP (Figure 4.6A). The decreased TEER values recovered after NAC addition to cells exposed to PEI-AgNPs thus suggesting a role for oxidative stress in increasing epithelial membrane permeability. Compared to Caco-2 cells, AgNP treated HIEC-6 cells experienced more significant TEER changes following relatively short exposure periods (Figure 4.6B). Similar findings were found in FITC-dextran transport assay (Figure 4.16) performed following the TEER assay. Confocal fluorescence images of the Caco-2 cells cultured on the transwell insert showed that FITC-dextran particles were localized at the cell junctions for negative control, SiO_2 FG-NP and TiO_2 FG-NP exposed cells (Figure 4.16). Localization of FITC-dextran particles was also observed on Citrate-AgNP treated cells with visually decreased intensity. PEI-AgNP exposed cells did not observe the uniform green fluorescence from FITC at cell junctions and decreased fluorescence intensity (Figure 4.16), indicating the passage of the FITC-dextran particles.

4.4.6. Antigen delivery and allergic responses

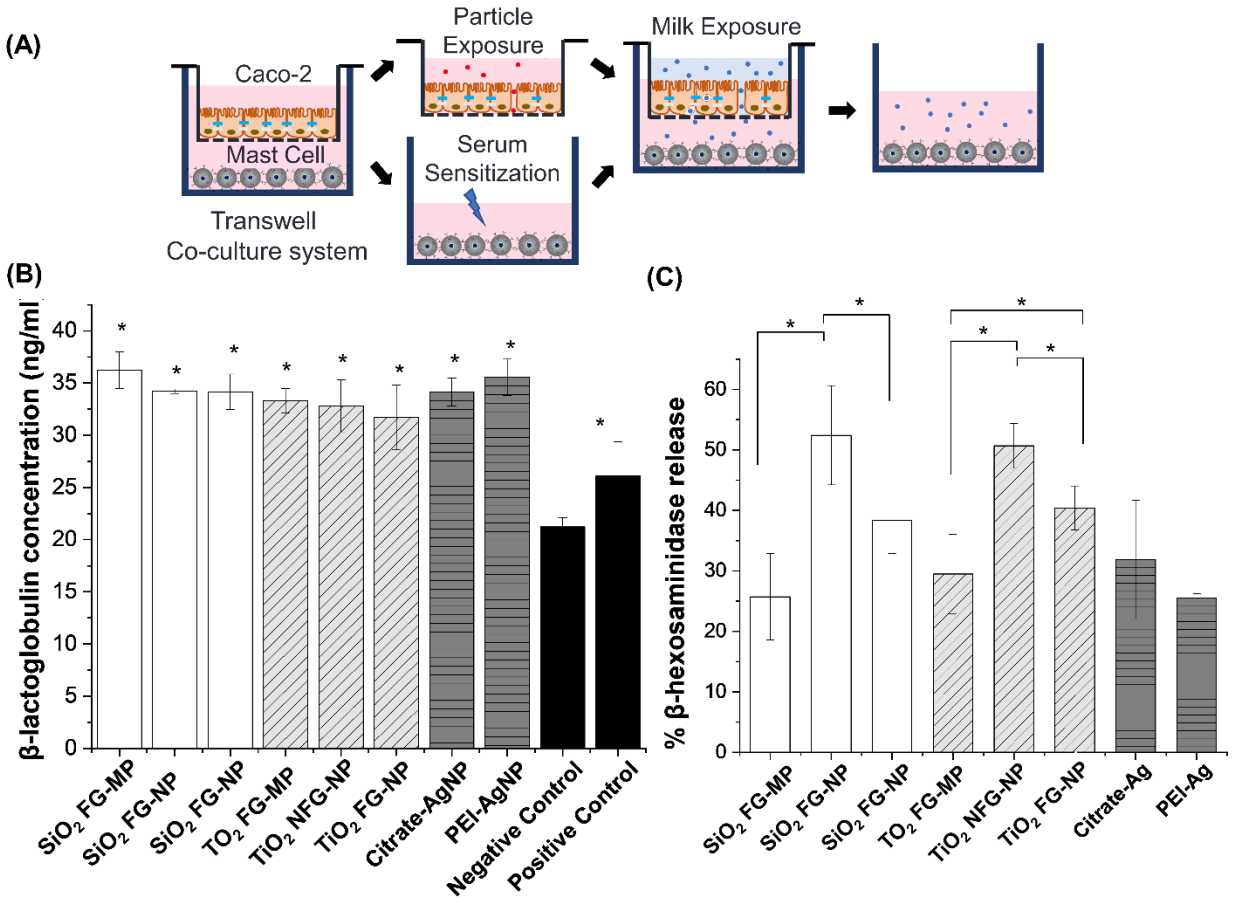

Figure 4.7 Transwell co-culture system designed to evaluate the effect of dietary particles on milk allergens delivery across intestinal epithelium and antigenic responses. In this (A) transwell co-culture system, Caco-2 cells were cultured and differentiated on the apical compartment and human mast cells (LUVA) were cultured separately in the basal compartment. Particles were exposed cells in the apical compartment for 24 h while mast cells were sensitized with milk allergy patients' sera. The particle suspension was replaced with milk for 6 h and the solution in the basal compartment was collected and quantified for (B) β-Lactoglobulin as a proxy of milk allergen content using ELISA and (C) mast cell (LUVA) degranulation (bars presented as mean±SD, n=3, *p<0.05).

The co-culture system consisting of Caco-2 cells and mast cells was established as an *in vitro* intestinal model aimed to understand the changes in epithelial barrier function mediated by NPs and the resulting effect on antigen delivery. After 24 h exposure, decreased TEER was observed in positive control (25 mM EDTA) and PEI-AgNP treated monolayers (data not shown). The ELISA assays for β-lactoglobulin were used to detect the common antigens for milk allergic

patients. The results indicated increased β-lactoglobulin delivery across epithelial layer in all sample treatments, but the amount of delivered antigens was not differentiable between different particle exposure (Figure 4.7B). Milk exposure for 6 h attained significant increase in β-Hexosaminidase release for all treatment groups (Figure 4.7C). We also noticed that NPs caused greater effect in mast cell degranulation compared to MPs, and FG NPs induced greater increase in β-Hexosaminidase release compared to NFG NPs.

4.5. Discussion

The rising nanotechnology applications in food and agriculture has increased human oral exposure to NPs despite the lack of sufficient knowledge on the health consequences of ingested dietary NPs.[21] In the current study we investigated common dietary NPs (SiO_2, TiO_2 and Ag), and demonstrated their cellular impacts on the GI system using two *in vitro* cell models (Figure 4.1). In all measured assays, AgNPs were the most potent of the three types of particles studied, while SiO_2 and TiO_2 exhibited milder toxic effects depending on the cell model and assay. Generally, HIEC-6 cells were more sensitive than Caco-2 cells (e.g., sublethal effects after 6 h NP exposure at 3.125 µg/mL in HIEC-6 cells *vs.* after 24 h exposure at 6.25 µg/mL for Caco-2 cells). We further demonstrated increased allergen delivery across epithelial layer and enhanced antigenicity of milk allergens as consequences of particle mediated changes in epithelial integrity.

NP-induced cell injury has been reported in several studies that emphasized the importance of ROS generation and oxidative stress as key early events mediating cellular responses.[22] Our study found that the production of intracellular ROS following 24 h exposure of 100 µg/mL all three types of

NPs. PEI-AgNPs were the most potent and were able to induce significant ROS generation at the lowest exposure concentration compared to the rest of particles. This high potency of PEI-AgNP might be attributed to the high cationic charge-density of PEI coated on the surface of PEI-AgNPs, which may interact with negatively charged cell membrane and facilitate cellular uptake compared to the negatively charged Citrate-AgNPs (Figure 4.10). The increased uptake may enhance Ag+ ion dissolution and accumulation inside cells, cause excess chloride influx, osmotic swelling and lysosome rupture according to the proton sponge theory. [23, 24] The decreased pH will further facilitate the intracellular dissolution of Ag^+ and induce downstream responses like ROS production.[25] The exposure of 100 µg/mL SiO_2, TiO_2 and Citrate-AgNPs could not initiate direct cell damages compared to PEI-AgNPs. However, the disruptions in the cellular redox homeostasis may further interplay with the changes in the spatiotemporal profiles of intracellular Ca^{2+} flux and mitochondrial activities.[26] The cellular responses mentioned above concurred with the "two-hit" theory, where Ca^{2+} flux changes coupled with other pathological stimulus may trigger mitochondrial dysfunction, one of the major checkpoints of apoptotic and necrotic cell death.[27] ROS overload may also trigger a cascade of proinflammatory cytokines such as IL-1β, IL-8, and TNF-α and mediators *via* activation of redox sensitive signaling pathways.[28] Our study found increased expressions of IL-1β, IL-8, TNF-α in AgNP treated cells, and increased IL-1β and TNF-α expression were observed for TiO_2 treated cells (Figure 4.13), suggesting possible inflammatory processes in response to oxidative stress.[29] IL-10 release was observed in AgNP treated cells, suggesting that anti-inflammatory cytokine had been induced by the production of pro-inflammatory cytokines to antagonizes the oxidative damage.[30] The low level of IL-10 in SiO_2,TiO_2 treated cells might be attributed to the lower release of pro-inflammatory cytokines which required minimal anti-inflammatory cytokine to restore homeostasis.[31]

Cytokines and chemokines may affect the structure and functions of cell junction complexes. For example, TNF-α was found to dissociate Claudin-1 from the TJ and increase Claudin-2 expression.[32] However, in the current study, the observed increases in both expression and release of TNF-α (Figure 4.13 and Figure 4.3C) in NP-exposed cells was not associated with changes in Claudin expression (Figure 4.12). As such, it is possible that NP exposure influenced the turnover rate of claudin without changing its expression level in cells, and thus the retained TJ components continued to regulate the barrier function.[33] Previous studies have also suggested the possibility of a "partially disrupted" TJ induced by TNF-α following an apoptosis-independent mechanism, where activation of myosin light-chain kinase (MLCK) can reversibly increase the paracellular permeability without dramatic reorganization or disassembly of TJ structure.[34] This was also supported in the current study by the immunofluorescence staining images for TJ proteins, showing only minor redistribution of TJ proteins and broadened staining bands for AJ proteins without major defects in junction complexes (Figure 4.5). FITC-dextran transport assay also suggested no passage of dextran particles conjugated with FITC fluorophore for all particle treated cells (except for PEI-AgNP) where dextran particles were localized at the cell junction (Figure 4.16). The results suggested that an enhancement of constitutive TJ remodeling, rather than loss or dissolution of TJ protein occurred at the junction complex while the maintaining the AJ undisturbed, and thus maintaining the barrier function. For PEI-AgNP exposed cells, increased fluorescence intensity in the basal compartment media and discontinuous fluorescence staining confirmed the disrupted junction complex and increased epithelial permeability.

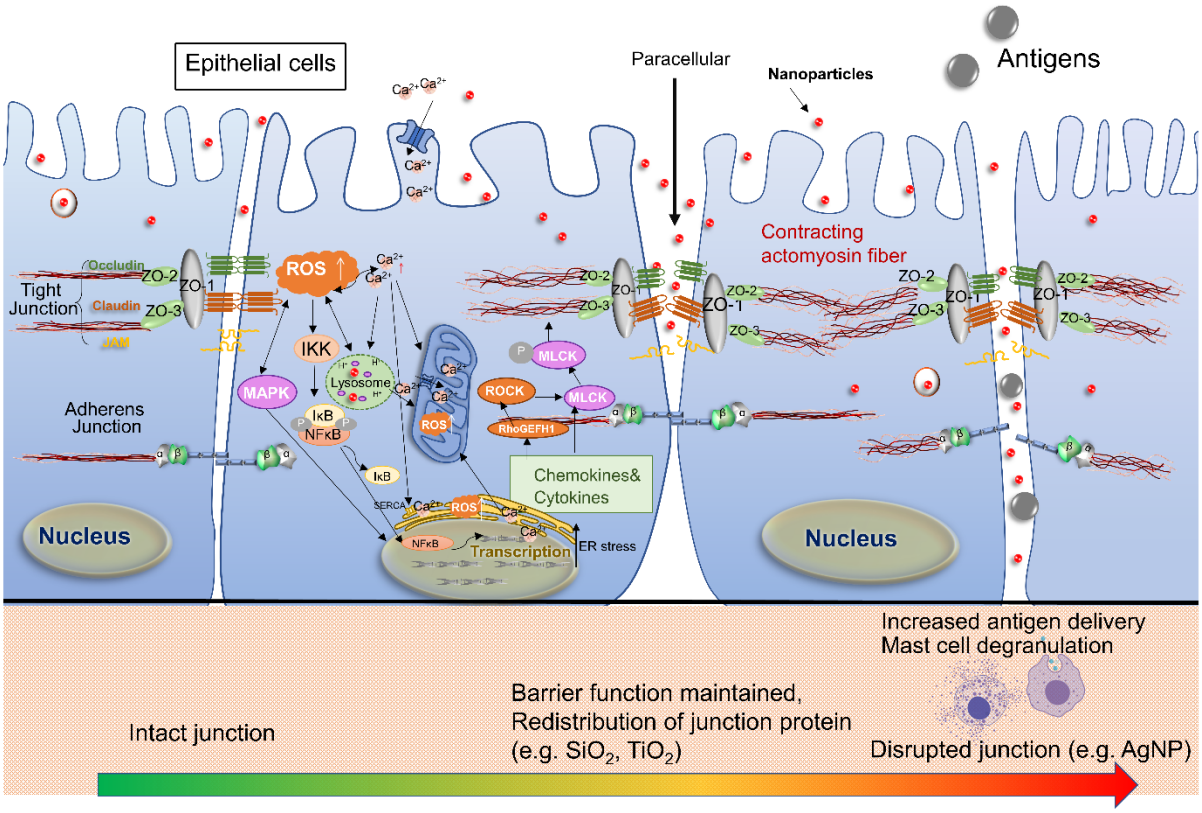

Figure 4.8 Proposed mechanism of NP-induced toxicity.

The proposed mechanism for disruption of junction complex is depicted in Figure 4.8 based on findings from this study and reports in literature.[27] Accordingly, we propose that NPs are first taken up by cells and transported by acidic organelles. Subsequently, the lysosomal release facilitates intracellular dissolution of Ag^+ ions and disrupts the oxidative stress homeostasis, which initiate changes in the intracellular calcium flux, ROS level and mitochondria membrane potential. The interplay between theses cellular responses further activate the nuclear factor kappa-light-chain-enhancer of activated B cells (NFκB) signaling pathway and affect the expression profiles and the release of inflammatory cytokines.[35] The inflammatory markers may then activate

signaling pathways involving rho kinase (ROCK) or MLCK, which regulate the junction complex stability *via* acting on the contraction of the actin filament that are linked to the junction complexes.[36] In the current study, we observed contraction of the actin filament in HIEC-6 cells (Figure 4.17) but not Caco-2 cells (Data not shown). This observation did not fully contradict a previous study from Cornu *et al.*that reported actin cytoskeleton disruption in FG SiO_2 treated Caco-2 cells only at 2 h after exposure probably due to the choice of measuring time, whereas the contraction of actin filaments had been restored from the tension stage by the time of the measurement.[7] Although the contraction of actin filaments was not able to alter the intestinal permeability in both studies, this destabilization might lead to partial disruption of the junction complex with undisturbed barrier function. Depending on the types of particles, epithelial layers exposed to SiO_2 and TiO_2 NPs may only experience partial remodeling of the junction complex without compromising barrier function, but may be disrupted completely following exposure to PEI-AgNPs. This particle-induced inflamed epithelium may further activate the immune system by stimulating the mast cells near the epithelium due to enhanced antigen exposure. We explored these possibilities by taking the delivery of food allergen across epithelial layer and antigenic response shown by primed mast cell.

Increased intestinal epithelial permeability plays a vital role in food hypersensitivity and exacerbates inflammation by introducing antigens *via* paracellular influx, which may underlie the pathogenesis of GI disorders like IBD.[37] The cross-linking between antigens and IgE antibodies on the surface of mast cells may initiate mast cell degranulation and release of pro-inflammatory mediators like β-hexosaminidase to further modulate epithelial permeability.[38] In addition to mast cells, intestinal epithelial cells also play active roles in antigen presentation and immunological

response due to the reaction with food allergens.[39] In the current study, NP-treated co-culture systems showed significantly higher delivery of β-lactoglobulins across the monolayer compared to the blanks and the positive control (Figure 4.7B), indicating that the paracellular transportation pathway might not be the only reason for this increased delivery within the 6 h exposure period. Instead, the enhanced transcytosis (endocytosis of the allergen from the upper chamber and exocytosis to the basal compartment) of β-lactoglobulins might be the major contributor. The turnover rate of allergen during transcytosis may be influenced by NP-induced cellular responses such as changes in Ca^{2+} influx, proton pumps, and endosome maturation due to the rate of the vesicle–plasma-membrane fusion.[40] However, no significant difference due to different particle treatment was observed, suggesting that the high delivery of β-lactoglobulins was not specific to particle types (Figure 4.7B).

All particle treatment significantly enhanced mast cell degranulation after milk exposure. We suspected the high β-hexosaminidase level to be first explained by the increased mast cell degranulation from enhanced antigen delivery (Figure 4.7B and C). Furthermore, the release might be enhanced by the lysosomal β-hexosaminidase from the Caco-2 monolayer during NP exocytosis due to the 24 h particle exposure prior to milk treatment.[41, 42] Notably, mast cell degranulation concorded with the release of pro-inflammatory cytokines in Caco-2 cells (Figure 4.3C). As evidenced in Figure 4.7C, NP treated epithelial layer also resulted in higher level of mast cell degranulation compared to MPs. As such, we argue that in addition to the enhanced deliver of allergens, the pro-inflammatory cytokines released by Caco-2 contribute to the enhanced degranulation. The results from the co-culture system confirmed the possible interference of dietary NPs on the antigen delivery and allergic responses across the intestinal epithelium.

4.6. Conclusion

This study investigated the effects of common dietary NPs on molecular, biochemical, and cellular level using cell line models, to investigate whether dietary NPs exposure could induce disruption of junction complex in epithelial cells and if this may subsequently lead to enhanced seepage and allergic response to food allergens. Based on the observed results, we propose a cascade of events following dietary NP exposure in human intestinal epithelial cells: oxidative stress coupled with changes in Ca^{2+} flux and impairment of mitochondrial function, followed by transcription of proinflammatory cytokines. These cytokines would activate signaling proteins to affect actin contraction and subsequent changes in cell junction. The results demonstrated that PEI-AgNP induced toxicity followed the complete proposed pathway, and resulted in disruption of cell junction complex and compromised intestinal barrier function. Highest concentrations (100 µg/mL) of SiO_2 and TiO_2 NPs partially followed this proposed pathway, and we found these NPs may cause remodeling in TJs while maintaining epithelial integrity. All types of particle treatment were able to increase the delivery of antigens across the intestinal epithelium and trigger allergic responses in pre-sensitized mast cells, but the allergic effects were more prominent in NPs exposed cells. The observations of this study revealed the potential adverse impacts of dietary NPs on human intestinal epithelium in affecting cellular junction complex, epithelium barrier function and subsequent antigen delivery and allergic responses under the scenario of cow's milk allergy. Although ingested NPs are unlikely to cause acute toxicity at the levels of daily exposure, synergistic effects that accompanied food allergy, long-term effects due to the changes in intestinal permeability and chronic oxidative stress deserve further recognition. Further chronic *in vivo* or *ex*

vivo exposure studies of these NPs are also suggested in order to appreciate the complexity of the human physiological systems and elucidate the actual effects of these NPs for risk assessment.

Taken together, the *in vitro* results in the current study probed possible mechanism of NP-mediated toxicity in intestinal cells and highlighted possible key early events in preclinical phase identifications of gastrointestinal disorders like IBD and allergy responses. The information may further complement preventatives strategies against GI diseases and emphasize the importance of including dietary NPs in food additives regulations.

4.7. Supplemental Information

4.7.1. Experimental Section

Table 4.1 Primers of selected genes. The primers used in study were selected from published literature and obtained from IDT, Iowa, USA

Gene		**Forward 5‘-3’**	**Reverse 5‘-3’**
Reference Gene	β-actin	CCACGAAACTACCTTCAAC	GATCTTCATTGTGTGCTGGG
	GAPDH	ATGGAAATCCCATCACCATCTT	CGCCCCACTTGATTTTGG
Inflammatory Response	TNF-a	CCCGAGTGACAAGCCTGTAG	GATGGCAGAGAGGAGGTTGAC
	IL-1β	CTGATGGCCCTAAACAGATGAAG	GGTGGTCGGAGATTCGTAGC
	IL-6	CCAGTACCCCCAGGAGAAGA	TTGTTTTCTGCCAGTGCCTC
	IL-8	CTGGCCGTGGCTCTCTTG	CTTGGCAAAACTGCACCTTCA
	IL-15	TGTTTCAGTGCAGGGCTTC	TTCCTCACATTCTTTGCATCC
Oxidative Stress	GSTP1	GGAGACCTCACCCTGTACCA	CTGCTGGTCCTTCCCATAGA
	HO-1	CAGGCAGAGAATGCTGAGTTC	GATGTTGAGCAGGAACGCAGT
	Catalase	AAGACCAGTTTACCAACTGGG	CAGATGGACATCGCCACATG
Epithelial and Mesenchymal cell markers	Claudin-1	AAGTGCTTGGAAGACGATGA	CTTGGTGTTGGGTAAGAGGTT
	Zonula occludens-1	ATCCCTCAAGGAGCCATTC	CACTTGTTTTGCCAGGTTTTA
	E-cadherin	TCCATTTCTTGGTCTACGCC	CACCTTCAGCCAACCTGTTT
	α-SMA	GTCCCCATCTATGAGGGCTAT	GCATTTGCGGTGGACAATGGA
	Vimentin	GCAGGCTCAGATTCAGGAACA	GTGAGGTCAGGCTTGGAAACA

4.7.2. Results

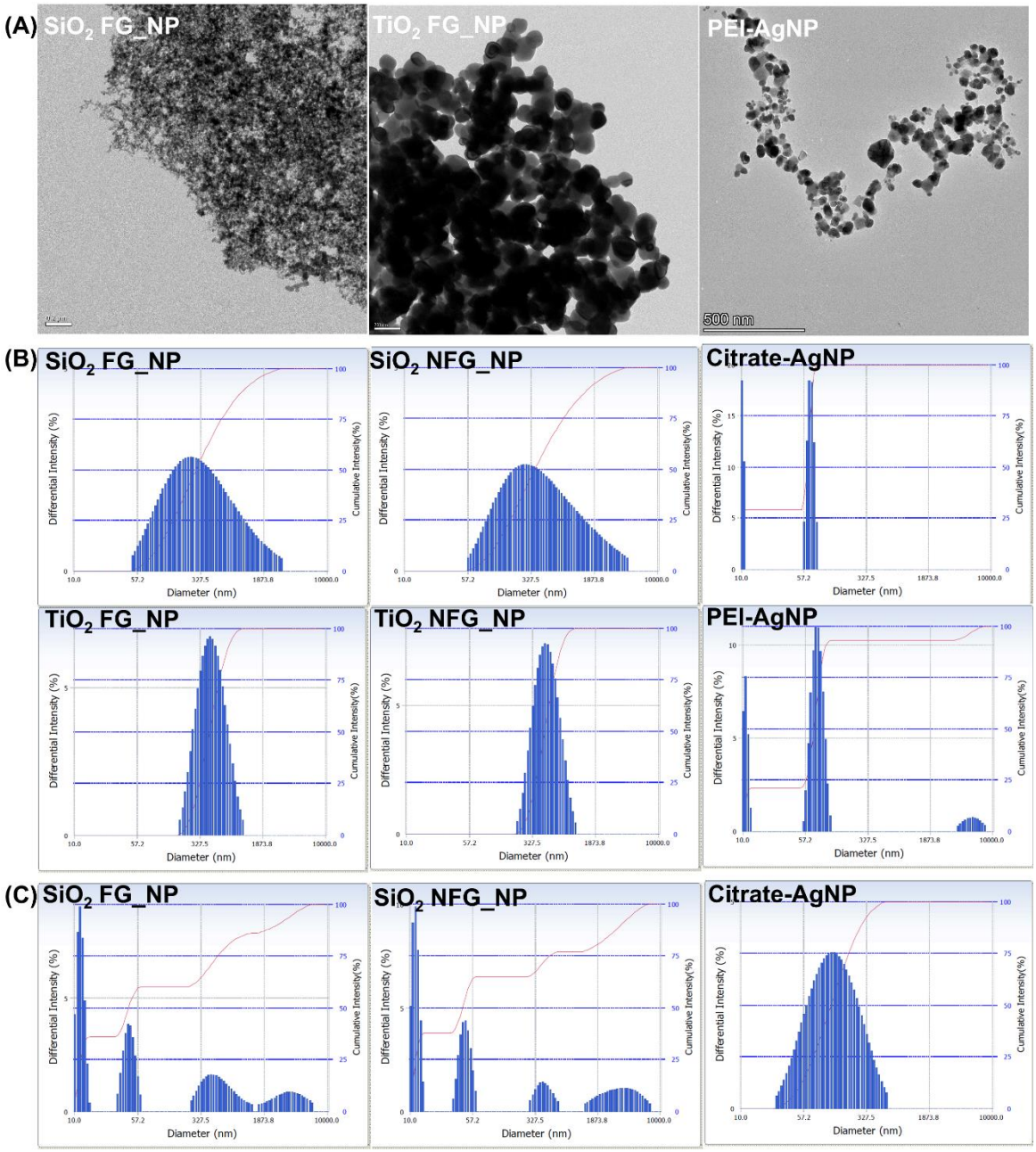

Figure 4.9 Characterization results for representative nanoparticles including (A) Transmission Electron microscopy (TEM) images for selected particles (scale bars for SiO_2 and TiO_2 particles are 200 nm and 500 nm for PEI-AgNP). DLS graphs for particle sizing analysis with representative particles suspended (B) in water and (C) in medium.

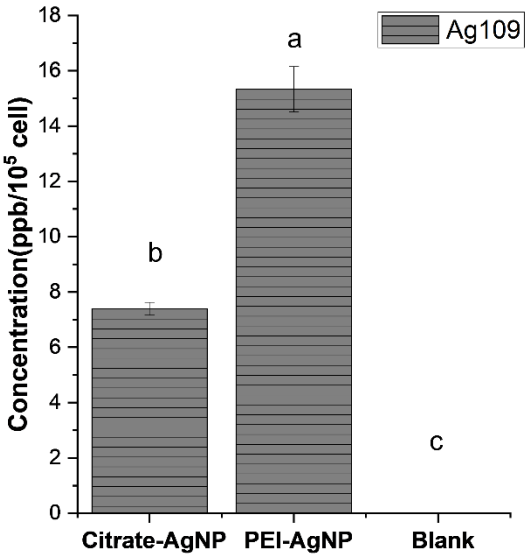

Figure 4.10 Cellular uptake of silver measured by ICP-MS. Cells exposed to two types of AgNPs were washed with serum free media and digested in 70% nitric acid at 90ºC for 1 h followed by 1 h H2O2 digestion before analysis. (n=2, compact letter display showed statistical significance by one-way ANOVA test, Tukey, p<0.05)

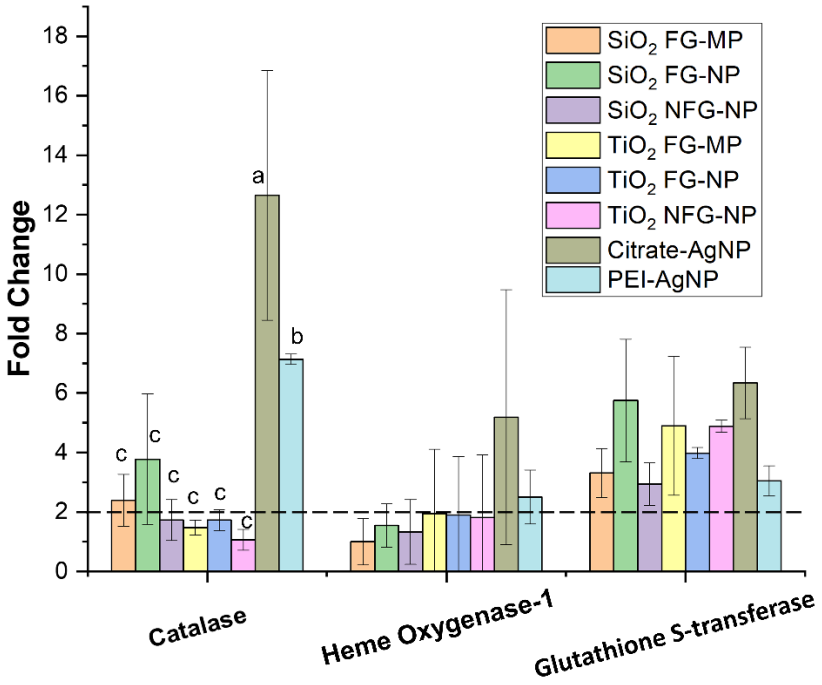

Figure 4.11 Oxidative stress related gene expression changes after particles exposure. Caco-2 cells were exposed to various particles for 24 hours before RNA extraction. Detailed protocol was listed in the materials and method section in the main manuscript. Glutathione S-transferase (GST) expression were increased by 2-fold after all particle treatment but there was no significant difference between particles. AgNPs can induce significant increases in catalase expression, compact letter display showed statistical significance by one-way ANOVA test (Tukey, p<0.05). (n=3, dashed line signifies Fold Change (FC)=2)

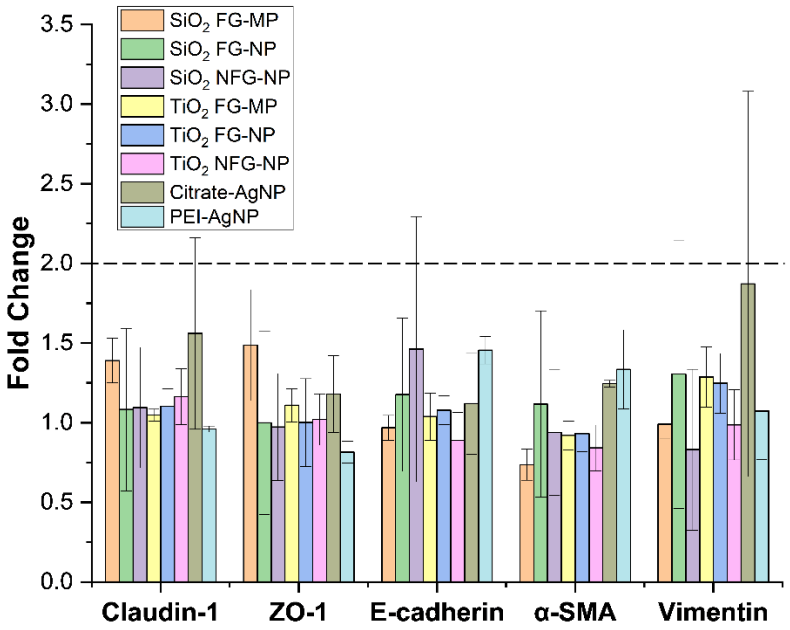

Figure 4.12 Gene expression changes of epithelial and mesenchymal junction proteins after 24 hours particles exposure on Caco-2 cells. Detailed protocol for qPCR is given in the materials and method section of the main manuscript. Expression level of any of the junction protein was not significantly affected when treated with dietary particles (FC<2), similarly no statistically significant differences were observed among different particles. (n=3, dashed line signifies FC=2)

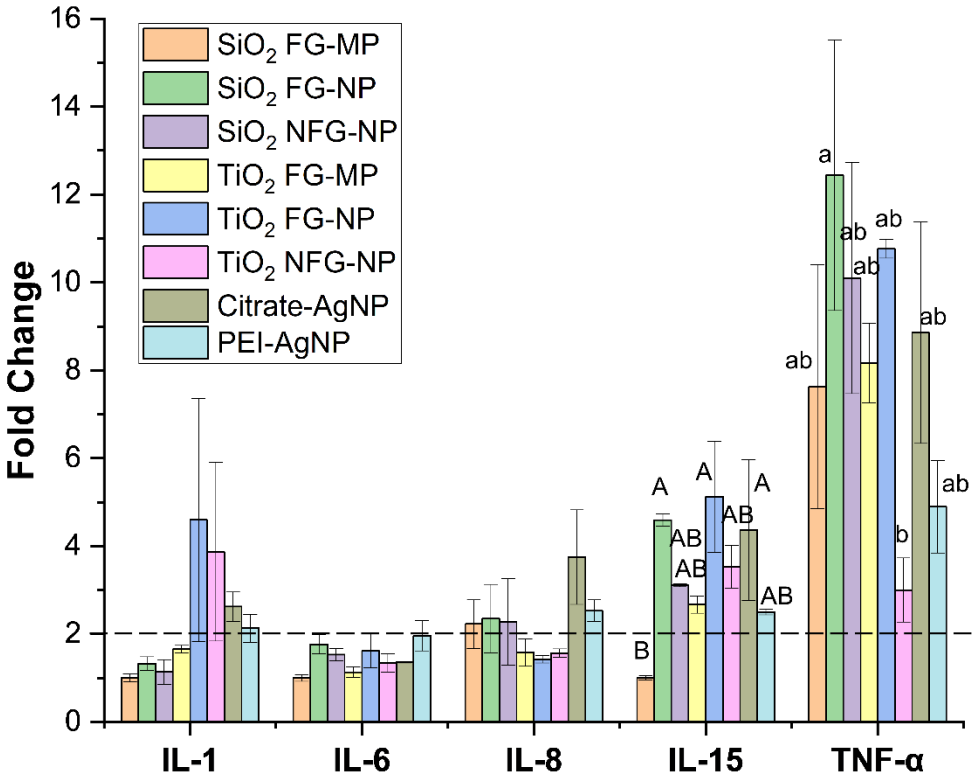

Figure 4.13 Gene expression changes of pro-inflammatory markers after 24 hours particles treatment on caco-2 cells. Detailed protocol is provided in the materials and method section of the main manuscript. AgNPs induced significantly higher expressions of IL-8, 15 and TNF-α, while TiO_2 NP and SiO_2 NP treatment increased IL-15 and TNF-α expressions (FC>2). Compact letter display indicate statistical significance by one-way ANOVA test (Tukey, $p<0.05$). The letters were assigned and compared among different particle exposure for each gene and not intended for comparison between different genes. (n=3, dashed line signifies FC=2)

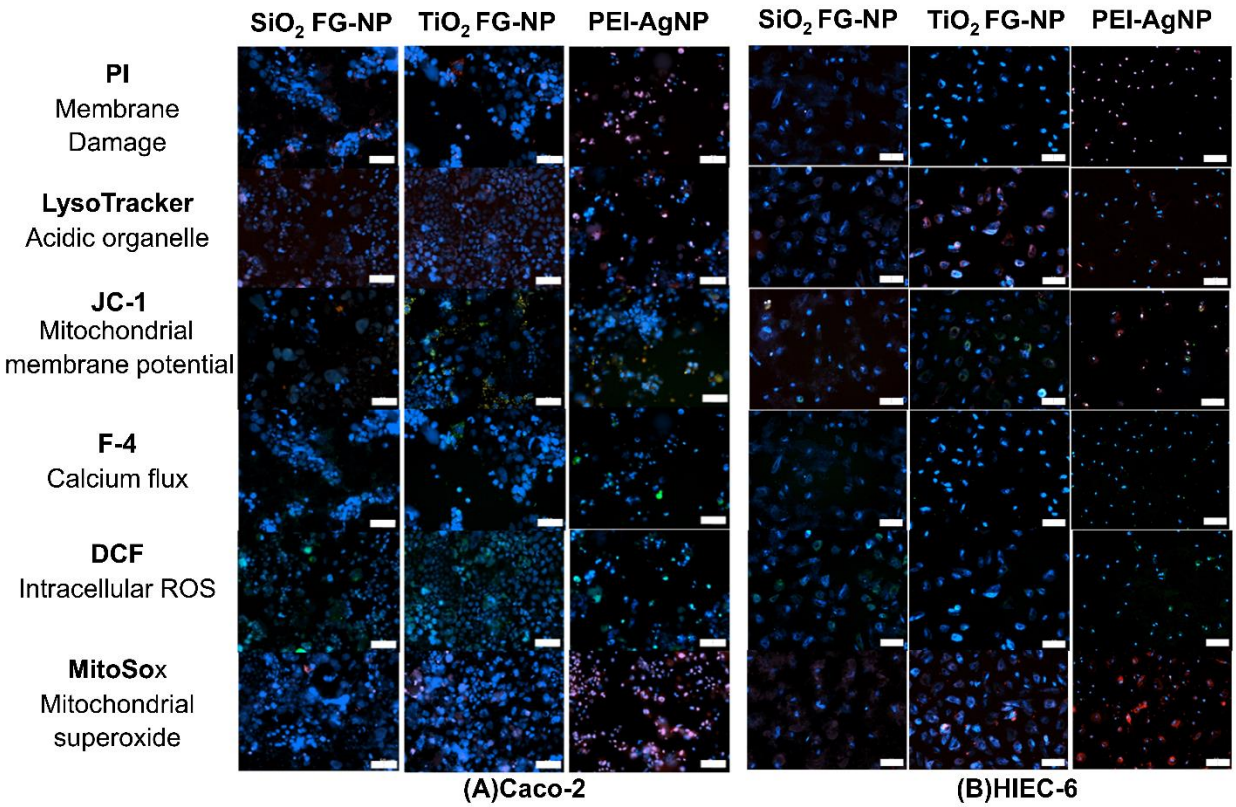

Figure 4.14 Representative high-content screening images of NP exposed cells.(A) Caco-2 cells and (B)HIEC-6 cells were stained using fluorescence indicators for cellular responses. Scale bar=50 μm.

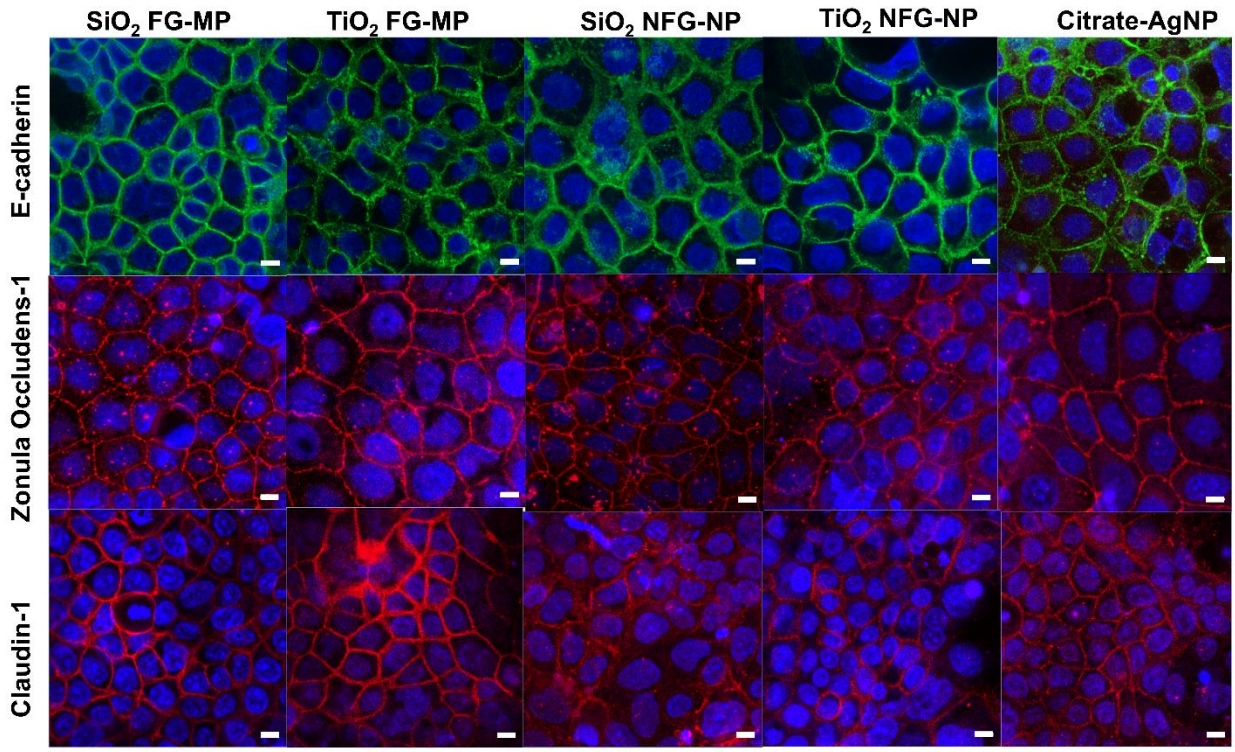

Figure 4.15 Selected confocal microscopy images of Caco-2 cells with and without NPs exposure. Confluent cells were treated with 100 μg/mL particles and stained for junction protein complexes (Claudin-1, Zonula Occludens-1, E-cadherin). Nucleus was stained by Hoechst 33342 (blue), E-cadherin is conjugated with anti-E-cadherin antibody and stained by Alexa-488(green). ZO-1 and Claudin-1 were conjugated with specific antibodies and stained by Alexa-594(red). No changes observed for adherens junction, but dislocations of tight junction proteins were observed for particles treated cells. Scale bar=10 μm

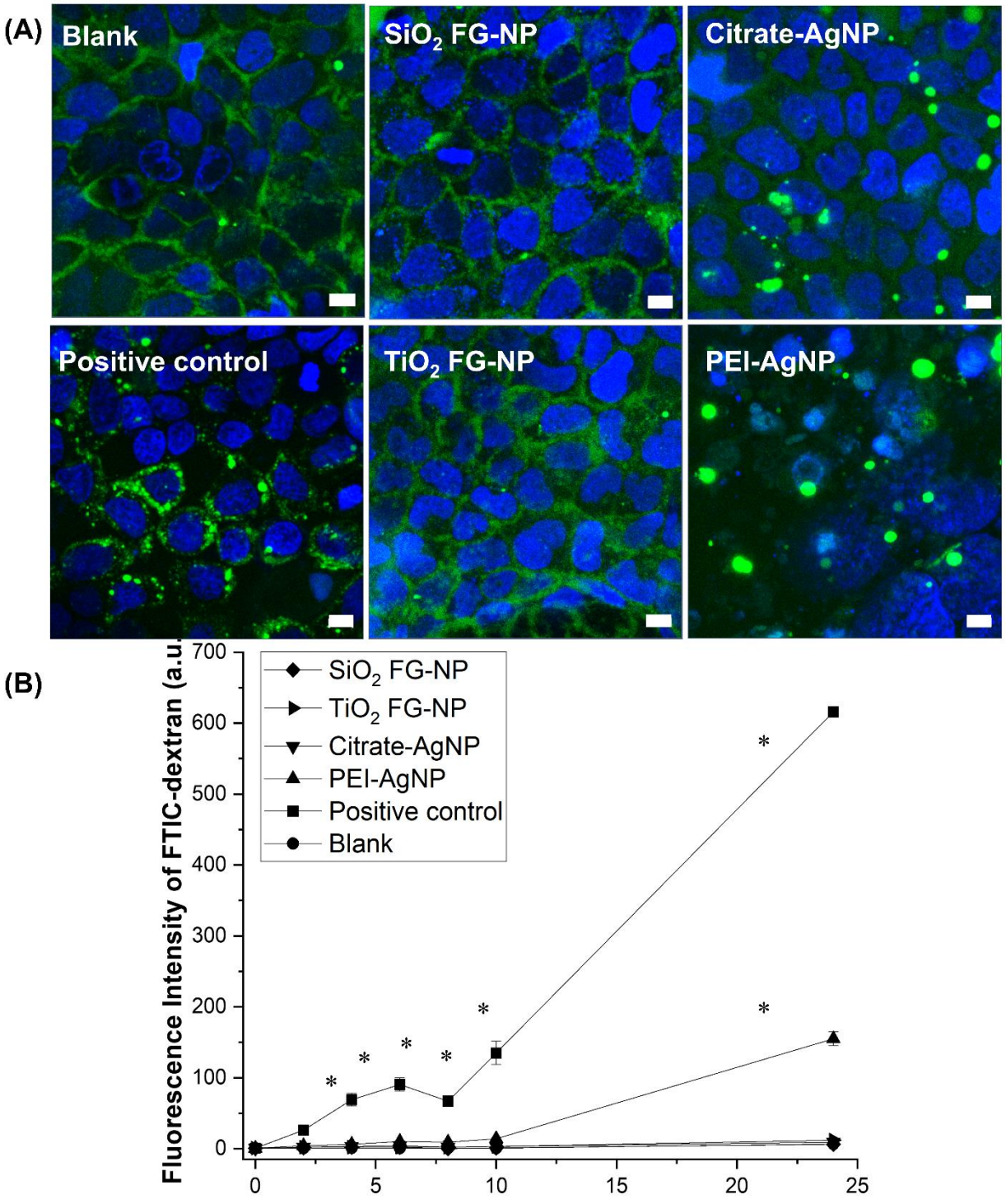

Figure 4.16 Representative confocal images of NP exposed cells. (A)FITC-dextran transport assay was performed with confocal fluorescence images for selected samples (scale bar= 10 μm) and (B) fluorescence intensity of the measured with microplate reader (n=3, * p<0.05).

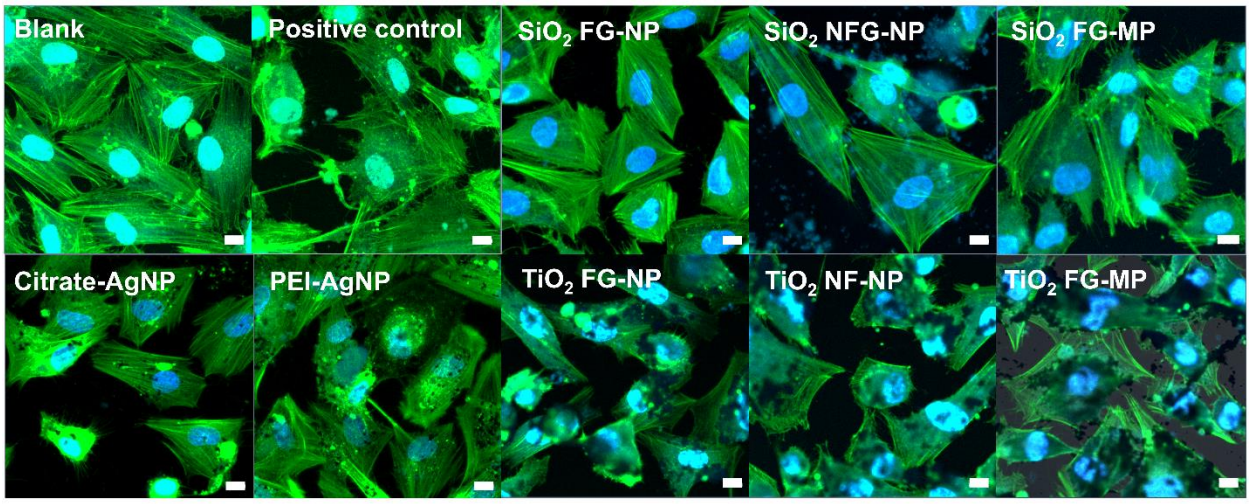

Figure 4.17 Confocal microscopy images of HIEC-6 cells with and without exposure to NPs. Cells were treated by 100 µg/mL particles for all except PEI-AgNPs which was 25 µg/mL and stained for intracellular actin filament (F-actin). Nucleus was stained by Hoechst 33342 (blue) and F-actin was stained by phalloidin (green). Contracted actin filament and stress fibers were observed in all particles treated cells. MPs exposed cells retaining more actin filament network while more bundles and polymerization observed in NPs treated cells. Scale bar=10 µm, objective= 63X, oil immersion

4.8. References

1. Lomer, M. C. E.; Thompson, R. P. H.; Powell, J. J., Fine and ultrafine particles of the diet: influence on the mucosal immune response and association with Crohn's disease. *Proc. Nutr. Soc.* **2002,** *61* (1), 123-130.

2. Frewer, L. J.; Gupta, N.; George, S.; Fischer, A. R. H.; Giles, E. L.; Coles, D., Consumer attitudes towards nanotechnologies applied to food production. *Trends Food Sci. Technol.* **2014,** *40* (2), 211-225.

3. George, S.; Kaptan, G.; Lee, J.; Frewer, L., Awareness on adverse effects of nanotechnology increases negative perception among public: survey study from Singapore. *J. Nanoparticle Res.* **2014,** *16* (12), 1-11.

4. Koeneman, B. A.; Zhang, Y.; Westerhoff, P.; Chen, Y.; Crittenden, J. C.; Capco, D. G., Toxicity and cellular responses of intestinal cells exposed to titanium dioxide. *Cell Biol. Toxicol.* **2010,** *26* (3), 225-238.

5. Williams, K. M.; Gokulan, K.; Cerniglia, C. E.; Khare, S., Size and dose dependent effects of silver nanoparticle exposure on intestinal permeability in an in vitro model of the human gut epithelium. *J. Nanobiotechnology* **2016,** *14* (1), 62.

6. Dorier, M.; Béal, D.; Tisseyre, C.; Marie-Desvergne, C.; Dubosson, M.; Barreau, F.; Houdeau, E.; Herlin-Boime, N.; Rabilloud, T.; Carriere, M., The food additive E171 and titanium dioxide nanoparticles indirectly alter the homeostasis of human intestinal epithelial cells in vitro. *Environ. Sci. Nano* **2019,** *6* (5), 1549-1561.

7. Cornu, R.; Chrétien, C.; Pellequer, Y.; Martin, H.; Béduneau, A., Small silica nanoparticles transiently modulate the intestinal permeability by actin cytoskeleton disruption in both Caco-2 and Caco-2/HT29-MTX models. *Arch. Toxicol.* **2020,** *94* (4), 1191-1202.

8. Chelakkot, C.; Ghim, J.; Ryu, S. H., Mechanisms regulating intestinal barrier integrity and its pathological implications. *Exp. Mol. Med.e* **2018,** *50* (8), 1-9.

9. Setyawati, M.; Tay, C.; Chia, S.; Goh, S.; Fang, W.; Neo, M.; Chong, H.; Tan, S.; Loo, S.; Ng, K., Titanium dioxide nanomaterials cause endothelial cell leakiness by disrupting the homophilic interaction of VE–cadherin. *Nat. Commun.* **2013,** *4* (1), 1-12.

10. Teahon, K.; Smethurst, P.; Levi, A.; Menzies, I.; Bjarnason, I., Intestinal permeability in patients with Crohn's disease and their first degree relatives. *Gut* **1992,** *33* (3), 320-323.

11. Flom, J. D.; Sicherer, S. H., Epidemiology of Cow's Milk Allergy. *Nutrients* **2019,** *11* (5), 1051.

12. Weir, A.; Westerhoff, P.; Fabricius, L.; Hristovski, K.; von Goetz, N., Titanium Dioxide Nanoparticles in Food and Personal Care Products. *Environ. Sci. Technol.* **2012,** *46* (4), 2242-2250.

13. Pageot, L. P.; Perreault, N.; Basora, N.; Francoeur, C.; Magny, P.; Beaulieu, J. F., Human cell models to study small intestinal functions: Recapitulation of the crypt-villus axis. *Microsc. Res. Tech.* **2000,** *49* (4), 394-406.

14. Wan, Y.; Guo, Z.; Jiang, X.; Fang, K.; Lu, X.; Zhang, Y.; Gu, N., Quasi-spherical silver nanoparticles: Aqueous synthesis and size control by the seed-mediated Lee–Meisel method. *J. Colloid Interface Sci.* **2013,** *394*, 263-268.

15. Toh, H. S.; Faure, R. L.; Mohd Amin, L. B.; Hay, C. Y. F.; George, S., A light-assisted in situ embedment of silver nanoparticles to prepare functionalized fabrics. *Nanotechnol. Sci. Appl.* **2017,** *10*, 147-162.

16. George, S.; Chua, M. L.; ZheWei, D. Z.; Das, R.; Bijin, V. A. U.; Connolly, J. E.; Lee, K. P.; Yung, C. F.; Teoh, O. H.; Thomas, B., Personal level exposure and hazard potential of particulate matter during haze and non-haze periods in Singapore. *Chemosphere* **2020,** *243*, 125401.

17. Chua, M. L.; Setyawati, M. I.; Li, H.; Fang, C. H. Y.; Gurusamy, S.; Teoh, F. T. L.; Leong, D. T.; George, S., Particulate matter from indoor environments of classroom induced higher cytotoxicity and leakiness in human microvascular endothelial cells in comparison with those collected from corridor. *Indoor Air* **2017,** *27* (3), 551-563.

18. George, S.; Pokhrel, S.; Xia, T.; Gilbert, B.; Ji, Z.; Schowalter, M.; Rosenauer, A.; Damoiseaux, R.; Bradley, K. A.; Mädler, L.; Nel, A. E., Use of a Rapid Cytotoxicity Screening Approach To Engineer a Safer Zinc Oxide Nanoparticle through Iron Doping. *ACS Nano* **2010,** *4* (1), 15-29.

19. George, S.; Xia, T.; Rallo, R.; Zhao, Y.; Ji, Z.; Lin, S.; Wang, X.; Zhang, H.; France, B.; Schoenfeld, D.; Damoiseaux, R.; Liu, R.; Lin, S.; Bradley, K. A.; Cohen, Y.; Nel, A. E., Use of a High-Throughput Screening Approach Coupled with In Vivo Zebrafish Embryo Screening To Develop Hazard Ranking for Engineered Nanomaterials. *ACS Nano* **2011,** *5* (3), 1805-1817.

20. Laidlaw, T. M.; Steinke, J. W.; Tiñana, A. M.; Feng, C.; Xing, W.; Lam, B. K.; Paruchuri, S.; Boyce, J. A.; Borish, L., Characterization of a novel human mast cell line that responds to stem cell factor and expresses functional FcεRI. *J. Allergy Clin. Immunol.* **2011,** *127* (3), 815-822.e5.

21. Stone, V.; Johnston, H. J.; Balharry, D.; Gernand, J. M.; Gulumian, M., Approaches to Develop Alternative Testing Strategies to Inform Human Health Risk Assessment of Nanomaterials. *Risk Anal.* **2016,** *36* (8), 1538-1550.

22. Li, N.; Xia, T.; Nel, A. E., The role of oxidative stress in ambient particulate matter-induced lung diseases and its implications in the toxicity of engineered nanoparticles. *Free Radic. Biol. Med.* **2008,** *44* (9), 1689-1699.

23. Akinc, A.; Thomas, M.; Klibanov, A. M.; Langer, R., Exploring polyethylenimine-mediated DNA transfection and the proton sponge hypothesis. *J. Gene Med.* **2005,** *7* (5), 657-663.

24. Xia, T.; Kovochich, M.; Liong, M.; Meng, H.; Kabehie, S.; George, S.; Zink, J. I.; Nel, A. E., Polyethyleneimine coating enhances the cellular uptake of mesoporous silica nanoparticles and allows safe delivery of siRNA and DNA constructs. *ACS nano* **2009,** *3* (10), 3273-3286.

25. Jiang, X.; Miclăuş, T.; Wang, L.; Foldbjerg, R.; Sutherland, D. S.; Autrup, H.; Chen, C.; Beer, C., Fast intracellular dissolution and persistent cellular uptake of silver nanoparticles in CHO-K1 cells: implication for cytotoxicity. Nanotoxicology **2015**, *9* (2), 181-189.

26. Xia, T.; Kovochich, M.; Brant, J.; Hotze, M.; Sempf, J.; Oberley, T.; Sioutas, C.; Yeh, J. I.; Wiesner, M. R.; Nel, A. E., Comparison of the Abilities of Ambient and Manufactured Nanoparticles To Induce Cellular Toxicity According to an Oxidative Stress Paradigm. *Nano Lett.* **2006,** *6* (8), 1794-1807.

27. Boya, P.; Kroemer, G., Lysosomal membrane permeabilization in cell death. *Oncogene* **2008,** *27* (50), 6434-6451.

28. Thannickal, V. J.; Fanburg, B. L., Reactive oxygen species in cell signaling. *Am. J. Physiol. Lung Cell Mol. Physiol.* **2000,** *279* (6), L1005-L1028.

29. Carlson, C.; Hussain, S. M.; Schrand, A. M.; K. Braydich-Stolle, L.; Hess, K. L.; Jones, R. L.; Schlager, J. J., Unique cellular interaction of silver nanoparticles: size-dependent generation of reactive oxygen species. *J. Phys. Chem. B* **2008,** *112* (43), 13608-13619.

30. Lorén, V.; Cabré, E.; Ojanguren, I.; Domènech, E.; Pedrosa, E.; García-Jaraquemada, A.; Mañosa, M.; Manyé, J., Interleukin-10 enhances the intestinal epithelial barrier in the presence of corticosteroids through p38 MAPK activity in Caco-2 monolayers: a possible mechanism for steroid responsiveness in ulcerative colitis. *PloS one* **2015,** *10* (6).

31. Li, X.; Mai, J.; Virtue, A.; Yin, Y.; Gong, R.; Sha, X.; Gutchigian, S.; Frisch, A.; Hodge, I.; Jiang, X., IL-35 is a novel responsive anti-inflammatory cytokine—a new system of categorizing anti-inflammatory cytokines. *PLoS One* **2012,** *7* (3), e33628.

32. Amasheh, M.; Fromm, A.; Krug, S. M.; Amasheh, S.; Andres, S.; Zeitz, M.; Fromm, M.; Schulzke, J.-D., TNFα-induced and berberine-antagonized tight junction barrier impairment via tyrosine kinase, Akt and NFκB signaling. *J. Cell Sci.* **2010,** *123* (23), 4145-4155.

33. Van Itallie, C. M.; Holmes, J.; Bridges, A.; Gookin, J. L.; Coccaro, M. R.; Proctor, W.; Colegio, O. R.; Anderson, J. M., The density of small tight junction pores varies among cell types and is increased by expression of claudin-2. *J. Cell Sci.* **2008,** *121* (3), 298-305.

34. Ivanov, A. I.; Parkos, C. A.; Nusrat, A., Cytoskeletal Regulation of Epithelial Barrier Function During Inflammation. *Am. J. Clin. Pathol.* **2010,** *177* (2), 512-524.

35. Choi, H. J.; Kim, J.; Park, S.-H.; Do, K. H.; Yang, H.; Moon, Y., Pro-inflammatory NF-κB and early growth response gene 1 regulate epithelial barrier disruption by food additive carrageenan in human intestinal epithelial cells. *Toxicol. Lett.* **2012,** *211* (3), 289-295.

36. Russo, J. M.; Florian, P.; Shen, L.; Graham, W. V.; Tretiakova, M. S.; Gitter, A. H.; Mrsny, R. J.; Turner, J. R., Distinct temporal-spatial roles for rho kinase and myosin light chain kinase in epithelial purse-string wound closure. *Gastroenterology* **2005,** *128* (4), 987-1001.

37. Perrier, C.; Corthesy, B., Gut permeability and food allergies. *Clin. Exp. Allergy* **2011,** *41* (1), 20-28.

38. Crowe, S. E.; Perdue, M. H., Gastrointestinal food hypersensitivity: basic mechanisms of pathophysiology. *Gastroenterology* **1992,** *103* (3), 1075-95.

39. Shao, L.; Serrano, D.; Mayer, L., The role of epithelial cells in immune regulation in the gut. *Semin. Immunol.* **2001,** *13* (3), 163-175.

40. Ramezani, M.; Wilkes, M. M.; Das, T.; Holowka, D.; Eliezer, D.; Baird, B., Regulation of exocytosis and mitochondrial relocalization by Alpha-synuclein in a mammalian cell model. *NPJ Parkinsons Dis.* **2019,** *5* (1), 12.

41. Yanes, R. E.; Tarn, D.; Hwang, A. A.; Ferris, D. P.; Sherman, S. P.; Thomas, C. R.; Lu, J.; Pyle, A. D.; Zink, J. I.; Tamanoi, F., Involvement of Lysosomal Exocytosis in the Excretion of Mesoporous Silica Nanoparticles and Enhancement of the Drug Delivery Effect by Exocytosis Inhibition. *Small* **2013,** *9* (5), 697-704.

42. Zhang, Y.; Wick, D. A.; Haas, A. L.; Seetharam, B.; Dahms, N. M., Regulation of lysosomal and ubiquitin degradative pathways in differentiating human intestinal Caco-2 cells. *Biochim. Biophys. Acta, Mol. Cell Res. Mol. Cell Res.* **1995,** *1267* (1), 15-24.

Preface to Chapter 5

The previous two chapters focused on the molecular, cellular, and intercellular effects of dietary NPs exposure on the intestinal epithelium. Founded in the Adverse Outcome Pathway (AOP) approach, we have identified good agreement between the changes in gene expression (Chapter 3) and apical cellular responses (e.g., oxidative stress, inflammation, and possibly immune responses; Chapter 4). In order to realize the ultimate goal of the study in organizing the NP-induced responses at different biological levels using an AOP approach, it is critical to connect these molecular and cellular responses to an adverse outcome at the organism level of public health concern.

Chapter 5 investigates the potential role that dietary NP exposure may play on disease progression associated with cow milk allergy. Here, an *in vitro* co-culture model for cow's milk allergy comprised of Caco-2 cells and sera-primed mast cells (LAD2) were exposed to the reference library of particles studied in the previous two chapters. The differences in allergen delivery across the intestinal epithelium, and subsequent allergy responses by mast cell degranulation were measured after co-exposure to the particles and commercial skim milk. The particle-dependent alterations were investigated for toxic responses by probing critical cytokines in type 2 immune responses. This chapter was designed to study the potential role of dietary particles in enhancing the antigenicity of the milk proteins, which is an immune response of real-world concern for children and patients with allergy histories.

This chapter is authored by the candidate and coauthored by Dr. Wut Hmone Phue and the candidate’s supervisors Dr. Niladri Basu and Dr. Saji George. This chapter was initiated and

designed by the candidate and the supervisor Dr. Saji George. The candidate performed all the experiments, data analysis and interpretation, discussion of the results, and manuscript preparation with the help of Dr. Wut Hmone Phue under the supervision of Dr. Saji George and Dr. Niladri Basu. The manuscript is under preparation and will be submitted shortly.

Chapter 5

5. Dietary nanoparticles enhance the allergenicity of milk proteins in both IgE-dependent and independent mechanism: an *in vitro* investigation

5.1. Abstract

Cow milk allergy, an allergy disease more prevalent in children at early ages, can induce hypersensitivity reactions in the immune system upon exposure to cow milk protein (CMP). In recent years, the popularity of dietary nanoparticles (NPs) in the food industry as additives has raised concerns due to the lack of knowledge about their toxicities and the potential interactions between NPs and the food matrix. In this study, we used a transwell culture system that consisted of human colorectal adenocarcinoma (Caco-2) cells in the apical insert and Laboratory of Allergic Diseases 2 (LAD2) mast cells in the basal compartment. This *in vitro* model captured the communication between the intestinal epithelium and mast cells in allergenic inflammation. The Caco-2 cells were exposed to a reference library of milk-interacted dietary NPs (SiO_2 NPs, TiO_2 NPs, and AgNPs) that varied in particle size, surface chemistry, and crystal structures. The interactions between milk and NPs were able to change the surface chemistry of the NPs and the bioavailability of milk allergen (casein and β-lactoglobulin) across the intestinal epithelial layer. The resulting effects of the communications between epithelial cells and the mast cells resulted in significant changes in the early-phase and late-phase activation of the mast cells. Such changes also led to a mechanism switch of the allergic response from an IgE-dependent mechanism to a mixed mechanism of both IgE-dependent and independent mechanisms during antigen challenge in the presence of dietary NPs.

5.2. Introduction

Food allergy refers to the adverse immune responses to food allergens (mostly proteins) that are responsible for a variety of symptoms and disorders in gastrointestinal (GI) tracts.[1] The prevalence of food allergy has increased dramatically over the past decades, affecting more than 7 % of the population in Canada.[2] This susceptible group of the population may experience adverse immune responses (Type 2 immunity) to the allergens that otherwise will be tolerated in non-allergic individuals. Food-induced allergic reactions can be primarily categorized by immunoglobulin E (IgE)-mediated and non-IgE-mediated mechanisms.[3] Cow milk protein (CMP) is the most common allergen that can induce both types of allergies in early childhood. In developed countries, allergy to milk protein affects approximately 2 to 3% of the population in the first year of life and often persists to school age.[4, 5] The major allergens in cow milk allergy (shortened as milk allergy) include caseins and whey proteins (β-lactoglobulin (BLG) and α-lactalbumin (ALA)), where the properties of the proteins may significantly affect the subsequent immune responses.[6] In 2010, the world allergy organization (WAO) released the guideline of the "Diagnosis and Rationale for Action against Cow's Milk Allergy".[7] The guideline emphasized the need for future research in probing the mechanism of the immune responses to ingested CMPs, and the roles of adverse GI conditions in the progress of milk allergy.

In recent years, the application of NPs in the food industry has expanded, with the most popular ones being silicon dioxide (SiO_2, E551), titanium dioxide (TiO_2, E171), and silver (Ag, E174).[8] Among these particles, however, about 35% of the particles are present in size of nanometers.[9, 10] Previous studies have shown the potential of NP-immune system interactions due to their unique physicochemical properties through critical effector cells (e.g., mast cells).[11, 12] However, much

less is known about the effects of simultaneous exposure of food allergens with NPs due to the possibility of biocorona formation on the particle surface in complexed biological systems.[13] A recent study from our group showed possible enrichment of milk allergens on food-grade (FG) NPs after interacting with milk.[14] Subsequent changes in structure, antigenicity, and degranulation status of the *in vitro* mast cells models, suggested their critical roles in altered allergenicity.[15] However, more complex *in vitro* models involving more cell types shall be used in allergy studies since food allergens were not directly exposed to immune cells after ingestion. The study in Chapter 4 used a transwell culture system that consisted of enterocytes model colorectal adenocarcinoma cells (Caco-2) on the transwell inserts and LUVA mast cells in the basal compartment.[16] We observed increased milk protein delivery and mast cell degranulation from a pre-exposure scenario where commercial skim milk samples were exposed to Caco-2 cells after one-day exposure to dietary NP. We then reasonably hypothesized that the co-exposure of the same reference library of NPs and milk may also affect the milk protein delivery across the intestinal epithelium and the subsequent immune responses.

After ingestion, milk allergens will first be exposed to the intestinal epithelial cells in the GI tract before encountering the immune system. Intestinal mast cells in the lamina propria beneath the epithelial layer may interact with epithelial cells in hypersensitivity and stress conditions.[17] In this study, a transwell culture system was used as the *in vitro* model to capture such interactions by having Caco-2 cells in the apical insert as intestinal epithelial layer and Laboratory of Allergic Diseases 2 (LAD2) mast cells in the basal compartment. The Caco-2 cells were exposed to different forms of milk-interacted SiO_2 NPs (FG and non-food-grade (NFG)), TiO_2 NPs (FG and NFG), SiO_2 FG microparticles (MP), TiO_2 FG MPs, and AgNPs (citrate coated AgNP (Citrate-

AgNP) and polyethyleneimine coated AgNP (PEI-AgNP)). NFG NPs were compared to their FG counterparts to probe the effect of compositional differences.[10] The effect of surface chemistry was also compared between positively charged PEI-AgNP and negatively charged Citrate-AgNPs. In addition to NPs, we also studied MPs of SiO_2 and TiO_2 given that food products contain particles of variable sizes.[10] We assessed the bioavailability of milk allergen (casein and BLG) delivery across the intestinal epithelial layer and the subsequent effects on the early-phase and late-phase activation of the mast cells. In addition to these responses in the common IgE-dependent mechanism, the possibility of IgE-independent mechanisms was also discussed.

5.3. Materials and Methods

5.3.1. Materials

Food-grade SiO_2 NP (AEROSIL 200F, lot # 625010907) and MPs (SIPERNAT 22, lot# 156032047) were obtained from Evonik Industries (Essen, Germany). NFG SiO_2 (cat# 637238, 10−20 nm particle size (BET), 99.5% trace metals basis) and NFG TiO_2 NPs were purchased from Sigma-Aldrich (St. Louis, USA). Food grade TiO_2 NPs were acquired from CNMI industry cooperation (Beijing, China) and MPs of TiO_2 were purchased from Pure Organic™ (Toronto, Canada).

Citrate-AgNPs were synthesized based on a modified method reported previously.[18] Briefly, aqueous solutions of 1 mM silver nitrate and 10 mM trisodium citrate solution were mixed at a 2:1 volume ratio and incubated in a 70 °C water bath for 3 hours (h). The product (greenish-yellow in color) solution was eluted twice with water for 30 minutes (min) at 16,000 g (Eppendorf 5430R

refrigerated centrifuge, Eppendorf Canada, Ontario, Canada) and resuspended in water for future use.

PEI coated AgNPs were prepared using light-assisted synthesis method based on a past study.[19] Briefly, 1% of silver nitrate and 1% w/v branched-PEI solution were dissolved in water and mixed at a 2:1 ratio. The mixture was covered with aluminum foil and sonicated in a water bath for 30 min. After sonication, the mixture was exposed directly to a light source (120 V, 160 W) for 4 min until the color of the solution turned to amber red. The product solution was washed twice with water for 30 min at 16,000 g with the Eppendorf 5430R refrigerated centrifuge (Eppendorf) and resuspended in water.

The milk sample (Quebon skimmed milk) used in this study was commercial skimmed milk purchased from local grocery stores (Agropur Dairy Cooperative, QC, Canada). The purchased milk was stored at 4 °C and centrifuged by Eppendorf 5430R Refrigerated centrifuge at 15,000 ×g for 15 min to remove any lipid debris, and the supernatant was collected for further use.

5.3.2. Particle characterization

The size and morphology of the particles were characterized by a Technai Spirit 120kV transmittance electron microscopy (TEM) (FEI, Oregon, USA). For this, pristine particles were suspended in water at 100 µg/mL, and 5 µL of each sample was dropped onto 200-mech Cu/C TEM grids. The samples were dried at room temperature for 1 hour (h) and imaged.

Milk-interacted particles were prepared by mixing 900 µL of prepared milk sample with 100 µL of 10 mg/mL dietary particle suspensions (final concentration 1 mg/mL) and incubated for 6 h at

37 °C. Particles were then pelleted out by centrifugation (18,000 g) for 15 min in the Eppendorf 5430R refrigerated centrifuge (Eppendorf) at 4 °C. The particle pellet was resuspended in 1 mL of water after removing the supernatant that contained unbound milk proteins. The mixture was centrifuged again at 18,000 g for 15 min followed by resuspending pellet in water. The solution was diluted 10 times to obtain a final concentration of 100 μg/mL for TEM imaging. For sample preparation, 5 μL of the 100 μg/mL milk-interacted particles suspension was dropped onto 200-mesh Cu/C TEM grids and air-dried at room temperature for 1 h. The images were acquired by Technai Spirit 120 kV transmittance electron microscopy (FEI, Oregon, USA).

5.3.3. Cell culture

Caco-2 was selected as the *in vitro* model of intestinal epithelium due to their morphological and functional similarities to mature human enterocytes. Caco-2 cell lines (ATCC #HTB-37, passage between 10-35) originally obtained from ATCC (ATCC, Virginia, USA) were seeded in 100 mm petri dish (Thermofisher, New York, USA). The cells were supplemented with 10 mL of complete culture media that contained Gibco Dulbecco's Modified Eagle Medium (DMEM) (Thermofisher), 10% fetal bovine serum (FBS) (WISENT, Quebec, Canada) and 1% PEN-STREP (WISENT). Cells were kept in the Caron's Oasis™ CO_2 incubator (Caron products, VWR International, California, USA) at 37 °C and 5% CO_2 with 95% humidity with media changed every two days. Upon reaching 90% confluency, cells were harvested using 0.25% Trypsin/EDTA (WISENT) and sub-cultured or seeded for subsequent experiments.

Human Laboratory of Allergic Diseases 2 (LAD2) cells were kindly supplied by Dr. A. S. Kirshenbaum's lab (National Institutes of Health, Bethesda, MD, USA). The LAD2 mast cell line

resembles the primary human mast cell whose growth is dependent on stem cell factor (SCF), has functional surface FcεRI receptors, and degranulates in response to immunologic stimuli.[20] The cells were cultured using StemPro®-34 SFM serum free medium for hematopoeitic stem cells (Thermofisher) supplemented with StemPro®-34 SFM nutrient supplement (Thermofisher), 1% PEN-STREP (WISENT), 2 mM L-glutamine (Thermofisher) and 100 µg/mL Primocin (Thermofisher). The cells were incubated at 37 °C and 5% CO_2 with 95% humidity and maintained weekly with hemi-depletions until seeding for subsequent assays.

The effects of the interactions between milk and NPs on antigen delivery and allergic responses across the intestinal barrier were assessed by a co-culture system that consisted of differentiated Caco-2 cells and LAD2 cells using transwell cell culture inserts. Caco-2 cells were cultured on transwell inserts (polycarbonate membrane filters, 0.4 µm pore size, 1×10^8 pores/cm) (Corning Incorporated) at 5×10^4 cells/cm^2. The inserts were placed in 24 well plates and 600 µL complete DMEM culture media was added to the basolateral chambers. Media were refreshed every two to three days until 21-25 days for differentiated and complete formation of cellular junction complex.

5.3.4. Exposure

5.3.4.1. Pre-exposure of particles

Two days before the assay, LAD2 cells were seeded at a density of 200,000 cells/well in empty wells of the 24 wells plate (37°C at 5% CO_2) and were kept separate from the Caco-2 cells. One day before the assay, the Caco-2 cells in the apical compartment were exposed to 100 µg/mL particle suspensions in sera-free media (25 µg/mL for AgNPs) for 24 h. Mast cells were sensitized overnight with milk allergy patients' sera diluted in Tyrode buffer (135 mM NaCl, 5 mM KCl, 1.8

mM $CaCl_2$, 1 mM $MgCl_2$, 5.6 mM glucose, 20 mM HEPES) in the ratio of 1:50. The sera were supplied by PlasmaLab International (Everett, WA, USA.), and the specific IgE levels for f2 allergen of patients' sera were 20.886 kU/L, 19.267 kU/L, 55.582 kU/L, 74.7 kU/L, and 41.9 kU/L, respectively. Non-sensitized (NS) controls were also prepared by adding an equal amount of Tyrode buffer.

On the day of exposure, the particle suspensions in the apical compartment were replaced with commercial skim milk (centrifuged at 16,000 g for 10 min before sampling the supernatant). The cells used as positive controls were exposed to 25 mM EDTA (S_positive control), and the cells used as negative controls were exposed to sera-free media (S_Media). Non-sensitized controls were prepared similarly for the LAD2 cells without exposure to patient sera (NS_Media and NS_positive control). Subsequently, the inserts containing milk exposed Caco-2 cells were transferred to the wells with mast cells and incubated for 6 h at 37 °C and 5% CO_2 before sampling. All exposure was repeated in triplicates.

5.3.4.2. Co-exposure of particles and milk

Two days before the assay, LAD2 cells were seeded at a density of 200,000 cells/well in empty wells of the 24 wells plate (37°C at 5% CO_2) and were kept separate from the Caco-2 cells. One day before the assay, mast cells were sensitized overnight with milk allergy patients' sera diluted in Tyrode buffer identical to the previous section.

On the day of exposure, the media in the apical compartment were replaced with 100 µg/mL particle suspensions in the prepared commercial skim milk (25 µg/mL for AgNPs) for 6 h. Non-sensitized (NS) negative control was prepared by exposing sera-free media (NS_Media) and 25

mM EDTA (NS_positive control) to Caco-2 cells and non-sensitized LAD2 cells. Then the inserts containing milk exposed Caco-2 cells were transferred to the wells that were seeded with mast cells and incubated for 6 h at 37 °C and 5% CO_2 before sampling. All exposure was repeated in triplicates.

5.3.5. Effect of NPs on cell junction complex and change in membrane permeability

The effects of the NPs and milk on the intestinal barrier were assessed in differentiated Caco-2 cells using transwell cell culture inserts. The changes in transepithelial electrical resistance (TEER) were monitored in both exposure scenarios (pre-exposure and co-exposure) to assess the epithelial barrier integrity. After the exposure, TEER measurements were taken at 2, 4, 6, 8,10 and 24 h by the Millicell-ERS system (ERS-2 Epithelial Volt-Ohm Meter, Millicell). Changes in TEER values of cells were recorded in triplicates.

5.3.6. Effect of NPs on allergen delivery

In order to measure the amount of milk allergens delivered to the basal compartment during the exposure, enzyme-linked immunosorbent assay (ELISA) assays targeting the major milk allergens (casein and BLG) were performed, as reported previously).[15] Primary antibody for casein (Anti-casein rabbit antibody-cat # ab166596), primary antibody for BLG (Anti-LGB rabbit antibody-cat # ab112893) and secondary anti-rabbit antibody (cat # 6721) were purchased from Abcam (Cambridge, UK). Supernatant from each basal compartment of the transwell plate was sampled 6 h after milk exposure and diluted in 3:2 with 0.1 M Na_2HPO_4 coating buffer (Sigma), and 100µL of the resulting mixture was added to 96 well plates and kept at 4 ºC overnight. The next day, the solution was discarded from the plate and the wells were filled with 100µL blocking buffer that

contained 2% BSA (Thermofisher) in 1X Tris-buffered saline (TBS) buffer. The buffer was prepared as 10 mM Tris (Sigma) and 150 mM NaCl (Bishop, Canada) in deionized water with pH adjusted to 7.5 with HCl (Sigma). After 1 h incubation, the blocking buffer was discarded and replaced with 100 µL primary antibodies diluted in the blocking buffer (1:5000) and incubated for 1 h at room temperature (RT). The primary antibody solution was aspirated, and the wells were washed with washing buffer (0.05% Tween-20 in TBS) 4 times before adding 100 µL secondary antibody (Abcam, USA) diluted 1:10000 in blocking buffer for 1 h at RT. The wells were washed 4 times again with washing buffer after discarding the secondary antibody solution. The substrate solution of 0.25 mg/mL 3,3',5,5'-tetramethylbenzidine (TMB) (Sigma) dissolved in 0.1 M citric acid buffer (pH 5) that also contained 0.625% of acetone, 5% methanol and 0.009% H_2O_2 was prepared and 100 µL was added to each well for 3 min before adding 100µL 0.2 M H_2SO_4 stop solution. The absorbance was read at 450 nm by Spectramax i3x plate reader (Molecular Devices, San Jose, USA).

5.3.7. Mast cell degranulation

After 6 h of particle-milk exposure, 50 µL of supernatant was taken from the basal compartment and mixed with 50 µL substrate solution (1 mM p-nitrophenyl-N-acetyl-b-D-glucopyranoside (PNAG) in 50 mM citric buffer) and incubated for 90 min at 37 °C. The reaction was stopped with 100 µL glycine solution (0.1M) and absorbance was read at 405 nm using Spectramax i3x plate reader (Molecular Devices, San Jose, USA). For the positive controls of the degranulation assay, 0.1% Triton X-100 in Tyrode buffer was added to the basal compartment for 1 h. The β-hexosaminidase release was expressed as the percentage of total β-hexosaminidase cell content, which was calculated as the percentage of the absorbance of the sample (after subtracting the

absorbance of unstimulated cells) over the asborbance of the positive control (after subtracting the absorbance of unstimulated cells). All experiments were performed in triplicates.

5.3.8. Change in inflammatory cytokines level

After 6 h incubation, 50 µL of supernatant was collected from the basal compartment of each transwell and centrifuged at 255×g, 4 ºC for 5 min with Eppendorf 5430R refrigerated centrifuge (Eppendorf) to remove cell debris, and the resulting supernatant was used to measure cytokines. Interleukin 33 (IL-33) and interleukin 13 (IL-13) ELISA kits (Sigma) were used following the instructions provided by the manufacturer. The absorbance of the reaction product was measured at 405 nm using a Spectramax i3x plate reader (Molecular Devices), and the results for each sample were calculated using a standard curve of provided recombinant proteins.

5.4. Results

5.4.1. Corona formation on the surface of milk-interacted particles

Physicochemical properties of the particles before and after milk exposure, including particle size, shape, and agglomeration status, and formation of biocorona on the surface of the particles, were visualized by TEM (Figure 5.1, Figure 5.5). We observed that all three samples of pristine TiO_2 particles (FG-NPs, NFG-NPs, and FG-MPs) contained both micro-size particles (diameter > 100 nm) and nano-sized particles (diameter < 100 nm). The primary particle size for pristine Citrate-AgNPs was about 30 - 40 nm. The majority of the particles were spherical particles, but we also observed the presence of a few Citrated coated silver nanorods (Citrate-AuNR). SiO_2 particles formed large agglomerates (diameter > 1 µm) with primary particle sizes of 20 nm. PEI-AgNPs

were well-dispersed as single particles in size of 30-50 nm. However, the size of the particles decreased significantly to less than 10 nm after interacting with milk for 6 h.

We were also able to verify the presence of surface corona after milk interaction for all three forms of TiO_2 particles and Citrate-AgNP (Figure 5.1). The lower electron density of the corona layer (pointed by arrows) resulted in lower contrast in the semi-transparent layer on the surface of the particles. The corona formation for SiO_2 particles was not as evident due to the minor differences in electron densities between SiO_2 and the corona layer. We could not visualize the corona formation on the surface of PEI-AgNPs because of the small size of the particles. However, the images still proved the interaction between PEI-AgNPs and milk from the decreased size of the particles, possibly resulting from Ag ion dissolution and reprecipitation as secondary particles.

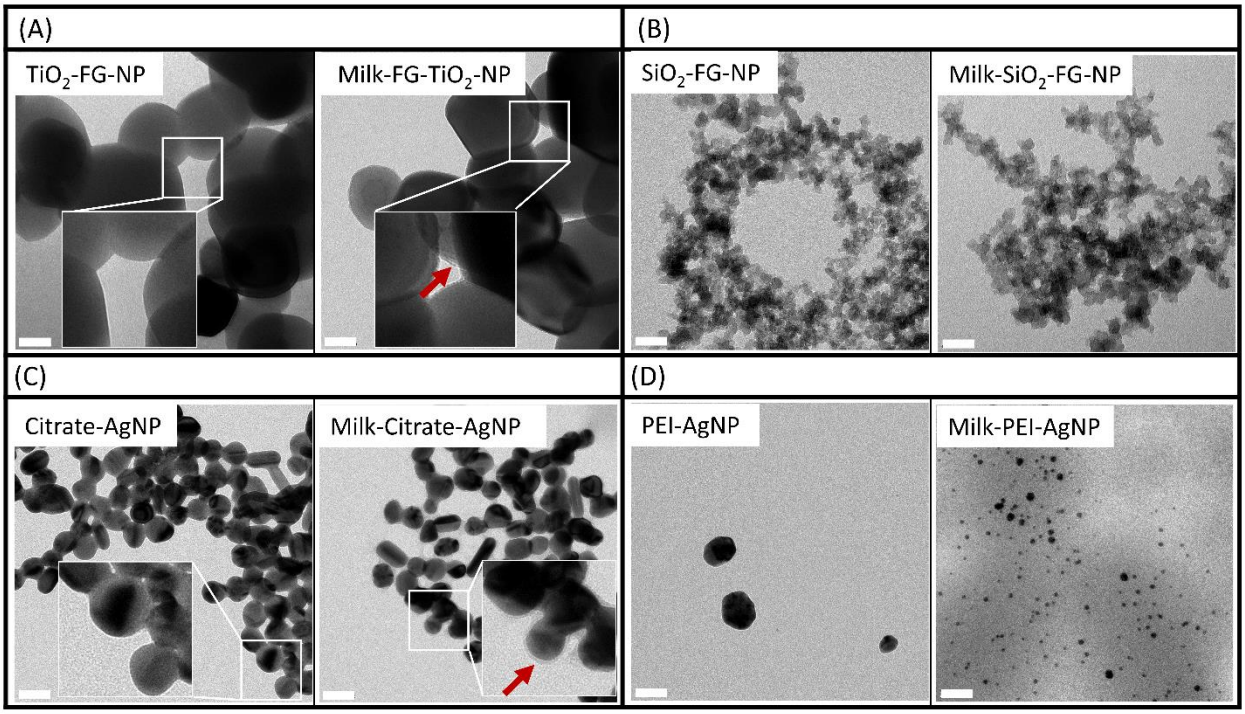

Figure 5.1 Transmittance Electron Microscopy (TEM) images of pristine and milk interacted particles for (A)TiO_2-FG-NP, (B) SiO_2-FG-NP, (C) Citrate-AgNP and (D) PEI-AgNP. The samples were prepared by drop-casting 5 µL of particles suspension (100

μg/mL) onto 200 -mesh Cu/C TEM grids and dried for 2 h. Images were acquired by Tecnai Spirit 120 kV TEM. Scale bar= 50 nm.

5.4.2. Pre-exposure of NPs to the intestinal epithelium changes the delivery and allergenicity of milk protein

The co-culture system consisting of Caco-2 cells and mast cells LAD2 was established as an *in vitro* intestinal model to understand the effect of dietary particles on intestinal responses in food allergy. The ELISA assays for casein and BLG were used to detect the two most common antigens for milk allergic patients. To begin with, we first tested the effect of particles on the mast cells without the Caco-2 cells for reference (Data now shown). The result showed that all sensitized cells could induce a higher percentage of degranulation than non-sensitized cells. However, the increased degranulation from the negative control (sera-free media exposed cells) for all samples was not dependent on the treatment, since the increments were not significantly different from each other. For non-sensitized cells, the percentage release of β-hexosaminidase was not significantly different between EDTA exposed cells and the negative control.

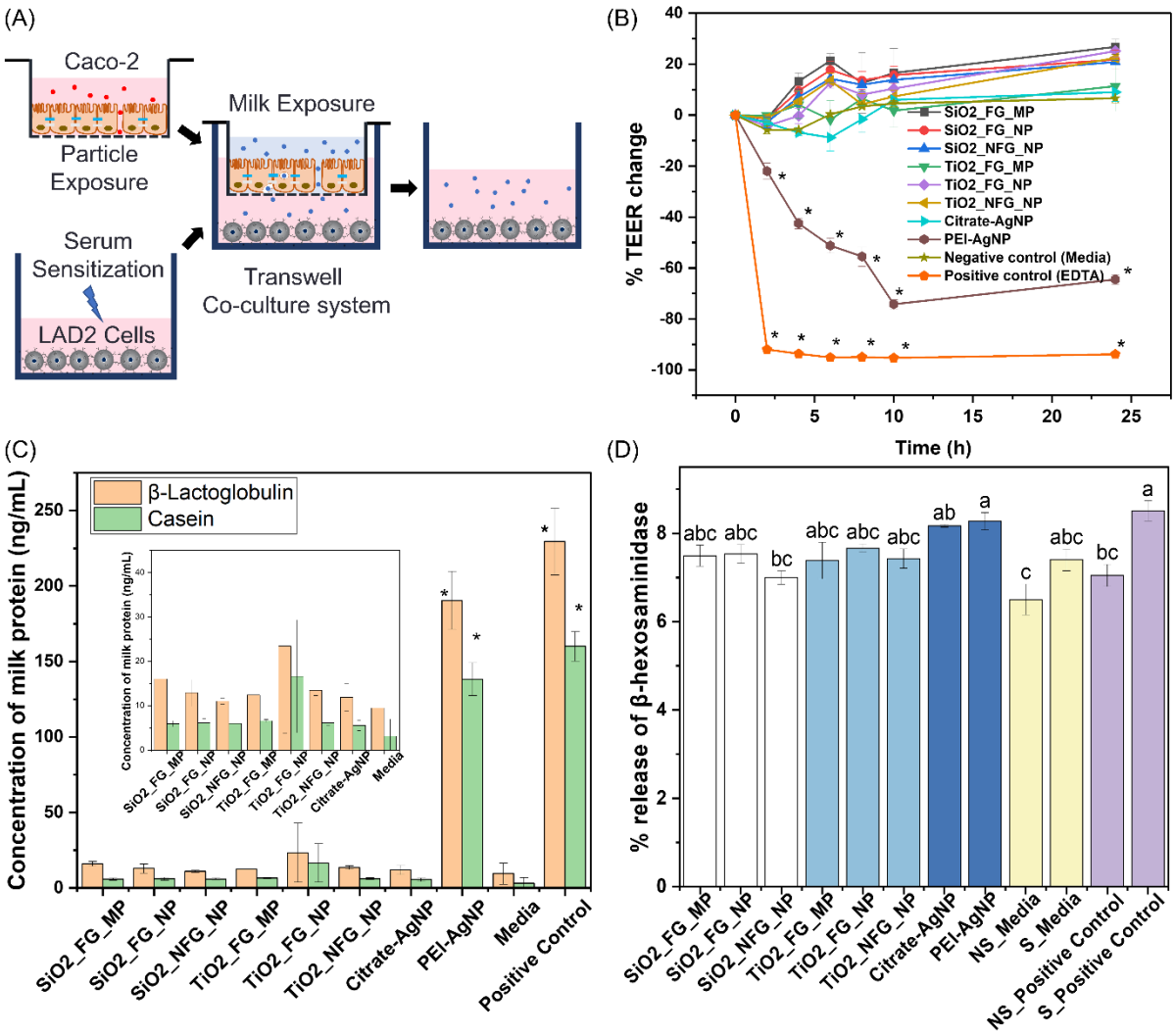

Figure 5.2 The exposure scheme (A) for the transwell allergy model pre-treated with dietary particles and subsequent responses in (B) electrical transepithelial resistance changes, (C) milk protein delivery across the intestinal epithelium model, and (D) % release of β-hexosaminidase as an indicator for degranulation level of LAD2 mast cells in the basal compartment (n=3, p<0.05).

This study considers two exposure scenarios of the ingested particles and milk proteins. The first one is the pre-exposure of dietary particles for 24 h followed by milk exposure (Figure 5.2A). In this scenario, we observed the compromised barrier function of the intestinal epithelium treated with PEI-AgNP and EDTA based on the decreased TEER value (Figure 5.2B), which resulted in the increased delivery of both casein and BLG (Figure 5.2C) across the epithelium. In contrast, the other particle treatments could not change the epithelial integrity, and thus the delivery of milk

protein was not affected compared to the negative control. For PEI-AgNP treated cells, the increased delivery was not coupled with a significant increase in mast cell degranulation (Figure 5.2D). The degranulation level was statistically different from the negative control and higher than other particle treatments.

5.4.3. Simultaneous exposure to milk and dietary particles enhanced the allergenicity of milk proteins

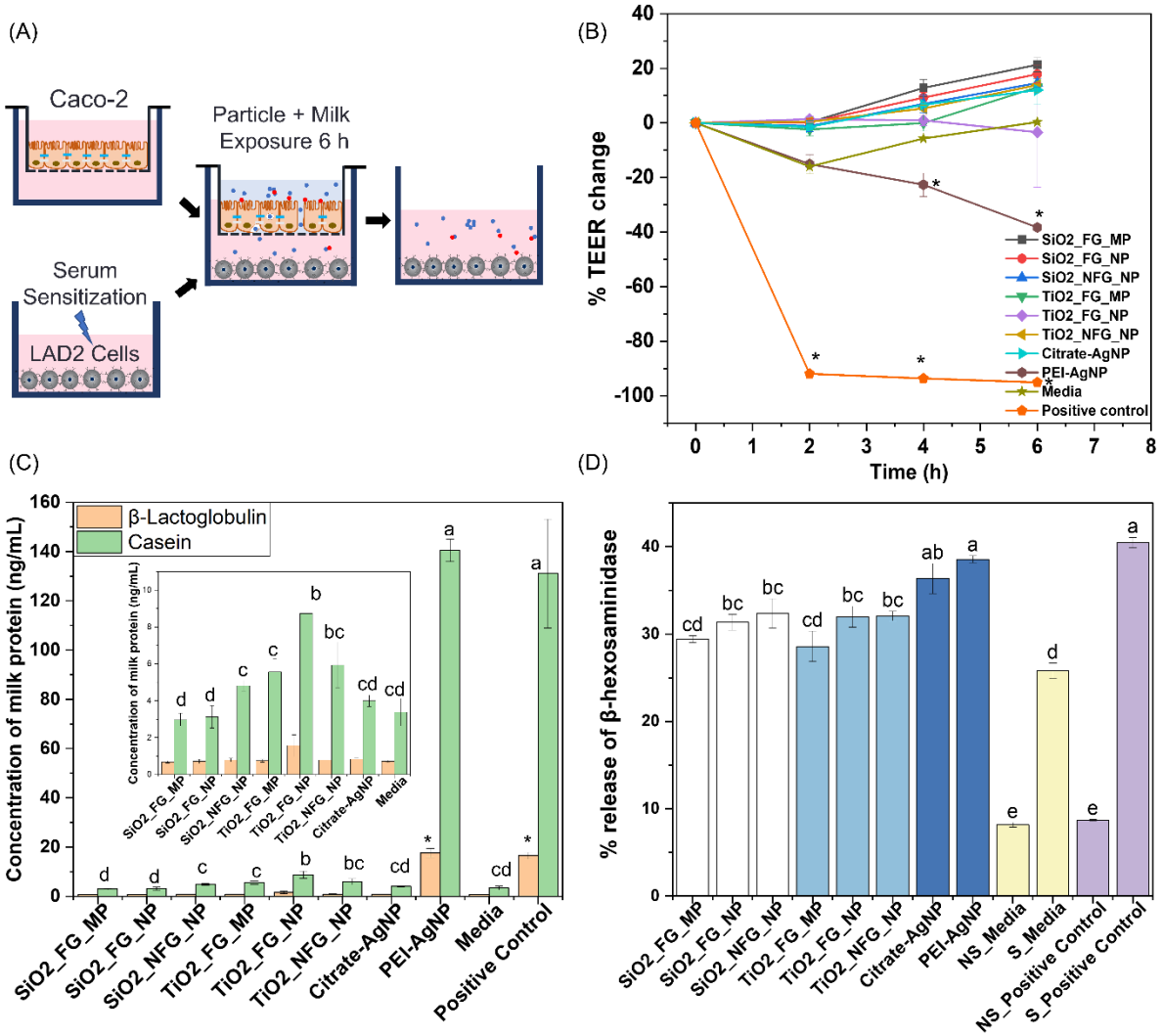

Figure 5.3 The exposure scheme (A) for the transwell allergy model simultaneously exposed to dietary particles and milk and the subsequent responses in (B) electrical transepithelial resistance changes, (C) milk protein delivery across the intestinal epithelium model, and (D) degranulation of LAD2 mast cells in the basal compartment. Significance was calculated by one-way ANOVA and was presented as compact letter display (n=3, p<0.05). The pairwise comparison was restricted to various particle tested samples for each protein in (C) and not between two proteins.

The co-exposure of milk and particles was intended to picture the other exposure scenario in this study where the dietary particles interacted with the food matrix. Similar to the pre-treated intestinal epithelium results, we observed decreased epithelium resistance only in PEI-AgNP

treated Caco-2 cells (Figure 5.3B). As a result, milk-interacted dietary particles treatment did not induce significant changes in casein and BLG delivery from the media control except for PEI-AgNP treated cells. The degranulation level of mast cells in the two exposure scenarios (Figure 5.2 and Figure 5.3) shall not be compared with each other due to the different exposure time after seeding and sensitization, where the number of mast cells can increase significantly in the additional 24 h for the first scenario (Figure 5.2A).

The simultaneous exposure of NPs with milk significantly enhanced the degranulation of mast cells, while MPs with milk were not statistically different from the media control. However, the difference between FG and NFG particles was not significant, suggesting the primary role of particle size in enhancing degranulation with the antigen. Both types of AgNPs were inducing higher degranulation compared to other types of particles, which can be affected by the compromised barrier function (PEI-AgNP) and sensitization process (both AgNPs). However, Citrate-AgNP was not compromising the barrier function (Figure 5.3B) while still significantly increasing the mast cell degranulation, suggesting the possibility of contributors other than the IgE-dependent mechanism.

5.4.4. Cytokines released by Caco-2 and LAD2 cells suggest non-IgE dependent mast cell activation

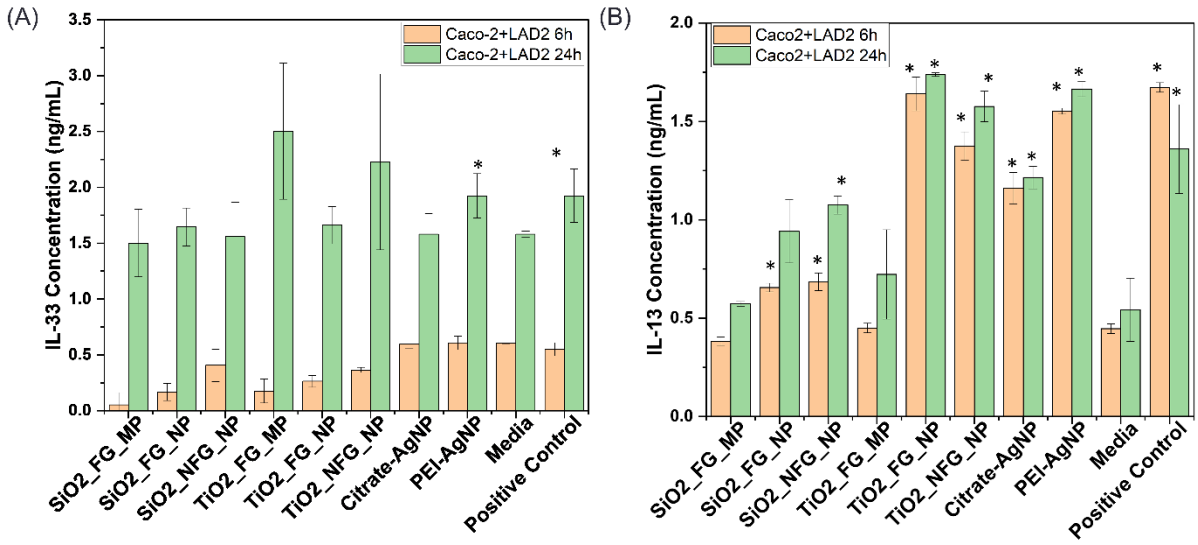

Figure 5.4 Concentration of (A)IL-33 and (B)IL-13 in the basal compartment of the transwell model after simultaneous exposure of milk and nanoparticles. The release of IL-33 and IL-13 was measured by ELISA assays following the manufacturer's instruction. The results were quantified by absorbance measurement. Data are expressed as fold change relative to the negative control (Mean ±SD (n=2))

In addition to the IgE-dependent mechanism of mast cell degranulation, mast cell degranulation can be initiated *via* other factors, including IgG , cytokines and chemokines, and infection.[21] Since the high-level degranulation cannot be completely explained by increased antigen presentation and IgE-dependent mechanism, we explored the possible IgE-independent mechanism with selective cytokines embedded in the IL-33/ST2 pathway.[22, 23] We observed increased IL-33 release in PEI-AgNP treated after 6 h exposed in the Caco-2 transwell system without LAD2 in the basal compartment (Figure 5.7). However, the release level was not different from each other in the Caco-2/LAD2 transwell system after 6 h of exposure. After 24 h of exposure, the IL-33 level increased for all samples, with that of PEI-AgNP treated cells significantly different from negative control (Figure 5.4). In contrast, we observed a distinctive IL-13 release pattern after 6 h of

exposure of particles in the Caco-2/LAD2 system that was otherwise not observed in the transwell system with Caco-2 and LAD2 cells alone (data not shown). Transwell systems exposed to NPs released higher levels of IL-13 than MPs treated samples, with SiO_2 NPs exposed cells releasing the lowest level. A similar trend was also observed after 24 h of exposure, with the level of IL-13 higher than 6 h.

5.5. Discussion

Allergic reactions to food proteins can be primarily categorized as single mechanism (IgE-dependent and IgE-independent) and mixed mechanisms.[3] The majority type of food allergy is IgE-dependent (type I reaction).[3] IgE is a primary immunoglobulin produced by the immune system in elevated concentrations in individuals with allergic diseases. The common IgE-mediated allergy mechanism has been well-characterized in the literature.[24, 25] Briefly, ingested allergens can be sampled by antigen-presenting cells (e.g., epithelial cells and dendritic cells) in the GI tract and enter tissues. As the allergens were transported and processed in regional lymph nodes or local mucosa, naive T cells acquired the characteristics of T helper 2 (TH2) cells, and B cells were stimulated to produce IgE. The produced IgE will then diffuse into lymphatic and blood vessels and be distributed systemically. Reintroducing the allergen-specific or non-specific IgE into the interstitial fluid allowed their binding to the high-affinity receptor for IgE (FcεRI) and a low-affinity receptor for IgE (CD23) on tissue-resident mast cells, resulting in the sensitization of the mast cells and preparing them to respond upon the subsequent allergen exposure.[24, 25] In the current study, we obtained sera from allergy patients with a high IgE level to sensitize the mast cells, so that LAD cells were primed with IgE and would respond to milk allergens when exposed.

From our past study, we identified the biocorona forming on the surface of the dietary particles that contain a high level of milk protein after 1 h incubation, which enhanced the allergenicity and antigenicity of the allergens.[15] In this study, we also identified the formation of biocorona as the translucent layer on the surface of most of the particles studied (red arrowed in Figure 5.1). SiO_2 particles were more agglomerated and smaller in primary particle size, and the corona formation was not visually evident with TEM. However, previous proteomic analysis for identical particles has proven higher protein adsorption on the surface of the SiO_2 particles than TiO_2 particles, possibly due to the higher surface area to volume ratio.[15] Surface charges of the AgNPs might be playing more critical roles in the corona formation due to surface coating. TEM images of Citrate-AgNP particles showed a more uniform and thicker corona coating than SiO_2 and TiO_2 particles (Figure 5.1), which can be attributed to the smaller size of the particles and mild aggregation state without agglomeration. The suspended state of the particles was maintained by the electrostatic forces between particles and biomolecules in milk and the resulting steric hindrance.[26] The milk-interacted PEI-AgNP was very different from Citrate-AgNP and other dietary particles, where primary particle size decreased significantly (<10 nm) and biocorona similar to other dietary particles were not evident. However, we observed the two types of particles on the grids with smaller particles having higher contrast and bigger particles with low contrast (Figure 5.6). The Energy-dispersive X-ray spectroscopy analysis confirmed the major element in the smaller NPs was silver. The background larger particles were abundant in calcium, phosphorus and nitrogen, suggesting the presence of milk proteins like caseins due to their Ca and P trapping properties.[27] The decrease in particle size and reaction with the biomolecules in the milk matrix suggested dissolution of the Ag^+ from the particles and reprecipitation into smaller particles.[28]

The interaction between PEI-AgNPs and milk also affects intestinal epithelial integrity. In Figure 5.2B, the TEER decreased by about 55 % after 6 h of pristine NP exposure while the milk-interacted PEI-AgNP only decreased by approximately 35% (Figure 5.3B). Although size-dependent effects of AgNPs on intestinal permeability[29] were reported, milk-interacted PEI-AgNPs were not inducing more significant TEER changes than the larger pristine counterparts. The allergen delivery across the intestinal epithelial layer was measured to identify the major transport mechanism. The compromised epithelial layer treated by PEI-AgNP (Figure 5.2C) and milk interacted PEI-AgNP (Figure 5.3C) resulted in enhanced delivery of allergens, while other deliveries were not significantly different from the media control. The results indicated the critical role of paracellular integrity other than transcellular transport during the exposure in this study. In contrast to the similar level of casein in the pre-treatment and co-exposure scenarios, the simultaneous exposure of particles and milk significantly decreased the delivery of BLG (Figure 5.3C), possibly due to the interaction with the small BLG particle and the particles that ended up not crossing the epithelium paracellularly. However, the caseins levels were similar, possibly due to the high abundance of casein naturally in milk.[27]

The delivered concentration of allergens across the intestinal epithelial layer did not fully explain the mast cell degranulation results. For the mast cells in the pre-treatment transwell systems (Figure 5.2D), the highest allergen delivery across the intestinal epithelium transferred to the highest degranulation level in the case of PEI-AgNP. However, the significant increase in Citrate-AgNP pre-treated cells was not resulted from higher allergen delivery, suggesting the possible roles of the epithelial cells in triggering mast cell degranulation.[30] The pre-treatment of particles on Caco-2 layers was shown to cause cellular responses in oxidative stress, mitochondria

dysfunctions, Ca^{2+} influx and resulted in the release of pro-inflammatory cytokines that can also trigger the degranulation of mast cells.[16] Similarly, in the case of simultaneous exposure of particles and milk (Figure 5.3D), the paracellular transport contributed to the highest level of mast cell degranulation. However, paracellular delivery was not the only reason for the high degranulation level for cells co-exposed to milk-interacted NPs. Possible reasons include the release of mediators for degranulation from the epithelial layers, suggesting a synergistic triggering system. In the case of IgE-dependent mechanism of degranulation, IgE is thought to be the primary mediator *via* binding receptors (FcεRI, CD23, etc.) expressed on mast cell surfaces.[31] Subsequent exposure to allergens will immediately trigger the degranulation of mast cells to release preformed, stored mediators for subsequent immune responses, namely, early phase activation.[32] The degranulation and the cytokines released after 6 h exposure should be considered as the early stage activation, and the cytokines measured after 24 h should be considered as *de novo* synthesized mediators during the late phase activation (8-24 h).[33] In addition to the IgE-dependent mechanism, non-IgE mediated responses have also been reported milk protein allergy.[4, 5, 34] IL-33/ST2 pathway is a well-studied mechanism initiated by the epithelial cells that activate mast cells, following an IgE-independent pathway in a late activated manner.[35] Basically, IL-33 is a cytokine that belongs to the IL-1 family that can be triggered due to the stimulus on the Caco-2 cells.[36] Our previous study had demonstrated the increased expression of IL-1 and release of other pro-inflammatory due to the exposure to dietary particles, and thus reasonably hypothesize similar responses may be encountered in this co-exposure scenario with the presence of milk.[16] IL-33 released by epithelial cells bind with the ST2 receptor present on the surface of mast cells. IL-33-ST2 binding triggered downstream responses that culminate in mast cell degranulation *via* the NF-κB pathway and the release of cytokines and chemokines such as IL-13 *via* the MAPK pathway.[37] We measured the

release of IL-13 from mast cells and IL-33 released from Caco-2 cells at 6 h and 24 h (Figure 5.4). The low level of IL-33 released from Caco-2 after 6 h of co-exposure to milk and dietary particles indicated that the release of IL-33 was not related to the early phase activation that accounted for the mast cell degranulation. However, IL-13 levels were significantly different from the media control after 6 h exposure, indicating that the released cytokines might be the pre-synthesized and stored cytokines in the granules of mast cells. As a result, the degranulation of the mast cells and the release of IL-13 at 6 h exposure could be attributed to the IgE-dependent mechanism. After 24 h, however, the dietary particles may exacerbate the immune responses by the increased amount of IL-33 and a higher level of IL-13 *via* a mixed mechanism that may include both IgE dependent and IgE-independent mechanisms.

5.6. Conclusion

Milk allergy can mediate both IgE-dependent and IgE-independent pathways.[5, 34] In this study, we used an *in vitro* model of transwell system consisting of enterocyte model Caco-2 cell and mast cell model LAD2. The simultaneous exposure of milk and dietary particles induced a higher level of mast cell degranulation than the pre-exposure of particles followed by milk, suggesting the role of particles in exacerbating the degranulation responses. In addition to early phase activation, mast cells can also be activated by the cytokines released by the epithelial cells in a late phase manner, which may follow a mixed mechanism including both IgE-dependent and IgE-independent pathways. The results in this study suggested that the widespread application of dietary particles and the potential interaction between milk proteins and particles shall be concerns for individuals susceptible to milk proteins. The study further emphasized the importance of re-evaluating novel

food ingredients like dietary NPs for immune-susceptible individuals and complementing strategies against milk allergy.

5.7. Supplemental Information

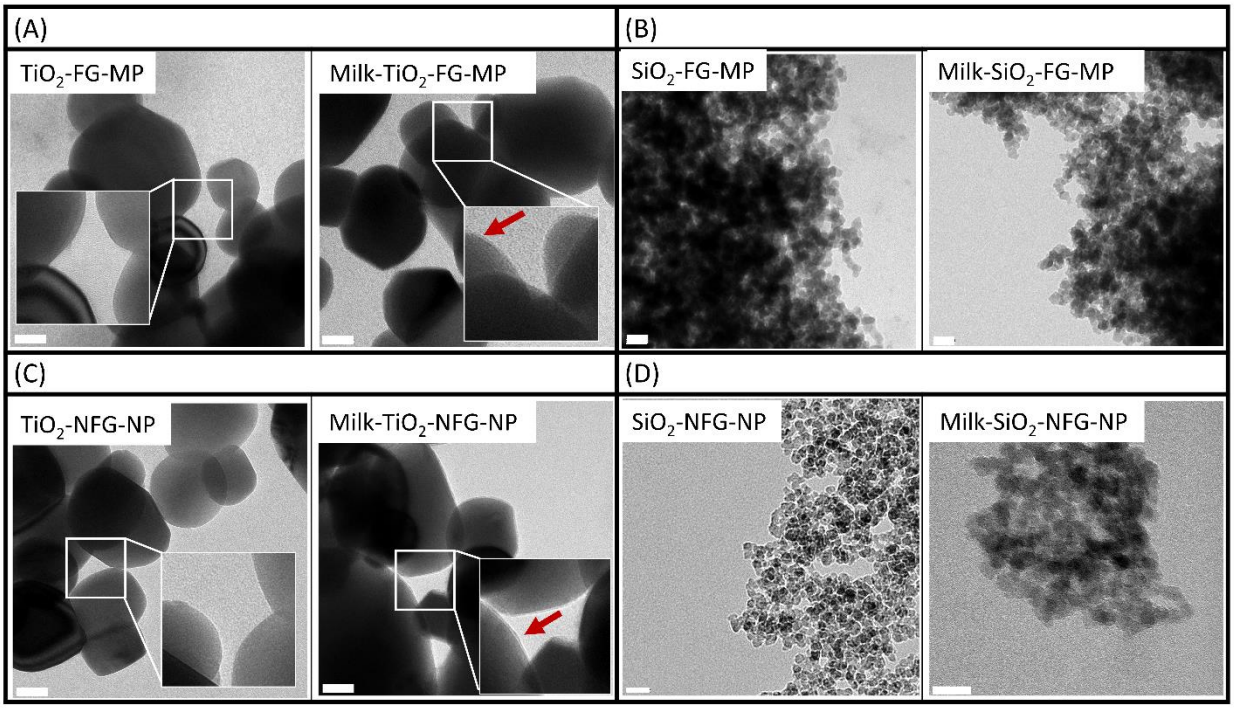

Figure 5.5 Transmittance Electron Microscopy (TEM) images of pristine and milk interacted particles for (A)TiO_2-FG-MP, (B) SiO_2-FG-MP, (C) TiO_2-NFG-NP and (D) SiO_2-NFG-NP. The samples were prepared by drop-casting 5 µL of particles suspension (100 µg/mL) onto 200 -mesh Cu/C TEM grids and dried for 2 h. Images were acquired by Tecnai Spirit 120 kV TEM. Scale bar= 50 nm.

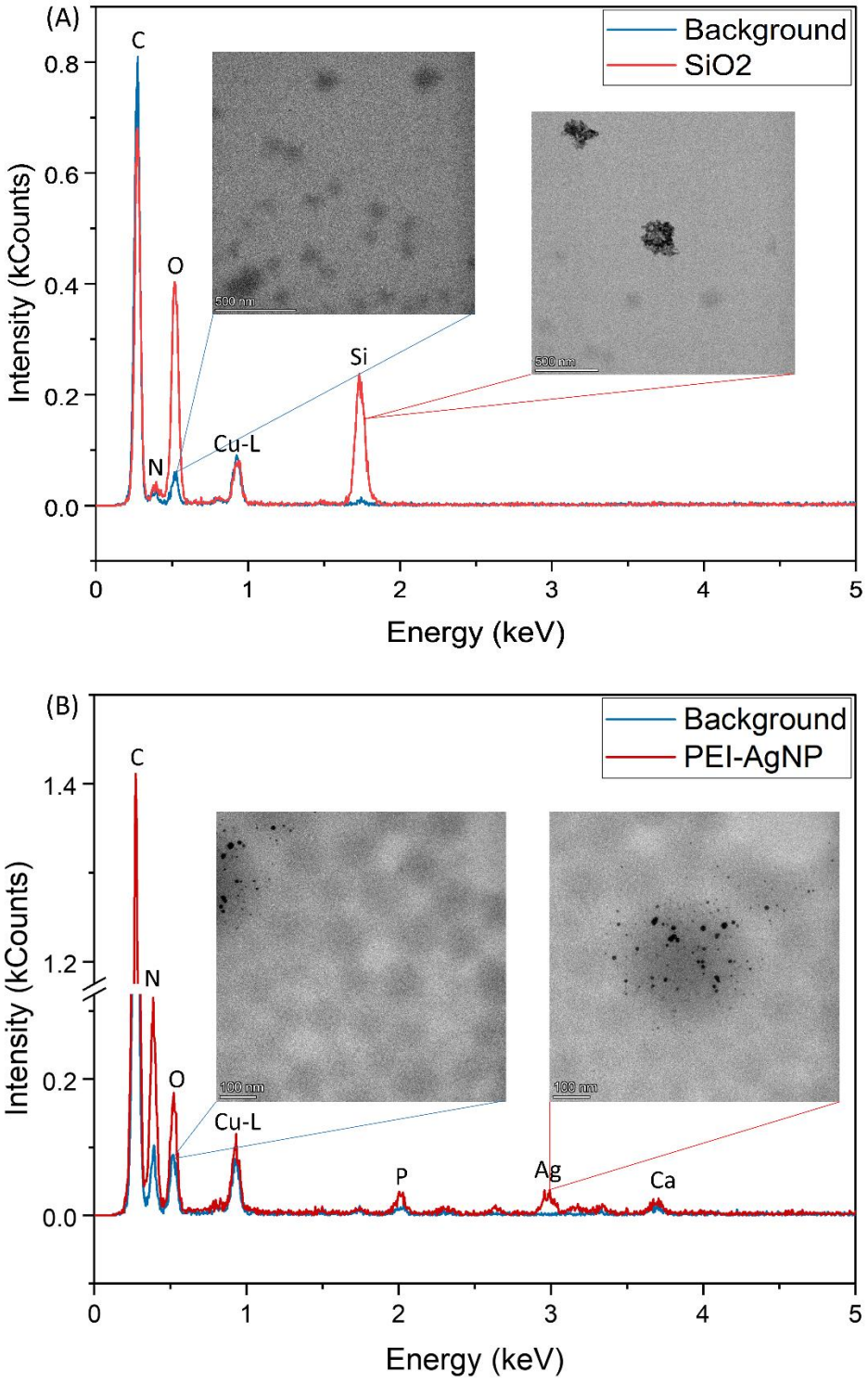

Figure 5.6 Energy-dispersive X-ray spectrostra and Transmittance Electron Microscopy (TEM) images of the milk-interacted particles and the respective background of (A)milk-interacted SiO_2-FG-NP (scale bar=500nm) and (B)PEI-AgNP (scale bar=100nm).

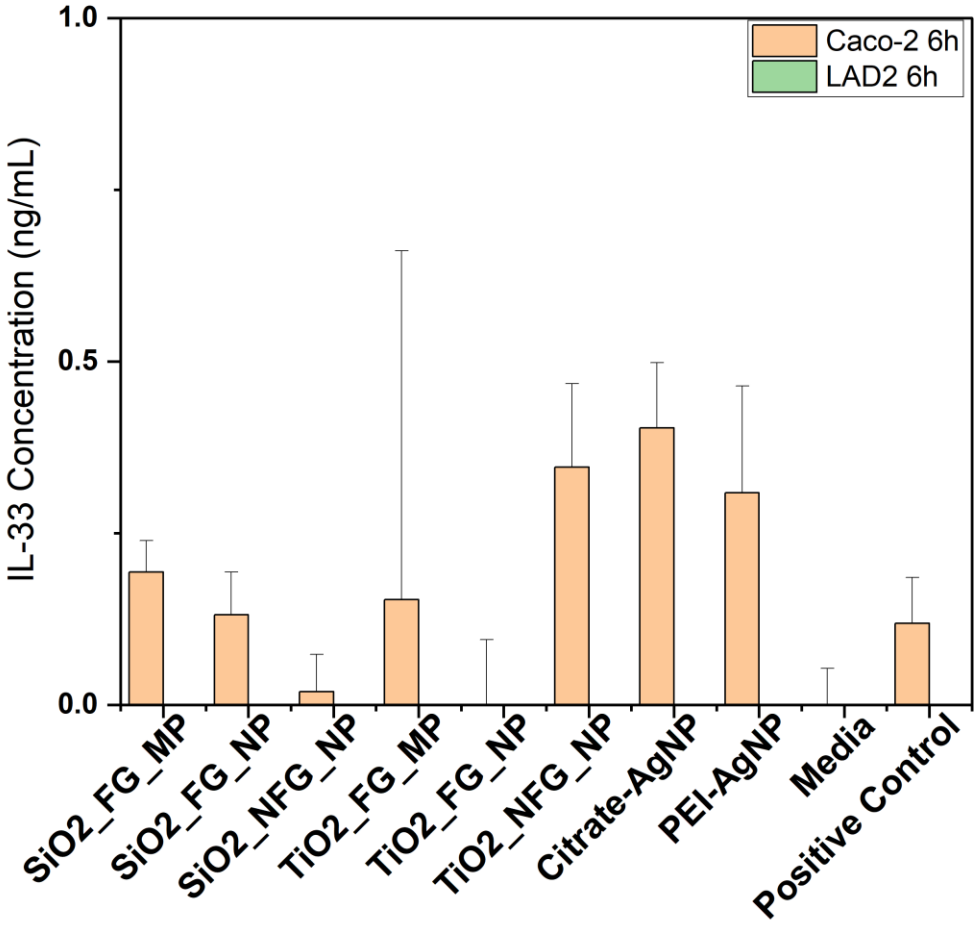

Figure 5.7 Concentration of IL-33 in the basal compartment of the transwell model with one cell model after simultaneous exposure of milk and nanoparticles. The release of IL-33 was measured by ELISA assays following the manufacturer's instruction. The results were quantified by absorbance measurement. Data are expressed as fold change relative to the negative control (Mean ±SD (n=2))

5.8. References

1. Johansson, S. G. O.; Bieber, T.; Dahl, R.; Friedmann, P. S.; Lanier, B. Q.; Lockey, R. F.; Motala, C.; Ortega Martell, J. A.; Platts-Mills, T. A. E.; Ring, J.; Thien, F.; Van Cauwenberge, P.; Williams, H. C., Revised nomenclature for allergy for global use: Report of the Nomenclature Review Committee of the World Allergy Organization, October 2003. *J. Allergy Clin. Immunol.* **2004,** *113* (5), 832-836.

2. Clarke, A. E.; Elliott, S. J.; Pierre, Y. S.; Soller, L.; La Vieille, S.; Ben-Shoshan, M., Temporal trends in prevalence of food allergy in Canada. *J. Allergy Clin. Immunol. Pract.* **2020,** *8* (4), 1428-1430. e5.

3. Sicherer, S. H.; Sampson, H. A., Food allergy. *J. Allergy Clin. Immunol.* **2010,** *125* (2, Supplement 2), S116-S125.

4. Høst, A., Frequency of cow's milk allergy in childhood. *Annals of Allergy, Asthma & Immunology* **2002,** *89* (6, Supplement), 33-37.

5. Saarinen, K. M.; Pelkonen, A. S.; Mäkelä, M. J.; Savilahti, E., Clinical course and prognosis of cow's milk allergy are dependent on milk-specific IgE status. *J. Allergy Clin. Immunol.* **2005,** *116* (4), 869-875.

6. Wal, J. M., Structure and function of milk allergens. *Allergy* **2001,** *56* (s67), 35-38.

7. Fiocchi, A.; Brozek, J.; Schünemann, H.; Bahna, S. L.; Von Berg, A.; Beyer, K.; Bozzola, M.; Bradsher, J.; Compalati, E.; Ebisawa, M., World Allergy Organization (WAO) diagnosis and rationale for action against cow's milk allergy (DRACMA) guidelines. *World Allergy Organ. J.* **2010,** *3* (4), 57-161.

8. Vance, M. E.; Kuiken, T.; Vejerano, E. P.; McGinnis, S. P.; Hochella, M. F.; Rejeski, D.; Hull, M. S., Nanotechnology in the real world: Redeveloping the nanomaterial consumer products inventory. *Beilstein J. Nanotechnol.* **2015,** *6*, 1769-1780.

9. Dekkers, S.; Krystek, P.; Peters, R. J.; Lankveld, D. P.; Bokkers, B. G.; van Hoeven-Arentzen, P. H.; Bouwmeester, H.; Oomen, A. G., Presence and risks of nanosilica in food products. *Nanotoxicology* **2011,** *5* (3), 393-405.

10. Weir, A.; Westerhoff, P.; Fabricius, L.; Hristovski, K.; von Goetz, N., Titanium Dioxide Nanoparticles in Food and Personal Care Products. *Environ. Sci. Technol.* **2012,** *46* (4), 2242-2250.

11. Alsaleh, N. B.; Persaud, I.; Brown, J. M., Silver Nanoparticle-Directed Mast Cell Degranulation Is Mediated through Calcium and PI3K Signaling Independent of the High Affinity IgE Receptor. *PloS one* **2016,** *11* (12), e016736.

12. Chen, E. Y.; Garnica, M.; Wang, Y.-C.; Mintz, A. J.; Chen, C.-S.; Chin, W.-C., A mixture of anatase and rutile TiO2 nanoparticles induces histamine secretion in mast cells. *Part. Fibre Toxicol* **2012,** *9* (1), 2.

13. Radauer-Preiml, I.; Andosch, A.; Hawranek, T.; Luetz-Meindl, U.; Wiederstein, M.; Horejs-Hoeck, J.; Himly, M.; Boyles, M.; Duschl, A., Nanoparticle-allergen interactions mediate human allergic responses: protein corona characterization and cellular responses. *Part. Fibre Toxicol.* **2016,** *13* (1), 3.

14. Phue, W. H.; Bahadi, M.; Dynes, J. J.; Wang, J.; Kuppili, V. S. C.; Ismail, A.; Hameed, A.; George, S., Protein–biomolecule interactions play a major role in shaping corona proteome: studies on milk interacted dietary particles. *Nanoscale* **2021,** *13* (31), 13353-13367.

15. Phue, W. H.; Xu, K.; George, S., Inorganic food additive nanomaterials alter the allergenicity of milk proteins. *Food Chem. Toxicol.* **2022,** *162*, 112874.

16. Xu, K.; Basu, N.; George, S., Dietary nanoparticles compromise epithelial integrity and enhance translocation and antigenicity of milk proteins: An in vitro investigation. *NanoImpact* **2021,** *24*, 100369.

17. Yu, L. C. H.; Perdue, M. H., Role of mast cells in intestinal mucosal function: studies in models of hypersensitivity and stress. *Immunol. Rev.* **2001,** *179* (1), 61-73.

18. Wan, Y.; Guo, Z.; Jiang, X.; Fang, K.; Lu, X.; Zhang, Y.; Gu, N., Quasi-spherical silver nanoparticles: Aqueous synthesis and size control by the seed-mediated Lee–Meisel method. *J. Colloid Interface Sci.* **2013,** *394*, 263-268.

19. Toh, H. S.; Faure, R. L.; Mohd Amin, L. B.; Hay, C. Y. F.; George, S., A light-assisted in situ embedment of silver nanoparticles to prepare functionalized fabrics. *Nanotechnol. Sci. Appl.* **2017,** *10*, 147-162.

20. Kirshenbaum, A. S.; Yin, Y.; Sundstrom, J. B.; Bandara, G.; Metcalfe, D. D., Description and Characterization of a Novel Human Mast Cell Line for Scientific Study. *Int. J. Mol. Sci.* **2019,** *20* (22), 5520.

21. Yu, Y.; Blokhuis, B. R.; Garssen, J.; Redegeld, F. A., Non-IgE mediated mast cell activation. *Eur. J. Pharmacol.* **2016,** *778*, 33-43.

22. Kakkar, R.; Hei, H.; Dobner, S.; Lee, R. T., Interleukin 33 as a mechanically responsive cytokine secreted by living cells. *J. Biol. Chem.* **2012,** *287* (9), 6941-6948.

23. Kakkar, R.; Lee, R. T., The IL-33/ST2 pathway: therapeutic target and novel biomarker. *Nat. Rev. Drug Discov.***2008,** *7* (10), 827-840.

24. Galli, S. J.; Tsai, M., IgE and mast cells in allergic disease. *Nat. Med.* **2012,** *18* (5), 693-704.

25. Gould, H. J.; Sutton, B. J., IgE in allergy and asthma today. *Nat. Rev. Immunol.* **2008,** *8* (3), 205-217.

26. Chanteau, B.; Fresnais, J.; Berret, J.-F., Electrosteric enhanced stability of functional sub-10 nm cerium and iron oxide particles in cell culture medium. *Langmuir* **2009,** *25* (16), 9064-9070.

27. Rogers, M. A., Naturally occurring nanoparticles in food. *Curr. Opin. Food Sci.* **2016,** *7*, 14-19.

28. Loza, K.; Diendorf, J.; Sengstock, C.; Ruiz-Gonzalez, L.; Gonzalez-Calbet, J.; Vallet-Regi, M.; Köller, M.; Epple, M., The dissolution and biological effects of silver nanoparticles in biological media. *J. Mat. Chem. B* **2014,** *2* (12), 1634-1643.

29. Williams, K. M.; Gokulan, K.; Cerniglia, C. E.; Khare, S., Size and dose dependent effects of silver nanoparticle exposure on intestinal permeability in an in vitro model of the human gut epithelium. *J. Nanobiotechnology* **2016,** *14* (1), 62.

30. Shao, L.; Serrano, D.; Mayer, L., The role of epithelial cells in immune regulation in the gut. *Semin. Immunol.* **2001,** *13* (3), 163-175.

31. Burton, O. T.; Oettgen, H. C., Beyond immediate hypersensitivity: evolving roles for IgE antibodies in immune homeostasis and allergic diseases. *Immunol. Rev.* **2011,** *242* (1), 128-143.

32. Johnson, M. M.; Mendoza, R.; Raghavendra, A. J.; Podila, R.; Brown, J. M., Contribution of engineered nanomaterials physicochemical properties to mast cell degranulation. *Sci. Rep.* **2017,** *7*, 43570.

33. Mendoza, R. P.; Brown, J. M., Mast Cells and Nanomaterials. In *Interaction of Nanomaterials with the Immune System*, Springer: 2020; pp 55-72.

34. Schouten, B.; van Esch, B. C. A. M.; van Thuijl, A. O. J.; Blokhuis, B. R. J.; Groot Kormelink, T.; Hofman, G. A.; Moro, G. E.; Boehm, G.; Arslanoglu, S.; Sprikkelman, A. B.; Willemsen, L. E. M.; Knippels, L. M. J.; Redegeld, F. A.; Garssen, J., Contribution of IgE and immunoglobulin free light chain in the allergic reaction to cow's milk proteins. *J. Allergy Clin. Immunol.* **2010,** *125* (6), 1308-1314.

35. Cayrol, C.; Girard, J.-P., IL-33: an alarmin cytokine with crucial roles in innate immunity, inflammation and allergy. *Curr. Opin. Immunol.* **2014,** *31*, 31-37.

36. Mertz, K. D.; Mager, L. F.; Wasmer, M.-H.; Thiesler, T.; Koelzer, V. H.; Ruzzante, G.; Joller, S.; Murdoch, J. R.; Brümmendorf, T.; Genitsch, V., The IL-33/ST2 pathway contributes to intestinal tumorigenesis in humans and mice. *Oncoimmunology* **2016,** *5* (1), e1062966.

37. Liew, F. Y.; Pitman, N. I.; McInnes, I. B., Disease-associated functions of IL-33: the new kid in the IL-1 family. *Nat. Rev. Immunol.* **2010,** *10* (2), 103-110.

Preface to Chapter 6

The previous three chapters studied the effects of dietary NPs exposure on subcellular, cellular responses, and barrier functions of the intestinal epithelium. Based on the findings, a series of experimental models and bioassay panels were identified to enable more efficient toxicity assessment of chemicals using *in vitro* models (these are defined as New Approach Methodologies, or NAMs, which have gained regulatory interest worldwide as a scheme to modernize toxicity testing into a practice that is more efficient, cost-effective, predictive, and ethical). To help ensure that the work of Chapters 3-5 were relevant, the identified changes were also linked (through the Adverse Outcome Pathway, AOP, framework) to the progression of cow milk protein allergy, a gastrointestinal (GI) disorder condition of public health concern.

The previous studies used pristine particles while recognizing that biological fluids in different compartments of the GI tract will modify the surface and properties of the particles during digestion, and thus may modify toxicity. The study in this chapter used a complex, multilayered NP model (quantum dots) and investigated the effects of the transformation of the NPs in the GI tract on their toxicity with the panel of bioassays from chapter 3. Chapter 6 applied the bioassay panels identified in previous chapters and investigated the toxicity of the quantum dots by investigating the contributions of individual components to the overall toxicity. The study also characterized the role of biological transformation (three-phase simulated digestion) in modifying the toxicity of ingested particles.

This chapter was initiated by the candidate and Dr. Aude Bechu under the supervision of Dr. Saji George, Dr. Audrey Moores, Dr. Subahsis Goshal, and Dr. Niladri Basu within The McGill

Sustainability Systems Initiative (MSSI). In collaboration with the coauthors, the candidate was responsible for the study design and conduction. Dr. Aude Bechu synthesized quantum dots and all the combinations of the individual component of quantum dots for this project and tracked the transformation of quantum dots in the digestive system. The candidate performed confocal microscopy imaging and Fourier-transform infrared spectroscopy for the transformation study. Transformation analysis were fully presented in Dr. Aude Bechu's thesis. The toxicity analysis for the pristine and transformed quantum dots was performed by the candidate and was fully included in this chapter. The data analysis and interpretation, discussion of the results, and manuscript preparation were shared between the candidate and Dr. Aude Bechu, under the supervision of Dr. Saji George, Dr. Audrey Moores, Dr. Subahsis Goshal, and Dr. Niladri Basu.

The toxicity analysis of the pristine quantum dots, titled "Hazard profiling of components constituting a commercially-relevant functional quantum dot revealed synergistic interactions between heavy metals and polymer" has been published in *Chemical Research in Toxicology* in 2022. The transformations of the quantum dots during simulated digestion and the corresponding effects on toxicology were presented in the manuscript "Cd-containing quantum dots transform during simulated human digestion, causing increased adverse subcellular effects to intestinal cells" and will be communicated shortly for publication.

Chapter 6

6. The role of individual components and material transformation under simulated digestion in determining hazard potential of a complex nanoparticle (Quantum Dot)

6.1. Abstract

Despite the popular application of the nanoparticles (NPs) in food, the toxicity of ingested NPs has not been fully investigated. Oral ingestion and the subsequent digestion processes in the gastrointestinal (GI) tract are critical in the transformation of the NPs inside the human body and may have significant impacts on their toxicity. Commercially used quantum dots (QDs) exemplify complex nanomaterials with multiple components and can be used as the model material for transformation analysis, enabled by easier tracking and characterization due to their fluorescence properties. We synthesized and characterized a functional QD (CdSe/ZnS_P&E) that was identical in structure and composition to a patented and commercially applied QD, and the combinations of its components (CdSe, CdSe/ZnS, ZnS, CdSe_P&E, ZnS_P&E, P&E). Cells exposed to incremental concentrations of these materials were investigated for cellular perturbations using high-content screening assays in model human intestinal epithelial cells (HIEC-6). Complete QD (core/shell-polymer) showed the highest toxic potential due to synergistic interactions between core, shell, and surface functional groups. The particles were further subjected to a three-phase simulated digestion process, including salivary, gastric, and intestinal digestions, to identify the effect of biotransformation on QD toxicity. Increasing toxicity of the QDs was identified along the simulated GI digestion, accompanied by changes in the QD structure and biomolecule interactions. Overall, this study advances our understanding of the collective contribution of individual

components of a functional QD towards its toxic potential and emphasizes the critical effects of biotransformation for the toxicity of ingested NPs.

6.2. Introduction

Consumers of a typical western diet are exposed to approximately 10^{12}-10^{14} nanoparticles (NPs) and micron-sized particles per day from oral ingestion,[1] for which insufficient knowledge remains about the fate and safety impacts of these materials. This widespread adoption and lack of safety management has led to concerns of possible unintended hazards of NPs and triggered intense research efforts.[2, 3] Some critical studies have contributed to regulatory restrictions on food applications of certain nanomaterials. For instance, recent data pointed to the possible genotoxicity of TiO_2 NPs and has led to the ban of TiO_2 NPs as food additives in Europe.[4]

Research on NP safety and toxicity has emphasized the importance of oral exposure as a key entry point and gastrointestinal (GI) digestion as a key contributor to human toxicity. One major discrepancy between *in vivo* animal studies and *in vitro* cell model studies for oral toxicity of nanomaterials lies in the transformation of nanomaterials in the GI tract.[5] Previous studies have used various static and dynamic models to simulate the physiological conditions (pH, temperature, ionic strength, digestive enzymes, etc.) of different compartments in the GI tract (mouth, stomach, and intestine).[3, 6-9] Often, studies might not follow the complete digestion process, and thus failed to consider the cumulative nature of the transformation.[10, 11] These experimental inconsistencies have recently been addressed in the field by the INFOGEST initiative, which standardized an *in vitro* digestion procedure. Furthermore, characterization of NPs and their by-products during transformation is absent from most works that explore the toxicity of transformed particles. Thus, a complete understanding of NP toxicity in the GI tract demands an integrated approach whereby transformation and toxicity are considered together sequentially.

In addition to the proper design of the simulated digestion process, another critical factor is the complex nature of relevant NPs themselves. NPs have distinct properties in their composition, structure, and surface modifications that greatly affect their interactions with the bio-interface and eventually change their toxicities.[5] The characterization and toxicity for commercially relevant multi-layered NPs can be even more challenging, as they are often complex mixtures of proprietary chemicals, carefully structured at the nano level. In our previous study, we synthesized such a model for commercially-relevant QD based on a published patent (US 9,199,842 B2) and our analysis of the various metal ratios in QD-containing TV screen films.[12] The QD model contained a CdSe core covered by a graded CdS and ZnS shell and a crosslinked polymer of polyethyleneimine and 1,2 epoxy-3-phenoxypropane (P&E).[13, 14] We found that the LC_{50} (lethal concentration that caused 50% death of the exposed HepG2 cells) of pristine QDs was on par with a simple mixture of its labile components, which is a combination of Cd^{2+}, Zn^{2+} ions, and the polymer.[12] The similar LC_{50} values between the pristine QDs and the component mixture suggested possible combinational effects, meaning that the toxicity of the commercially-relevant QDs with the core, shell, and polymer coating may equal, increase, or decrease the sum of the toxicity of individual components. An additional technical benefit of taking QD as model NP is the featured fluorescence properties, which enable easier tracking and characterization of the chemical and structural compositions in each digestion phase. Using such a representative NP model to understand their GI tract toxicity will be vital in understanding the complex nature of digestion and deriving useful knowledge for the transformations of ingested complex NPs.

In this study, we used the developed QD model and studied the cytotoxic effects of the components of the pristine QD on Human Intestinal Epithelial Cell-6 (HIEC-6), which is an intestinal

epithelium crypt cell[15] model, and used the results to quantitatively probe the potential combinational effects of the individual QD components based on combination index calculation. The sublethal effects were further investigated using multiparametric toxicity assays to identify the mechanism of toxicity. The synthesis of different permutations of QD components enabled the identification of the differential effect of QD components on cell viability, oxidative stress, and other responses. In addition, we probed both transformations and toxicity of the QDs at every digestion stage, in a "stage-by-stage" approach with an acquired INFOGEST procedure.[16] The toxicity of QDs at each stage of the simulated digested was also studied on the HIEC-6 to test for cellular responses using multiparametric bioassays. We observed decreased particle size and gradual loss of the shell, and the dissolution of Cd ions from the QD core as simulated digestion progressed, which resulted in increasing toxicity mediated by increased bioavailability.

6.3. Materials and Methods

6.3.1. Materials

The QDs used in this study are as follows: (1) cadmium selenide core with cadmium sulfide and zinc sulfide shell with octadecylamine ligand (CdSe/ZnS), (2) cadmium selenide core with myristic acid ligand (CdSe), (3) zinc sulfide QD with oleylamine ligand (ZnS). The QDs were then covered with a coating polymer (P&E) composed of polyethyleneimine complexed with 1,2-epoxy-3-phenoxypropane and were labeled as CdSe/ZnS_P&E, CdSe_P&E, and ZnS_P&E. All particles were synthesized and provided by Dr. Aude Bechu. The composition of the particles was briefly summarized in the SI (Table 6.2), and a detailed synthesis protocol can be found in the previous publication.[12]

6.3.2. Simulated human digestion

The QDs were subjected to a three-stage (salivary, gastric, and intestinal stage) simulated human digestion process based on a modified protocol according to Brodkorb *et al.*,[16] and are described briefly below. The general composition of each digestion fluid is listed in the SI (Table 6.6, modeled after Table 2 in Brobkorb *et al.*). QDs were initially dispersed in sera-free media containing media at 1250 µg/mL. Then, 1 mL of this solution was mixed with the same volume of simulated salivary fluid (SSF) in the salivary digestion stage (2 mL final volume). The mixture was placed on an orbital shaker (Forma Scientific 420) and incubated at 120 rpm at 37°C for 2 minutes (min). Samples were taken as SSF digested QDs, and the mixture was further mixed in a 1:1 ratio with simulated gastric fluid (SGF) and incubated on the shaker for 2 hours (h). After incubation, the pH of the solution was adjusted to pH=7 with 1M NaOH before samples were taken. Then, simulated intestinal fluid (SIF) was mixed at the ratio of 1:1 with the solution in the previous step. The mixture was kept in the incubated orbital shaker for another 2 h at 120 rpm, 37°C. To stop the enzyme digestion, samples taken at each stage were subjected to heat-shock treatment (placed in boiling water for 5 min) to inactivate enzymes. The inactivated samples were then subjected to ultracentrifugation (Optima)

6.3.3. Visualization of digested QD with confocal microscopy

The aliquots from each digestion phase were deactivated (5 min boiling) and drop-casted onto a microscope slide. The dried samples were then imaged with the LSM 710 confocal laser scanning microscopy (Carl Zeiss, Oberkochen, Germany).

6.3.4. Cell culture

HIEC-6 cells are normal cell models that do not differentiate upon confluency and exhibit markers resembling undifferentiated lower crypt cell functions.[15] In this study, HIEC-6 cells (ATCC# CRL-3266) were purchased from ATCC(ATCC, VA, USA), and passages between 7 and 20 were cultured in 100 mm Petri dishes supplemented with 10 mL complete media. The complete media consisted of OptiMEM I Reduced Serum Medium (Gibco, Thermofisher), 4% fetal bovine serum (FBS) (WISENT, QC, Canada), 1% PEN-STREP (WISENT), 20 mM HEPES (Thermofisher), 10 mM GlutaMAX (Thermofisher), and 10 ng/mL Epidermal Growth Factor (EGF) (Thermofisher). Cells were incubated at 37 °C and supplied with 5% CO_2 and 95% humidity, with media changed every two days. As HIEC-6 cells are adherent, they were harvested upon reaching 90% confluency using Trypsin/EDTA (WISENT) and sub-cultured or seeded for subsequent experiments.

6.3.5. Particle exposure to cells

HIEC-6 cells were seeded at a density of 1×10^4 in each well of 96 well plates (volume 100 µL), 2×10^3 in 384 well plates (volume 30 µL) or 5×10^4 in 24 well plates (volume 0.5 mL) overnight before exposure. To prepare samples for exposure, 100 µg/mL particle suspensions were prepared for each type of particle in sera-free media (complete culture media without 4% FBS). Particles without P&E polymer were first suspended in 1:1 chloroform and dimethyl sulfoxide (DMSO) solution at 10 mg/mL and sonicated with the MISONIX S-4000 ultrasonicator at 12 W for 30 seconds (s) with a pulse every 10 s (Qsonica, Newton, CT, USA) to disperse in the aqueous phase. The mixture was then suspended in sera-free media followed by serial dilutions (two-fold) from 100 µg/mL to 1.56 µg/mL for all particle samples. The original culture media in each well were aspirated and replaced with prepared particle suspensions and incubated for 24 h. $CdCl_2$ (99.99%,

Sigma) was used as Cd^{2+} source in the ion control. Cells used as the ion controls were exposed to working concentrations of $CaCl_2$ dissolved in sera-free media. Cells used as negative controls were incubated in sera-free media alone. Three replicates of each test concentration were assayed in the 96 well plates for cell viability and cytokines release measurement. Four replicates of each treatment were performed in 384 well plates for the assays targeting other sub-lethal cellular responses.

Digested QDs from each of the stages, separated in the pellet by ultracentrifugation at 234,000g for 30 min (Optima XL-100K Beckman Coulter, California, USA), were diluted to 100µg/mL in sera-free media and two-fold serial dilution was performed subsequently until concentrations of 1.5625 µg/mL were reached for all particle samples. Particle suspensions at prepared concentrations (1.5625, 3.125, 6.25, 12.5, 25, 50, 100 µg/mL) were subsequently added to wells in 384 well plates containing confluent HIEC-6 cells originally seeded at a density of 2×10^3. These plates were then incubated for 24 h. Cells exposed to sera-free media were considered negative controls, and pristine QD suspensions with the same concentration range were used as positive controls. Four replicates were performed for each sample concentration.

6.3.6. Cell viability assessment for pristine QD

After 24 h of QD particle exposure, cells in 96 wells plates were washed three times with fresh sera-free media, followed by the addition of 50 µg/mL resazurin (Abcam, USA). Fluorescence intensity was measured at 530 nm excitation and 590 nm emission with the Spectramax i3x plate reader (Molecular Devices, San Jose, USA) after 4 h of incubation. The positive controls of this assay include $CdCl_2$ (99.99%, Sigma) and $ZnSO_4$ (99%, Sigma) dispersed in the same

concentration gradients as the samples (1.56 µg/mL to 100 µg/mL). Percentage cell viability was calculated based on non-exposed cells, and statistical comparison was conducted using the student t-test (p<0.05, n=3).

6.3.7. Combination index for identifying interactions between individual components in overall pristine QD toxicity

Combination indexes were calculated based on the method originally developed by Chou and Talalay[17], which provides a quantitative estimate of the contribution of individual compounds to the overall toxicity of the mixture.[18] The combination index, CI, can be calculated by the following general equation:

$$CI = \frac{C_1}{(C_x)_1} + \frac{C_2}{(C_x)_2} + \ldots \frac{C_n}{(C_x)_n} \quad (1)$$

C_n represents the concentration of the component that yields a certain percentage (%) increase in cellular perturbation in combination with n components. $(C_x)_n$ is the concentration of C_n alone that exerts a certain % increase in cellular perturbation. CI < 1 indicates synergism, CI = 1 suggests addition, and CI >1 represents antagonism of the combinations.

Curve fitting was performed using 4 parameter logistics equation between the concentration of the sample (x) and the % viability (y) (Equation 2), the 4 parameters (A1, A2, x0, and p) were then used to derive EC_{20} (Equation 3). Fitting and parameter calculations were performed by Origin Pro 2018 software (version 95E [2018])

$$y = A2 + \frac{A1-A2}{1 + \left(\frac{x}{x0}\right)^p} \quad (2)$$

$$EC_{20} = 10^{log(x0)+\frac{log(0.25)}{p}} \quad (3)$$

6.3.8. Pristine QD induced the release of inflammatory cytokines

After 24 h particle exposure, the media from the wells of the 96 well plates were collected and centrifuged at 1500 rpm, 4 ºC for 5 min to remove cell debris. Subsequently, Interleukin-8 (IL-8), Tumour Necrosis Factor- α (TNF-α), and Interleukin-10 (IL-10) levels in the supernatant were determined using enzyme-linked immunosorbent assay (ELISA) kits according to instructions provided by the manufacturer (Sigma). The absorbance of the reaction product was measured at 405 nm using Spectramax i3x plate reader (Molecular Devices) and converted to cytokine concentration using a standard curve prepared from the respective kit. The presented fold changes were calculated based on the negative control (sera-free media without particle exposure) as mean +SD (n=3). $CdCl_2$ was used as the positive control. Significance was calculated by one-way ANOVA tests with 0.05 significance level and presented in the compact letter display. Comparison between different particle exposures was only conducted for the same cytokines.

6.3.9. Multiparametric cytotoxicity assay in cells exposed to test samples

High-content screening assays were carried out with cells exposed to pristine QDs, components of QDs, and digested QDs in the clear bottom black 384 chamber plates (Nunc cell culture, Thermofisher), as detailed previously.[20] Cellular perturbations contributing to the final pathway of cell death were measured using fluorescent probes. Accordingly, wavelength-compatible fluorescent probes were mixed in Dulbecco′s Phosphate Buffered Saline (DPBS) buffer (Invitrogen, Thermofisher) as described in Table 6.7. The first cocktail consisted of Hoechst 33342 (1 μM), 2',7'-dichlorodihydrofluorescein diacetate (H_2DCFDA, abbreviated as DCF) (10 μM), and

LysoTracker (75 nM); the second cocktail was comprised of Hoechst 33342 (1 μM), Fluo-4 (5 μM) and propidium iodide (PI) (5 μM); the third cocktail contained Hoechst 33342 (1 μM) and MitoSox Red (5 μM); the last cocktail included Hoechst 33342 (1 μM) and JC-1 (1 μM). Thirty μL (cocktails 1 and 2) or 20 μL (cocktails 3 and 4) of dye mixture was added to each well of the 384 well plates containing particle-exposed cells. Incubation was continued for another 30 min under standard culture conditions in the incubator. Zeiss Cell Discoverer 7 was used to capture fluorescence images of the cells from each well (Carl Zeiss Microscopy, Oberkochen, Germany). Three pictures were collected from each well in three different positions (upper-middle, middle, and lower-middle section of the well) using 10× magnification.

Images captured were analyzed with Zeiss ZEN software (version 3.1 [2020]) to determine the cellular responses. For data analysis, the intensity sum of each channel in a well was normalized by the number of cells, which was counted based on morphological features of the nucleus stain. The resulting normalized intensity values of the three pictures collected from one well were averaged to represent each replicate, and the results of each sample were calculated based on 4 replicates from four respective wells. Heatmap was constructed by calculating strictly standardized mean difference (SSMD). Samples with SSMD score <1 were not significantly different from the control group and were colored green; SSMD scores between 1-2 denoted moderate difference from the control and were colored yellow; SSMD between 2-3 denoted strong differences and were colored orange; SSMD>3 represented samples strongly different from the control and were colored red.

6.3.10. Cellular uptake of QDs

6.3.10.1. Localization of QD uptake

The cellular uptake of QDs was visualized by LSM 710 confocal laser scanning microscopy (Carl Zeiss, Oberkochen, Germany) with Argon ion laser at 488 nm. Confluent HIEC-6 cells were seeded in 8 chamber culture slides (Falcon, Fisher Scientific, ON, Canada) and were exposed to 25 µg/mL particle suspensions (CdSe/ZnS and CdSe/ZnS_P&E) for 6 h. After exposure, cells were washed three times with DPBS buffer (pH =7.4), fixed with 4% formaldehyde (Sigma) for 15 min, and permeabilized with 0.25% Triton X-100 (Sigma) in PBS (PBST) for 10 min. F-actin filaments were stained by Phalloidin conjugated with Alexa 488 (Sigma), and cell nuclei were stained by Hoechst 33342 (Thermofisher). Stained cells were incubated at RT in the dark for 10 min. The cells were then imaged by LSM 710 confocal laser scanning microscopy (Carl Zeiss). Based on the emission wavelength (590 nm) identified in the previous study, the red channel was used to capture images and measure the fluorescence intensity of the QDs.[12]

6.3.10.2. Quantifying QD cellular uptake

The differences in bioavailability of QD-derived heavy metals (Cd, Se, Zn) after exposure to different test materials were measured using inductively coupled plasma mass spectroscopy (ICP-MS) in cell digests. HIEC-6 cells were seeded in 6 well plates at a density of 2.5×10^5 overnight and were exposed to 25 µg/mL particle suspensions for 6 h. After exposure, the particle suspensions were aspirated, and cells in 6 wells plates were washed three times with fresh sera-free culture media. The cells were then trypsinized by 0.25% Trypsin-EDTA (Gibco) and harvested by centrifugation (Eppendorf 5430R Refrigerated centrifuge, 255×g, 5 min). In each

case, 10 µL cell suspension was used to count cells. Cells were then digested with 400 µL 70 % (v/v) HNO_3 in open 15ml Digitubes at 90 °C using a heating block for 1 h, followed by 400 µL H_2O_2 digestion in the same condition. The digestion product was diluted with Milli-Q water to 1.3% (v/v) HNO_3 acid for ICP-MS analysis. Total amounts of Cd, Se, and Zn in the cell digest were determined using Perkin Elmer NexION 300X ICP-MS by reading wavelengths 82, 66, 114 for Se, Zn, Cd, respectively. Zn, Se, and Cd standards of 1-20 ng/mL were made from TraceCERT standard solutions. The measured values were normalized to cell counts in respective wells and were presented as the mass of the designated elements in micrograms per one million cells. Significance was calculated by one-way ANOVA tests with a 0.05 significance level and presented in the compact letter display.

6.4. Results

6.4.1. Particle characterization

The QD model used in this study (CdSe/ZnS_P&E) has been well-characterized in our prior study.[12] The average sizes of all components were about 3-5 nm (CdSe/ZnS =4.8 ± 0.8 nm, CdSe =3.2 ± 0.4 nm, ZnS =4.0 ± 0.6 nm). CdSe and ZnS particles were spherical, while CdSe/ZnS particles were more angular due to uneven growth of sulfide shells, which is common in both commercial and lab-synthesized QDs.[19, 20] A known amount of polymer was added onto the QDs such that the inorganic portion of the mixture (Cd, Se, Zn, and S) was 4 wt%. After adding the polymer, all particles were positively charged as indicated by zeta potential measurements (data presented in Aude's thesis). The hydrodynamic diameter of the polymer-coated QDs (66-141 nm) was much larger than the primary diameter of the inorganic core-shell alone (measured

by TEM), due to the presence of the polymer and possible aggregation in the solution. The CdSe_P&E and the ZnS_P&E particles were synthesized wherein the amount of Cd and Zn were comparable to CdSe/ZnS_P&E.

6.4.2. Cytotoxicity of QDs and combination index calculation

HIEC-6 cells were exposed to the CdSe/ZnS_P&E QDs and their components, and the resulting cytotoxic responses in Figure 6.1 were measured with a resazurin assay. CdSe/ZnS_P&E QD was identified to be the most cytotoxic particle of all tested samples as it caused 20% cell death (EC_{20}) at the lowest concentration (2.47 µg/mL from Table 6.1). Generally, polymer-coated particles (CdSe_P&E, ZnS_P&E, CdSe/ZnS_P&E) were more toxic as their EC_{20} values were at or below 10 µg/mL in comparison to particles without surface coating. Other components, including CdSe, ZnS, and CdSe/ZnS, were less toxic than their coated counterparts (EC_{20} values greater than 20 µg/mL). Ion control samples ($CdCl_2$ and $ZnSO_4$) also exhibited higher cytotoxicity than the individual components of QD, as both $CdCl_2$ and $ZnSO_4$ were able to induce about 20% cell death at concentrations below 10 µg/mL (Figure 6.1).

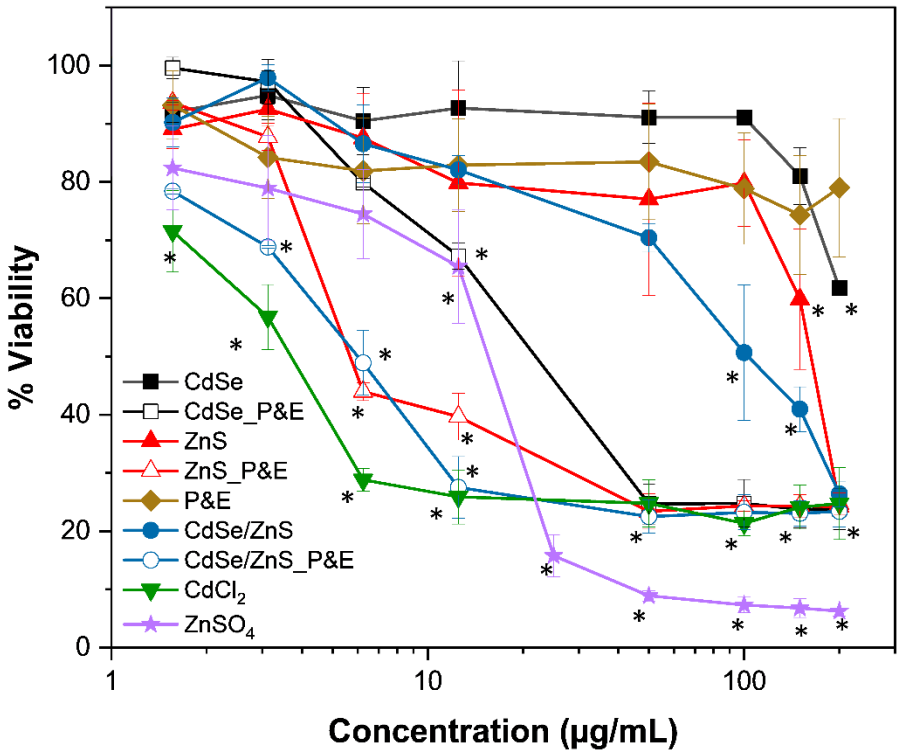

Figure 6.1 Cytotoxic effects of particles measured with resazurin assay on confluent HIEC-6 cells exposed to incremental concentrations of particles for 24 h. Cell viability is expressed as % change relative to negative control with no particle exposure (n=3, *p<0.05).

Combination indexes were calculated based on the EC_{20} values derived from the cell viability assay (Figure 6.1) and presented in Table 6.1. According to the combination index table, combinations between QD component and coating polymer (e.g., CdSe_P&E, ZnS_P&E, and CdSe/ZnS_P&E) yielded CI<1 and thus suggested strong synergistic effects due to the coating of polymer. On the other hand, the combination of ZnS shell and CdSe has an antagonistic effect towards cell viability (CI>1), suggesting its protective role. CdSe/ZnS_P&E showed the lowest CI of 0.20, demonstrating synergistic cytotoxicity effects for complete QD containing all components.

Table 6.1 Combination index calculations for QD samples based on EC_{20}.

Component or combination	EC_{20} (µg/mL)	Combination Index

CdSe	194.26	N/A
ZnS	28.98	N/A
P&E	11.98	N/A
CdSe/ZnS	61.73	1.13
CdSe_ P&E	10.86	0.79
ZnS_ P&E	4.89	0.40
CdSe/ZnS_ P&E	2.47	0.20

6.4.3. Sublethal effects of QDs

To analyze the mechanism of toxicity of the QDs, cellular responses potentially embedded in the toxicity pathway were measured for CdSe/ZnS_P&E QDs and their components (Figure 6.2). CdSe/ZnS_P&E QDs were able to induce the most significant changes (SSMD>3, red color in heatmap) at the lowest concentration compared to all the other particles for most cellular responses. They can cause significant changes in intracellular reactive oxygen species (ROS) production at 50 µg/mL, mitochondrial ROS production at 12.5 µg/mL, changes in $[Ca^{2+}]_i$ influx at 25 µg/mL, and mitochondrial membrane potential at 6.25 µg/mL in a concentration-dependent manner. For the other QD components, polymer-coated particles (CdSe/ZnS_P&E, CdSe_P&E, and ZnS_P&E) induced significant changes (SSMD>2, orange or red color in the heatmap) in mitochondrial superoxide production at lower concentrations compared to their uncoated counterparts. CdSe and ZnS samples only demonstrated statistically significant (SSMD>3) cellular responses at 100 µg/mL, while CdSe/ZnS responses were significantly different from blank (SSMD>3) from 12.5-50 µg/mL. Cells exposed to P&E alone were significantly different (SSMD>3) than the media

blank only in the mitochondrial superoxide generation (MitoSox) at concentrations greater than 12.5 µg/mL.

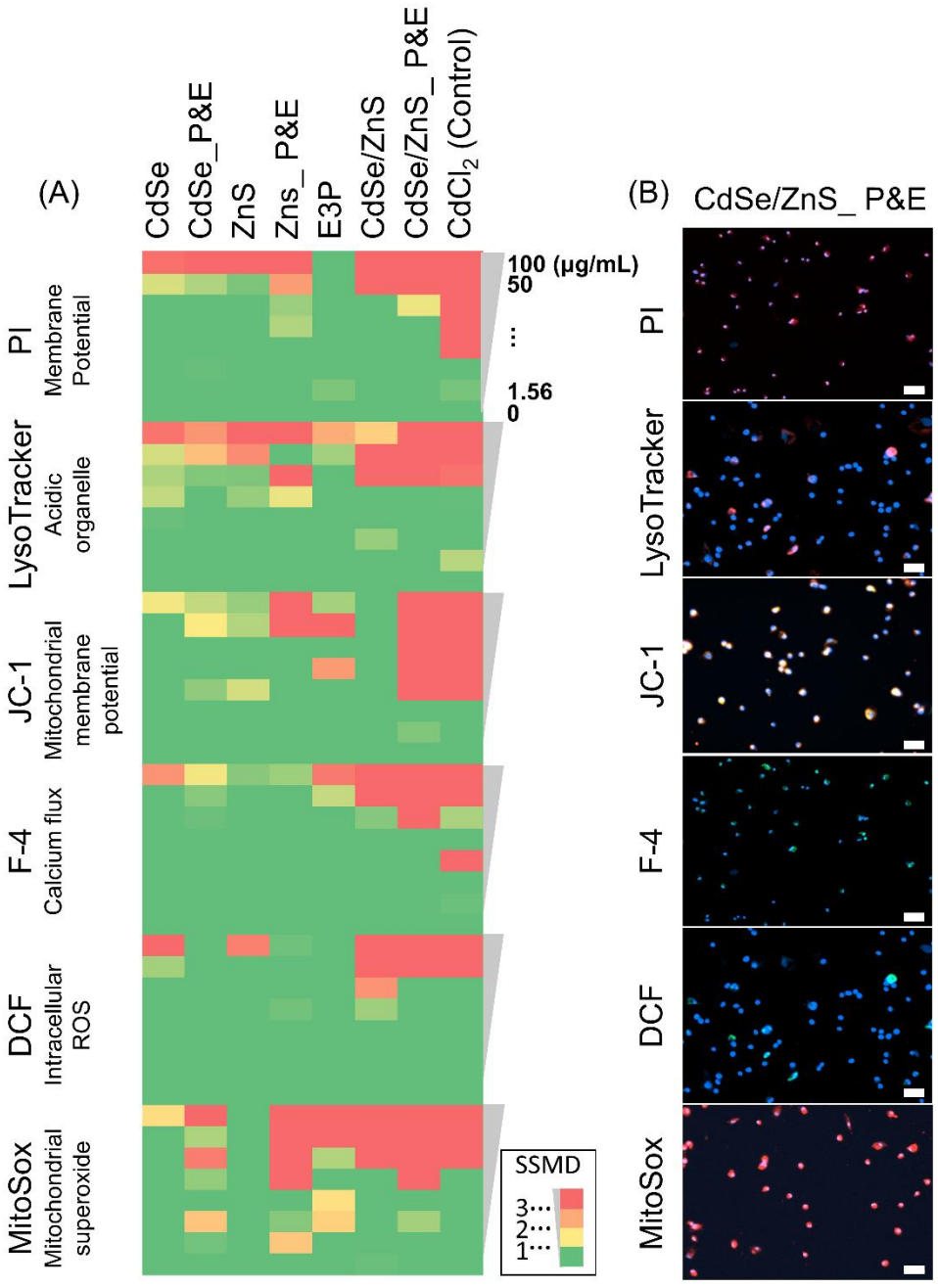

Figure 6.2 Multiparametric cellular responses after 24 h exposure of HIEC-6 cells to complete QDs and combinations of individual components measured by high-content screening. (A) Heat map developed from normalized raw data based on strictly standardized mean difference (SSMD) transformation (n=4). The rows and columns in the heat map correspond to the dose range and sample

types, respectively. Green colors indicate no significant toxic effects (SSMD<1) compared to the negative control (cells exposed to sera-free media), while yellow (1<SSMD<2), orange (2<SSMD<3), and red (SSMD>3) denotes moderate, fairly strong and strong difference from the control, respectively. The responses are designated from top to bottom: (i) PI = cell viability by membrane permeability *via* propidium iodide uptake. (ii) LysoTracker=acidic organelles (iii) JC-1= perturbation of mitochondrial membrane potential measured by JC-1. (iv) F4 = increased intracellular Ca^{2+} flux measured by Fluo-4. (v) DCF= intracellular reactive oxygen species measured by DCF. (vi) MitoSox= mitochondrial superoxide generation measured by MitoSox Red. (B) Representative images obtained from high-content screening showing respective cellular responses at 100 μg/mL QD exposure (scale bar= 50 μm).

In addition to the cellular responses analyzed by the high-content screening assays, inflammatory responses of HIEC-6 cells due to particles treatments were also assessed by measuring pro- and anti-inflammatory cytokines IL-8, TNF-α (Figure 6.3), and IL-10 (Figure 6.7) using ELISA. On an equal mass basis, CdSe/ZnS_P&E induced the highest level of all three inflammatory markers. Similar to the cellular responses, polymer-coated particles induced a 2-fold increase in the production of chemokine IL-8 release than uncoated particles (CdSe_P&E *vs.* CdSe; ZnS_P&E *vs.* ZnS). A similar trend was observed for TNF-α as CdSe_P&E and ZnS_P&E induced a 2-fold and 3-fold increase of TNF-α, respectively, while CdSe and ZnS did not induce changes in release compared to the negative control. A high level of anti-inflammatory cytokines production of IL-10 (fold change>2) was observed in all treatments except CdSe_P&E particles, but no statistically significant differences were observed between different particle exposures. The high standard error for IL-10 might be contributed to the fluctuation in the bioactive IL-10 dimers level since dissociation into monomers was possible at the experiment condition (37 °C and low protein concentrations in sera-free media).[23]

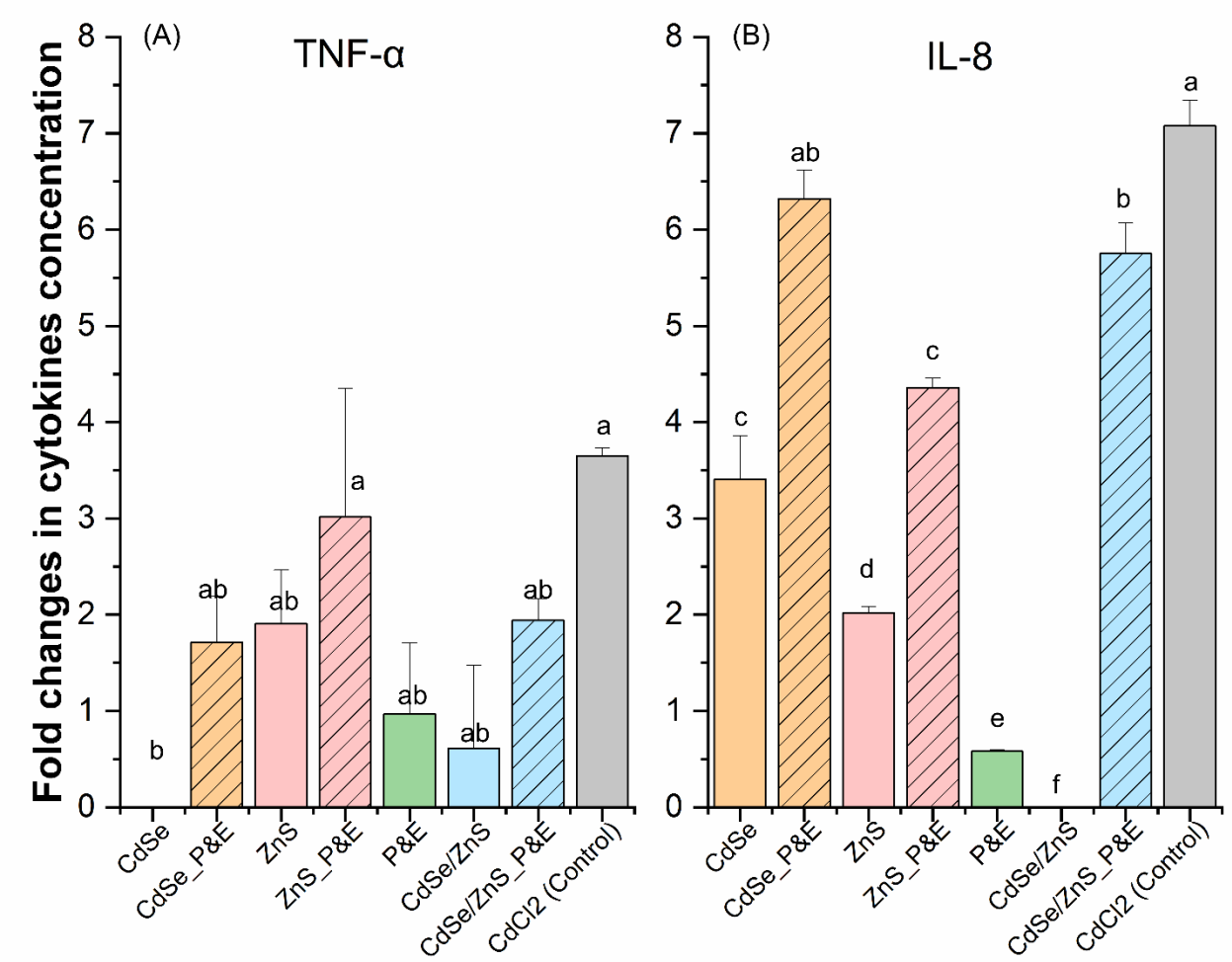

Figure 6.3 Inflammatory responses measured by (A) TNF-α and (B) IL-8 release. Confluent HIEC-6 cells were exposed to 25 µg/mL of different types of particles for 24 h, and the supernatants were collected for cytokines quantification using ELISA kits. The results are expressed as the fold change from the negative control (cells exposed to sera-free media). Average values +SD (n=3) are plotted in the graph with compact letter display indicating significant differences (one-way ANOVA test, $p< 0.05$).

To explain the differential responses induced by polymer-coated and uncoated QDs, cellular uptake of all QDs was studied using confocal microscopy and ICP-MS. Confocal fluorescence images (projected view after z-stacking and 3D view) suggested higher uptake of polymer-coated samples into HIEC-6 cells (Figure 6.4A). Single particles or particle aggregates that were not taken up by cells were observed in red color and projected through different imaging layers, while polymer-coated particles displayed orange color due to a combination of red (QDs) and green

(intracellular fibers) colors. Determination of bioavailability of heavy metals such as Cd, Zn, and Se concurred with the microscopic observation. Acid digestates of cells analyzed by ICP-MS suggested polymer coating enhanced QDs uptake into cells by the higher levels of all three elements (Zn, Se, Cd). We observed that measured concentrations for coated QDs were about 4 times higher than the equal mass of uncoated particles (Figure 6.8). In addition, the Cd uptake for cells exposed to QDs was also higher than equivalent concentrations of $CdCl_2$ salt exposed cells, suggesting that Cd in polymer-coated QDs is more bioavailable than dissolved Cd ions.

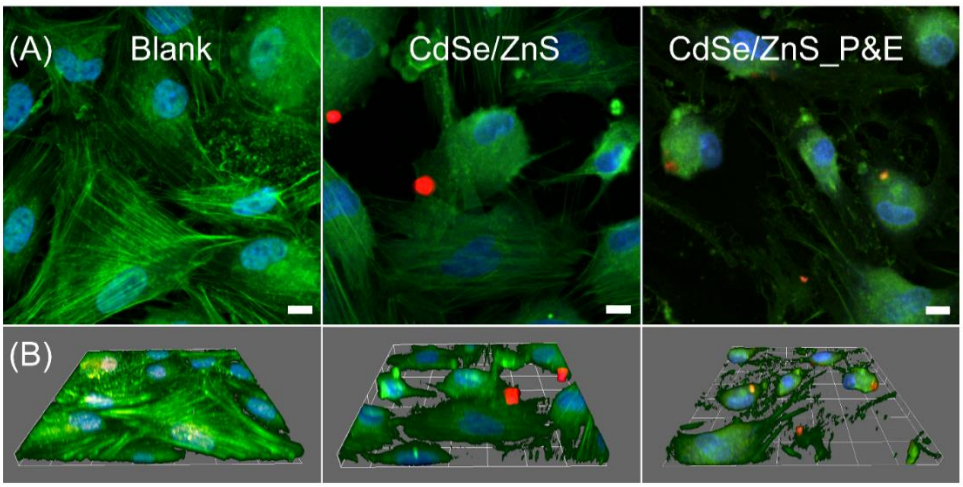

Figure 6.4 Cellular uptake of CdSe/ZnS and CdSe/ZnS_P&E particles analyzed by scanning confocal microscopy images of HIEC-6 exposed to QDs (red fluorescence) and stained with Phalloidin (green fluorescence) for F-actin and Hoechst (blue fluorescence) for nuclei (scale bar =10 μm, objective lens 63× in oil immersion) in (A) projected top view and (B) 3-D reconstructed side view.

6.4.4. Transformations in different stages of digestion changed the toxicity of QD

The characterization of the transformations of QDs at each stage of the digestion was included in Aude's thesis, and the resulting changes in QD toxicity towards HIEC-6 cells were presented in this work. The cellular responses after digested QDs recovered from each stage of the simulated digestions (Figure 6.5A) were measured and paired with the analysis of QDs localization in cells

with confocal microscopy (Figure 6.5B) as well as an analysis of the uptake of Cd, Zn, and Se into cells (Figure 6.5C).

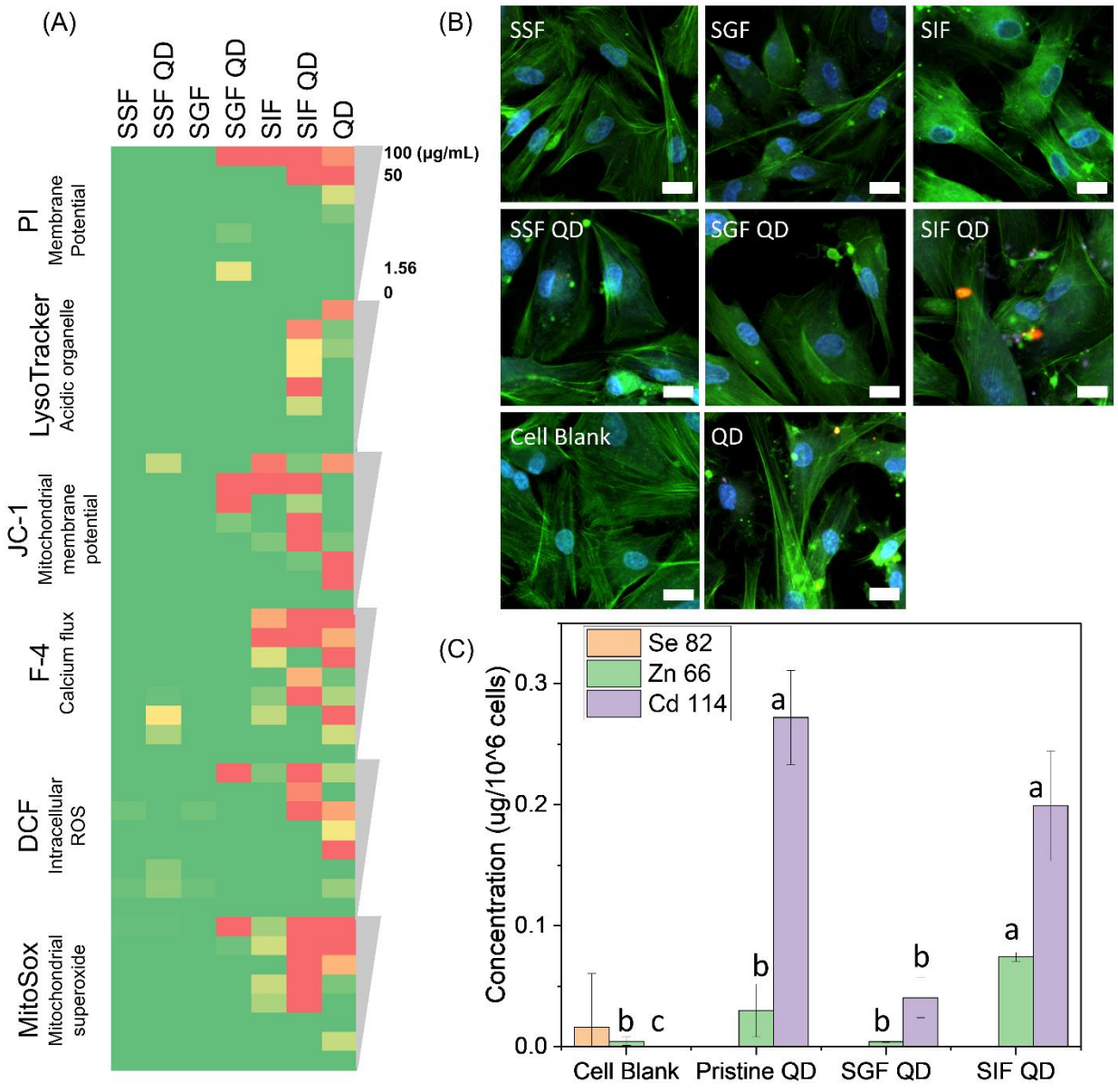

Figure 6.5 Toxicity of QDs after different stages of digestion with the accompanying blanks characterized as (A) Multi-parametric cellular responses after 24 h exposure of HIEC-6 cells measured by high-content screening (HCS). Heat map developed from normalized raw data based on strictly standardized mean difference transformation. The rows and columns in the heat map correspond to the dose range and sample types, respectively, in each cell type (average value from n=4). Green colors indicate no significant toxic effects compared to negative control (no QD exposure) while yellow/red indicated significant increases in cellular

responses. The responses are designated from top to bottom: (i) PI = cell viability by membrane permeability *via* propidium iodide uptake. (ii) LysoTracker=acidic organelles (iii) JC-1= perturbation of mitochondrial membrane potential measured by JC-1. (iv)F4 = increased intracellular Ca^{2+} flux measured by Fluo-4. (v) DCF= intracellular reactive oxygen species measured by DCF. (vi) MitoSox= mitochondrial superoxide generation measured by MitoSox Red. (B) Cellular distribution of digested particles(red) imaged by Scanning Confocal Microscope and HIEC-6 intracellular component F-actin and cell membrane(green) after 3 h exposure to selected nanoparticles. Scale bar =10 μm, objective lens 63X oil immersion and (C)ICP-MS for metal uptake after 3 h exposure. The results were presented as mass of the element (μg) normalized by the number of cells(n=3, $p<0.05$).

Compared to the pristine QDs, the cytotoxicity of salivary digested QDs (SSF-QD) decreased. SSF-QDs were not inducing cell death at the highest exposure concentration (Figure 6.5A). We also did not observe the generation of intracellular ROS (SSMD<1) and mitochondrial ROS, with moderate changes in mitochondria membrane potential (1<SSMD<2). SSF-QDs were not observed inside of cells by microscopy (Figure 6.5B).

After the gastric stage, QDs significantly increased in toxicity at 50-100 μg/mL (Figure 6.5A). Using membrane potential (PI) as a proxy of cytotoxicity, we found that QDs only cause cell death at the highest exposure concentration (100 μg/mL). However, we observed significant changes (SSMD>3, red in the heatmap) in calcium flux even at the concentration of 3.125 μg/mL. Other subcellular responses were also noticed to be significant (SSMD>3) at higher exposure concentrations (>50 μg/mL), including generation of intracellular ROS, generation of mitochondrial ROS, and mitochondria membrane potential. However, uptake of individual QDs by cells was not evident from confocal microscope images (Figure 6.5B). Compared to pristine QDs, SGF-QDs have decreased uptake into cells (Figure 6.5C).

After the intestinal stage, SIF-QDs induced significant cell death at 50-100 μg/mL (Figure 6.5A). At lower concentrations (6-12 μg/mL), impacts on mitochondrial membrane potential and mitochondrial superoxide were significant (SSMD>3). Acidic organelles like lysosomes were also impacted at these low concentrations. The presence of SIF-QDs was observed in confocal

microscopic images of cells as orange-colored dots in Figure 6.5B, suggesting possible cellular uptake of the SIF-QDs. The uptake of SIF-QDs was further confirmed by ICP-MS measurement (Figure 6.5C), where the amount of internalized SIF-QDs by cells increased significantly compared to SGF-QDs. The amount of Cd in the cells increases to 0.2 µg Cd/10^6 cells, which is only slightly less than the pristine uptake of QDs into cells (0.27 µg Cd/10^6 cells).

6.5. Discussion

While the unique optical characteristics are making QDs competitive candidates for next-generation display technologies, the safety aspects of these materials have raised serious concerns due to the presence of highly toxic metals.[21] Although previous studies have analyzed the roles of single components in the overall toxicity of QDs by changing the specific component, few have attempted to study the potential combinational effects of the individual QD components in a quantitative manner.[22, 23] In this study, the complete QD (CdSe/ZnS_P&E) and combinations of its components were tested for cytotoxicity, cellular responses, and uptake to determine the roles of each component and the mechanism of toxicity as they are dosed to model intestinal cells.

Dissolution and release of toxic heavy metal ions have been reported as one of the major mechanisms of QD toxicity in previous studies.[24, 25] In the current study, we identified the roles of ion release by comparing the cytotoxic effects between commercially-relevant QDs and equivalent concentrations of metal ions. We found that equivalent concentrations of $CdCl_2$ salt and $ZnSO_4$ salt (2 wt% and 1 wt% of CdSe/ZnS_P&E, respectively) failed to induce the same level of cytotoxicity (Figure 6.1). The cell viability decreased by 80% after the exposure of 100 µg/mL commercially-relevant QDs, while the equivalent concentration of $CdCl_2$ salt and $ZnSO_4$ salt

caused about 30% and 20% cell death, respectively. Our finding was consistent with another study showing that intact Cd-based QDs were more toxic compared to their equivalent Cd^{2+} salts, suggesting that the amount of metal ions released by dissolution alone is not the major source of toxicity for commercially-relevant QDs.[26]

In addition to the metal content, we explored the effect of the ZnS shell and compared the cytotoxic effects between CdSe and CdSe/ZnS. At 100 μg/mL, the cytotoxicity of CdSe core alone was significantly different than that of CdSe/ZnS (4 times higher). The reduced cytotoxicity of CdSe/ZnS also yielded a CI greater than 1, representing an antagonism in the cytotoxic effect upon combining the involving components (CdSe + ZnS) (Table 6.1). This result suggests that the ZnS shell shielded the core from Cd dissolution and release at least for the exposure time used in this investigation. The protective effect of the ZnS shell on Cd dissolution from the QD breakdown and ion dissolution has also been reported in other studies.[27]

In this study, we also used mathematical models to discern the individual constituents' contributions to the toxicity of multicomponent nanomaterials in a quantitative manner. While predictive computational models have been developed for assessing the hazard potential of nanomaterials, most of the available studies assumed the nature of the core material as the dominant contributor to the quantitative structure-activity relationship (QSAR).[28, 29] In the current study, we were able to discern the interplay between different components using the Chou-Talalay model.[17] Accordingly, shell (ZnS) showed an antagonistic effect (CI=1.13) on the toxic potential of the core (CdSe). However, the surface coating (P&E) showed synergistic effects (CI=0.79, 0.4, and 0.2) on the toxicity of the core, shell, and core/shell structure (Table 6.1). Using percentage weight content and the EC_{20} value of each content, we can quantitatively compare the

combinational effects of multiple constituents of the QD model based on a single-ended cytotoxicity assay.

Besides the dissolutions of QD to release toxic heavy metals, surface chemistry is another critical factor determining the toxicity of QDs. In the commercially-relevant electronic display QD model, polymer P&E coating on the surface of the particles yielded a positive charge and thus modified the surface chemistry to alter the toxicity. Polymer P&E initially caused a 20% decrease in cell viability at a concentration around 10 μg/mL (Figure 6.1) but then failed to cause more than 20% of cell death at all higher concentrations. Yet, QDs decorated with P&E affected cell viability and other cytotoxicity parameters, much more than QDs (core and core/shell structure) without P&E. P&E is synthesized from PEI and, as such, contains multiple amine groups that positively charge QDs upon deposition of their surface. As supported by a recent study using primary amine-terminated QDs, the polymer on the QDs can interact with negatively charged cell membranes and facilitate the QD internalization *via* lipid raft-mediated endocytosis.[30] Likewise, previous studies identified 25 kDa branched PEI as the "gold standard" for delivering genes into cells, a process often coupled with a decreased cell viability.[31] Therefore, we reasoned that the synergistic effect of P&E with the QDs resulted from the increased uptake of heavy metals (from the core/shell) into the cells when P&E was present. Accordingly, we observed significantly enhanced Cd uptake of coated QDs compared to non-coated ones (4 times higher in μg Cd uptake per 10^6 cells) (Figure 6.8). Furthermore, the cell uptake data presented in Figure 6.8 resulted from dosing cells with 25 μg/mL of QD sample. When factoring in the differences in Cd present in the QD samples, the uptake efficiency (ratio between Cd inside cells and Cd in solution) is 77-fold higher for Cd in polymer-coated QDs *vs.* Cd in non-polymer coated QDs (calculation described in SI). Chandran

et al. also found similar behaviors in PEI-capped Au NPs, which had 10-fold higher uptake than PEG or lactic acid-coated AuNPs in human umbilical vein endothelial cells.[32]

As the QDs used in this study might be subjected to sedimentation, we can not overlook the possible changes in cellular QD uptake due to the amount of QDs sedimented onto the adherent cells at the bottom of the culture container.[33] The delivery rate of the particles can be determined by various factors, including gravitational settling and diffusion, depending on the properties of the particles and the suspending liquid. The delivered concentrations to cells remain challenging to be experimentally determined but have been estimated using the *In vitro* Sedimentation, Diffusion, and Dosimetry model (ISDD) model.[34] We chose to use the model without dissolution due to the limited dissolution of QDs noted in our past work.[9] According to the ISDD model (see SI for calculations), the delivered dose of the polymer-coated QDs to cells was lower than that of the uncoated QDs (Figure 6.9). Based on a previous study, we rationalize this observation by the surface stabilization of the QDs due to electrostatic repulsion and steric stabilization effects of the coating polymer.[35] In contrast, the uncoated QDs may agglomerate and settle faster due to hydrophobic interactions and gravitational settling. This argument concurred with our observation in that the measured cellular uptake of each element (Cd, Zn, and Se) was very close to the calculated delivered mass for uncoated QDs (Figure 6.9). Thus, the good agreement between the ISDD model calculated delivery concentrations and the measured metal uptake suggests that gravitational sedimentation and diffusion play major roles in determining the bioavailability of the uncoated QDs. However, the actual delivery of polymer-coated QD was higher compared to the estimated delivery. ICP-MS results showed that the cellular uptake of Cd and Zn was about 160-times and 80-times higher than the estimated delivery of the respective element (Figure 6.9). This

discrepancy indicates that sedimentation and diffusion are not the critical factors for the high uptake of coated QDs. Instead, we believe that the polymer coating is the major contributor to the enhanced bioavailability. The higher toxicity of the polymer-coated QD also confirmed the critical role of surface chemistry in QD toxicity.

In addition to facilitating higher intracellular delivery, the cationic polymeric coating on QD is suspected of causing additional organelle injuries stemming from perturbations in subcellular organelles such as lysosomes and mitochondria. We observed enhanced intracellular transport of coated QDs into lysosomes based on the LysoTracker staining (Figure 6.2), possibly due to the increased vesicle trafficking of endosome-lysosome fusion.[36] The low pH inside the lysosomes could further increase the protonation of PEI and induce an influx of protons and chloride ions, subsequently leading to osmotic pressure buildup inside the lysosomes.[37, 38] The lowering of pH and subsequent rupturing of the lysosome is reasoned to enhance the disintegration of QDs and the burst release of heavy metal into the cytosol. Such "proton sponge" effect[39] may induce mitochondrial damage and increase cytosolic and mitochondrial Ca^{2+} flux, as observed in our study for coated QD. The perturbations in intracellular Ca^{2+} homeostasis and mitochondria function can aggravate cellular oxidative stress and lead to apoptosis. A previous study has demonstrated that inflammatory responses can be facilitated by QDs-induced oxidative stress, a mechanism connected by mitochondrial dysfunction.[40] In this study, the polymer P&E coated particles induced a higher increase of pro-inflammatory cytokines IL-8 and TNF-α than uncoated samples (Figure 6.3). The higher release of the anti-inflammatory cytokines IL-10 (Figure 6.7) during the exposure time in this study compared to the pro-inflammatory cytokines suggested the inducible nature of IL-10 after being stimulated by pro-inflammatory cytokines production.[41] The antagonistic effect

of endogenous IL-10 can be regarded as a compensatory mechanism to reverse the oxidative damage due to the exposure of QDs, which also confirmed the mechanism of QDs toxicity *via* oxidative stress and subsequent mitochondria dysfunction. In short, the presence of cationic polymer not only enhances the cellular uptake of QD but also increases its lysosomal dissolution and heavy metal release into the cytosol to aggravate oxidative stress and cell death.

The critical role of surface chemistry on pristine QD toxicity further highlights the importance of examining the biotransformation of the QD during simulated digestion to identify the resulting toxicity of relevance. The digestion of QDs changes the structure of individual particles and particle aggregates, and the impact of particles on intestinal cells. Detailed characterization of the QDs at each step was presented in Aude's thesis and briefly summarised in the scheme below (Figure 6.6).

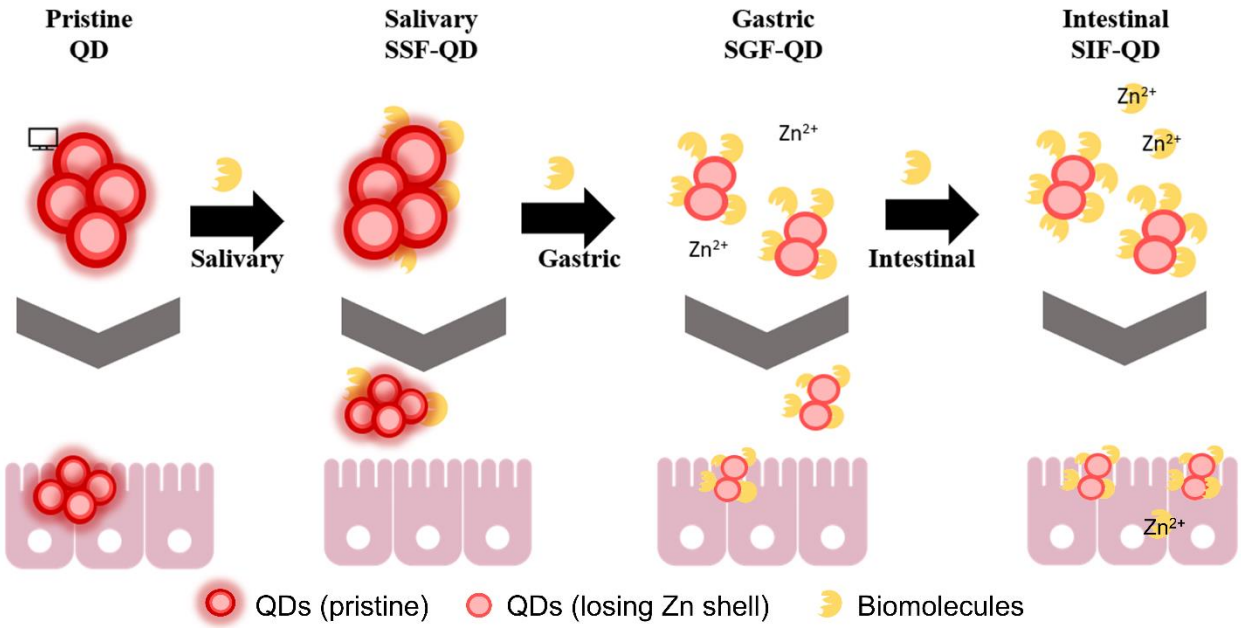

Figure 6.6 Stage-by-stage representation of the transformations of QDs (top line) and the impact of these transformations on uptake and toxicity (bottom line).

Characterization of the size of the pristine QDs suggested that the particles were in a highly aggregated state (69% Cd is present in aggregates that are > 210 QDs) when dispersed in cell culture media (results presented in Aude's thesis). These bigger aggregates could lead to faster settling of QD due to gravitational settling, which increased the effective delivery of QDs to intestinal cells adhering to the bottom of the well.[33] However, the increased effective delivery did not necessarily lead to enhanced cellular uptake. As discussed before, the determining factor of bioavailability of pristine QDs was identified as surface chemistry, where the cationic charges on the surface experienced protonation and mediated toxicity by the oxidative stress pathway following the "proton sponge" mechanisms.[42] These results provide a needed baseline for interpreting changes to both the QD and its toxicity in later digestion stages.

At the salivary stage, there is a significant decrease in QD-induced toxicity compared to the pristine QD. The size of the particles remained relatively unchanged, although a significant portion of the Zn shells (40% released Zn ion) was lost (results presented in Aude's thesis). This might be explained by the metal-protein complex formed between the released Zn and α-amylase in the simulated salivary fluid due to the binding of Zn on the metal-binding site of the enzyme.[43] As a result, the released Zn was quenched by the enzymes and was not inducing adverse effects on the cells.

At the gastric stage, we observed dramatic transformations in both the structure of individual QDs and QD aggregates. Individual QDs lost the Zn-containing shells while aggregates decreased in size (80% became less than 210 QDs) (results presented in Aude's thesis). These changes to QD shells were in part expected due to the low pH, as previous work had demonstrated the instability of the Zn-containing shell.[12] These dramatic changes started to translate into changes in toxicity

and cellular uptake. At the highest concentration, significant impacts on the mitochondrial function, ROS generation, and membrane potential were recorded at 24 h of exposure (Figure 6.5A). The lower indication of perturbation of the acidic organelles or calcium flux might be attributed to the chronological order of these events, where these two perturbations were initiated earlier in the oxidative stress mediated pathway and had returned to normal levels by the time of the measurement.[44] These cellular impacts, however, did not translate into a higher cellular uptake for QDs at this stage of digestion (Figure 6.5C). Possible reasons might be attributed to the interaction between QDs and the proteins (enzymes). The loss of the inorganic shell at the gastric phase might disclose the CdSe core and allowed subsequent local binding with digestive enzyme (pepsin) to form CdSe–pepsin complex. The confocal microscopic images of particles recovered from this stage support the formation of such structures (Figure 6.10) which also concur with observations made by Wang, *et al*..[45] Confocal microscopic analysis of cells treated with QDs recovered from this phase showed no evidence of QD taken up. The QD-pepsin complexes might not be taken up by the cells and were thus washed away during sample preparation for uptake analysis.

At the intestinal stage, aggregation of QDs decreased slightly from the gastric stage (from 10% to 5%). These seemingly slight transformations were correlated to a large increase in subcellular impacts. The subcellular impacts at >5 ug/mL SIF-QD were significant (compared to >50 ug/mL for SGF-QD) and uptake of QDs increased 4-fold for Cd. However, the comparison between the Zn uptake for SIF QD and pristine QD will be inconclusive because of the background Zn concentration in the intestinal fluid. SIF-QDs were able to induce more significant changes in acidic organelles and superoxide generation in the mitochondria compared to the pristine QDs, suggesting that the major responses captured for SIF-QD treated cells at 24 h of exposure are early

key events in the oxidative stress pathway.[44, 46] The reason for the increased toxicity might be attributed to the surface modification of the QDs by bile salt, which may facilitate the uptake of the digested QDs in the intestinal due to its emulsifying properties as well as the apical sodium-dependent bile acid transporter (ASBT) on the surface of cells.[47] The resulting digested particles shared a similar mechanism of toxicity with the pristine QD but showed differences in the point of departure concentration of the cellular response (i.e., the lowest concentration of an adverse response), depending on the subcellular impact analyzed. This indicates possible changes in the toxicokinetics (i.e., transport of QDs by cells and the body) brought on by GI-induced transformations that warrant future studies.

6.6. Conclusion

Granular discussions based on the commercially-relevant QD as a model complex material are necessary to understand the toxicity mechanisms of such multi-layered nanomaterials on the human GI tract. Results from this study emphasize that the toxicity of multi-layered material can be higher than its components due to synergistic effects, which can help the industry to maximize the benefits of the materials while balancing the potential hazards from a safe-by-design perspective. Moreover, the transformation of the materials in the surrounding matrix may also yield significant changes in their structure and subsequent toxicity properties, and thus deserves further studies probing the relationship between environmental fate and the toxicity of the target materials. The toxicity of QD decreased at the salivary digestion stage compared to pristine QDs, with the increase in toxicity in the gastric state and highest in the intestinal phase. We hypothesize that this could be due to the interaction with biomolecules at each stage that altered bioavailability, but further study is needed to establish the exact reasons for the increased toxicity of QDs. This

study advances our understanding of the toxicity of complex NPs. It provides evidence for the toxicity changes during digestion due to the dynamic surface changes of NPs. The results of the study warrant more transformations to be examined, in the same stage-by-stage method, to discern the hazard, and therefore risk, of other ingested NPs.

6.7. Supporting Information

6.7.1. Materials and methods

6.7.1.1. Composition of the QDs

Table 6.2 Composition of the QDs and combination of the components. Cd and Zn contents were measured with ICP-OES, and P&E contents were calculated from the synthesis. The remaining percent weight of the compounds is composed of Se and/or S and different organic ligands resulting from the synthesis.

Weight Percent (% wt)	**CdSe**	**CdSe_P&E**	**ZnS**	**ZnS_PEI&E3P**	**CdSe/ZnS**	**CdSe/ZnS_P&E**	**P&E**
%wt Cd	13	2	0	0	30	2	0
%wt Zn	0	0	31	1	15	1	0
%wt P&E	0	83	0	95	0	93	100

6.7.1.2. Uptake efficiency and delivery dosimetry calculation

6.7.1.2.1. Uptake efficiency

The uptake efficiency (UE) calculation was based on the ratio of intracellular Cd ions (Figure 6.8) over the Cd ions in the solution based on the ICP-MS results Table 6.2).

$$UE = \frac{Cd_{cell}}{Cd_{solution}} \quad (4)$$

We derived a 77-fold increase (z) in uptake efficiency by dividing the uptake efficiency of the polymer-capped QDs by the uptake efficiency of the uncoated QDs.

$$z = \frac{UE_{polymercapped\ QD}}{UE_{noncapped\ QD}} \quad (5)$$

There are differences in Cd concentration in polymer capped and uncapped cell toxicity experiments since we normalized the QD doses by the weight of the entire substance. The z calculation, therefore, involves two different values for Cd in solution (Table 6.2) as well as two values for uptake into cells (Figure 6.8).

6.7.1.2.2. Simulation of delivered exposure concentration

The delivery efficiency calculation was based on the *In vitro* Sedimentation, Diffusion and Dosimetry (ISDD) model software (ISDD, v2018) from the Pacific Northwest National media. These two samples were established due to the very similar contents of polymer and Cd/Zn (Table 6.2). We expect there to be a limited dissolution of these particles due to past work illustrating that Cd in CdSe/ZnS_P&E did not dissolve in pH 7 after 24 h.[12] Therefore, we opted to use the ISDD model [34, 48] rather than the ISD3 model.[49]

The ISDD model requires a range of inputs, some of which we could provide with high certainty (Table 6.3 & Table 6.4). For the inputs that could not be measured, we provide a range of values for these factors, which are outlined in Table 6.5. The simulated time was set as 6 h to be identical to the exposure time for cellular uptake analysis using ICP-MS.

Table 6.3 ISDD inputs with a high degree of certainty due to either direct measurement (see Fig. 1) or due to past published work.[12] These inputs relate to the primary particle characteristics.

Factor	Polymer Coated	Uncoated
Particle diameter (nm)	4.8	4.8
Particle density (g/mL)*	3.4	3.4
Particle Concentration (ug/mL)**	25	25
Agglomerate Diameter (nm)	110	160 (90 - 250)

* Reflects 35 wt% of octadecylamine (0.862 g/mL) with 65 wt% of inorganic particle (4.8 g/mL)

** Reflects the large amount of polymer in the polymer-coated particles, which left a comparatively lower concentration of inorganic CdSe/ZnS

Table 6.4 ISDD inputs related to the exposure conditions of cells (see Methods for more information).

Factor	Value
Dish Depth (m)	0.0157
Volume (mL)	0.5
Temperature (K)	310
Viscosity (N s/m^2)	0.0009
Density (g/mL)	1

Table 6.5 ISDD inputs that were estimated, with a middle ground and a range in parentheses.

Factor	Polymer Coated	Uncoated
Packing Factor (PF)	0.50 (0.40 - 0.60)	0.634 (0.57 – 0.74)
Agglomerate Density (g/mL)	1.25 (1.05-1.5)	1.5 (1.25-2.0)

The hydrodynamic diameter of uncoated QDs represents a large range due to experimental difficulties (performed by Aude). The presence of 1:1 DMSO/chloroform (2 wt%) caused a high background signal, as these formed micelles in solution. The difference between the averages of these solutions (with and without QDs) was 94 nm, so we chose that as the low end of the estimate (rounded to 100 nm).

The packing factor for the uncoated QD was based on the value for uniform spheres. This approach was validated by DeLoid *et al.*, who investigated metal and metal oxide NPs.[50] The range reflects the average measured values for two metal oxides (0.57) to the theoretical maximum (0.74).[50] For the polymer-coated NPs, we expect the particles to be in a looser aggregate due to the large presence of a polymer. Therefore, we estimated the packing factor to be 0.50, with a wide range of possible values (0.40-0.60) than the sample without polymer.

Agglomerate density was also estimated due to instrumental limitations (i.e., a lack of packed cell volume tubes and ultracentrifugation).[49] The use of the Sterling equation was not deemed practical due to the nature of the ligands (either polymer or octadecylamine), which could not be fully dried for BET analysis. Therefore, we estimated the "uncoated" agglomerate density using the work of Liu *et al*.[51] They evaluated the effective density of 8 metal oxide NPs (with similar particle density as CdSe/ZnS QDs) and found that the effective density was roughly 1.25-2 g/mL. The agglomerate density with the polymer was expected to be lower due to the presence of the polymer (polyethyleneimine, which is the backbone of P&E, has a density of 1.03 g/mL). Therefore, we decided to use an effective density of 1.25 (with a range of 1.05-1.5 g/mL).

6.7.1.3. Composition of the simulated fluid

Table 6.6 Composition of the simulated fluid at each stage, which was adapted from Infogest[16] and the activity of enzymes of this specific study. Ionic strength calculated from the procedure's standard electrolyte solutions.

Digestion Stage	**Salivary**	**Gastric**	**Intestinal**	
Biomolecule	Salivary amylase	Pepsin	Pancreatin	Bile
Biomolecule concentration	0.005 mg/mL	6.0 mg/mL	30 mg/mL	15 mg/mL
Ionic strength	38 mM	98 mM	142 mM	

6.7.2. Results

Table 6.7 Fluorophore cocktails used in the high-content screening assays with detailed chemical information and principles of assays.

	Fluorophore	**Target**	**Working concentration**	**Assay principle**
Dye cocktail 1	Hoechst 33342	Nucleus	1 μM	Nucleus stain that emits blue fluorescence upon binding to dsDNA.
	2',7'-dichlorodihydrofluorescein diacetate (H_2DCFDA)	Intracellular reactive oxygen species (H_2O_2)	10 μM	Nonfluorescent dye that can be oxidized by reactive oxygen species into highly fluorescent DCF.
	LysoTracker	Acidic organelles	75 nM	Red fluorescent dye that stains acidic organelles (e.g., lysosomes)
Dye cocktail 2	Hoechst 33342	Nucleus	1 μM	Nucleus stain that emits blue fluorescence upon binding to dsDNA.
	Fluor 4	Intracellular [Ca^{2+}] flux	5 μM	Calcium indicator that increases fluorescence when binding to cytosolic Ca^{2+} ions.
	Propidium Iodide	Plasma membrane damage	5 μM	Nucleus dye that enters cells with compromised membrane and fluoresces red
Dye cocktail 3	Hoechst 33342	Nucleus	1 μM	Membrane permeating nucleus stain that emits blue fluorescence upon binding to dsDNA.
	MitoSOX	Mitochondria puperoxide	5 μM	Red fluorescence dye that reacts to mitochondrial superoxide

Dye cocktail 4	Hoechst 33342	Nucleus	1 μM	Nucleus stain that emits blue fluorescence upon binding to dsDNA.
	JC-1	Mitochondria membrane depolarization	1 μM	Mitochondrial dye that fluoresces red when aggregated at polarized mitochondria membrane but shifts to green with a drop in the mitochondrial membrane potential

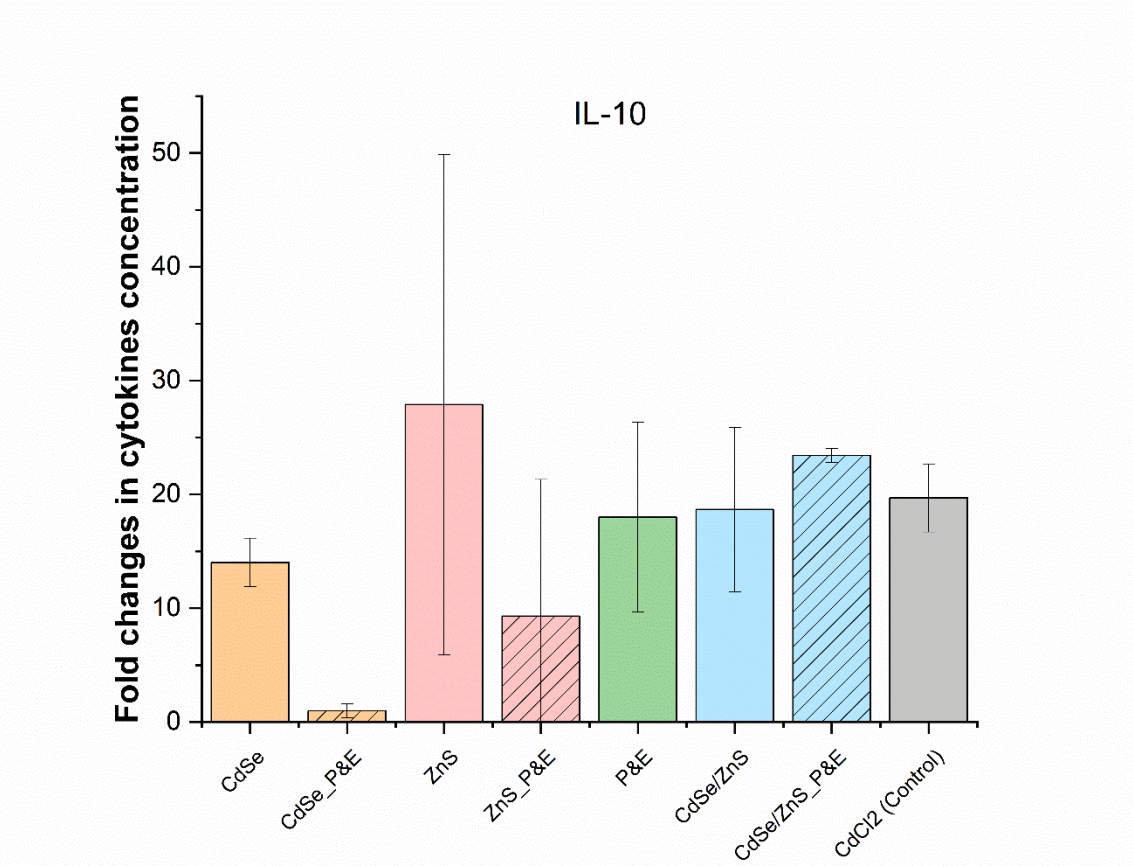

Figure 6.7 Inflammatory response measured by IL-10 induction with ELISA assay. Confluent HIEC-6 cells were exposed for 24 h to 25 µg/mL to different types of particles as indicated in the figure. The results were quantified by absorbance measurement and presented as fold change from the negative control (cells exposed to sera-free media) as Mean +SD (n=3). Significance was calculated by one way ANOVA test with a 0.05 significance level.

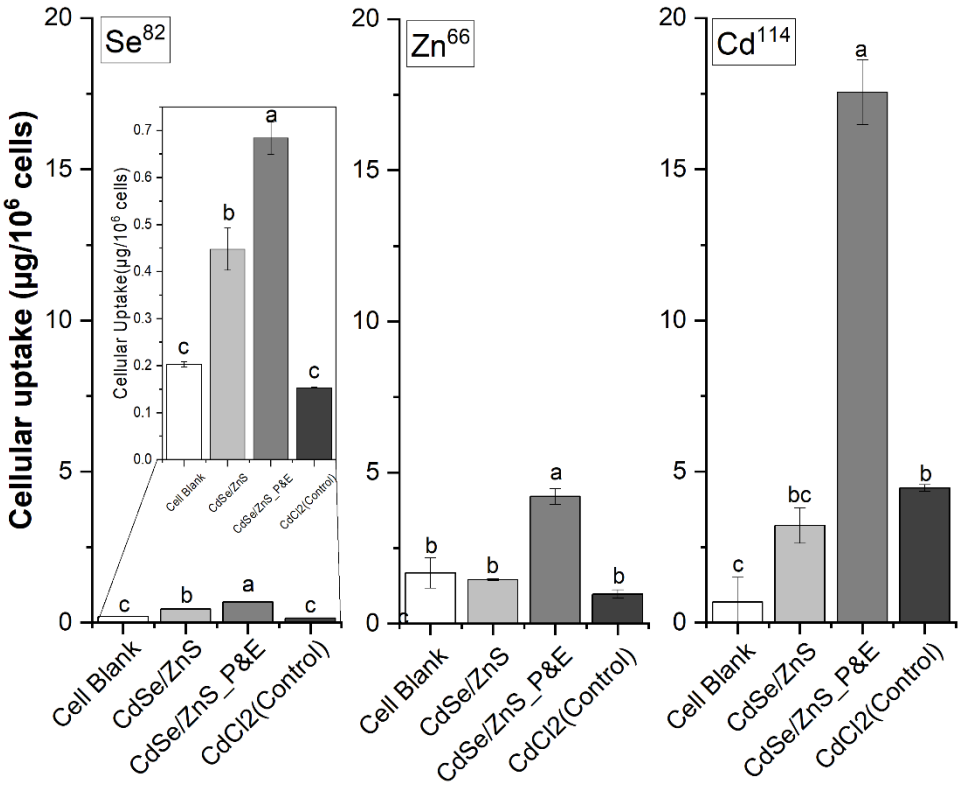

Figure 6.8 ICP-MS for the tested three element (Se, Zn, and Cd) from HIEC-6 cells after 6 h exposure. The results were presented as the mass of the element (µg) normalized by the number of cells. Significance was calculated by one-way ANOVA test with 0.05 significance level and presented in compact letter display (n=3).

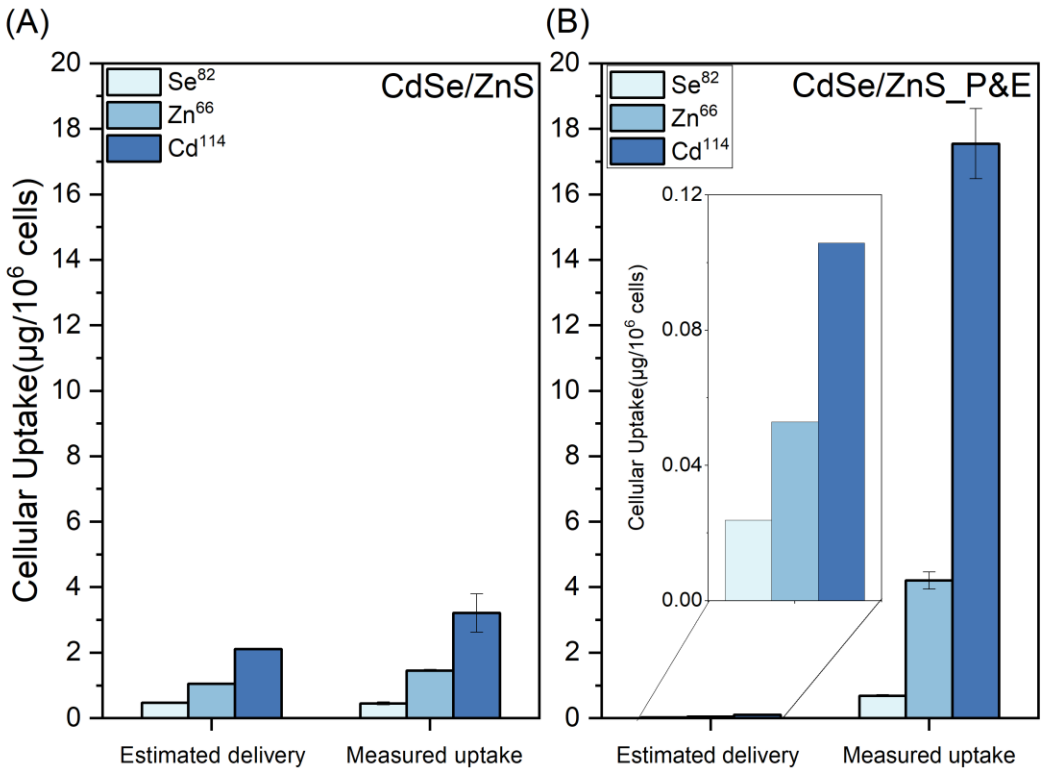

Figure 6.9 Comparison between the estimated delivered mass on the cells and the measured uptake of each element after 6 h exposure by ICP-MS for (A) uncoated and (B)polymer-coated QD.

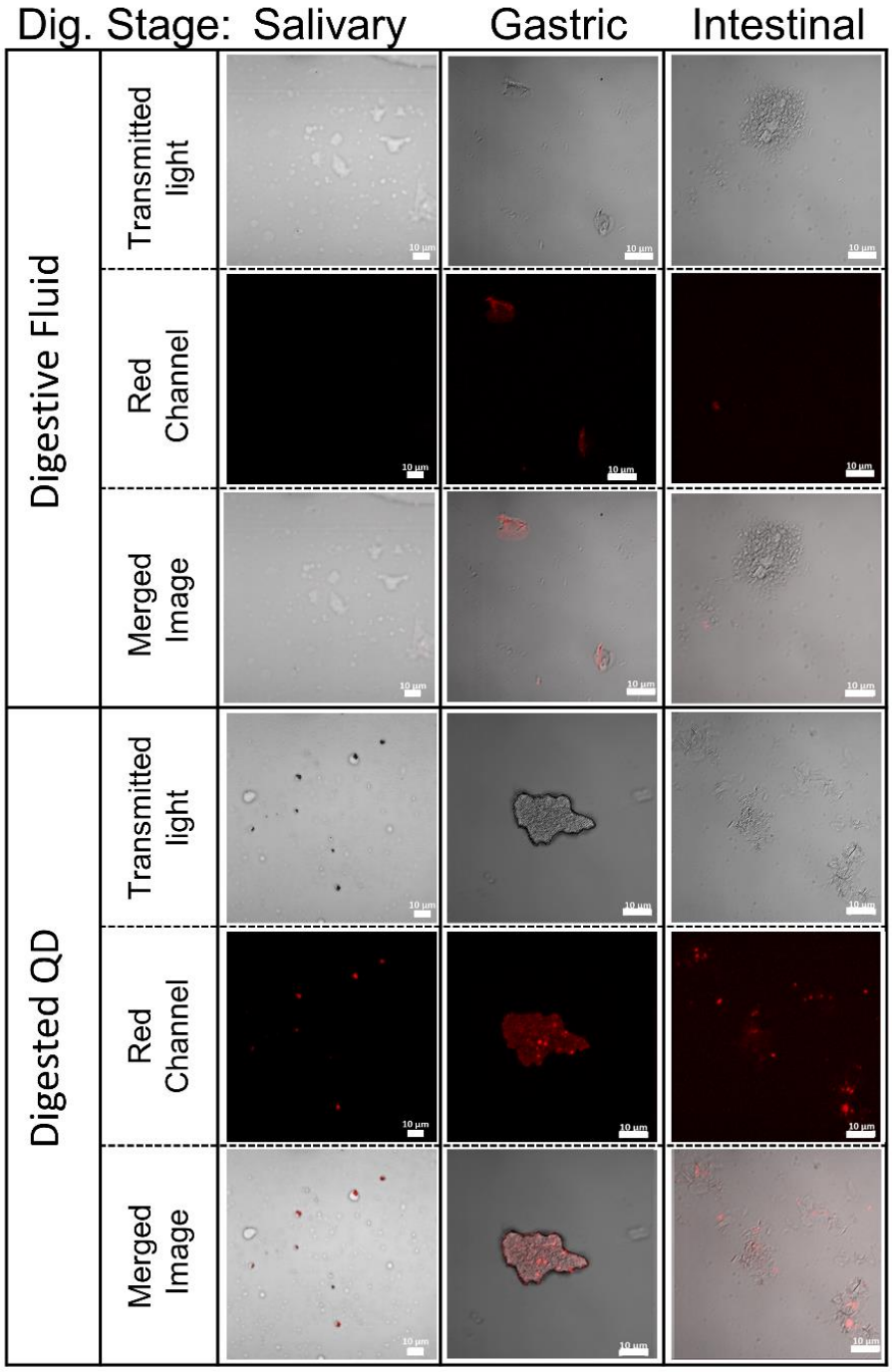

Figure 6.10 Confocal microscopy images of (A) three digestion stages without QDs present and (B) three digestion stages with QDs present, with QD presence indicated by red fluorescence (red channel) (scale bar=10 µm).

6.8. References

1. Lomer, M. C. E.; Thompson, R. P. H.; Powell, J. J., Fine and ultrafine particles of the diet: influence on the mucosal immune response and association with Crohn's disease. *Proc. Nutr. Soc.* **2002,** *61* (1), 123-130.

2. Mwilu, S. K.; El Badawy, A. M.; Bradham, K.; Nelson, C.; Thomas, D.; Scheckel, K. G.; Tolaymat, T.; Ma, L.; Rogers, K. R., Changes in silver nanoparticles exposed to human synthetic stomach fluid: Effects of particle size and surface chemistry. *Sci. Total Environ.* **2013,** *447*, 90-98.

3. Wu, W.; Zhang, R.; McClements, D. J.; Chefetz, B.; Polubesova, T.; Xing, B., Transformation and Speciation Analysis of Silver Nanoparticles of Dietary Supplement in Simulated Human Gastrointestinal Tract. *Environ. Sci. Technol.* **2018,** *52* (15), 8792-8800.

4. Additives, E. Panel o. F.; Flavourings; Younes, M.; Aquilina, G.; Castle, L.; Engel, K.-H.; Fowler, P.; Frutos Fernandez, M. J.; Fürst, P.; Gundert-Remy, U.; Gürtler, R.; Husøy, T.; Manco, M.; Mennes, W.; Moldeus, P.; Passamonti, S.; Shah, R.; Waalkens-Berendsen, I.; Wölfle, D.; Corsini, E.; Cubadda, F.; De Groot, D.; FitzGerald, R.; Gunnare, S.; Gutleb, A. C.; Mast, J.; Mortensen, A.; Oomen, A.; Piersma, A.; Plichta, V.; Ulbrich, B.; Van Loveren, H.; Benford, D.; Bignami, M.; Bolognesi, C.; Crebelli, R.; Dusinska, M.; Marcon, F.; Nielsen, E.; Schlatter, J.; Vleminckx, C.; Barmaz, S.; Carfí, M.; Civitella, C.; Giarola, A.; Rincon, A. M.; Serafimova, R.; Smeraldi, C.; Tarazona, J.; Tard, A.; Wright, M., Safety assessment of titanium dioxide (E171) as a food additive. *EFSA J.* **2021,** *19* (5), e06585.

5. Nel, A. E.; Madler, L.; Velegol, D.; Xia, T.; Hoek, E. M. V.; Somasundaran, P.; Klaessig, F.; Castranova, V.; Thompson, M., Understanding biophysicochemical interactions at the nano-bio interface. *Nat. Mater.* **2009,** *8* (7), 543-557.

6. Ault, A. P.; Stark, D. I.; Axson, J. L.; Keeney, J. N.; Maynard, A. D.; Bergin, I. L.; Philbert, M. A., Protein corona-induced modification of silver nanoparticle aggregation in simulated gastric fluid. *Environ. Sci. Nano* **2016,** *3* (6), 1510-1520.

7. Gerloff, K.; Pereira, D. I. A.; Faria, N.; Boots, A. W.; Kolling, J.; Förster, I.; Albrecht, C.; Powell, J. J.; Schins, R. P. F., Influence of simulated gastrointestinal conditions on particle-induced cytotoxicity and interleukin-8 regulation in differentiated and undifferentiated Caco-2 cells. *Nanotoxicology* **2013,** *7* (4), 353-366.

8. He, X.; Zhang, H.; Shi, H.; Liu, W.; Sahle-Demessie, E., Fates of Au, Ag, ZnO, and CeO2 Nanoparticles in Simulated Gastric Fluid Studied using Single-Particle-Inductively Coupled Plasma-Mass Spectrometry. *J. Am. Soc. Mass Spectrom.* **2020,** *31* (10), 2180-2190.

9. Zhou, P.; Guo, M.; Cui, X., Effect of food on orally-ingested titanium dioxide and zinc oxide nanoparticle behaviors in simulated digestive tract. *Chemosphere* **2021,** *268*, 128843.

10. Wang, L.; Nagesha, D. K.; Selvarasah, S.; Dokmeci, M. R.; Carrier, R. L., Toxicity of CdSe Nanoparticles in Caco-2 Cell Cultures. *J. Nanobiotechnology* **2008,** *6* (1), 11.

11. Böhmert, L.; Girod, M.; Hansen, U.; Maul, R.; Knappe, P.; Niemann, B.; Weidner, S. M.; Thünemann, A. F.; Lampen, A., Analytically monitored digestion of silver nanoparticles and their toxicity on human intestinal cells. *Nanotoxicology* **2014,** *8* (6), 631-642.

12. Bechu, A.; Liao, J.; Huang, C.; Ahn, C.; McKeague, M.; Ghoshal, S.; Moores, A., Cadmium-Containing Quantum Dots Used in Electronic Displays: Implications for Toxicity and Environmental Transformations. *ACS Appl. Nano Mater.* **2021,** *4* (8), 8417-8428.

13. Chopra, S. S.; Bi, Y.; Brown, F. C.; Theis, T. L.; Hristovski, K. D.; Westerhoff, P., Interdisciplinary collaborations to address the uncertainty problem in life cycle assessment of nano-enabled products: case of the quantum dot-enabled display. *Environ. Sci. Nano* **2019,** *6* (11), 3256-3267.

14. Dubrow, R. S.; Freeman, W. P.; Lee, E.; Furuta, P. Quantum dot films, lighting devices, and lighting methods. 2015.

15. Pageot, L. P.; Perreault, N.; Basora, N.; Francoeur, C.; Magny, P.; Beaulieu, J. F., Human cell models to study small intestinal functions: Recapitulation of the crypt-villus axis. *Microsc. Res. Tech.* **2000,** *49* (4), 394-406.

16. Brodkorb, A.; Egger, L.; Alminger, M.; Alvito, P.; Assunção, R.; Ballance, S.; Bohn, T.; Bourlieu-Lacanal, C.; Boutrou, R.; Carrière, F., INFOGEST static in vitro simulation of gastrointestinal food digestion. *Nat. Protoc.* **2019,** *14* (4), 991-1014.

17. Chou, T.-C., Theoretical Basis, Experimental Design, and Computerized Simulation of Synergism and Antagonism in Drug Combination Studies. *Pharmacol. Rev.* **2006,** *58* (3), 621.

18. Zhou, H.; George, S.; Li, C.; Gurusamy, S.; Sun, X.; Gong, Z.; Qian, H., Combined toxicity of prevalent mycotoxins studied in fish cell line and zebrafish larvae revealed that type of interactions is dose-dependent. *Aquat. Toxicol.* **2017,** *193*, 60-71.

19. Supiandi, N. I.; Charron, G.; Tharaud, M.; Cordier, L.; Guigner, J. M.; Benedetti, M. F.; Sivry, Y., Isotopically Labeled Nanoparticles at Relevant Concentrations: How Low Can We Go? The Case of CdSe/ZnS QDs in Surface Waters. *Environ. Sci. Technol.* **2019,** *53* (5), 2586-2594.

20. Durisic, N.; Godin, A. G.; Walters, D.; Grütter, P.; Wiseman, P. W.; Heyes, C. D., Probing the "Dark" Fraction of Core–Shell Quantum Dots by Ensemble and Single Particle pH-Dependent Spectroscopy. *ACS Nano* **2011,** *5* (11), 9062-9073.

21. Moon, H.; Lee, C.; Lee, W.; Kim, J.; Chae, H., Stability of quantum dots, quantum dot films, and quantum dot light‐emitting diodes for display applications. *Adv. Mater.* **2019,** *31* (34), 1804294.

22. Nagy, A.; Steinbrück, A.; Gao, J.; Doggett, N.; Hollingsworth, J. A.; Iyer, R., Comprehensive Analysis of the Effects of CdSe Quantum Dot Size, Surface Charge, and Functionalization on Primary Human Lung Cells. *ACS Nano* **2012,** *6* (6), 4748-4762.

23. Tarantini, A.; Wegner, K. D.; Dussert, F.; Sarret, G.; Beal, D.; Mattera, L.; Lincheneau, C.; Proux, O.; Truffier-Boutry, D.; Moriscot, C.; Gallet, B.; Jouneau, P. H.; Reiss, P.; Carrière, M., Physicochemical alterations and toxicity of InP alloyed quantum dots aged in environmental conditions: A safer by design evaluation. *NanoImpact* **2019,** *14*, 100168.

24. Kirchner, C.; Liedl, T.; Kudera, S.; Pellegrino, T.; Muñoz Javier, A.; Gaub, H. E.; Stölzle, S.; Fertig, N.; Parak, W. J., Cytotoxicity of Colloidal CdSe and CdSe/ZnS Nanoparticles. *Nano Lett.* **2005,** *5* (2), 331-338.

25. Derfus, A. M.; Chan, W. C.; Bhatia, S. N., Probing the cytotoxicity of semiconductor quantum dots. *Nano Lett.* **2004,** *4* (1), 11-18.

26. Wang, Y.; Tang, M., Review of in vitro toxicological research of quantum dot and potentially involved mechanisms. *Sci. Total Environ.* **2018,** *625*, 940-962.

27. Su, Y.; Hu, M.; Fan, C.; He, Y.; Li, Q.; Li, W.; Wang, L.-h.; Shen, P.; Huang, Q., The cytotoxicity of CdTe quantum dots and the relative contributions from released cadmium ions and nanoparticle properties. *Biomaterials* **2010,** *31* (18), 4829-4834.

28. Fourches, D.; Pu, D.; Tassa, C.; Weissleder, R.; Shaw, S. Y.; Mumper, R. J.; Tropsha, A., Quantitative Nanostructure−Activity Relationship Modeling. *ACS Nano* **2010,** *4* (10), 5703-5712.

29. Epa, V. C.; Burden, F. R.; Tassa, C.; Weissleder, R.; Shaw, S.; Winkler, D. A., Modeling Biological Activities of Nanoparticles. *Nano Lett.* **2012,** *12* (11), 5808-5812.

30. Mensch, A. C.; Melby, E. S.; Laudadio, E. D.; Foreman-Ortiz, I. U.; Zhang, Y.; Dohnalkova, A.; Hu, D.; Pedersen, J. A.; Hamers, R. J.; Orr, G., Preferential interactions of primary amine-terminated quantum dots with membrane domain boundaries and lipid rafts revealed with nanometer resolution. *Environ. Sci. Nano* **2020,** *7* (1), 149-161.

31. Mintzer, M. A.; Simanek, E. E., Nonviral Vectors for Gene Delivery. *Chem. Rev.* **2009,** *109* (2), 259-302.

32. Chandran, P.; Riviere, J. E.; Monteiro-Riviere, N. A., Surface chemistry of gold nanoparticles determines the biocorona composition impacting cellular uptake, toxicity and gene expression profiles in human endothelial cells. *Nanotoxicology* **2017,** *11* (4), 507-519.

33. Teeguarden, J. G.; Hinderliter, P. M.; Orr, G.; Thrall, B. D.; Pounds, J. G., Particokinetics In Vitro: Dosimetry Considerations for In Vitro Nanoparticle Toxicity Assessments. *Toxicol. Sci.* **2007,** *95* (2), 300-312.

34. Hinderliter, P. M.; Minard, K. R.; Orr, G.; Chrisler, W. B.; Thrall, B. D.; Pounds, J. G.; Teeguarden, J. G., ISDD: A computational model of particle sedimentation, diffusion and target cell dosimetry for in vitro toxicity studies. *Part. Fibre Toxicol.* **2010,** *7* (1), 36.

35. Jiang, J.; Oberdörster, G.; Biswas, P., Characterization of size, surface charge, and agglomeration state of nanoparticle dispersions for toxicological studies. *J. Nanopart. Res.* **2009,** *11* (1), 77-89.

36. Bright, N. A.; Gratian, M. J.; Luzio, J. P., Endocytic delivery to lysosomes mediated by concurrent fusion and kissing events in living cells. *Curr. Biol.* **2005,** *15* (4), 360-365.

37. Boussif, O.; Lezoualc'h, F.; Zanta, M. A.; Mergny, M. D.; Scherman, D.; Demeneix, B.; Behr, J. P., A versatile vector for gene and oligonucleotide transfer into cells in culture and in vivo: polyethylenimine. *Proc. Natl. Acad. Sci. U. S. A.* **1995,** *92* (16), 7297-7301.

38. Sonawane, N. D.; Szoka, F. C.; Verkman, A., Chloride accumulation and swelling in endosomes enhances DNA transfer by polyamine-DNA polyplexes. *J. Biol. Chem.* **2003,** *278* (45), 44826-44831.

39. Xia, T.; Kovochich, M.; Liong, M.; Meng, H.; Kabehie, S.; George, S.; Zink, J. I.; Nel, A. E., Polyethyleneimine coating enhances the cellular uptake of mesoporous silica nanoparticles and allows safe delivery of siRNA and DNA constructs. *ACS nano* **2009,** *3* (10), 3273-3286.

40. Zhu, J.; Wang, K. Z. Q.; Chu, C. T., After the banquet. *Autophagy* **2013,** *9* (11), 1663-1676.

41. Lorén, V.; Cabré, E.; Ojanguren, I.; Domènech, E.; Pedrosa, E.; García-Jaraquemada, A.; Mañosa, M.; Manyé, J., Interleukin-10 enhances the intestinal epithelial barrier in the presence of corticosteroids through p38 MAPK activity in Caco-2 monolayers: a possible mechanism for steroid responsiveness in ulcerative colitis. *PloS one* **2015,** *10* (6), e0130921.

42. Akinc, A.; Thomas, M.; Klibanov, A. M.; Langer, R., Exploring polyethylenimine-mediated DNA transfection and the proton sponge hypothesis. *J. Gene. Med.* **2005,** *7* (5), 657-663.

43. Agarwal, R. P.; Henkin, R. I., Metal binding characteristics of human salivary and porcine pancreatic amylase. *Int. J. Biol. Chem.* **1987,** *262* (6), 2568-2575.

44. Xu, K.; Basu, N.; George, S., Dietary nanoparticles compromise epithelial integrity and enhance translocation and antigenicity of milk proteins: An in vitro investigation. *NanoImpact* **2021,** *24*, 100369.

45. Wang, Y.; Mo, Y.; Zhou, L., Synthesis of CdSe quantum dots using selenium dioxide as selenium source and its interaction with pepsin. *Spectrochim. Acta A Mol. Biomol. Spectrosc.* **2011,** *79* (5), 1311-1315.

46. Lee, J.; Giordano, S.; Zhang, J., Autophagy, mitochondria and oxidative stress: cross-talk and redox signalling. *Biochem. J.***2012,** *441* (2), 523-540.

47. Balakrishnan, A.; Polli, J. E., Apical sodium dependent bile acid transporter (ASBT, SLC10A2): a potential prodrug target. *Mol. Pharm.* **2006,** *3* (3), 223-230.

48. Pacific Northwest National Laboratory, P. https://nanodose.pnnl.gov/default.aspx?topic=ISDD (accessed Feburary 2022).

49. Thomas, D. G.; Smith, J. N.; Thrall, B. D.; Baer, D. R.; Jolley, H.; Munusamy, P.; Kodali, V.; Demokritou, P.; Cohen, J.; Teeguarden, J. G., ISD3: a particokinetic model for predicting the combined effects of particle sedimentation, diffusion and dissolution on cellular dosimetry for in vitro systems. *Part. Fibre Toxicol.* **2018,** *15* (1), 6.

50. DeLoid, G.; Cohen, J. M.; Darrah, T.; Derk, R.; Rojanasakul, L.; Pyrgiotakis, G.; Wohlleben, W.; Demokritou, P., Estimating the effective density of engineered nanomaterials for in vitro dosimetry. *Nat. Commun.* **2014,** *5* (1), 3514.

51. Liu, R.; Liu, H. H.; Ji, Z.; Chang, C. H.; Xia, T.; Nel, A. E.; Cohen, Y., Evaluation of Toxicity Ranking for Metal Oxide Nanoparticles via an in Vitro Dosimetry Model. *ACS Nano* **2015,** *9* (9), 9303-9313.

Chapter 7

7. Summary and Conclusions

7.1. Summary of Results

This thesis aimed to characterize the mechanisms by which ingested NPs elicited responses at the molecular, cellular, and intercellular levels for intestinal cellular models. The roles that such effects may have on immune cells underlying disease progression in the context of cow milk allergy were also evaluated. The critical perturbations identified were then applied to study the effects of biotransformation in the GI tract on NP toxicity using a complex NP model. Here I summarize the major findings from my thesis:

- Exposure to the most popular dietary particles used in the food industry can induce transcriptomic (molecular) changes in epithelial cells. These transcriptomic data can derive t-POD values that may be used to rank/prioritize the toxicity of particles based on the chemical type and particle size. This is one of the first studies to apply the t-POD approach to *in vitro* studies of NPs in the dietary contexts on multiple cell lines. Functional pathway enrichment analysis highlighted potential downstream responses, including oxidative stress, inflammation, and immune responses. (Chapter 3)
- The identified transcriptomic responses were in good agreement with phenotypic responses. The particles taken up by the cells were shown to affect organelle functions inside the epithelial cells and disrupt cellular homeostasis, which was reflected by fluorescence-based bioassays targeting the identified perturbations from the transcriptomic study. The responses at the cellular level were inferred to then induce subsequent inter-cellular

responses in changing the cellular junction complex structure and barrier function of the intestinal epithelium. (Chapter 4)

- The disrupted cellular homeostasis and membrane integrity may further impact disease progression, which I investigated here through the context of milk allergy. The intestinal epithelium that was pre-exposed to NPs showed a higher level of allergen (milk protein) delivery and mast cell degranulation. Simultaneous exposure of cells to the NPs and milk further increased the degranulation level and induced the release of inflammatory mediators that can exacerbate the local inflammation. The mechanism of toxicity also switched from an IgE-dependent pathway into a mixed mechanism consisting of both IgE-dependent and independent pathways, bringing more challenges to allergy remediation. (Chapter 5)
- The panel of bioassays identified in the previous chapters was applied for toxicity screening of multilayered NPs in pristine and digested form. The results suggested synergistic effects of the individual components on the complete NPs, with surface chemistry being the critical contributor to bioavailability. The biotransformation of the NPs at each stage of the simulated digestion in the GI tract further altered the surface properties of the NPs and enhanced the toxicity.
- The overall approach was designed according to the AOP framework. To my knowledge, this is one of the first works to comprehensively examine the intestinal effects of a dietary contaminant using this framework (i.e., responses were linked from the molecular to the cellular level and ultimately to an adverse outcome of relevance to population health).

7.2. Discussion

7.2.1. The paradigm shift in toxicity assessment

The growing market of nanotechnology and the application of NPs has inevitably increased the general public's oral exposure to NPs from food products.[154] The safety aspects of these exposures, however, are not fully backed up with detailed risk assessment information for the materials being used. The current regulation of nano-containing food products in Canada still follows the existing legislation for chemical additives in food, and does not consider the distinctive properties of the nanomaterials from their bulk counterparts.[155] Similarly, the Food and Drug Administration (FDA) in the U.S. does not have specific regulations for nanotechnology-based products, but does recommend preliminary safety assessments for finishing products at the nanoscale with a case-by-case approach.[156] The current toxicity tests for food additives or new dietary ingredients primarily comprise repeated (28[157] and 90[158] days) oral dosing studies in rodents. However, realizing that such traditional approaches for toxicity assessment of a chemical are resource-intensive, it is thus challenging to evaluate every nano-containing product on the market.[159]

The limited efficiency (i.e., they take lots of time, cost lots of money, and use many animal lives and are thus unethical) in current approaches taken for toxicity assessment, coupled with the recent paradigm shift in toxicity testing, has raised interest in the research and regulatory community to develop New Approach Methodologies (NAMs).[4] A major driver of this newfound focus on NAMs was the influential 2007 National Research Council (NRC) report "Toxicity Testing in the 21st Century-a Vision and Strategy" which articulated a paradigm shift in toxicology toward the use of mechanistic pathway-based testing methods instead of traditional animal-based assays.[4]

Since these pathways contain responses at various biological levels that, when disturbed, can cause adverse health effects, the hope is that *in vitro* methods measuring early biological events can complement and eventually replace animal models to inform hazard assessments.[160]

The versatile and comprehensive information offered by *in vitro* methods is enabled by emerging biotechnologies. First, the increasing affordability of high-throughput transcriptomic analysis by RNA sequencing (RNA-seq) provides comprehensive information for key events at the molecular level. Transcriptomics is one of the most widely applied techniques to identify perturbations in biological pathways by probing changes in the expression of all mRNAs in cells or tissues.[161, 162] Targeted transcriptomic analysis using 1,000-3,000 target genes further reduced the cost while still providing representative gene-expression profiling information.[163-165] In this thesis, the L1000 panel[165] coupled with a high-throughput sequencing platform based on 96 well plates was used, which significantly reduced the time and amount of reagent for sequencing. When applied in Chapter 3, this approach provided critical information about the affected pathways (oxidative stress, inflammation, and immune responses) from the molecular level, allowing comparisons to other perturbations from phenotypic assays (Chapter 4).

Second, the increasing availability of adequate high-throughput *in vitro* tests allowed simultaneous characterization of various biological functions inside tissues and cells. The high-content screening (HCS) system has emerged as a visual detection instrument that can measure a panel of functional biomarkers for the biological status of cells, tissues, or small organisms (e.g., fish embryos).[166, 167] The fluorescence microscopy imaging system can visualize living cells and organisms in real-time during the exposure and track a panel of biomarkers (fluorophores) overtime to provide quantitative measurements of key cellular effects. In this thesis, I used the HCS system to perform

high-throughput screening of cellular response in 384 well plates in Chapters 4 and 6 to characterize cellular responses after exposure to different NPs. Changes in cell membrane integrity, ROS generation, mitochondrial function, lysosome acidity, and calcium flux were characterized in a concentration-dependent (Chapters 4 and 6) and time-dependent Chapter 4) manner. Like the aforementioned high-throughput transcriptomics approach (Chapter 3), the HCS system here also satisfies the interest of the NAMs community as a method that is cost-effective and rapid, designed for use with *in vitro* models, and yields rich biological information.

Third, the increasing power of computational tools is facilitating data analysis. In this thesis, the sequencing data was demultiplexed *via* online data processing hubs (GeneGlobe) and analyzed by online tools (FastBMD) specifically developed for DEG analysis and t-POD derivation (Chapter 3). The images acquired by the HCS system were also analyzed and processed by specific software (Zeiss) to extract quantitative fluorescence intensity values from images (Chapter 4). Publicly accessible databases that contain biological networks and pathways, such as the Kyoto Encyclopedia of Genes and Genomes (KEGG)[168] and AOP wiki[143], provide a comprehensive representation of the current knowledge and set the base for new studies. All these enabling technologies allow this thesis to bring together bioassays at molecular, cellular, and intracellular levels to understand a "system level" response, and in doing so, they meet the challenges articulated in the aforementioned 2007 US NRC report and contemporaneous interest in NAMs.

7.2.2. Adverse outcome pathway (AOP) approach

After obtaining *in vitro* results from various assays, frameworks like the AOP can be applied to integrate and organize the knowledge to provide mechanistic information for hazard assessment and eventually for regulatory purposes.[144, 169] The AOP framework assembles existing toxicity knowledge based on the causal relationships between the molecular initiating events, key events, and adverse outcomes from lower to higher biological levels.[144] As a result, the adverse outcomes due to exposure to a substance can be reasonably predicted using measurable perturbations at lower biological levels. Currently, the AOP repository (AOP wiki) does not contain any finalized (endorsed) AOPs that focus on GI disorders.[143] This thesis used the AOP approach to examine and organize the effects of ingested NPs in the context of GI disorders with the ultimate goal that the identified measurable perturbations can be used for screening other materials in risk assessment. Recognizing that AOP is not specific to chemicals[144], we exposed the *in vitro* model cell lines to a reference library of NPs for both industrial relevance and more comprehensive responses. In order to frame the toxicity effects along an AOP continuum, I first needed to identify the mechanism of toxicity and assemble relevant *in vitro* assays (MIEs and KEs) along an AOP. In this thesis, I first identified the changes at the molecular level by RNA-sequencing (Chapter 3). The affected molecular functions, biological processes, and enriched pathways suggested the potential mechanisms of toxicity were likely mediated *via* the oxidative stress pathways. Based on the findings in Chapter 3, the bioassays that target the critical perturbations (KEs) embedded in the oxidative stress pathway at various biological levels were tested in Chapter 4 (Figure *7.1*). The listed *in vitro* cellular assays were identified to be relevant for all tested particles (with varying lowest observed effect concentrations), and thus can be incorporated as a panel of assays in the

testing platform. In Chapter 5, we moved further to identify the KEs and AOs higher biological levels that aligned in the disease progression of the immune responses and other subsequent reactions in milk allergy.

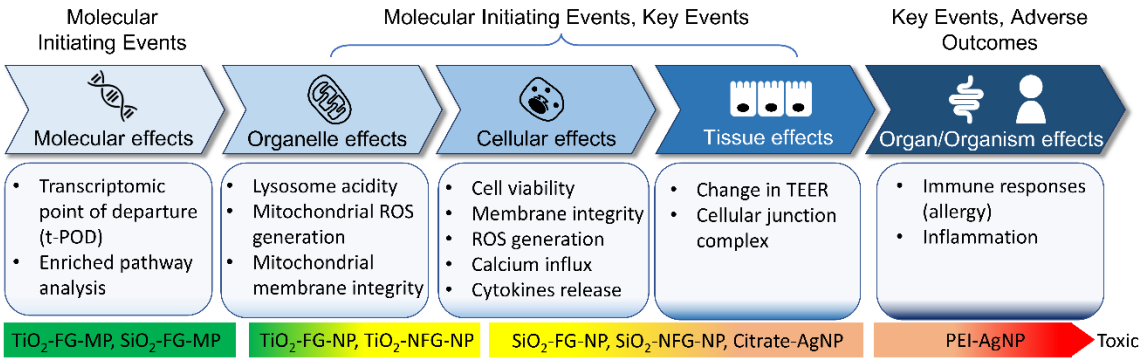

Figure 7.1 Critical changes due to nanoparticle exposure identified in this thesis organized along the adverse outcome pathway from the molecular level (Chapter 3) to key events at organelle, cellular, and tissue levels (Chapter 4) and adverse outcomes at the highest biological level (Chapter 5).

In addition to the identified critical perturbations, the KERs are also suggested in this study. Chapter 3 demonstrated that the toxicity of the reference library of particles is the highest for AgNPs, followed by SiO_2 and TiO_2, which were confirmed to induce oxidative stress, inflammation, and compromised barrier integrity at the cellular level (Chapter 4). The t-POD values derived in Chapter 3 were mostly lower than the lowest observed effect concentrations identified in the bioassays in Chapter 4, suggesting that the downstream responses were induced at higher concentrations. Furthermore, temporal responses were also reported in this chapter for HIEC-6 cells, further confirming the sequence of events. Similarly, in Chapter 5, the time-dependent release of cytokines and phase progression in the activation of mast cells indicated the causal relationship between the events and adverse outcomes.

7.2.3. Biological relevancy

Since the ultimate goal of the alternative toxicity testing methods is to inform regulatory bodies by facilitating the prioritization and toxicity screening of chemicals, the *in vitro* assays need to provide biologically relevant results.[170] This goal requires the proposed adverse outcomes to be of public health concern and the chemicals and cell models used for method development to be biologically relevant. I address the relevancy of my findings using several approaches.

First, my thesis was anchored on adverse outcomes prevalent in the population, including cow milk allergy[131, 171], and inflammation[172] in the GI tract. Constructing the platform of assays in an AOP approach also ensures that the identified critical perturbations in the proposed bioassays align with the GI disorders' disease progression.

Second, as mentioned in previous chapters, the reference library of particles is industrially relevant and includes FG-NPs that may be ingested. The concentration ranges used in the thesis are also relevant in real-world scenarios. From the literature, the oral exposure concentration varied significantly for SiO_2 (1.8 mg/kg bw/day of nano-sized silica[23] ; 1.3–16.3 mg Si/g product[28]), TiO_2 (0.36 - 1. 08 mg/kg bw/day[25] ; 0.02 to 9.0 mg TiO_2/g product[173]) and Ag (0.012-0.42 mg/kg bw/day[26, 174]). Rough estimations of the intestinal burden of the NPs based on exposure to x mg/kg bw/day of respective compounds were calculated assuming the total area of the intestine is about 30 m^2 [175] and the average body weight of an adult is 60 kg:

$$\frac{x\ \frac{mg}{kg\ bw/day} * 60\ kg}{30\ m^2 * \frac{10000\ cm^2}{m^2}} = 0.0002x\ \frac{mg}{day * cm^2}$$

After normalizing the exposure area to the liquid volume and growth area in the multi-well plates[176] (100 μL, 0.32 cm^2 for 96 well plates and 30 μL, 0.056 cm^2 for 384 well plates), the relevant concentration for the bioassays is calculated and presented in (Table 7.1). The concentration range was covered in the studies of Chapter 3 and was comparatively smaller than the derived t-POD values and the lowest observed effect concentration in the apical assays in Chapter 4 (Table 7.1). However, since the rough estimate did not consider any interactions during digestion, excretion and accumulation in the body, and differences between the nominal and experimental concentration, this relevant daily exposure range warrants more accurate studies before being considered non-toxic. In order to further make use of the exposure data, the *in vitro* results from HCS may be converted to equivalent doses ($POD_{Bioactivity}$) through reverse dosimetry by toxicokinetic models. The ratios of the $POD_{Bioactivity}$ values against the exposure estimates yield bioactivity-to-exposure ratios (BER), which can be used to guide risk-based ranking for regulatory agencies.[177]

Table 7.1 Comparison of estimated exposure concentrations of the particles to t-POD_{mode} values (Chapter 3), LC20 and lowest concentration of observed effects from sublethal phenotypic assay (Chapter 4) results.

Concentration (ppm)	**SiO_2 FG-NP**	**TiO_2 FG-NP**	**AgNP**
$tPOD_{mode}$	7.15-31.56	13.18-58.85	0.42-7.02
LC20	62.78	NA	28.14
Sublethal responses	6.25	3.125	3.125
Estimated exposure	0.672-1.152	0.13-0.69	0.008-0.27

Using bio-relevant cell models and exposure scenarios are also critical for *in vitro* toxicity studies. The different results in Caco-2 and HIEC-6 cells in the derived tPOD (Chapter 3) and the phenotypic responses (Chapter 4) confirmed cell-dependent responses in evaluating respective changes of interests. Although HIEC-6 was more sensitive to particle exposure in a more significant decrease in TEER, it is not considered a relevant model for membrane permeability due

to the absence of junction complex formation.[178] The difference in exposure scenario resulted in significant changes in mast cell degranulation in Chapter 5, where the co-exposure scenario suggested mechanism difference in mediating allergic responses. The exposure model is also relevant to the interaction between the NPs and the biological environment, where the formation of biocorona has been evident in changing the surface properties of the NPs.[80, 146, 179-181] The continuous transformation of QDs at various stages of simulated digestion and the increasing toxicity compared to the pristine form (Chapter 6) further confirmed the critical effects of the relevant biological environment in modifying toxicity.

The proposed methods also need to be applicable to other screening studies. The inclusion of Chapter 6 not only explored the effects of digestion on particle toxicity but also served as a primary test for the assay platform for its possible application to screen other particles. The ability of the panel of assays to compare the toxicity of pristine NPs (multilayered QDs) and bio-transformed NPs (digested QDs) suggested further demonstrated the potential of the platform in toxicity screening.

7.2.4. Regulatory uptake

Regulatory acceptance of *in vitro* assays for toxicity screening is a constantly evolving process that requires collaborative efforts from diverse stakeholders.[182] One example is TiO_2 (E171), which I studied in my dissertation. Before this thesis work commenced in 2016, the European Food Safety Authority (EFSA) Panel on Food Additives and Nutrient Sources added to Food (ANS) published a report evaluating the use of TiO_2 as a food additive because of identified adverse effects, though it did not establish an acceptable daily intake (ADI) and believed that exposure

levels would not be of concern.[183] In 2018, an updated report from the EFSA panel concluded no changes in the existing opinion of TiO_2 safety.[184] However, in response to a request by the European Commission in March 2020, EFSA updated its safety assessment in 2021 and concluded that E171 could no longer be considered as safe when used as a food additive.[185] In a recent report released in June 2022, the food directorate of Health Canada is also concerning the safety of TiO_2 as a food additive due to its role in food allergy based on some of the recently published studies.[186] The collective efforts from the scientific community and the continuous re-evaluation of the regulatory agencies from evidence-based studies will continuously promote regulatory amendment to protect consumer safety.

Through the aforementioned case study of TiO_2, a key challenge in informing regulatory changes has been the difficulty in determining the public health relevance of limited *in vitro* and *in vivo* studies. Compared to the respiratory toxicity of NPs[187, 188], the effects of ingested NPs are largely understudied. In addition, most of the evaluated studies in the EFSA reports were *in vitro* studies or *in vivo* ones with single-ended apical tests focused on a few primary responses. Due to the differences in the weight of evidence of each study and the limitations in reproducibility, it is rather difficult for regulatory agencies to provide recommendations based on contradicting results.[170] This also confirms the importance of including a panel of assays underlying the mechanism of toxicity while interpreting toxicity results. In this thesis work, the mechanism of toxicity was also identified based on multiple assays. For example, the partial disruption and re-distribution of the proteins in the cellular junction complex by SiO_2 and TiO_2 particles (Chapter 4) was not suggested at the gene expression level (Chapter 3) and was only realized by fluorescence imaging. In addition, it is also critical to obtain reproducible and reliable data across laboratories for regulatory

acceptance.[189] In this study, various quality control measures (positive controls and negative controls) were included in the study design. For the future application of this study, the results can be evaluated jointly with other mechanistic studies for comprehensive risk assessment.

7.2.5. Limitations and future works

In this thesis, the identified perturbations embedded in the AOP were further connected to the disease progression of milk allergy, and suggested the possibility of performing gene expression and cell assays for primary toxicity screening of other chemicals. However, this work is still limited in the choice of cell models and relevancy in exposure scenario. First, the culture models are limited to a few types of cells (single-cell model for Chapters 3-4 and two-cell model for Chapter 5), which cannot represent the complicated multi-cell environment in the small intestine.[190] Future studies using more realistic models, such as intestine-on-a-chip[191], can achieve more relevant results. Another model to be considered is the *ex vivo* culture model[192], which is developed from human tissue (intestinal) biopsies. This model minimized the inter-species extrapolation while maintaining certain complexity in the types of cells and thus can provide more relevant information than *in vitro* models. In the context of this thesis, *ex vivo* cultures developed with intestinal biopsies from patients with GI disorders and healthy individuals can be exposed to the reference library of particles. The bioassay results of the control (healthy) and diseased model can be compared with the *in vitro* results to take this work further into the organism and human populations level. Second, the release of NPs from food products and the digestion in the GI system should also be concerned for the complete ingestion and digestion process. The reference library of NPs can be subjected to simulated human ingestion and digestion before exposing to the abovementioned culture models to improve the weight of evidence in future studies.

With the improved cell model selection and relevant exposure design, more studies may be performed in detailing the role of NPs in the molecular mechanisms of allergic inflammation. Future studies include and were not limited to the applications of "Omics Sciences" in unravelling how dietary NPs may shape the proteome, transcriptome, and metabolome of the exposed cell models. These detailed approaches can provide versatile data to capture the changes at the gene expression and resulting phenotypic levels for clinically relevant allergens. Moreover, identifying the detailed toxicity mechanism also helps to determining the type of allergy (IgE-dependent, independent, or mixed mechanism) and subsequently supports the development of targeted immunotherapies.

7.3. Conclusion

This doctoral thesis performed laboratory studies to advance knowledge about the effects of ingested NPs on the gastrointestinal system at molecular, cellular, and higher biological levels. The organization of the key perturbations using an AOP approach allowed reasonable connections to be made between the results at different levels in a causal manner. The targeted bioassays applied for toxicity screening further confirmed the changes in particle toxicity after biotransformation in the GI tract. Given the increasing number of NPs used in food products without mechanistic toxicity information, this study suggests an integrated testing strategy that can be used to screen NPs of interest, which has the potential of expanding to a larger scale to facilitate regulatory decision-making practices.

References

1. Chaudhry, Q.; Scotter, M.; Blackburn, J.; Ross, B.; Boxall, A.; Castle, L.; Aitken, R.; Watkins, R., Applications and implications of nanotechnologies for the food sector. *Food Addit. Contam. Part A* **2008,** *25* (3), 241-258.

2. Chey, W. D., The role of food in the functional gastrointestinal disorders: introduction to a manuscript series. *Am. J. Gastroenterol. Suppl.* **2013,** *108* (5), 694.

3. Bergin, I. L.; Witzmann, F. A., Nanoparticle toxicity by the gastrointestinal route: evidence and knowledge gaps. *Int. J. Biomed. Nanosci. Nanotechnol.* **2013,** *3* (1-2), 163-210.

4. National Research Council (NRC), *Toxicity Testing in the 21st Century: A Vision and a Strategy*. The National Academies Press: Washington, DC, 2007; p 216.

5. Nel, A.; Xia, T.; Meng, H.; Wang, X.; Lin, S.; Ji, Z.; Zhang, H., Nanomaterial toxicity testing in the 21st century: use of a predictive toxicological approach and high-throughput screening. *Acc. Chem. Res.* **2012,** *46* (3), 607-621.

6. Damoiseaux, R.; George, S.; Li, M.; Pokhrel, S.; Ji, Z.; France, B.; Xia, T.; Suarez, E.; Rallo, R.; Mädler, L., No time to lose—high throughput screening to assess nanomaterial safety. *Nanoscale* **2011,** *3* (4), 1345-1360.

7. Thomas, C. R.; George, S.; Horst, A. M.; Ji, Z.; Miller, R. J.; Peralta-Videa, J. R.; Xia, T.; Pokhrel, S.; Mädler, L.; Gardea-Torresdey, J. L., Nanomaterials in the environment: from materials to high-throughput screening to organisms. *ACS nano* **2011,** *5* (1), 13-20.

8. Calder, P. C., Fatty acids and inflammation: the cutting edge between food and pharma. *Eur. J. Pharmacol.* **2011,** *668*, S50-S58.

9. Kolodziejczyk, A. A.; Zheng, D.; Elinav, E., Diet–microbiota interactions and personalized nutrition. *Nat. Rev. Microbiol.* **2019,** *17* (12), 742-753.

10. Chassaing, B.; Koren, O.; Goodrich, J. K.; Poole, A. C.; Srinivasan, S.; Ley, R. E.; Gewirtz, A. T., Dietary emulsifiers impact the mouse gut microbiota promoting colitis and metabolic syndrome. *Nature* **2015,** *519* (7541), 92.

11. Choi, H. J.; Kim, J.; Park, S.-H.; Do, K. H.; Yang, H.; Moon, Y., Pro-inflammatory NF-κB and early growth response gene 1 regulate epithelial barrier disruption by food additive carrageenan in human intestinal epithelial cells. *Toxicol. Lett.* **2012,** *211* (3), 289-295.

12. Lomer, M. C.; Harvey, R. S.; Evans, S. M.; Thompson, R. P.; Powell, J. J., Efficacy and tolerability of a low microparticle diet in a double blind, randomized, pilot study in Crohn's disease. *Eur. J. Gastroenterol.* **2001,** *13* (2), 101-106.

13. Ruiz, P. A.; Morón, B.; Becker, H. M.; Lang, S.; Atrott, K.; Spalinger, M. R.; Scharl, M.; Wojtal, K. A.; Fischbeck-Terhalle, A.; Frey-Wagner, I.; Hausmann, M.; Kraemer, T.; Rogler, G., Titanium dioxide nanoparticles exacerbate DSS-induced colitis: role of the NLRP3 inflammasome. *Gut* **2017,** *66* (7), 1216-1224.

14. Rogers, M. A., Naturally occurring nanoparticles in food. *Curr. Opin. Food Sci.* **2016,** *7*, 14-19.

15. Ridout, M. J.; Parker, M. L.; Hedley, C. L.; Bogracheva, T. Y.; Morris, V. J., Atomic force microscopy of pea starch granules: granule architecture of wild-type parent, r and rb single mutants, and the rrb double mutant. *Carbohydr. Res.* **2003,** *338* (20), 2135-2147.

16. Limbach, L. K.; Wick, P.; Manser, P.; Grass, R. N.; Bruinink, A.; Stark, W. J., Exposure of Engineered Nanoparticles to Human Lung Epithelial Cells: Influence of Chemical Composition and Catalytic Activity on Oxidative Stress. *Environ. Sci. Technol.* **2007,** *41* (11), 4158-4163.

17. Gonzalez, L.; Lison, D.; Kirsch-Volders, M., Genotoxicity of engineered nanomaterials: a critical review. *Nanotoxicology* **2008,** *2* (4), 252-273.

18. Vance, M. E.; Kuiken, T.; Vejerano, E. P.; McGinnis, S. P.; Hochella, M. F., Jr.; Rejeski, D.; Hull, M. S., Nanotechnology in the real world: Redeveloping the nanomaterial consumer products inventory. *Beilstein J. Nanotechnol.* **2015,** *6*, 1769-1780.

19. Philpott, H. L.; Nandurkar, S.; Lubel, J.; Gibson, P. R., Drug-induced gastrointestinal disorders. *Frontline Gastroenterol.* **2014,** *5* (1), 49-57.

20. Frewer, L. J.; Gupta, N.; George, S.; Fischer, A. R. H.; Giles, E. L.; Coles, D., Consumer attitudes towards nanotechnologies applied to food production. *Trends Food Sci. Technol.* **2014,** *40* (2), 211-225.

21. Verleysen, E.; Van Doren, E.; Waegeneers, N.; De Temmerman, P.-J.; Abi Daoud Francisco, M.; Mast, J., TEM and SP-ICP-MS analysis of the release of silver nanoparticles from decoration of pastry. *J. Agric. Food Chem.* **2015,** *63* (13), 3570-3578.

22. Boutillier, S.; Fourmentin, S.; Laperche, B., History of titanium dioxide regulation as a food additive: a review. *Environ. Chem. Lett.* **2022,** *20* (2), 1017-1033.

23. Dekkers, S.; Krystek, P.; Peters, R. J. B.; Lankveld, D. P. K.; Bokkers, B. G. H.; van Hoeven-Arentzen, P. H.; Bouwmeester, H.; Oomen, A. G., Presence and risks of nanosilica in food products. *Nanotoxicology* **2011,** *5* (3), 393-405.

24. Wang, H.; Du, L.-J.; Song, Z.-M.; Chen, X.-X., Progress in the characterization and safety evaluation of engineered inorganic nanomaterials in food. *Nanomedicine* **2013,** *8* (12), 2007-2025.

25. Weir, A.; Westerhoff, P.; Fabricius, L.; von Goetz, N., Titanium Dioxide Nanoparticles in Food and Personal Care Products. *Environ. Sci. Technol.* **2012,** *46* (4), 2242-2250.

26. EFSA Panel on Food Additives Nutrient Sources added to Food, Scientific opinion on the re-evaluation of silver (E 174) as food additive. *EFSA Journal* **2016,** *14* (1), 4364.

27. Doshi, R.; Braida, W.; Christodoulatos, C.; Wazne, M.; O'Connor, G., Nano-aluminum: transport through sand columns and environmental effects on plants and soil communities. *Environ. Res.* **2008,** *106* (3), 296-303.

28. Yang, S.-T.; Wang, T.; Dong, E.; Chen, X.-X.; Xiang, K.; Liu, J.-H.; Liu, Y.; Wang, H., Bioavailability and preliminary toxicity evaluations of alumina nanoparticles in vivo after oral exposure. *Toxicol. Res.* **2012,** *1* (1), 69-74.

29. Hong, S. U.; Miller, M. D.; Bruening, M. L., Removal of Dyes, Sugars, and Amino Acids from NaCl Solutions Using Multilayer Polyelectrolyte Nanofiltration Membranes. *Ind. Eng. Chem. Res.* **2006,** *45* (18), 6284-6288.

30. Fathi, M.; Mozafari, M. R.; Mohebbi, M., Nanoencapsulation of food ingredients using lipid based delivery systems. *Trends Food Sci. Technol.* **2012,** *23* (1), 13-27.

31. Espitia, P. J. P.; Soares, N. d. F. F.; Coimbra, J. S. d. R.; de Andrade, N. J.; Cruz, R. S.; Medeiros, E. A. A., Zinc Oxide Nanoparticles: Synthesis, Antimicrobial Activity and Food Packaging Applications. *Food Bioproc. Tech.* **2012,** *5* (5), 1447-1464.

32. Llorens, A.; Lloret, E.; Picouet, P. A.; Trbojevich, R.; Fernandez, A., Metallic-based micro and nanocomposites in food contact materials and active food packaging. *Trends Food Sci. Technol.* **2012,** *24* (1), 19-29.

33. Cho, J. W.; Paul, D. R., Nylon 6 nanocomposites by melt compounding. *Polymer* **2001,** *42* (3), 1083-1094.

34. Abdellah, A.; Abdelhalim, A.; Loghin, F.; Köhler, P.; Ahmad, Z.; Scarpa, G.; Lugli, P., Flexible carbon nanotube based gas sensors fabricated by large-scale spray deposition. *IEEE Sens. J.* **2013,** *13* (10), 4014-4021.

35. Yoshioka, Y.; Higashisaka, K.; Tsunoda, S.-i.; Tsutsumi, Y., The Absorption, Distribution, Metabolism, and Excretion Profile of Nanoparticles. In *Engineered Cell Manipulation for Biomedical Application*, Springer: 2014; pp 259-271.

36. Lomer, M. C. E.; Thompson, R. P. H.; Powell, J. J., Fine and ultrafine particles of the diet: influence on the mucosal immune response and association with Crohn's disease. *Proc. Nutr. Soc.* **2002,** *61* (1), 123-130.

37. Harris, A. T.; Bali, R., On the formation and extent of uptake of silver nanoparticles by live plants. *J. Nanopart. Res.* **2008,** *10* (4), 691-695.

38. Emamifar, A.; Kadivar, M.; Shahedi, M.; Soleimanian-Zad, S., Effect of nanocomposite packaging containing Ag and ZnO on inactivation of Lactobacillus plantarum in orange juice. *Food Control* **2011,** *22* (3), 408-413.

39. Boland, M., Human digestion–a processing perspective. *J. Sci. Food Agric.* **2016,** *96* (7), 2275-2283.

40. Go, M.-R.; Bae, S.-H.; Kim, H.-J.; Yu, J.; Choi, S.-J., Interactions between Food Additive Silica Nanoparticles and Food Matrices. *Front. Microbiol.* **2017,** *8*, 1013.

41. Lichtenstein, D.; Ebmeyer, J.; Knappe, P.; Juling, S.; Böhmert, L.; Selve, S.; Niemann, B.; Braeuning, A.; Thünemann, A. F.; Lampen, A., Impact of food components during in vitro digestion of silver nanoparticles on cellular uptake and cytotoxicity in intestinal cells. *Biol. Chem.* **2015,** *396* (11), 1255-1264.

42. Hollander, D., Intestinal permeability, leaky gut, and intestinal disorders. *Curr. Gastroenterol. Rep.* **1999,** *1* (5), 410-416.

43. Laukoetter, M. G.; Bruewer, M.; Nusrat, A., Regulation of the intestinal epithelial barrier by the apical junctional complex. *Curr. Opin. Gastroenterol.* **2006,** *22* (2), 85-89.

44. Behzadi, S.; Serpooshan, V.; Tao, W.; Hamaly, M. A.; Alkawareek, M. Y.; Dreaden, E. C.; Brown, D.; Alkilany, A. M.; Farokhzad, O. C.; Mahmoudi, M., Cellular uptake of nanoparticles: journey inside the cell. *Chem. Soc. Rev.* **2017,** *46* (14), 4218-4244.

45. Oh, N.; Park, J.-H., Endocytosis and exocytosis of nanoparticles in mammalian cells. *Int. J. Nanomedicine* **2014,** *9* (Suppl 1), 51-63.

46. Parkar, N. S.; Akpa, B. S.; Nitsche, L. C.; Wedgewood, L. E.; Place, A. T.; Sverdlov, M. S.; Chaga, O.; Minshall, R. D., Vesicle Formation and Endocytosis: Function, Machinery, Mechanisms, and Modeling. *Antioxid. Redox Signal.* **2009,** *11* (6), 1301-1312.

47. Sonaje, K.; Chuang, E.-Y.; Lin, K.-J.; Yen, T.-C.; Su, F.-Y.; Tseng, M. T.; Sung, H.-W., Opening of Epithelial Tight Junctions and Enhancement of Paracellular Permeation by Chitosan: Microscopic, Ultrastructural, and Computed-Tomographic Observations. *Mol. Pharm.* **2012,** *9* (5), 1271-1279.

48. Jani, P.; Halbert, G. W.; LANGRIDGE, J.; Florence, A. T., Nanoparticle uptake by the rat gastrointestinal mucosa: quantitation and particle size dependency. *J. Pharm. Pharmacol.* **1990,** *42* (12), 821-826.

49. Ge, Y.; Zhang, Y.; Xia, J.; Ma, M.; He, S.; Nie, F.; Gu, N., Effect of surface charge and agglomerate degree of magnetic iron oxide nanoparticles on KB cellular uptake in vitro. *Colloids Surf. B: Biointerfaces* **2009,** *73* (2), 294-301.

50. Chen, L.; Mccrate, J. M.; Lee, J. C.; Li, H., The role of surface charge on the uptake and biocompatibility of hydroxyapatite nanoparticles with osteoblast cells. *Nanotechnology* **2011,** *22* (10), 105708.

51. Brandenberger, C.; Rothen-Rutishauser, B.; Mühlfeld, C.; Schmid, O.; Ferron, G. A.; Maier, K. L.; Gehr, P.; Lenz, A.-G., Effects and uptake of gold nanoparticles deposited at the air–liquid interface of a human epithelial airway model. *Toxicol. Appl. Pharmacol.* **2010,** *242* (1), 56-65.

52. Villanueva, A.; Canete, M.; Roca, A. G.; Calero, M.; Veintemillas-Verdaguer, S.; Serna, C. J.; del Puerto Morales, M.; Miranda, R., The influence of surface functionalization on the enhanced internalization of magnetic nanoparticles in cancer cells. *Nanotechnology* **2009,** *20* (11), 115103.

53. Lunov, O.; Syrovets, T.; Loos, C.; Beil, J.; Delacher, M.; Tron, K.; Nienhaus, G. U.; Musyanovych, A.; Mailander, V.; Landfester, K., Differential uptake of functionalized polystyrene nanoparticles by human macrophages and a monocytic cell line. *ACS nano* **2011,** *5* (3), 1657-1669.

54. Saptarshi, S. R.; Duschl, A.; Lopata, A. L., Interaction of nanoparticles with proteins: relation to bio-reactivity of the nanoparticle. *J. Nanobiotechnology* **2013,** *11* (1), 26.

55. Peters, R.; Kramer, E.; Oomen, A. G.; Herrera Rivera, Z. E.; Oegema, G.; Tromp, P. C.; Fokkink, R.; Rietveld, A.; Marvin, H. J. P.; Weigel, S.; Peijnenburg, A. A. C. M.; Bouwmeester, H., Presence of Nano-Sized Silica during In Vitro Digestion of Foods Containing Silica as a Food Additive. *ACS Nano* **2012,** *6* (3), 2441-2451.

56. Phue, W. H.; Liu, M.; Xu, K.; Srinivasan, D.; Ismail, A.; George, S., A Comparative Analysis of Different Grades of Silica Particles and Temperature Variants of Food-Grade Silica Nanoparticles for Their Physicochemical Properties and Effect on Trypsin. *J. Agric. Food Chem.* **2019,** *67* (44), 12264-12272.

57. Phue, W. H.; Bahadi, M.; Dynes, J. J.; Wang, J.; Kuppili, V. S. C.; Ismail, A.; Hameed, A.; George, S., Protein–biomolecule interactions play a major role in shaping corona proteome: studies on milk interacted dietary particles. *Nanoscale* **2021,** *13* (31), 13353-13367.

58. Phue, W. H.; Xu, K.; George, S., Inorganic food additive nanomaterials alter the allergenicity of milk proteins. *Food Chem. Toxicol.* **2022,** *162*, 112874.

59. Cho, W.-S.; Kang, B.-C.; Lee, J. K.; Jeong, J.; Che, J.-H.; Seok, S. H., Comparative absorption, distribution, and excretion of titanium dioxide and zinc oxide nanoparticles after repeated oral administration. *Part. Fibre Toxicol.* **2013,** *10*, 9.

60. Kim, Y. S.; Kim, J. S.; Cho, H. S.; Rha, D. S.; Kim, J. M.; Park, J. D.; Choi, B. S.; Lim, R.; Chang, H. K.; Chung, Y. H.; Kwon, I. H.; Jeong, J.; Han, B. S.; Yu, I. J., Twenty-Eight-Day Oral Toxicity, Genotoxicity, and Gender-Related Tissue Distribution of Silver Nanoparticles in Sprague-Dawley Rats. *Inhal. Toxicol.* **2008,** *20* (6), 575-583.

61. Cho, K.; Wang, X.; Nie, S.; Chen, Z.; Shin, D. M., Therapeutic Nanoparticles for Drug Delivery in Cancer. *Clin. Cancer Res.* **2008,** *14* (5), 1310.

62. Champion, J. A.; Katare, Y. K.; Mitragotri, S., Particle shape: A new design parameter for micro- and nanoscale drug delivery carriers. *J. Control. Release* **2007,** *121* (1), 3-9.

63. Geng, Y.; Dalhaimer, P.; Cai, S.; Tsai, R.; Tewari, M.; Minko, T.; Discher, D. E., Shape effects of filaments versus spherical particles in flow and drug delivery. *Nat. Nanotechnol* **2007,** *2*, 249.

64. Akashi, M.; Akagi, T.; Matsusaki, M., *Engineered Cell Manipulation for Biomedical Application*. Springer Japan: 2014.

65. Furumoto, K.; Ogawara, K.-i.; Yoshida, M.; Takakura, Y.; Hashida, M.; Higaki, K.; Kimura, T., Biliary excretion of polystyrene microspheres depends on the type of receptor-mediated uptake in rat liver. *Biochim. Biophys. Acta. Gen. Subj.* **2001,** *1526* (2), 221-226.

66. Ogawara, K.-I.; Yoshida, M.; Furumoto, K.; Takakura, Y.; Hashida, M.; Higaki, K.; Kimura, T., Uptake by hepatocytes and biliary excretion of intravenously administered polystyrene microspheres in rats. *J. Drug Target* **1999,** *7* (3), 213-221.

67. Choi, H. S.; Liu, W.; Misra, P.; Tanaka, E.; Zimmer, J. P.; Ipe, B. I.; Bawendi, M. G.; Frangioni, J. V., Renal clearance of quantum dots. *Nat. Biotechnol.* **2007,** *25* (10), 1165-1170.

68. Council, N. R.; Studies, D. E. L.; Sciences, B. L.; Toxicology, B. E. S.; Toxicology, C. A. T. T. P., *Applications of Toxicogenomic Technologies to Predictive Toxicology and Risk Assessment*. National Academies Press: 2007.

69. Seaton, A.; Godden, D.; MacNee, W.; Donaldson, K., Particulate air pollution and acute health effects. L*ancet* **1995,** *345* (8943), 176-178.

70. Peters, A.; Döring, A.; Wichmann, H. E.; Koenig, W., Increased plasma viscosity during an air pollution episode: a link to mortality? *Lancet* **1997,** *349* (9065), 1582-1587.

71. Schulz, H.; Harder, V.; Ibald-Mulli, A.; Khandoga, A.; Koenig, W.; Krombach, F.; Radykewicz, R.; Stampfl, A.; Thorand, B.; Peters, A., Cardiovascular effects of fine and ultrafine particles. *J. Aerosol. Med.* **2005,** *18* (1), 1-22.

72. Renwick, L.; Brown, D.; Clouter, A.; Donaldson, K., Increased inflammation and altered macrophage chemotactic responses caused by two ultrafine particle types. *Occup. Environ. Med.* **2004,** *61* (5), 442-447.

73. Byrne, J. D.; Baugh, J. A., The significance of nanoparticles in particle-induced pulmonary fibrosis. *Mcgill J. Med.* **2008,** *11* (1), 43-50.

74. Turrens, J. F., Mitochondrial formation of reactive oxygen species. *J. Physiol.* **2003,** *552* (Pt 2), 335-344.

75. Khanna, P.; Ong, C.; Bay, H. B.; Baeg, H. G., Nanotoxicity: An Interplay of Oxidative Stress, Inflammation and Cell Death. *Nanomaterials* **2015,** *5* (3), 1163–1180.

76. Meng, H.; Xia, T.; George, S.; Nel, A. E., A Predictive Toxicological Paradigm for the Safety Assessment of Nanomaterials. *ACS Nano* **2009,** *3* (7), 1620-1627.

77. Fu, P. P.; Xia, Q.; Hwang, H.-M.; Ray, P. C.; Yu, H., Mechanisms of nanotoxicity: Generation of reactive oxygen species. *J. Food Drug Anal.* **2014,** *22* (1), 64-75.

78. Nel, A. E.; Mädler, L.; Velegol, D.; Xia, T.; Hoek, E. M. V.; Somasundaran, P.; Klaessig, F.; Castranova, V.; Thompson, M., Understanding biophysicochemical interactions at the nano–bio interface. *Nat. Mater.* **2009,** *8*, 543.

79. Nel, A.; Xia, T.; Mädler, L.; Li, N., Toxic Potential of Materials at the Nanolevel. *Science* **2006,** *311* (5761), 622.

80. Nel, A. E.; Madler, L.; Velegol, D.; Xia, T.; Hoek, E. M. V.; Somasundaran, P.; Klaessig, F.; Castranova, V.; Thompson, M., Understanding biophysicochemical interactions at the nano-bio interface. *Nat. Mater.* **2009,** *8* (7), 543-557.

81. Halliwell, B.; Gutteridge, J. M., *Free radicals in biology and medicine*. Oxford University Press, USA: 2015.

82. Stohs, S. J.; Bagchi, D., Oxidative mechanisms in the toxicity of metal ions. *Free Radic. Biol. Med.* **1995,** *18* (2), 321-336.

83. Valko, M.; Rhodes, C. J.; Moncol, J.; Izakovic, M.; Mazur, M., Free radicals, metals and antioxidants in oxidative stress-induced cancer. *Chem. Biol. Interact.* **2006,** *160* (1), 1-40.

84. Misawa, M.; Takahashi, J., Generation of reactive oxygen species induced by gold nanoparticles under x-ray and UV Irradiations. *Nanomed.: Nanotechnol. Biol. Med.* **2011,** *7* (5), 604-614.

85. Avalos, A.; Haza, A. I.; Mateo, D.; Morales, P., Cytotoxicity and ROS production of manufactured silver nanoparticles of different sizes in hepatoma and leukemia cells. *J. Appl. Toxicol.* **2014,** *34* (4), 413-423.

86. Yin, J.-J.; Liu, J.; Ehrenshaft, M.; Roberts, J. E.; Fu, P. P.; Mason, R. P.; Zhao, B., Phototoxicity of nano titanium dioxides in HaCaT keratinocytes—Generation of reactive oxygen species and cell damage. *Toxicol. Appl. Pharmacol.* **2012,** *263* (1), 81-88.

87. Manke, A.; Wang, L.; Rojanasakul, Y., Mechanisms of Nanoparticle-Induced Oxidative Stress and Toxicity. *Biomed Res. Int.* **2013,** *2013*, 15.

88. Staniek, K.; Gille, L.; Kozlov, A. V.; Nohl, H., Mitochondrial superoxide radical formation is controlled by electron bifurcation to the high and low potential pathways. *Free Radic. Res.* **2002,** *36* (4), 381-387.

89. Richter, C.; Gogvadze, V.; Laffranchi, R.; Schlapbach, R.; Schweizer, M.; Suter, M.; Walter, P.; Yaffee, M., Oxidants in mitochondria: from physiology to diseases. *Biochim. Biophys. Acta. Mol. Basis. Dis.* **1995,** *1271* (1), 67-74.

90. Hensley, K.; Robinson, K. A.; Gabbita, S. P.; Salsman, S.; Floyd, R. A., Reactive oxygen species, cell signaling, and cell injury. *Free Radic. Biol. Med.* **2000,** *28* (10), 1456-1462.

91. Toyokuni, S.; Okamoto, K.; Yodoi, J.; Hiai, H., Persistent oxidative stress in cancer. *FEBS Lett.* **1995,** *358* (1), 1-3.

92. Fisichella, M.; Berenguer, F.; Steinmetz, G.; Auffan, M.; Rose, J.; Prat, O., Intestinal toxicity evaluation of TiO 2 degraded surface-treated nanoparticles: a combined physico-chemical and toxicogenomics approach in caco-2 cells. *Part. Fibre Toxicol.* **2012,** *9* (1), 18.

93. Song, Y.; Guan, R.; Lyu, F.; Kang, T.; Wu, Y.; Chen, X., In vitro cytotoxicity of silver nanoparticles and zinc oxide nanoparticles to human epithelial colorectal adenocarcinoma (Caco-2) cells. *Muta. Res.-Fund. Mol. M.* **2014,** *769*, 113-118.

94. Zhang, H.; Ji, Z.; Xia, T.; Meng, H.; Low-Kam, C.; Liu, R.; Pokhrel, S.; Lin, S.; Wang, X.; Liao, Y.-P.; Wang, M.; Li, L.; Rallo, R.; Damoiseaux, R.; Telesca, D.; Mädler, L.; Cohen, Y.; Zink, J. I.; Nel, A. E., Use of Metal Oxide Nanoparticle Band Gap To Develop a Predictive Paradigm for Oxidative Stress and Acute Pulmonary Inflammation. *ACS Nano* **2012,** *6* (5), 4349-4368.

95. Buzea, C.; Pacheco, I. I.; Robbie, K., Nanomaterials and nanoparticles: sources and toxicity. *Biointerphases* **2007,** *2* (4), MR17-MR71.

96. Medzhitov, R., Origin and physiological roles of inflammation. *Nature* **2008,** *454* (7203), 428.

97. Kirsner, J. B.; Sartor, R. B.; Sandborn, W. J., *Kirsner's inflammatory bowel disease*. Saunders: Edinburgh; New York, 2004.

98. Medzhitov, R., Inflammation 2010: new adventures of an old flame. *Cell* **2010,** *140* (6), 771-776.

99. Donaldson, K.; Stone, V., Current hypotheses on the mechanisms of toxicity of ultrafine particles. *Ann. Ist. Super. Sanita* **2003,** *39* (3), 405-410.

100. Baumgart, D. C.; Carding, S. R., Inflammatory bowel disease: cause and immunobiology. *Lancet* **2007,** *369* (9573), 1627-1640.

101. Hanauer, S. B., Inflammatory bowel disease: Epidemiology, pathogenesis, and therapeutic opportunities. *Inflamm. Bowel Dis.* **2006,** *12* (5), S3-S9.

102. MacDonald, T. T.; Monteleone, G., Immunity, inflammation, and allergy in the gut. *Science* **2005,** *307* (5717), 1920-1925.

103. Krüger, K.; Cossais, F.; Neve, H.; Klempt, M., Titanium dioxide nanoparticles activate IL8-related inflammatory pathways in human colonic epithelial Caco-2 cells. *J. Nanopart. Res.* **2014,** *16* (5), 2402.

104. Powell, J.; Harvey, R.; Ashwood, P.; Wolstencroft, R.; Gershwin, M.; Thompson, R., Immune potentiation of ultrafine dietary particles in normal subjects and patients with inflammatory bowel disease. *J. Autoimmun.* **2000,** *14* (1), 99-105.

105. Oberdörster, G.; Stone, V.; Donaldson, K., Toxicology of nanoparticles: a historical perspective. *Nanotoxicology* **2007,** *1* (1), 2-25.

106. Fasano, A., Leaky Gut and Autoimmune Diseases. *Clin. Rev. Allergy Immunol.* **2012,** *42* (1), 71-78.

107. Liu, Z.; Li, N.; Neu, J., Tight junctions, leaky intestines, and pediatric diseases. *Acta Paediatr.* **2005,** *94* (4), 386-393.

108. Hartsock, A.; Nelson, W. J., Adherens and tight junctions: Structure, function and connections to the actin cytoskeleton. *Biochim. Biophys. Acta. Biomembr.* **2008,** *1778* (3), 660-669.

109. Gumbiner, B., Structure, biochemistry, and assembly of epithelial tight junctions. *Am. J. Physiol. Cell Physiol.* **1987,** *253* (6), C749-C758.

110. Schneeberger, E. E.; Lynch, R. D., The tight junction: a multifunctional complex. *Am. J. Physiol. Cell Physiol.* **2004,** *286* (6), C1213-C1228.

111. Anderson, J. M.; Van Itallie, C. M., Physiology and Function of the Tight Junction. *Cold Spring Harb. Perspect. Biol.* **2009,** *1* (2), a002584.

112. Meng, W.; Takeichi, M., Adherens junction: molecular architecture and regulation. *Cold Spring Harb. Perspect. Biol.* **2009,** *1* (6), a002899.

113. Nagafuchi, A., Molecular architecture of adherens junctions. *Curr. Opin. Cell Biol.* **2001,** *13* (5), 600-603.

114. Capaldo, C. T.; Macara, I. G., Depletion of E-cadherin disrupts establishment but not maintenance of cell junctions in Madin-Darby canine kidney epithelial cells. *Mol. Biol. Cell* **2007,** *18* (1), 189-200.

115. Sambuy, Y.; De Angelis, I.; Ranaldi, G.; Scarino, M. L.; Stammati, A.; Zucco, F., The Caco-2 cell line as a model of the intestinal barrier: Influence of cell and culture-related factors on Caco-2 cell functional characteristics. *Cell Biol. Toxicol.* **2005,** *21* (1), 1-26.

116. Li, N.; Gu, L.; Qu, L.; Gong, J.; Li, Q.; Zhu, W.; Li, J., Berberine attenuates pro-inflammatory cytokine-induced tight junction disruption in an in vitro model of intestinal epithelial cells. *Eur. J. Pharm. Sci.* **2010,** *40* (1), 1-8.

117. Cereijido, M.; Contreras, R. G.; Flores-Benítez, D.; Flores-Maldonado, C.; Larre, I.; Ruiz, A.; Shoshani, L., New Diseases Derived or Associated with the Tight Junction. *Arch. Med. Res.* **2007,** *38* (5), 465-478.

118. Farquhar, M. G.; Palade, G. E., JUNCTIONAL COMPLEXES IN VARIOUS EPITHELIA. *J. Cell Biol.* **1963,** *17* (2), 375.

119. Setyawati, M.; Tay, C. Y.; Chia, S.; Goh, S.; Fang, W.; Neo, M.; Chong, H. C.; Tan, S.; Loo, S. C. J.; Ng, K., Titanium dioxide nanomaterials cause endothelial cell leakiness by disrupting the homophilic interaction of VE–cadherin. *Nat. Commun.* **2013,** *4*, 1673.

120. Sun, X.; Shi, J.; Zou, X.; Wang, C.; Yang, Y.; Zhang, H., Silver nanoparticles interact with the cell membrane and increase endothelial permeability by promoting VE-cadherin internalization. *J. Hazard. Mater.* **2016,** *317*, 570-578.

121. Long, Y.-M.; Zhao, X.-C.; Clermont, A. C.; Zhou, Q.-F.; Liu, Q.; Feener, E. P.; Yan, B.; Jiang, G.-B., Negatively charged silver nanoparticles cause retinal vascular permeability by activating plasma contact system and disrupting adherens junction. *Nanotoxicology* **2016,** *10* (4), 501-511.

122. Zhang, W.; Kalive, M.; Capco, D. G.; Chen, Y., Adsorption of hematite nanoparticles onto Caco-2 cells and the cellular impairments: effect of particle size. *Nanotechnology* **2010,** *21* (35), 355103.

123. Setyawati, M. I.; Sevencan, C.; Bay, B. H.; Xie, J.; Zhang, Y.; Demokritou, P.; Leong, D. T., Nano-TiO2 Drives Epithelial–Mesenchymal Transition in Intestinal Epithelial Cancer Cells. *Small* **2018,** *14* (30), 1800922.

124. Johansson, S. G. O.; Bieber, T.; Dahl, R.; Friedmann, P. S.; Lanier, B. Q.; Lockey, R. F.; Motala, C.; Ortega Martell, J. A.; Platts-Mills, T. A. E.; Ring, J.; Thien, F.; Van Cauwenberge, P.; Williams, H. C., Revised nomenclature for allergy for global use: Report of the Nomenclature Review Committee of the World Allergy Organization, October 2003. *J. Allergy Clin. Immunol.* **2004,** *113* (5), 832-836.

125. Sicherer, S. H.; Sampson, H. A., Food allergy. *J. Allergy Clin. Immunol.* **2010,** *125* (2, Supplement 2), S116-S125.

126. Kumar, S.; Verma, A. K.; Das, M.; Dwivedi, P. D., Molecular mechanisms of IgE mediated food allergy. *Int. Immunopharmacol.* **2012,** *13* (4), 432-439.

127. Galli, S. J.; Tsai, M., IgE and mast cells in allergic disease. *Nat. Med.* **2012,** *18* (5), 693-704.

128. Gould, H. J.; Sutton, B. J., IgE in allergy and asthma today. *Nat. Rev. Immunol.* **2008,** *8* (3), 205-217.

129. Lyons, D. O.; Pullen, N. A., Beyond IgE: Alternative Mast Cell Activation Across Different Disease States. *Int. J. Mol. Sci.* **2020,** *21* (4),1498.

130. Yu, Y.; Blokhuis, B. R.; Garssen, J.; Redegeld, F. A., Non-IgE mediated mast cell activation. *Eur. J. Pharmacol.* **2016,** *778*, 33-43.

131. Høst, A., Frequency of cow's milk allergy in childhood. *Ann. Allergy Asthma Immunol.* **2002,** *89* (6, Supplement), 33-37.

132. Saarinen, K. M.; Pelkonen, A. S.; Mäkelä, M. J.; Savilahti, E., Clinical course and prognosis of cow's milk allergy are dependent on milk-specific IgE status. *J. Allergy Clin. Immunol.* **2005,** *116* (4), 869-875.

133. Johnson, M. M.; Mendoza, R.; Raghavendra, A. J.; Podila, R.; Brown, J. M., Contribution of engineered nanomaterials physicochemical properties to mast cell degranulation. *Sci. Rep.* **2017,** *7*, 43570-43570.

134. Chen, E. Y.; Garnica, M.; Wang, Y.-C.; Mintz, A. J.; Chen, C.-S.; Chin, W.-C., A mixture of anatase and rutile TiO2 nanoparticles induces histamine secretion in mast cells. *Part. Fibre Toxicol.* **2012,** *9* (1), 2.

135. Radauer-Preiml, I.; Andosch, A.; Hawranek, T.; Luetz-Meindl, U.; Wiederstein, M.; Horejs-Hoeck, J.; Himly, M.; Boyles, M.; Duschl, A., Nanoparticle-allergen interactions mediate human allergic responses: protein corona characterization and cellular responses. *Part. Fibre Toxicol.* **2016,** *13* (1), 3.

136. Kruger, C.; Mann, S., Safety evaluation of functional ingredients. *Food Chem. Toxicol.* **2003,** *41* (6), 793-805.

137. Food, U.; Administration, D., 'Toxicological Principles for the Safety Assessment of Food Ingredients: Redbook 2000. *secs. IV. C. 4b and IV. C* **2003,** *5*.

138. Shanks, N.; Greek, R.; Greek, J., Are animal models predictive for humans? *Philos. Ethics Humanit. Med.* **2009,** *4* (1), 2.

139. Kathawala, M. H.; Xiong, S.; Richards, M.; Ng, K. W.; George, S.; Loo, S. C. J., Emerging In Vitro Models for Safety Screening of High-Volume Production Nanomaterials under Environmentally Relevant Exposure Conditions. *Small* **2013,** *9* (9-10), 1504-1520.

140. Hartung, T., Toxicology for the twenty-first century. *Nature* **2009,** *460* (7252), 208-212.

141. Villeneuve, D. L.; Crump, D.; Garcia-Reyero, N.; Hecker, M.; Hutchinson, T. H.; LaLone, C. A.; Landesmann, B.; Lettieri, T.; Munn, S.; Nepelska, M.; Ottinger, M. A.; Vergauwen, L.; Whelan, M., Adverse Outcome Pathway (AOP) Development I: Strategies and Principles. *Toxicol. Sci.* **2014,** *142* (2), 312-320.

142. Groh, K. J.; Carvalho, R. N.; Chipman, J. K.; Denslow, N. D.; Halder, M.; Murphy, C. A.; Roelofs, D.; Rolaki, A.; Schirmer, K.; Watanabe, K. H., Development and application of the adverse outcome pathway framework for understanding and predicting chronic toxicity: I. Challenges and research needs in ecotoxicology. *Chemosphere* **2015,** *120*, 764-777.

143. Society for the Advancement of Adverse Outcome Pathways (SAAOP). AOPWiki. https://aopwiki.org/ (accessed 01/29).

144. Ankley, G. T.; Bennett, R. S.; Erickson, R. J.; Hoff, D. J.; Hornung, M. W.; Johnson, R. D.; Mount, D. R.; Nichols, J. W.; Russom, C. L.; Schmieder, P. K., Adverse outcome pathways: a conceptual framework to support ecotoxicology research and risk assessment. *Environ. Toxicol. Chem.* **2010,** *29* (3), 730-741.

145. Docter, D.; Distler, U.; Storck, W.; Kuharev, J.; Wünsch, D.; Hahlbrock, A.; Knauer, S. K.; Tenzer, S.; Stauber, R. H., Quantitative profiling of the protein coronas that form around nanoparticles. *Nat. Protoc.* **2014,** *9* (9), 2030.

146. Di Silvio, D.; Rigby, N.; Bajka, B.; Mayes, A.; Mackie, A.; Baldelli Bombelli, F., Technical tip: high-resolution isolation of nanoparticle-protein corona complexes from physiological fluids. *Nanoscale* **2015,** *7* (28), 11980-11990.

147. Strutz, F.; Zeisberg, M.; Ziyadeh, F. N.; Yang, C.-Q.; Kalluri, R.; Müller, G. A.; Neilson, E. G.; Renziehausen, A.; Sisic, Z., Role of basic fibroblast growth factor-2 in epithelial-mesenchymal transformation. *Kidney Int.* **2002,** *61* (5), 1714-1728.

148. Bates, R. C.; Mercurio, A. M., Tumor necrosis factor-α stimulates the epithelial-to-mesenchymal transition of human colonic organoids. *Mol. Biol. Cell* **2003,** *14* (5), 1790-1800.

149. Lee, S. H., Intestinal permeability regulation by tight junction: implication on inflammatory bowel diseases. *Intest. Res.* **2015,** *13* (1), 11.

150. Breese, E. J.; Michie, C. A.; Nicholls, S. W.; Murch, S. H.; Williams, C. B.; Domizio, P.; Walker-Smith, J. A.; Macdonald, T. T., Tumor necrosis factor α-producing cells in the intestinal mucosa of children with inflammatory bowel disease. *Gastroenterology* **1994,** *106* (6), 1455-1466.

151. Rachmilewitz, D.; Stamler, J. S.; Bachwich, D.; Karmeli, F.; Ackerman, Z.; Podolsky, D. K., Enhanced colonic nitric oxide generation and nitric oxide synthase activity in ulcerative colitis and Crohn's disease. *Gut* **1995,** *36* (5), 718.

152. Halliwell, B., Oxygen and nitrogen are pro-carcinogens. Damage to DNA by reactive oxygen, chlorine and nitrogen species: measurement, mechanism and the effects of nutrition. *Mutat. Res. Genet. Toxicol. Environ. Mutagen.* **1999,** *443* (1), 37-52.

153. Furuse, M.; Izumi, Y.; Oda, Y.; Higashi, T.; Iwamoto, N., Molecular organization of tricellular tight junctions. *Tissue Barriers* **2014,** *2*, e28960.

154. Cao, Y.; Li, J.; Liu, F.; Li, X.; Jiang, Q.; Cheng, S.; Gu, Y., Consideration of interaction between nanoparticles and food components for the safety assessment of nanoparticles following oral exposure: A review. *Environ. Toxicol. Pharmacol.* **2016,** *46*, 206-210.

155. Canada, H., Policy Statement on Health Canada's Working Definition for Nanomaterial. Health Canada Ottawa: 2011.

156. Tyler, L. C., FDA issues draft guidance on use of nanotechnology in food and food packaging. *Nanotech. Law Bus.* **2012,** *9*, 149.

157. EPA, Health Effects Test Guidelines: OCSPP 870.3050 – Repeated Dose 28-Day Oral Toxicity Study in Rodents. Agency., U. S. E. P., Ed. Washington, DC, 2000.

158. EPA, Health Effects Test Guidelines: OCSPP 870.3100 – 90-Day Oral Toxicity in Rodents. Agency, U. S. E. P., Ed. Washington, DC, 1998.

159. Mittal, K.; Crump, D.; Head, J. A.; Hecker, M.; Hickey, G.; Maguire, S.; Hogan, N.; Xia, J.; Basu, N., Resource requirements for ecotoxicity testing: A comparison of traditional and new approach methods. *bioRxiv* **2022**.

160. OECD, Proposal for a template, and guidance on developing and assessing the completeness of adverse outcome pathways. OECD Publishing Paris: 2012.

161. Kukurba, K. R.; Montgomery, S. B., RNA Sequencing and Analysis. *Cold Spring Harb. Protoc.* **2015,** *2015* (11), 951-969.

162. Ozsolak, F.; Milos, P. M., RNA sequencing: advances, challenges and opportunities. *Nat. Rev. Genet.***,** *12* (2), 87-98.

163. Mav, D.; Shah, R. R.; Howard, B. E.; Auerbach, S. S.; Bushel, P. R.; Collins, J. B.; Gerhold, D. L.; Judson, R. S.; Karmaus, A. L.; Maull, E. A., A hybrid gene selection approach to create the S1500+ targeted gene sets for use in high-throughput transcriptomics. *PloS one* **2018,** *13* (2), e0191105.

164. Soufan, O.; Ewald, J.; Viau, C.; Crump, D.; Hecker, M.; Basu, N.; Xia, J., T1000: a reduced gene set prioritized for toxicogenomic studies. *PeerJ* **2019,** *7*, e7975.

165. Subramanian, A.; Narayan, R.; Corsello, S. M.; Peck, D. D.; Natoli, T. E.; Lu, X.; Gould, J.; Davis, J. F.; Tubelli, A. A.; Asiedu, J. K.; Lahr, D. L.; Hirschman, J. E.; Liu, Z.; Donahue, M.; Julian, B.; Khan, M.; Wadden, D.; Smith, I. C.; Lam, D.; Liberzon, A.; Toder, C.; Bagul, M.; Orzechowski, M.; Enache, O. M.; Piccioni, F.; Johnson, S. A.; Lyons, N. J.; Berger, A. H.; Shamji, A. F.; Brooks, A. N.; Vrcic, A.; Flynn, C.; Rosains, J.; Takeda, D. Y.; Hu, R.; Davison, D.; Lamb, J.; Ardlie, K.; Hogstrom, L.; Greenside, P.; Gray, N. S.; Clemons, P. A.; Silver, S.; Wu, X.; Zhao, W.-N.; Read-Button, W.; Wu, X.; Haggarty, S. J.; Ronco, L. V.; Boehm, J. S.; Schreiber, S. L.; Doench, J. G.; Bittker, J. A.; Root, D. E.; Wong, B.; Golub, T. R., A Next Generation Connectivity Map: L1000 Platform and the First 1,000,000 Profiles. *Cell* **2017,** *171* (6), 1437-1452.e17.

166. Lu, S.; Jessen, B.; Strock, C.; Will, Y., The contribution of physicochemical properties to multiple in vitro cytotoxicity endpoints. *Toxicol. In Vitro* **2012,** *26* (4), 613-620.

167. Buchser, W.; Collins, M.; Garyantes, T.; Guha, R.; Haney, S.; Lemmon, V.; Li, Z.; Trask, O. J., Assay development guidelines for image-based high content screening, high content analysis and high content imaging. *Assay guidance manual [Internet]* **2014**.

168. Kanehisa, M.; Goto, S., KEGG: kyoto encyclopedia of genes and genomes. *Nucleic Acids Res.* **2000,** *28* (1), 27-30.

169. Hartung, T.; Daston, G., Are in vitro tests suitable for regulatory use? *Toxicol. Sci.* **2009,** *111* (2), 233-237.

170. Locke, P. A.; Westphal, M.; Tischler, J.; Hessler, K.; Frasch, P.; Myers, B.; Krewski, D., Implementing toxicity testing in the 21st century: challenges and opportunities. *Int. J. Risk Assess. Manag.* **2017,** *20* (1-3), 198-225.

171. Flom, J. D.; Sicherer, S. H., Epidemiology of Cow's Milk Allergy. *Nutrients* **2019,** *11* (5), 1051.

172. Alatab, S.; Sepanlou, S. G.; Ikuta, K.; Vahedi, H.; Bisignano, C.; Safiri, S.; Sadeghi, A.; Nixon, M. R.; Abdoli, A.; Abolhassani, H., The global, regional, and national burden of inflammatory bowel disease in 195 countries and territories, 1990–2017: a systematic analysis for the Global Burden of Disease Study 2017. *Lancet Gastroenterol. Hepatol.* **2020,** *5* (1), 17-30.

173. Peters, R. J. B.; van Bemmel, G.; Herrera-Rivera, Z.; Helsper, H. P. F. G.; Marvin, H. J. P.; Weigel, S.; Tromp, P. C.; Oomen, A. G.; Rietveld, A. G.; Bouwmeester, H., Characterization of Titanium Dioxide Nanoparticles in Food Products: Analytical Methods To Define Nanoparticles. *J. Agric. Food Chem.* **2014,** *62* (27), 6285-6293.

174. Cushen, M.; Kerry, J.; Morris, M.; Cruz-Romero, M.; Cummins, E., Migration and exposure assessment of silver from a PVC nanocomposite. *Food Chem.* **2013,** *139* (1), 389-397.

175. Helander, H. F.; Fändriks, L., Surface area of the digestive tract – revisited. *Scand. J. Gastroenterol.* **2014,** *49* (6), 681-689.

176. Scientific, T. Useful information for various sizes of cell culture dishes and flasks. https://www.thermofisher.com/ca/en/home/references/gibco-cell-culture-basics/cell-culture-protocols/cell-culture-useful-numbers.html.

177. Canada, H., Science Approach Document–Bioactivity Exposure Ratio: Application in Priority Setting and Risk Assessment. Existing Substance Risk Assessment Bureau Canada: 2021.

178. Escaffit, F.; Perreault, N.; Jean, D.; Francoeur, C.; Herring, E.; Rancourt, C.; Rivard, N.; Vachon, P. H.; Paré, F.; Boucher, M.-P.; Auclair, J.; Beaulieu, J.-F., Repressed E-cadherin expression in the lower crypt of human small intestine: a cell marker of functional relevance. *Exp. Cell Res.* **2005,** *302* (2), 206-220.

179. Ault, A. P.; Stark, D. I.; Axson, J. L.; Keeney, J. N.; Maynard, A. D.; Bergin, I. L.; Philbert, M. A., Protein corona-induced modification of silver nanoparticle aggregation in simulated gastric fluid. *Environ. Sci. Nano* **2016,** *3* (6), 1510-1520.

180. Shannahan, J. H.; Podila, R.; Aldossari, A. A.; Emerson, H.; Powell, B. A.; Ke, P. C.; Rao, A. M.; Brown, J. M., Formation of a protein corona on silver nanoparticles mediates cellular toxicity via scavenger receptors. *Toxicol. Sci.* **2014,** *143* (1), 136-146.

181. Winuprasith, T.; Chantarak, S.; Suphantharika, M.; He, L.; McClements, D. J., Alterations in nanoparticle protein corona by biological surfactants: Impact of bile salts on β-lactoglobulin-coated gold nanoparticles. *J. Colloid Interface Sci.* **2014,** *426*, 333-340.

182. Sachana, M.; Willett, C.; Pistollato, F.; Bal-Price, A., The potential of mechanistic information organised within the AOP framework to increase regulatory uptake of the developmental neurotoxicity (DNT) in vitro battery of assays. *Reprod. Toxicol.* **2021,** *103*, 159-170.

183. EFSA Panel on Food Additives Nutrient Sources added to Food, Re-evaluation of titanium dioxide (E 171) as a food additive. *EFSA Journal* **2016,** *14* (9), e04545.

184. EFSA Panel on Food Additives Nutrient Sources added to Food; Younes, M.; Aggett, P.; Aguilar, F.; Crebelli, R.; Dusemund, B.; Filipič, M.; Frutos, M. J.; Galtier, P.; Gott, D.; Gundert-Remy, U.; Kuhnle, G. G.; Lambré, C.; Leblanc, J.-C.; Lillegaard, I. T.; Moldeus, P.; Mortensen, A.; Oskarsson, A.; Stankovic, I.; Waalkens-Berendsen, I.; Wright, M.; Lodi, F.; Rincon, A. M.; Smeraldi, C.; Woutersen, R. A., Evaluation of four new studies on the potential toxicity of titanium dioxide used as a food additive (E 171). *EFSA Journal* **2018,** *16* (7), e05366.

185. EFSA Panel on Food Additives Flavourings; Younes, M.; Aquilina, G.; Castle, L.; Engel, K.-H.; Fowler, P.; Frutos Fernandez, M. J.; Fürst, P.; Gundert-Remy, U.; Gürtler, R.; Husøy, T.; Manco, M.; Mennes, W.; Moldeus, P.; Passamonti, S.; Shah, R.; Waalkens-Berendsen, I.; Wölfle, D.; Corsini, E.; Cubadda, F.; De Groot, D.; FitzGerald, R.; Gunnare, S.; Gutleb, A. C.; Mast, J.; Mortensen, A.; Oomen, A.; Piersma, A.; Plichta, V.; Ulbrich, B.; Van Loveren, H.; Benford, D.; Bignami, M.; Bolognesi, C.; Crebelli, R.; Dusinska, M.; Marcon, F.; Nielsen, E.; Schlatter, J.; Vleminckx, C.; Barmaz, S.; Carfí, M.; Civitella, C.; Giarola, A.; Rincon, A. M.; Serafimova, R.; Smeraldi, C.; Tarazona, J.; Tard, A.; Wright, M., Safety assessment of titanium dioxide (E171) as a food additive. *EFSA Journal* **2021,** *19* (5), e06585.

186. Health Canada, State of the Science of Titanium Dioxide (TiO2) as a Food Additive. Food Directorate, **2022**.

187. Muller, J.; Huaux, F.; Moreau, N.; Misson, P.; Heilier, J.-F.; Delos, M.; Arras, M.; Fonseca, A.; Nagy, J. B.; Lison, D., Respiratory toxicity of multi-wall carbon nanotubes. *Toxicology and applied pharmacology* **2005,** *207* (3), 221-231.

188. Nemery, B., Metal toxicity and the respiratory tract. *Eur. Clin. Respir.* **1990,** *3* (2), 202-219.

189. Leist, M.; Hasiwa, N.; Daneshian, M.; Hartung, T., Validation and quality control of replacement alternatives–current status and future challenges. *Toxicol. Res.* **2012,** *1* (1), 8-22.

190. Brittan, M.; Wright, N. A., Gastrointestinal stem cells. *J. Pathol.* **2002,** *197* (4), 492-509.

191. Donkers, J. M.; Amirabadi, H. E.; van de Steeg, E., Intestine-on-a-chip: Next level in vitro research model of the human intestine. *Curr. Opin. Toxicol.* **2021,** *25*, 6-14.

192. Foulke-Abel, J.; In, J.; Kovbasnjuk, O.; Zachos, N. C.; Ettayebi, K.; Blutt, S. E.; Hyser, J. M.; Zeng, X.-L.; Crawford, S. E.; Broughman, J. R., Human enteroids as an ex-vivo model of host–pathogen interactions in the gastrointestinal tract. *Exp. Biol. Med.* **2014,** *239* (9), 1124-1134.